Spring 2024

Thermo-Elasto-Plastic Stability of Biaxially Loaded Hollow Rectangular Section Steel Beam-Columns with Applied Torsion

George Adomako Kumi
Old Dominion University, gadom002@odu.edu

THERMO-ELASTO-PLASTIC STABILITY OF BIAXIALLY LOADED HOLLOW RECTANGULAR SECTION STEEL BEAM-COLUMNS WITH APPLIED TORSION

by

George Adomako Kumi
B.Sc. June 2011, Kwame Nkrumah University of Science and Technology
M.S. July 2018, Chongqing University

A Dissertation Submitted to the Faculty of
Old Dominion University in Partial Fulfillment of the
Requirements for the Degree of

DOCTOR OF PHILOSOPHY

CIVIL ENGINEERING

OLD DOMINION UNIVERSITY
May 2024

Approved by:

Zia Razzaq (Director)

Mojtaba B. Sirjani (Member)

Shahin N. Amiri (Member)

Mamadou Konate (Member)

Gene W. Hou (Member)

ABSTRACT

THERMO-ELASTO-PLASTIC STABILITY OF BIAXIALLY LOADED HOLLOW RECTANGULAR SECTION STEEL BEAM-COLUMNS WITH APPLIED TORSION

George Adomako Kumi
Old Dominion University, 2024
Advisor: Dr. Zia Razzaq

Presented herein is an experimental and theoretical study of biaxially loaded hollow rectangular section steel beam-columns with applied torsion at elevated temperatures. The theoretical analysis is based on a system of simultaneous materially nonlinear differential equations of equilibrium for which an iterative semi-analytic solution approach is formulated. Although the primary goal of this research is to study the influence of elevated temperatures on the steel member with the complex loading, rigorous analysis is also conducted of the member at ambient temperature for comparison. The experimental part of the study involves conducting tests on the members at both ambient and high temperatures. A biaxial bending apparatus with a pair of gimbals and means to apply an axial load as well as torsion is used to perform the experiments. The elevated temperatures are introduced by means of a heat chamber surrounding each test specimen. The theory is validated by a comparison to the experimentally observed behavior and strength. A set of general dimensionless interaction expressions are developed that can be used for determining the ultimate strength of biaxially loaded beam-columns with applied torsion at elevated temperatures. The substantial reduction of the member strength due to temperature-dependent nonlinear material properties and second-order effects is also quantified.

This dissertation is dedicated to the proposition that success doesn't come from what you do occasionally, but what you do consistently.

ACKNOWLEDGEMENTS

Special Praise goes to the Almighty God for his provision of life, blessings, wealth and health in my life thus far. The author would like to express his profound gratitude to Dr. Zia Razzaq for his guidance, reviews, criticisms, and instructions during this research study at Old Dominion University.

I also wish to express my special appreciation to the workers of the Engineering Workshop for their help in fabricating and mounting of the test specimens and my family for their support, counsel and encouragement throughout this important stage in my academic career.

NOMENCLATURE

A	Area
B	Section width
D	Section depth
dA	Elemental Area
E, E_T	Modulus of elasticity at ambient and elevated temperature
G	Shear modulus
Ix, Iy	Moment of inertia about x-axis and y-axis
Ixy	Product moment of inertia relative to x-axis and y-axis
Iwx, Iwy	Warping product of inertia relative to x-axis and y-axis
$[T]$, $[T]_T$	Member global tangent stiffness matrix at ambient and elevated temperature
k_{BX}, k_{TX}	End rotational stiffness about x-axis
k_{BY}, k_{TY}	End rotational stiffness about y-axis
L	Member length
m_{BX}, m_{TX}	Restraint moments at bottom and top about x-axis
m_{BY}, m_{TY}	Restraint moments at bottom and top about y-axis
M_{BX}, M_{TX}	Applied moments at bottom and top end about x-axis
M_{BY}, M_{TY}	Applied moments at bottom and top end about y-axis
M_{xp}, M_{yp}	Moments due to plastification
M_{xre}, M_{yre}	Moments due to residual stress
M_{xthe}, M_{ythe}	Moments due to thermal deformation
M_{rz}	Torsional moment due to residual stress

Mzp	Torsional moment due to plastification
P	Applied axial load
Pp	Plastic load
Pr	Residual load
P_{the}	Axial load due to thermal expansion
T	Temperature
Rx, Ry	Reaction at the bottom end of the beam-column
Sx, Sy	Elastic section modulus about x and y-axis
S_{wx}, S_{wy}	Warping section modulus about x and y-axis
T	Applied Torque
U	Total deflection in x-direction
V	Total deflection in y-direction
u	Deflection due to applied load in x-direction
v	Deflection due to applied load in y-direction
u_T	Deflection due to applied load and increased temperature in x-direction
v_T	Deflection due to applied load and increased temperature in y-direction
u_o	Midspan initial member crookedness in x-direction
v_o	Midspan initial member crookedness in y-direction
u_{oi}	Initial member crookedness in x-direction
v_{oi}	Initial member crookedness in y-direction
u''	The second order derivative of u
v''	The second order derivative of v
Zx,Zy	Plastic section modulus about x-axis and y-axis

β	Angle between the column and base plate
ε	Normal strain
ε_r	Residual strain
ε_O	Average axial strain
ε_{th}	Thermal strain
ε_w	Normal strain due to warping
ϕ_x, ϕ_y	Bending curvatures
σ_y, σ_{yT}	Yield normal stress at ambient and elevated temperature
σ_{rt}, σ_{rc}	Compressive and tensile residual stress
τ_y	Yield shear stress
Φ	Angle of twist

TABLE OF CONTENTS

Page

Chapter Page

LIST OF TABLES

Table Page

LIST OF FIGURES

Figure Page

Figure Page

Figure Page

Figure Page

Figure Page

Figure Page

Figure Page

Figure Page

CHAPTER 1 INTRODUCTION

1.1 Introduction

The primary focus of the research presented herein is on a theoretical and experimental study of the elasto-plastic behavior of biaxially loaded hollow rectangular section steel beam-columns subjected to biaxial bending, axial load, and applied torsion under elevated temperature conditions. A parallel set of analyses and experiments is conducted at ambient temperature for the purpose of comparison. The current study is focused on non-sway thin-walled hollow square or rectangular section steel members. The study of such members has gained significant importance due to the 9/11 events as well as fire hazards which a building can experience.

The theoretical part of this research is based on an approximated semi-analytic iterative solution of a system of coupled nonlinear differential equations of quasi-static equilibrium. Closed-form solutions of elasto-plastic stability problems are not possible [1-4]. Hence, a theoretical solution procedure based on the semi-analytic method is adopted to iteratively solve the governing differential equations. The experimentally verified analysis is used to develop expressions relating biaxial bending, axial load, and torsion for various ranges of high temperatures for practical use for both square and rectangular section steel members.

Although a considerable body of literature exists on the elasto-plastic behavior of biaxially loaded beam-columns, a rather limited amount of research has been conducted in the past when such members are also subjected to applied torsion. Furthermore, to the best of the author's knowledge, the influence of elevated temperatures on such members in the presence of applied torsion has not been investigated in the past.

1.2 Literature Review

1.2.1 Review of Beam-Column Behavior under Ambient Temperature

The behavior of beam-columns under ambient temperatures subjected to varying loads have been studied by many researchers in the past. In 1954, Ketter [5] applied the method of virtual displacement in his study which was related to the behavior of simply supported wide flange beam-columns. The method of solution that was consequently developed was applied to determine the critical load value for members which had been subjected to concentric, eccentric and lateral loads.

By applying the Newmark's method, Galambos and Ketter [6] determined load deflection curves of wide-flange columns subjected to combined thrust and bending. The theoretical results obtained in the research investigations were later validated with results conducted by popular astute researchers Mason, Fisher and Winter [7].

Birnstiel [8] as well as Birnstiel and Michalos [9] both developed an analytical procedure to investigate the inelastic response of biaxially loaded beam-columns with equal end eccentricities. Galambos and Fukumoto [10] conducted experimental research into the inelastic lateral-torsional buckling strength of rolled-steel wide flange beam-columns. The beam-columns were subjected to axial loads as well as bending moments applied at one end only. Through finite difference approximation, the characteristic determinants of the variable coefficients of the differential equations were subsequently solved. This research was conducted to serve as the framework in providing theoretical background behind the inelastic behavior of beam-columns, derivations, and eventual solution of the system of differential equations.

Beam-columns subjected to axial load and bending moments applied at either one end of a member or at both ends of a member were investigated by Galambos et al [11]. Important

behaviors such as strength reduction, yield stress, residual stress, cross-sectional size, and its effect on lateral torsional buckling strength were determined as part of the experimental study. The theoretical solutions were subsequently compared with the empirical reduction formula for design purposes. The test results were also compared with the theoretical results using the reduction formula approach.

Milner [12] conducted both theoretical and experimental investigation into the behavior of elastic-plastic, elastic restrained and H-section columns (10 in number) that were carefully designed to bend in symmetrical single curvature about two axes. Harstead [13] successfully succeeded in modifying the analytical approach introduced by Birnstiel [8] by reducing the amount of trial and error leading to the computation of the ultimate capacity of the member whilst giving considerations to warping strains, shearing stresses and torsional rigidity.

Rectangular tubular cross-section beam columns that were biaxially loaded with both ends being simply supported as well as axially loaded with a constant increasing moment applied at one end were studied by Razzaq [14] at the University of Windsor. The results of the tests predominantly showed that the predicted deflections were lower as compared to the actualized experimental results.

Marshall and Ellis [15] also performed tests on thin-walled box sections subjected to biaxial bending and compression. The results were found to compare favorably with the results obtained through theoretical solutions.

Sakda [16] conducted a study of biaxially loaded columns by applying the limit theorem and tangent stiffness method to determine the elastic-plastic behavior of the cross-sections. This led to the derivation of interaction equations that depicted the elastic-plastic behavior of biaxially loaded columns. Baseheart [17] investigated the deformational response of biaxially loaded

beam-columns using three coupled differential equations that depicted the members behavior. The proposed solution procedure was found capable of being extended to cover the deformational response of biaxially loaded beam-columns with unequal end eccentricities.

A designed experimental program to evaluate the load deflection behavior and failure modes of rolled, mild steel beams and beam-columns were carried out by Thompson [18]. It was observed from the research that short span beam-columns had more reserve strength, and they were found to exhibit certain characteristics such as load deterioration, stiffness and dissipated energy that correlated the buckling and load deflection trends at large deflections when exposed to monotonic loading. Hobbs and Jowharzadeh [19] explored the use of computer based analysis to examine the effects of off-diagonal flexibilities in the tangent flexibility matrix of a beam-column in a frame section. These off-diagonal terms were adopted as increments of bending moments and axial load to alterations in both curvature and centroidal strains. As part of research observations, small effects of flexural flexibility due to the presence of axial load on the maximum load carrying capacity were realized.

Hollow rectangular non-sway beam-columns were also subsequently studied by both Razzaq and McVinnie [20,21]. Both experimental and theoretical studies were performed on selected hollow rectangular non-sway beam-columns that were subjected to nonproportional loading. It was observed from the tests that twisting was insignificant for either hollow square or rectangular section beam-columns. Furthermore, in attempting to investigate and offer predictions on the inelastic behavior of steel tubular beam-columns subjected to post-buckling and cyclic loading conditions, Han and Chen [22] employed the use of finite segment and influence coefficient method. Subsequently, the results of this study led to the successful representation of moment-thrust-curvature and moment-thrust-axial strain relations for the post

yield behavior of tubular cross-sections. Sugimoto and Chen [23] established a finite segment computer-based simulation to study the post-buckling, post-peak and cyclic behavior of beam-columns. They proposed the application of automatic load control techniques intertwined with the generalized cyclic stress-strain relationships. The conclusion of this research led to a successful application in tubular beam-columns and frames with large shape factor values and various distinct end conditions.

In 1985, W shaped beam-columns were investigated by Dawe and Kulak [24] for their buckling behavior via the application of a computerized based technique. This was done whilst taking consideration to the effects of flange, web interaction, inelastic behavior, and the presence of residual stresses in beam-columns. The research findings were later found to be conservative when compared with the standards stipulated in both the US and Canadian specifications. Chen [25] investigated the ultimate strength of beam-columns, secondary effects namely, P-δ and P-Δ effects and second-order elastic as well as inelastic analysis based on a simplified computerized approach. This research led to the development and consequent ultimate strength design interactions which has subsequently been applied in the United States.

Darbhamulla [1] investigated the elasto-plastic behavior of steel beam-columns under combined effects of various imperfections, flexible connections and non-proportional loads. This was achieved by applying second order finite difference algorithm to a set of materially nonlinear equilibrium equations interconnected with the tangent stiffness approach. Results of the study revealed the very important effects of non-proportional loads on the behavior and strength of beam-columns. Eidan [4] solved a set of materially nonlinear differential equilibrium equations to be used for both biaxially loaded and planar beam-columns with sidesway uninhibited. With analysis centered on the effects of initial imperfections and flexible

connections, an iterative numerical solution procedure using the central difference approach was adopted in solving the problem.

Hancock and Rasmussen [26] conducted experiments on the interaction buckling behavior of beam-columns with thin-walled hollow square and I-shaped sections bent about the major and minor principal axes. For the majority of sections tested, local buckling was observed to occur before overall buckling. The results of the tests were subsequently found to correlate with the AS4100:98, EC3 and AISC LRFD specifications. Torkomani and Sonmez [27] also performed a comparative study of two beam-column models for inelastic analysis and large deformation of planar steel structural systems. The models proposed were based on the derivations of different stiffness matrices.

Boissonnade et al [28] formulated a new design proposal for beam-column interaction formulae based on the theoretical background, physical meaning and consistency with other Eurocode 3 formulae. Boissonnade and his team of researchers validated the experimental results with more than 15,000 results of finite element simulations. Based on a research investigation carried out by Pi and Trahair [29] on steel beam-columns subjected to biaxial bending and torsion, a finite element model was developed for the successful nonlinear incremental analysis of the biaxial bending and torsion of thin-walled beam columns. Meanwhile, Hasham and Rasmussen [30] also studied interaction curves of slender cross-sections of beam-columns. Consequently, the experimental interaction curves were found to be closely correlated with the design interaction curves stipulated by the Australian, British and European specifications.

Law and Gardner [31] carried out both experimental and numerical tests on selected number of beam-column specimens under various combinations of compressive loadings and bending moments acting on the principal axes. The numerical methods were successfully applied

in further parametric studies to determine the slenderness and cross-sectional aspect ratios and their effects on the overall response of the beam-column member.

Marques et al [32] also examined the various methodologies used in verifying the stability of members and frames using tapered beam-columns. To achieve the research objectives, various web tapered beam-columns subjected to in-plane loading were adopted using the interaction formulae in EC3-1-1 and subsequently validated against finite element method numerical modelling techniques.

Kucukler, Gardner and Macorini [33] developed a stiffness reduction method for the flexural-torsional buckling assessment of steel beam-columns subjected to major axis bending and axial compression. In validating the developed method, the proposed stiffness reduction method was found to compare favorably with the European 3 design standards.

Konate [3] presented the results of the highly complex and detailed research investigation into the experimental and theoretical inelastic behavior of beam-columns subjected to torsion. In this research, the theoretical study revolved around the application of the finite integral method used in solving materially non-linear differential equations. The outcome of Mamadou's research led to new load-moment-torsion interaction equations that have been adopted in various international steel design specifications. Zhao [34] conducted tests on 48 beam-columns that were subjected to both constant bending and various moment gradients to investigate their buckling behavior. The results of this test led to the development of new and accurate design rules pertaining to the structural performance of stainless steel elements under the action of combined axial load and bending moments.

Ferritic stainless steel beam-column specimens with several contrasting bending moment-to-axial load rations were tested and compared with developed finite element models to evaluate

the beam-column design provisions in practice. Zhao, Gardner and Young [35] later discovered that the Australian / New Zealand standards of practice offered the most reliable design provisions concurrent with the experimental and numerical procedures. Gizejowski et al [36] meanwhile proposed an analytical model to study the inelastic out-of-plane buckling resistance of beam-columns subjected to moment gradient. The developed model was consequently modified to adhere to the standard European technique of simulating buckling resistance of main steel elements subjected to either bending moments or compression loading about the cross-sectional axis.

Konate and Razzaq [37] examined and proceeded to present yield limit interaction equations for a typical biaxially loaded I-shaped and rectangular shaped non-sway beam columns with a torsional moment present at the bottom end. The analysis involved p-delta and initial residual stresses effects. The resultant interaction equations were observed to compare favorably with previous experimental tests conducted by Konate [3]. Kucukler et al [38] did investigate the flexural buckling of beam-columns whilst considering several ranges of member slenderness and differing loading conditions. The test results were later validated by reliability analysis in compliance with the European design standards.

1.2.2 Review of Beam-Column Behavior under Elevated Temperature

Liew [39] modeled the inelastic behavior of beam-columns of steel framing members when subjected to high temperature conditions. Research results obtained by Real et al [40] and Lopes et al [41] validated the accuracy of the beam-column design requirements in the European standards. This was achieved by subjecting wide flange steel beam-columns to a supply of uniform temperature whilst placing emphasis on lateral-torsional buckling.

Knobloch et al [42] analyzed the spatial buckling behavior of steel beam-columns

subjected to combined axial loading and biaxial bending moments with both uniform and non-uniform bending moment distributions. Results of the test led to the development of temperature-dependent non-dimensional M-N interaction curves. In attempting to validate the results with the European design standards, it was realized that the interaction curves as well as plasticity factors were inconclusive and required further modifications.

Also, Kodur and Dwaikat [43] carried out several numerical tests which were later validated against experimental tests on the response of steel beam-columns under real fire load and other restraint scenarios. Results of the study showed that the form of fire scenario, magnitude of load, end-restraint degrees and high temperature creep had adverse effects on the fire performance of steel beam-columns. Chloe et al [44] performed experimental investigations on steel beam-columns subjected to high temperature. For the experimental setup, test specimens were exposed to various loading conditions in the form of axial, thermal and monotonically increasing flexure loading to investigate the fundamental behavior of steel beam-columns. By innovative radiant heating and digital imaging processing techniques, the load-moment-curvature temperature responses of steel members were subsequently derived and were found to compare favorably with 3D finite element models and analyses.

Further experimental efforts were made by Chloe et al [45] to determine the behavior of steel beam-columns and their responses mainly, moment-curvature and axial load behaviors at high temperatures. The method used in the testing process involved the application of thermal loads and photogrammetry in connection with digital imaging processing techniques to determine the deformations in the heating region of the beam-column. Overall, it was discovered that the stiffness of beam-columns was significantly affected when the temperature reached 500°C and beyond. Also, it was realized that the lateral force-lateral displacement-temperature

behavior was non-linear at the beginning stages of loading as temperature was steadily increased. The normalized moment capacities were also observed to suffer significant decreases especially in the temperature range of 300°C -500°C.

Lopes et al [46] investigated the resistance of stainless steel beam-columns under combined axial compression and bending moment subjected to high temperature conditions. Through the finite element program SAFIR, the numerical analyses for this study were performed. After successfully validating the results of the numerical and the interaction curves in the Eurocode 3, the results showed the urgent need for specific design approach to be adopted for the behavior of stainless steel members in elevated temperature conditions. Zhao [2] investigated the behavior of biaxially loaded steel beam-columns subjected to elevated temperatures. Upon validating the experimental and numerical study, the results were extended to offer a prediction of the beam-columns that were used in the World Trade Center buildings.

Kucukler et al [47] replicated the structural behavior of stainless steel I-section beam-columns when subjected to elevated temperatures by creating finite element models that were successfully validated against experimental data. Furthermore, by carrying out parametric studies the major imperfections such as geometric and material nonlinearity were also validated against the finite element models. The design rules that were proposed as part of this research were found to offer both consistent and safe resistance predictions than the EN 1993-1-2.

1.2.3 Review of Torsion in Steel Members under Ambient Temperature

In 1951, Abramyan [48] reported on a given solution to a generalized problem relating to torsion and bending of prismatic rods of hollow rectangular sections. In obtaining the solutions, the formulae used were indicative of the torsional stiffness and bending as a function of the geometric parameters of the selected section. Through upper and lower approximations, the

interaction curve of the bending and twisting couples at yielding for the case of a combined bending and twisting cylinders of plastic-rigid rectangular, I and box sections were studied in detail by Gaydon and Nuttal [49]. They concluded that the method adopted in this study can be used for any section in addition to the fact that the excellent upper approximations were determined through the use of appropriate warping functions.

Imegwu [50] conducted research on prismatic beams to determine the plastic flexure and torsion whilst simultaneously loaded by terminal bending and twisting moments to cause full plastic flow. The results of this numerical study were determined through the Handelman equation for a Levy-Mises material. The results realized were found consistent with previous research undertaken by Steele.

Furthermore, Imegwu [51] extended his previous research in [50] by introducing the loading of a uniform prismatic beam to satisfy the Treca-Levy-Mises hypothesis to a member experiencing both bending moments about the two main axes of symmetry and an applied torque to cause plastic flow. No deformation was found to exist with any combination of moments Mx, My and torque T to result in yielding of the entire beam cross-section. The experimental results were successfully validated against the numerical tests. Boulton [52] developed an approximate lower bound solution for the fully plastic twisting and bending of I-beams in which warping was restrained at the ends of the beam. An increase in twisting moment was also observed for I-beams twisted in pure torsion beyond the full plasticity point.

Nethercot [53] explored the results of torsion tests conducted on the torsional rigidity of I-sections. As a result of this study, a simplified formula dependent on a single geometrical parameter was proposed to be utilized in torsional rigidity. Research highlighting the use of a 3D finite element for the elasto-plastic analysis of beams subjected to both pure and warping torsion

was performed by May and Al-Shaarbaf [54]. In order to meet the research objectives, the researchers employed the use of a 20- node iso-parametric brick element in their research study. The results of the numerical study were seen to provide a correct assessment of the elasto-plastic behavior of beams under pure and warping torsion conditions. Furthermore, the results obtained from the tests was also found to provide an accurate approximation of the plastic collapse of I-section beams under warping torsion conditions.

Research conducted by Trahair and Bild [55] sought to determine the non-linear elastic biaxial bending and torsion of thin-walled open section members. As part of the assumptions of this research, shear strain in the mid-section of the member was assumed to be non-existent however, effects due to initial deformation, loads, stresses and strains were considered. The results of this study led to the development of non-linear equilibrium and tangent stiffness equations.

Billinghurst et al [56] worked on developing a mitre model for determining the shear strain distribution in steel members subjected to uniform torsion. The main emphasis of the research was concentrated on the inelastic torsional behavior of steel beams of open cross-section. The proposed model was found to provide an accurate relationship of both the elastic and inelastic torque-twist behavior of selected steel members. A model using Vlasov's warping strain was developed by Chen and Trahair [57] to represent the warping torsion and for analyzing the elastic plastic non uniform torsion behavior of thin-walled steel I-beams. In order to conduct the elastic-plastic analysis, the incremental theory of plasticity based on the Prandtl-Reuss flow rule and Von Mises yield criterion was employed. Chen and Trahair's proposed model led to the prediction of more accurate and realistic results at higher rotations than previously established models.

Zheng et al [58] also performed a holistic analysis of the variations of the damage parameter with the average compressive axial strain at different locations of the steel type SAE 1020 and 1045. Zheng et al resorted to applying torsion and compressive loads to obtain alterations in stress, specimen length and effect strain. The results were found consistent with that of the experimental study. Rowan et al [59] subsequently studied the torsional properties of stainless steel and nickel-titanium endodontic files subjected to either clockwise or anticlockwise torsional load rotations. The clockwise torsional rotations were found to be considerably higher in the stainless steel based material whereas the nickel-titanium based material experienced a substantially higher anticlockwise torsional rotation.

Trahair and Pi [60] carried out a series of investigations into the behavior, analysis and design of members subjected to combined bending and torsion. Interaction equations were developed for the member behavior as a result of the application of the combined loadings. Further research was carried out by Trahair and Pi [61] into the behavior, analysis and design of steel members subjected to combined loadings such as torsion and bending. The findings of this research led to the development of interaction equations capable of describing the behavior of steel beams under combined action of torsion and bending.

Wagner and Gruttman [62] developed an unknown warping function through a process of performing exact approximations using the isoparametric concept based on variational formulation. Subsequently, Wagner and Gruttman were able to determine the ultimate torque of the member through a simple single load step. The numerical predictions obtained were found to compare favorably with the analytical results. Based on geometric nonlinear analysis, the behavior of cold-formed beams under the action of torsion and bending such as local buckling, effect of support conditions and magnitude of spring stiffness were also studied by Gotluru,

Schafer and Pekoz [63]. Trahair and Teh [64] examined the elastic flexural buckling of structural members subjected to torsion whilst considering second order moments. Ridley-Ellis et al [65] carried out full scale torsion tests on rectangular hollow sections to observe their torque-twist behavior in comparison with the extended version of Marshall's simplified thick wall torsion theory and finite element analysis. The measured results revealed that both the elastic and plastic torsional capacities were lower than both the theoretical and finite element solutions. Lee et al [66] carried out a research investigation into 3D finite beam elements that were initially formulated to represent the typical behavior of two or three span composite double T-beam under the combined action of flexural and torsional loads. Results showed the tendency of the steel section originally designed to increase flexural stiffness rather resulted in a maximum increase of 20% in the torsional stiffness of the composite double T-beam.

Through the Laplace transform equations, solutions for determining the distributional differential equations of equilibrium for thin-walled structural members in a continuous uniform torsion were determined by Gosowksi [67]. The solutions that were derived were in closed generalized functions form and were observed to be effective in providing distinctive results for both non-uniform torsion displacements and internal forces and their influence lines. Melcher and Karmazinova [68] presented results of a study on the torsional analysis of thin-walled open cross sections made from steel sections. This research highlighted the beneficial effects of the modified torsion analysis and proceeded to offer comparisons with the technical theory and the method supplying the torsion by the couple of forces.

Mahata et al [69] also conducted torsion tests on selected Titanium modified austenitic stainless steels at ambient temperature conditions. The stainless steel used showed periodic hardening and softening when strain was considered at low strain rates with considerable shear

ductility whilst at higher strain rates, shear ductility was found to be lower. Peterman et al [70] developed parameters for torsional stiffness, buckling and yielding by validating experimental results with that of commercially available finite element software ABAQUS. With the conclusion of this research activity, sufficient results and shell finite elements which predicts the torsional behavior of selected cold formed steel type 400s162-54 were established.

Wan and Mahendran [71] subjected several selected channels sized to both uniform and non-uniform torsion as well as bending. Through this research, it was discovered how torsion was seen to reduce the bending strength in short span channel beams whereas long span channel beams achieved their design moment capacities irrespective of the effects of applied torsion. Bian et al [72] provided benchmark test results for cold formed steel lipped channels that were subjected to torsion dominated by warping effects. Through this research, the direct strength method provided accurate results for predicting torsion in members with warping effects. Aminbaghai et al [73] also investigated the effects of torsional warping of cross-sections of twisted beams on eigen vibrations with angle of twist due to secondary deformations. Secondary torsion moment in the non-uniform torsional eigen frequency was also studied as part of this research investigation. The results were later validated with the torsional eigen frequencies obtained by using the standard solid and warping beam finite elements.

Lorkowski and Gosowski [74] carried out both numerical and experimental investigations to determine the equivalent second moment of area of the uniform torsion of two-chord steel single laced members. The setup of the experimental investigation involved arresting two-chord steel single span members with rotations at their ends whilst simultaneously loaded by torque at their mid-span. The numerical studies were conducted using finite element software ABAQUS and SOFiSTik program for sophisticated range of cross-sections.

Muhammad et al [75] conducted parametric numerical studies to examine the torsional stiffness and strength of wide-flange steel members. Results showed that the basic flexural theory as well as the simple empirical relationship were found to offer good predictions which correlated with the results of the experimental tests.

Devi et al [76] worked on sets of perforated and unperforated cold-formed steel hollow section members subjected to torsion. Nandhakumar et al [77] also prepared a summary of various research efforts related to the behavior of beams under torsion. Main observations from this research included that for every significant increase in rotational stiffness a resultant decrease in maximum stress was recorded.

To determine the actual boundary conditions for the lateral torsional beam effects, torsional joints were experimentally investigated by Gil et al [78]. A parametric study was conducted after the conclusion of the experimental tests to validate the results of the experimental work. Winkler et al [79] also studied the influence of torsion on structural integrity of structural members. Through both numerical and experimental methods, the behavior of structural members subjected to biaxial bending, axial loading and torsion were investigated with consideration given to load-deflection curves, plastic yielding of cross-section, ultimate capacities, and failure modes. Furthermore, Devi and Singh [80] performed parametric investigation on selected hollow section members under torsion. The research findings were subsequently extended to generate design equations for both perforated and unperforated steel structural members.

1.2.4 Review of Torsion in Steel Members under Elevated Temperatures

An experimental investigation involving AISI 316L stainless steel with a constant equivalent strain rate of 0.006/s under the action of high temperatures was undertaken by

Angella et al [81]. Other secondary effects such as grain size distribution as well as strain rates were investigated.

Also, Matheron et al [82] investigated the tension-torsion tests on selected steel specimens at high temperature conditions ranging from 450°C - 500°C. Observations from the tests led to the subsequent definition of the revised efficiency diagram suitable for 9Cr steel.

A review of the existing literature shows that the problem of biaxially loaded beam-column subjected to torsion at elevated temperatures has not been studied in the past.

1.3 Problem Statement

This dissertation is focused on a study of the inelastic stability of biaxially loaded steel beam-columns subjected to torsion at elevated temperatures. Figure 1 is a schematic of an imperfect steel beam-column member AB which is subjected to an axial load P, biaxial bending moments M_{BX}, M_{BY}, M_{TX}, M_{TY} as well as a concentrated torsional moment M_Z. The subscripts B and T denote the bottom and top ends of the member. The stiffnesses of the end rotational restraints are represented by K_{BX}, K_{BY}, K_{TX} and K_{TY}.

The theoretical aspect of the research is based on solving a system of materially nonlinear and temperature-dependent ordinary differential equations of equilibrium. An iterative semi-analytic approach is developed and intertwined with a cross-sectional inelastic tangent stiffness procedure with various types of boundary equations. A series of laboratory experiments is conducted to study the inelastic behavior of the member at both ambient and elevated temperatures in order to verify the theoretical predictions. Upon validating the theoretical solutions, the analysis is then used to formulate ultimate strength interaction expressions to capture the combined effects of an axial load, biaxial bending and torsion at elevated temperatures.

1.4 Objectives and Scope

The specific objectives of this study are:

1. To develop a semi-analytic solution procedure to predict the behavior and stability of biaxially loaded steel beam-columns with applied torsion at elevated temperatures.
2. To experimentally investigate the behavior of biaxially loaded steel beam-columns with applied torsion at ambient and elevated temperatures and compare the results with theoretical predictions.
3. Develop interaction expressions based on the theory for members subjected to elevated temperatures.

The experimental study is conducted on a 1.5 x 1.5 x 0.125 in. hot-rolled hollow steel section member with a clear length of 33.65 in. A total of 30 tests are conducted at both ambient and elevated temperatures.

1.5 Assumptions and Conditions

The primary assumptions and conditions in this research are outlined below:

1. Small deflection theory is implemented in this research.

2. The steel beam-column material is assumed to have an elastic-perfectly plastic normal and shear stress -strain relationship at both ambient and elevated temperatures with material elastic loading.

3. The stress-strain relationships for either compression or tension remains the same.

4. External loads are applied in a quasi-static manner up until ultimate strength is reached.

5. Axial force is applied to the centroid of the cross-section and its position remains unchanged until the member load carrying capacity is achieved.

6. Local buckling does not occur in the member.

7. Effects emanating from creep due to elevated temperature conditions are neglected.

8. Material unloading is neglected.

9. A concentrated torsional moment is applied only at the bottom end of the steel beam-column member.

10. Temperature distribution over the cross-section and along the member covered by the electric furnace is assumed to be uniform.

11. Residual stresses are neglected for the theoretical investigations conducted at elevated temperatures.

12. Lateral torsional buckling is not considered in this research.

CHAPTER 2

THEORETICAL FORMULATION AT ELEVATED TEMPERATURES

The theoretical study of biaxially loaded steel beam-columns with applied torsion under elevated temperature conditions is outlined in this chapter.

2.1 Thrust-Moment-Curvature Relations under Elevated Temperatures

2.1.1 Material Properties at Elevated Temperatures

Previous research and design standards [87-93] have proposed material properties reduction factors for yield strengths and elastic modulus at high temperatures. The subscript T is used to denote high temperature induced material properties. For this proposed research, only the reduction factors proposed in the EC3 [87] will be used.

The yield strength σ_{YT} and elastic modulus E_T at any given high temperature is shown as follows:

$$\sigma_{YT} = K_{1T}\,\sigma_Y \tag{1}$$

$$E_T = K_{2T}\,E \tag{2}$$

where K_{1T} and K_{2T} are the yield stress and elastic modulus reduction factors at elevated temperature T.

The reduction factors in the EC3 [87] are as follows:

$$\begin{aligned}
K_{1T} &= 1.00 && 20°C < T \leq 400°C \\
K_{1T} &= -0.0022T+1.88 && 400°C \leq T \leq 500°C \\
K_{1T} &= -0.0031T+2.33 && 500°C \leq T \leq 600°C \\
K_{1T} &= -0.0024T+1.91 && 600°C \leq T \leq 700°C \\
K_{1T} &= -0.0012T+1.07 && 700°C \leq T \leq 800°C \\
K_{1T} &= -0.0005T+0.51 && 800°C \leq T \leq 900°C
\end{aligned} \tag{3}$$

K_{1T} = -0.0002T+0.24 900°C ≤ T ≤ 1200°C

K_{1T} = 0.00 1200°C ≤ T

The reduction factors for the elastic modulus are as follows:

K_{2T} = 1.00 20°C ≤ T ≤ 100°C

K_{2T} = -0.001T+1.1 100°C ≤ T ≤ 500°C

K_{2T} = -0.0029T+2.05 500°C ≤ T ≤ 600°C (4)

K_{2T} = -0.0018T+1.39 600°C ≤ T ≤ 700°C

K_{2T} = -0.0004T+0.41 700°C ≤ T ≤ 800°C

K_{2T} = -0.000125T+0.15 800°C ≤ T ≤ 1200°C

K_{2T} = 0.00 1200°C ≤ T

Equations 3-4 will be used in this dissertation research to modify both the yield stress and elastic modulus at high temperatures. Figures 2-3 also shows the reduction factors for the yield stress and elastic modulus.

2.2 Total Mechanical Strain at Elevated Temperatures

The beam-column is subjected to a uniformly distributed temperature T, axial load P, uniaxial moment M_y, biaxial bending moments M_x and M_y as well as torsional moment M_z as shown in Figure 4. Unlike the ambient temperature analysis, there are no residual stress distribution patterns for the typical hollow rectangular section at high temperatures. This is because residual stresses are released during the event of high temperatures [2]. However, since this study is being compared to ambient temperature tests, the residual stress distribution pattern at ambient temperature is shown in Figure 5. Hence, considering a point (x,y) of the cross-section subjected to an axial load in addition to bending moments M_x , M_y and M_z about both the x and y axes, the mechanical strain ε_T is given as

$$\varepsilon_T = \varepsilon_0 + \phi_x y - \phi_y x + \varepsilon_{th} \quad (5a)$$

$$\tau = G \Upsilon \qquad \text{for } -\Upsilon_Y < \Upsilon < \Upsilon_Y \quad (5b)$$

in which ε_0 represents the average strain, ϕ_x and ϕ_y represents the bending curvatures about the x and y axes respectively, ε_{th} denotes the thermal strain. τ is the shear stress, G is the shear modulus, Υ is the shear strain and Υ_Y is the shear yield strain. For this research study, an elastic-perfectly plastic material stress strain relationship will be utilized as shown in Figures 6-7. This relationship comprises of both the material loading and unloading segments. Outlined below are the material loading relationships [2]:

$$\sigma_T = E_T \varepsilon_T \qquad -\varepsilon_{YT} < \varepsilon_T < \varepsilon_{YT} \quad (6)$$

$$\sigma_T = +\sigma_{YT} \qquad \varepsilon_T \geq \varepsilon_{YT} \quad (7)$$

$$\sigma_T = -\sigma_{YT} \qquad \varepsilon_T \leq -\varepsilon_{YT} \quad (8)$$

The material unloading relationship is as follows:

$$\sigma_T = \sigma_{Tf} - E_T (\varepsilon_{Tf} - \varepsilon_T) \quad (9)$$

where σ_{Tf} and ε_{Tf} represents the strain and stress values of the previous load levels.

The predictions of the thermal strain based on the EC3[87] are utilized in this research are:

$$\varepsilon_{TH} = 1.2\text{x}10^{-5}T + 0.4\text{x}10^{-8}T^2 - 2.416\text{x}10^{-4} \qquad T<750°C$$

$$\varepsilon_{TH} = 1.1\text{x}10^{-2} \qquad 750°C \leq T \leq 860°C \quad (10)$$

$$\varepsilon_{TH} = 2\text{x}10^{-5}T - 6.2\text{x}10^{-3} \qquad 860°C \leq T \leq 1200°C$$

From Equation 10, the thermal strain decreases linearly with an increase in temperature whereas thermal strain remains constant for temperature ranges 750°C - 860°C.

2.3 Elasto-plastic Cross-sectional Equilibrium Conditions

The equilibrium equations for the member as a function of temperature when subjected to axial load, biaxial bending moment and torsion are [2]:

$$P = -\int_{Ae} \sigma_{eT}\, dA - \int_{Ap} \sigma_{yT}\, dA \quad (11)$$

$$M_x = \int_{Ae} \sigma_{eT} y\, dA + \int_{Ap} \sigma_{yT}\, y\, dA \quad (12)$$

$$M_y = -\int_{Ae} \sigma_{eT}\, x\, dA - \int_{Ap} \sigma_{yT}\, x\, dA \quad (13)$$

$$M_{zT} = (C_{te})\Phi' - C_{we}\, \Phi''' + M_{zpT} \quad (14)$$

In this section, σ_{eT} and σ_{YT} represents the normal elastic and yield stress at temperature T, $\int_{Ae}$ and $\int_{Ap}$ denotes the integrals over the elastic and plastic regions respectively whilst dA is the elemental area of the steel beam-column cross-section. Also, a total of 2048 elemental areas which contributes to greater convergence (512 elemental areas per plate) will be utilized in this theoretical investigation.

Meanwhile, due to the presence of additional forces caused because of the presence of high temperatures the initial applied axial load is altered. This change leads to a modification of the equilibrium expressions used previously in equations (11-14). The modified equations then are as follows:

$$P^* = -\int_{Ae} E_T\, \varepsilon_T dA - \int_{Ap} \sigma_{yT}\, dA \quad (15)$$

$$M_x^* = \int_{Ae} E_T\, \varepsilon_T\, dA + \int_{Ap} \sigma_{yT}\, y\, dA \quad (16)$$

$$M_y^* = -\int_{Ae} E_T\, \varepsilon_T dA - \int_{Ap} \sigma_{yT}\, x\, dA \quad (17)$$

$$M_{zT} = (C_{te})\, \Phi' - C_{we}\, \Phi''' + M_{zpT} \quad (18)$$

2.4 Modified Differential Equations for Elevated Temperature Conditions

Based on research efforts by Zhao [2], the following equations are modified and applied for the elevated temperature conditions in this research study:

$$-g_{11}\epsilon_o + g_{12} v_T'' + g_{13}\, u_T'' + g_{14}\Phi_T'' - P_p - P_T = P \quad (19)$$

$$-g_{21}\epsilon_o + g_{22} v_T'' + g_{23}\, u_T'' + g_{24}\Phi_T'' - M_{xp} - M_{xT} = -M_x \quad (20)$$

$$-g_{31}\epsilon_o + g_{32} v_T'' + g_{33}\, u_T'' + g_{34}\Phi_T'' - M_{yp} - M_{yT} = M_y \quad (21)$$

$C_{we}\Phi_T'''$- $(C_{te} + K)\Phi_T'$ + $v_T'[m_{BY}+ \frac{z}{L}(M_{TY} + m_{TX} – m_{BX}) + u_T'[-m_{BX}+ \frac{z}{L}(M_{TX}- m_{TX} + m_{BX})$

$- \frac{vT}{L}(M_{TY} + m_{TY} – m_{BY}) - \frac{uT}{L}(M_{BX} + M_{TX} – m_{TX} – m_{BX})$ $= - M_{RZ} + M_{zpT}$ (22)

where P_T, M_{xT} and M_{yT} are the axial, biaxial bending moments about x and y axes as a result of thermal strain. P_p, M_{xp} and M_{yp} are the axial force and moment parameters for the plastified members. The coefficients g_{ij} have been defined in Appendix B. ϵ_o is solved explicitly in order to obtain the following differential equilibrium equations:

Hence, the modified general differential equilibrium equations to be applied for elevated temperature conditions are:

$B_{xx}v_T'' + B_{xy}u_T''+ B_{xw}\Phi_T'' - A_eM_{RZ}u_T' + A_ePv_T + A_e\Phi_T(m_{BY}+ \frac{z}{L}(M_{TY} – m_{TY}- m_{BY})$

$- A_em_{BX} + A_e\frac{z}{L}(-m_{TX} + m_{BX}) = - A_ePv_i - A_e\frac{z}{L}(M_{TX}) - S_{xe}P + S_{xe}P_T + A_eM_{xT}$

$- S_{xe}P_p + A_eM_{xp}$ (23)

$B_{yx}v_T'' + B_{yy}u_T''+ B_{yw}\Phi_T'' - A_eM_{RZ}v_T' + A_ePu_T + A_e\Phi_T(- m_{Bx}+ \frac{z}{L}(M_{TX}- m_{TX}+m_{BX})- A_em_{BY} -$

$A_e\frac{z}{L}(m_{TY} – m_{BY}) = - A_ePu_i + A_e\frac{z}{L}(M_{TY}) - S_{ye}P - S_{ye}P_T + A_eM_{yT} - S_{ye}P_p + A_eM_{yp}$ (24)

$C_{we}\Phi_T'''$ - $(C_{te} + K)\Phi_T'$ + $v_T'[m_{BY}+ \frac{z}{L}(M_{TY} + m_{TX} – m_{BX}) + u_T'[-m_{BX}+ \frac{z}{L}(M_{TX}- m_{TX} + m_{BX})$

$- \frac{vT}{L}(M_{TY} + m_{TY} – m_{BY}) - \frac{uT}{L}(M_{BX} + M_{TX} – m_{TX} – m_{BX}) = - M_{RZ} + M_{zpT}$ (25)

Equations 23-25 can be written as the following system of 3N simultaneous nonlinear differential equations and programmed.

$[T_T]\ \{\Delta_T\} = \{F_T\}$ (26)

where $[T_T]$ represents the global stiffness matrix of the order 3n x 3n at elevated temperatures; the vector $\{\Delta_T\}$ comprises of derivatives of v_T,u_T and Φ_T are :

$\{\Delta_T\}^T = \{v_{1T}\ v_{2T}\ v_{3T}.....v_{(N-2)T}\ v_{(N-1)T}\ v_{(N)T}\ u_{1T}\ u_{2T}\ u_{3T}.....u_{(N-2)T}\ u_{(N-1)T}\ u_{(N)T}\ .....\ \Phi_{1T}\ \Phi_{2T}$

$\Phi_{3T}.....\ \Phi_{(N-2)T}\ \Phi_{(N-1)T}\ \Phi_{(N)T}\}$ (27)

The load vector $\{F_T\}$ is determined as follows:

$$\{F_T\} = \begin{Bmatrix} \{F_{xT}\} + \{F_{xp}\} \\ \{F_{yT}\} + \{F_{yp}\} \\ \{F_{yT}\} + \{F_{zp}\} \end{Bmatrix} \quad (28)$$

Equation 26 is solved iteratively for each applied load until the member reaches the collapse state. The collapse state is reached when the determinant of $[T_T]$ matrix becomes zero. For the elastic range, the residual and plastic moment vectors are zero whereas for the inelastic range, they are computed iteratively.

2.5 Boundary Conditions

The moment versus rotation relations for the partial rotational end restraints are shown below:

$m = k\theta$ for $\theta < \theta_p$ (29)

$m = m_p$ for $\theta \geq \theta_p$ (30)

where m is spring bending moment, k is the end spring stiffness and θ is the corresponding end slope.

The geometric boundary conditions for the pinned end boundary conditions only are:

At z = a;

$u(a) = a \times u'(a)$ (31)

$v(a) = a \times v'(a)$ (32)

$\Phi(a) \neq 0$ (33)

$\Phi'(a) = 0$ (34)

At z = L+a;

$$u(L+a) = a \times u'(L+a) \quad (35)$$

$$v(L+a) = a \times v'(L+a) \quad (36)$$

$$\Phi(L+a) = 0 \quad (37)$$

$$\Phi'(L+a) = 0 \quad (38)$$

The natural boundary conditions are as follows:

$$m_{BX} = k_{BX}\theta_{BX} \quad (39)$$

$$m_{BY} = k_{BY}\theta_{BY} \quad (40)$$

$$m_{TX} = k_{TX}\theta_{TX} \quad (41)$$

$$m_{TY} = k_{TY}\theta_{TY} \quad (42)$$

k_{BX}, k_{BY}, k_{TX} and k_{TY} are the partial rotational end restraint stiffness values and θ_{BX}, θ_{BY}, θ_{TX} and θ_{TY} represents the corresponding end slopes. The end slopes are defined as follows:

$$\theta_{BX} = u'(a) \quad (43)$$

$$\theta_{BY} = v'(a) \quad (44)$$

$$\theta_{TX} = -u'(L+a) \quad (45)$$

$$\theta_{TY} = -v'(L+a) \quad (46)$$

If the member end at z = a and z = L+a is flexurally fixed, the geometric boundary conditions to be applied are:

$$u'(a) = u(a) / a \quad (47)$$

$$v'(a) = v(a) / a \quad (48)$$

$$u'(L+a) = u(L+a) / a \quad (49)$$

$$v'(L+a) = v(L+a) / a \quad (50)$$

$$\Phi'(a) = 0 \quad (51)$$

$$\Phi'(L+a) = 0 \quad (52)$$

Equations 31 through 52 are used in conjunction with the governing differential equations, namely, Equations 23-25.

2.6 Semi-Analytic Solution Formulation

The Semi-Analytic solution has been used with great accuracy in the past to determine the numerical solutions of non-linear ordinary differential equations. This solution is based on determining derivatives which comprises of function values at that point and neighboring points. The procedure also involves subdividing a domain into segments. The differential equations are then approximated by piecewise trial functions over each of the sub-divided finite elements to obtain a solution.

For this research investigation, the beam-column member will be divided into ten segments, therefore $\Delta z = \frac{h}{10}$. The deflection in the y, x and z axis is labelled as v,u and Φ respectively. By taking into consideration the rigid end fixtures at the bottom and top end of the experimental setup, the following assumed solutions were developed:

$$u = A_o z(z^2-L^2) + A_1 z(z-L) + \Sigma^*(A_K \sin(\frac{K\pi z}{L})) \quad (53)$$

$$v = B_o z(z^2-L^2) + B_1 z(z-L) + \Sigma^*(B_K \sin(\frac{K\pi z}{L})) \quad (54)$$

$$\Phi = C_o(L-z) + \Sigma^* C_K(1-\cos\frac{2\pi z}{L}) \qquad \text{For only } \Phi(z) \quad (55)$$

$$\Phi = C_o + \Sigma^* C_K(1-\cos\frac{2\pi z}{L}) \qquad \text{For only } \Phi'(z) \quad (56)$$

It is not possible to obtain a single equation that satisfies Φ(z) is not equal to zero and Φ'(z) equal to zero because these conditions are contradictory. Hence, a piecewise function is used in this case.

However, for a mixed boundary condition (fixed at the bottom – pinned at the top), the following expressions will be used:

$$u = A_o z\left(\frac{1}{4L} - \frac{3}{4z} + \frac{1}{2z}\right) + A_1 z\left(-\frac{1}{4L} + \frac{3}{4z} - \frac{1}{2z}\right) + \Sigma^*(A_K \sin(\frac{K\pi z}{L})) \quad (57)$$

$$v = B_o z\left(\frac{1}{4L} - \frac{3}{4z} + \frac{1}{2z}\right) + B_1 z\left(-\frac{1}{4L} + \frac{3}{4z} - \frac{1}{2z}\right) + \Sigma^*(B_K \sin(\frac{K\pi z}{L})) \quad (58)$$

where Σ represents both odd and even numbers (K=2,3,4,5…) summations made over K.

Substituting Equations 53 – 56 into the General Equilibrium Equations 23-25, the following expressions are obtained:

$$B_{xx}(-B_1\frac{\pi^2}{L^2}\sin\frac{\pi z}{L} - B_2\frac{4\pi^2}{L^2}\sin\frac{2\pi z}{L})dz + B_{xy}(-A_1\frac{\pi^2}{L^2}\sin\frac{\pi z}{L} - A_2\frac{4\pi^2}{L^2}\sin\frac{2\pi z}{L})dz + B_{xw}(C\frac{4\pi^2}{L^2}\cos\frac{2\pi z}{L})\,dz -$$

$$A_e M_{RZ}\,(A_o(z^2-L^2) + A_1(z-L) + A_2\frac{\pi}{L}\cos\frac{\pi z}{L} + A_3\frac{2\pi}{L}\cos\frac{2\pi z}{L})dz + A_e P(B_o z(z^2-L^2) + B_1 z(z-L)$$

$$+B_2\sin\frac{\pi z}{L} + B_3\frac{2\pi}{L}\sin\frac{2\pi z}{L})dz \; -A_e C(1-\cos\frac{2\pi z}{L})(\, m_{BY} + \frac{z}{L}(M_{TY} + m_{TY} - m_{BY})dz - A_e m_{BX} + A_e\frac{z}{L}(\, -$$

$$m_{Tx} + m_{BX}) - A_e P\frac{L}{1000}(B_o z(z^2-L^2) + B_1 z(z-L) + B_2\sin\frac{\pi z}{L} + B_3\frac{2\pi}{L}\sin\frac{2\pi z}{L})$$

$$-A_e\frac{z}{L}(\, M_T x) - S_{xe}P \; = 0 \quad (59)$$

$$B_{yx}(-B_1\frac{\pi^2}{L^2}\sin\frac{\pi z}{L} - B_2\frac{4\pi^2}{L^2}\sin\frac{2\pi z}{L}\;)dz + B_{yy}\,(-A_1\frac{\pi^2}{L^2}\sin\frac{\pi z}{L} - A_2\frac{4\pi^2}{L^2}\sin\frac{2\pi z}{L}\;)dz + B_{yw}(C\frac{4\pi^2}{L^2}\cos\frac{2\pi z}{L})\,dz +$$

$$A_e M_{RZ}\,(A_o(z^2-L^2) + A_1(z-L) + B_2\frac{\pi}{L}\cos\frac{\pi z}{L} + B_3\frac{2\pi}{L}\cos\frac{2\pi z}{L})dz + A_e P(\, A_o z(z^2-L^2) + A_1 z(z-L)$$

$$+A_2\sin\frac{\pi z}{L} + A_3\frac{2\pi}{L}\sin\frac{2\pi z}{L} +)dz \; + A_e C(1-\cos\frac{2\pi z}{L})(\, m_{BX} + \frac{z}{L}(M_{TX} + m_{TX} - m_{BX})dz - A_e m_{BX} + A_e\frac{z}{L}(-m_{TY}$$

$$+m_{BY}) - A_e P\,(B_o z(z^2-L^2) + B_1 z(z-L) + B_2\sin\frac{\pi z}{L} + B_3\frac{2\pi}{L}\sin\frac{2\pi z}{L})dz$$

$$- S_{ye}P = 0 \quad (60)$$

$$\text{Cwe}\,C(-\frac{8\pi^3}{L^3}\sin\frac{2\pi z}{L})dz - (Cte + K)(C(\frac{2\pi}{L}\sin\frac{2\pi z}{L}\;))dz + ([m_{BY} + \frac{z}{L}(\, M_{TX} + m_{TY} - m_{BY}) - \;))dz +$$

$$\frac{1}{L}(A_o(z^2-L^2) + A_1(z-L) + A_2\frac{\pi}{L}\cos\frac{\pi z}{L} + A_3\frac{2\pi}{L}\cos\frac{2\pi z}{L}\,)\,dz\,[-m_{BX} + \frac{z}{L}(\, M_{TX} - m_{TX} - m_{BX}) - \frac{1}{L}(B_o(z^2-L^2) +$$

$$B_1(z-L) + B_2\frac{\pi}{L}\cos\frac{\pi z}{L} + B_3\frac{2\pi}{L}\cos\frac{2\pi z}{L}\,)dz - \;\frac{1}{L}(A_o z(z^2-L^2) + A_1 z(z-L) + A_2\frac{\pi}{L}\sin\frac{\pi z}{L} + A_3\frac{2\pi}{L}\sin\frac{2\pi z}{L})dz \; -$$

$$\frac{1}{L}B_o z(z^2-L^2) + B_1 z(z-L) + B_2\frac{\pi}{L}\sin\frac{\pi z}{L} + B_3\frac{2\pi}{L}\sin\frac{2\pi z}{L})dz + M_{RZ} - M_{zp} = 0 \quad (61)$$

Equations 59-61 are the final governing nonlinear differential equations of equilibrium obtained.

2.7 Proposed Solution Procedure for Biaxially Loaded Beam-Columns with Applied Torsion under Elevated Temperatures

The theoretical solution procedure for the elastic-plastic behavior of biaxially loaded steel beam-columns with applied torsion under elevated temperatures is outlined as follows:

1. Evaluate the material and geometric properties of the steel beam-column member at the designated elevated temperature.
2. Specify the external loads to be applied.
3. Determine the Tangent Stiffness Matrix $[T_T]$.
4. Determine the deformation vector $\{\Delta_T\}$ using the General Equation 26.
5. Segregate each of the cross-sections N along the length of the member and determine the normal stress $\sigma_{i,j}$ and strain $\epsilon_{i,j}$ in which case i,j represents the x and y coordinate system of the elemental area respectively.
6. Apply the von Mises yield criterion in determining σ_p for the N cross-sections whilst also determining the shear stresses $\tau_{i,j}$ and plastic stresses $\sigma_{pi,j}$ for the various N cross-sections.
7. Determine whether all the N cross-sections are elastic or plastic. If $|\sigma_{i,j}|<|\sigma_{pi,j}|$, elasticity condition is satisfied whereas in the case of $|\sigma_{i,j}|>|\sigma_{pi,j}|$, the plasticity condition is satisfied. For the case of elasticity, proceed to step 8 whereas for plasticity proceed to step 10.
8. Apply external loads.
9. Check for the determinant of the Tangent Stiffness matrix $[T_T]$. If $|[T_T]|$ approaches zero, proceed to Step 12.

10. Compute the inelastic coefficients and generate new Tangent Stiffness [$T_{Tinelastic}$]. By iteration, determine deformation vectors $\{\Delta_T\}$. Perform the error tolerance check.
11. If the tolerance check fails, recompute the inelastic coefficients and update the Tangent stiffness [$T_{Tinelastic}$] and determine further updated deformation vectors $\{\Delta_T\}$until the error tolerance is within limits.
12. Stop

2.8 Structural Load Paths

Load paths to be implemented to study the biaxially loaded beam-columns with applied torsion under elevated temperatures are as follows.

- HPT : Under elevated temperature conditions, the axial load P is initially applied incrementally and then held constant, followed by steadily increasing torsional moment T until the load carrying capacity of the member is reached.
- HUT : Under elevated temperature conditions, the uniaxial moment M_{TX} is initially applied incrementally and then held constant followed by steadily increasing torsional moment T until the load carrying capacity of the member is reached.
- HBT : Under elevated temperature conditions, the biaxial end moments M_{TX} and M_{TY} are initially applied incrementally and then held constant followed by steadily increasing torsional moment T until the load carrying capacity of the member is reached.
- HPUT : Under elevated temperature conditions, the axial load P and uniaxial end moment M_{TX} are initially applied incrementally and then held constant followed by steadily increasing torsional moment T until the load carrying capacity of the member is reached.
- HPBT : Under elevated temperature conditions, the axial load P and biaxial end moments M_{TX} and M_{TY} are initially applied incrementally and then held constant followed by

steadily increasing torsional moment T until the load carrying capacity of the member is reached.

2.9 Temperature-Time Curve

The relationship between the increase in elevated temperature as a function of the time duration was also established by observing an increasingly heated beam-column sample. A stabilization period of 15 minutes was allowed for uniform temperature distribution throughout the specimen. The results of the test have been compared with the ASTM E119 [93] and previous research conducted by Zhao [2] as shown in Figures 8-9.

CHAPTER 3

EXPERIMENTAL INVESTIGATION

This chapter outlines the experimental investigation conducted on biaxially loaded steel beam-columns under axial load, biaxial bending moment and torsion. Material property tests were initially performed, and the subsequent tests conducted were to determine the elastic and inelastic behavior under ambient and elevated temperatures.

3.1 Test Equipment for Material Property Tests

A Tinius Olsen Universal Testing machine of 400K capacity is used to conduct preliminary tensile and column stub tests. The testing setup used has been shown in Figure 10. Residual stresses are also determined using the sectioning method.

3.2 Test Equipment for Beam-Column Experimental Tests

The test equipment for the main experimental investigation primarily consisted of 4 main components: the gimbals, the setup for applying uniaxial and or biaxial bending moment, the setup for applying torsional moment and an electric furnace for generating high temperatures.

3.2.1 Gimbals

Razzaq and McVinnie [20,21], Zhao [2] and Konate [3] conducted experimental research involving biaxially loaded steel beam-columns using gimbals. For this experimental study, a four-sided gimbal outer and inner box supported by a pair of inner bearings and a shaft along the x-axis was used. The inner bearings of the gimbal box are situated in two opposite walls of the gimbal outer box whilst the opposite walls of the gimbal box are equipped with a pair of shafts and outer bearings along the y-axis. The lower end gimbal is attached to a steel plate which has a gliding steel chamber beneath it as shown in Figure 11. The gliding steel chamber is also equipped with a 55 kips capacity load cell connected to a hydraulic jack. The upper end gimbal

on the other hand has been attached to a steel cross-beam which is bolted at its respective ends to the steel beam-columns.

The end columns are fixed to a laboratory test bed to form a large reaction frame whilst the upper end gimbals are supported by the presence of a cross-beam element. The gimbal setup arrangement enables the application of axial load by using the hydraulic jack whilst measuring the load output on a load cell. The load cell pushes the steel plate whilst transmitting the axial load to the lower gimbal outer box through the pair of outer bearings and shafts. Finally, the test specimen: steel beam columns receive the load through the gimbal inner box.

3.2.2 Uniaxial and Biaxial Bending Moment Setup

To apply either the uniaxial and or biaxial bending moment, a moment arm machined to the upper gimbal inner box as shown in Figure 12 is used. The moment arm is a 1.0 x 2.0 x 24.0 in. solid rectangle steel section. The moment is applied through the presence of two 0.75in diameter tie rods. Both rods are 75 inches long and are separated by a 12-inch long 0.5-in thick steel plate forming a closed ring at the upper and lower ends. With the aid of a ball and socket arrangement, the Top Plate B rests on a machined arm. A bottom placed plate is fitted to a 22-kips capacity load cell. The load cell has been attached to hydraulic jack and further bolted to a small steel reaction frame in an inverted position. The small steel reaction frame is mounted to the laboratory test bed. Applying the moment requires manually adjusting the hydraulic jack. In the case of the uniaxial bending moment, angle 0° is adopted between the moment arm and the x-axis of the gimbal. By welding a set of steel beam-columns at an angle of 45°, the biaxial moments M_x and M_y can be applied. Hence, M_{TX} and M_{TY} are both equal to M(sin45°) in this research.

3.2.3 Torsional Moment Setup

Torsional moment is applied through the bottom end by means of an applied eccentric force through a hydraulic jack and conveyed to the test specimen member via a revolving chain as shown in Figures 13-15. The torsional moment value equals the load output from the load cell multiplied by the eccentricity e.

3.2.4 High Temperature Furnace

A 28 x 28 x 18.5in. electric furnace with a maximum heating capacity of 1000°F is used to conduct the elevated temperature tests. The electric furnace manufactured in-house is built using silica refractory insulation boards and covered by flat-thin aluminum bars. The heating elements consists of both flat-thin bronze and stainless-steel bars located inside the chamber of the furnace. A controller which is equipped with an optical pyrometer detects, controls, and is used to adjust the various temperature gradients generated by the electric furnace. The electric furnace together with the controller has been shown in Figure 16. The heating rate of the furnace is observed to be 15°F/min.

3.3 Test Specimen

For this experimental process, commercially available standardized ASTM 513 Type 1 hollow steel sections of nominal sizes 1.5 x 1.5 x 0.125in. as shown in Figure 17 are used. The standardized ASTM A513 Type 1 steel specimens are ordered in compliance with the requirements of EN 10204 type 3.1. The chemical composition of the ASTM A513 Type 1 steel specimen is shown in Table 1.

The steel specimens are made from low carbon steel produced by the hot rolling process. A total of 30 specimens will be tested. 15 will be used for ambient temperature tests whilst the remaining 15 will be for elevated temperature tests.

The measured length of the specimen is 33.65 inches including the end plates thickness. In addition, the distance measured from the center lines of the upper and lower fixtures is included in the total length of specimen. Hence, the total length of the specimen is 37.4 inches as seen in Figure 18. The minimum yield strength for this type of steel is 72 kips.

Samples of the ASTM A513 Type1 hollow steel specimens as shown in Figure18 are also fabricated into 6 coupon specimens based on the EN 10002-5 [94] to determine the stress-strain curves, the shear modulus G and shear yield stress τ_Y. Each coupon specimen had a circular section with a diameter of 6mm. The gauge length for the coupon specimen is 30mm.The details of the coupon specimens have been shown in Figures 19 and 20. Stub columns are also cut off from the steel specimen to conduct compression tests to determine the young's modulus and yield stress. The specifications, details and results of the stub-column tests have been shown in Figures 21 and 22.

3.4 Test Procedure

Four dial gages are set up at the midspan of the specimen to measure both the deflections in the x and y axes for the ambient temperature tests. To measure the temperature of the specimens for the elevated temperature tests, the optical pyrometer located in the electric furnace will be used. Dial gages will also be placed at both the top and bottom ends of the specimens to measure the deflections that occur when the specimen is subjected to elevated temperatures. The axial loads, biaxial bending moment as well as torsional moments will be applied gradually and incrementally with intermittent stops to manually record test data. Further increase in deformations without any increase in load, bending moments and temperature results in achieving the load-carrying capacity of the steel specimen member. The various tests conducted are outlined in Table 2.

3.5 Test Results

3.5.1 Material Property Tests

From the tests conducted, the average yield stress σ_Y and elastic modulus E are 58.64 ksi and 29988 ksi respectively. Also, the shear modulus G, shear yield stress τ_Y and residual stress σ_r are also found to be 11236 ksi, 32.56 ksi and 23.33 ksi respectively. These properties are utilized especially in the ambient temperature theoretical studies and modified by reduction factors for use in the high temperature theoretical studies.

3.5.2 Member Tests

Table 2 outlines the details of the tests such as boundary conditions and structural load paths. Figures 23-79 show the various load deflection curves, comparisons involving both ambient and elevated temperature results. The following symbols are used to define the various load types in this research:

P = Axial load

U = Uniaxial Bending Moment

B = Biaxial Bending Moment

T = Torsional Moment

A = Ambient Temperature

H = High Temperature

Table 3 presents the results for Tests 1 through 5. The first column shows the load type namely APT, AUT, ABT, APUT and APBT for a pinned boundary condition. The second column shows the ultimate axial load applied. The third column shows the maximum bending moment whilst the fourth column shows ultimate torsional moment applied. The maximum mid-span deflections and angle of twist are shown in the fifth and sixth column respectively.

Table 4 summarizes the results for Tests 6 through 10. The first column shows the load type namely APT, AUT, ABT, APUT and APBT for a fixed boundary condition. The second column shows the ultimate axial load applied. The third column shows the maximum bending moment whilst the fourth column shows ultimate torsional moment applied. The maximum mid-span deflections and angle of twist are shown in the fifth and sixth column respectively.

In Table 5, the results for Tests 11 through 15 are shown. The first column shows the load type namely APT, AUT, ABT, APUT and APBT for a mixed boundary condition. The second column shows the ultimate axial load applied. The third column shows the maximum bending moment whilst the fourth column shows ultimate torsional moment applied. The maximum mid-span deflections and angle of twist are shown in the fifth and sixth column respectively.

Table 6 summarizes the results for Tests 16 through 20. The first column shows the load type namely HPT, HUT, HBT, HPUT and HPBT for a pinned boundary condition. The second column shows the ultimate axial load applied. The third column shows the maximum bending moment whilst the fourth column shows ultimate torsional moment applied. The maximum mid-span deflections and angle of twist are shown in the fifth and sixth column respectively.

Table 7 shows the results for Tests 21 through 25. The first column shows the load type namely HPT, HUT, HBT, HPUT and HPBT for a fixed boundary condition. The second column shows the ultimate axial load applied. The third column shows the maximum bending moment whilst the fourth column shows ultimate torsional moment applied. The maximum mid-span deflections and angle of twist are shown in the fifth and sixth column respectively.

Table 8 presents the results for Tests 26 through 30. The first column shows the load type namely HPT, HUT, HBT, HPUT and HPBT for a mixed boundary condition. The second column

shows the ultimate axial load applied. The third column shows the maximum bending moment whilst the fourth column shows ultimate torsional moment applied. The maximum mid-span deflections and angle of twist are shown in the fifth and sixth column respectively.

From the tests conducted, it was observed that for APT & HPT, AUT & HUT, ABT & HBT, APUT & HPUT and APBT & HPBT for a pinned boundary condition, the reduction in strength of the member is 50 percent, 7 percent, 36 percent, 53 percent, and 36 percent respectively.

For tests involving APT & HPT, AUT & HUT, ABT & HBT, APUT & HPUT and APBT & HPBT for a fixed boundary condition, the strength reduction of the member is 39 percent, 45 percent, 27 percent, 62 percent, and 29 percent respectively.

For tests such as APT & HPT, AUT & HUT, ABT & HBT, APUT & HPUT and APBT & HPBT for a mixed boundary condition, the strength reduction of the steel member is 39 percent, 53 percent, 32 percent, 43 percent, and one percent respectively.

CHAPTER 4

COMPARISON OF EXPERIMENTAL AND THEORETICAL RESULTS

This Chapter presents the results of the theoretical formulation of the semi-analytic solution under both ambient and elevated temperature conditions as well as comparison with experimentally obtained results.

4.1. Combined Axial Load and Torsion under Ambient Temperature

Figures 80-88 present the results of the combined axial load and torsion for the boundary conditions used in this research. Tables 9-11 summarize theoretical results of load type APT for pinned, fixed and mixed boundary conditions. The first column shows the load type whilst the second column and third column are showing the ratio of the theoretical peak load to the experimental peak of the axial load and torsional moment respectively.

The fourth column shows also shows the ratio of the maximum theoretical mid-span deflections to the maximum experimental mid-span deflection whereas the fifth column also shows ratio for the angle of twist.

It was observed that the theoretical peak loads for the load type APT for pinned, fixed and mixed boundary condition was three percent,6 percent and 8 percent respectively lower than the experimental peak loads. The maximum theoretical mid-span deflection was found to be 17 percent higher than the experimental mid-span deflection for APT with pinned boundary condition. The theoretical mid-span deflection for the same load type under fixed and mixed boundary condition was 8 percent and three percent lower than the maximum mid-span deflection obtained experimentally. The maximum theoretical angles of twist for the load type APT were 7 percent and 6 percent greater than the maximum experimental angles of twist for the pinned and fixed boundary conditions respectively.

However, for the mixed boundary condition the maximum theoretical angle of twist was 8 percent lower than the maximum experimental angle of twist.

4.2 Combined Uniaxial Moment and Torsion under Ambient Temperature

Figures 89-97 summarize the results of the combined uniaxial moment and torsion for the boundary conditions used in this research. Tables 9-11 also shows the theoretical results of load type AUT for pinned, fixed and mixed boundary conditions.

The first column shows the load type whilst the second column and third column are showing the ratio of the theoretical peak load to the experimental peak of the biaxial and torsional moment respectively. The fourth column shows also shows the ratio of the maximum theoretical mid-span deflections to the maximum experimental mid-span deflection whereas the fifth column also shows ratio for the angle of twist.

It was observed that the theoretical peak loads for the load type ABT for pinned, fixed and mixed boundary condition was 8 percent,6 percent and one percent lower than the experimental peak loads. The maximum theoretical mid-span deflection was found to be two percent and one percent higher than the experimental mid-span deflection for ABT with pinned and fixed boundary condition. The theoretical mid-span deflection for the mixed boundary condition was four percent lower than the maximum experimental mid-span deflection. However, the maximum theoretical angles of twist were 14 percent and 43 percent higher than the maximum experimental angles of twist for the load type AUT under pinned and mixed boundary conditions. The maximum theoretical angle of twist for the fixed boundary condition for the AUT was five percent lower than the maximum experimental angle of twist.

4.3 Combined Biaxial Moment and Torsion under Ambient Temperature

Figures 98-106 show the results of the combined biaxial moment and torsion for the boundary conditions used in this research. Tables 9-11 present theoretical results of load type ABT for pinned, fixed and mixed boundary conditions. The first column shows the load type whilst the second column and third present the biaxial moment and torsional moment respectively. The fourth column shows the mid-span deflections whereas the fifth column shows the angle of twist.

Results showed that the difference between the experimental and theoretical peak loads for the load type ABT for pinned, fixed and mixed boundary condition was 8 percent,6 percent and one percent respectively. The maximum theoretical mid-span deflections were one percent and two percent higher than the maximum experimental mid-span deflections for ABT with fixed and pinned boundary conditions. The maximum theoretical mid-span deflection for the same load type with fixed boundary condition was four percent lower than the maximum mid-span deflection measured experimentally. The ratios of the theoretical maximum angles of twist to the maximum experimental angles of twists were also 1.125, 1.29 and 1.09 for the pinned, fixed and mixed boundary conditions respectively.

4.4 Combined Axial Load, Uniaxial Moment and Torsion under Ambient Temperature

Figures 107-118 show the results of the combined axial load, uniaxial moment and torsion for the boundary conditions used in this research. Tables 9-11 present theoretical results of load type APUT for pinned, fixed and mixed boundary conditions. The first column shows the load type whilst the second, third and fourth present the axial loading, uniaxial moment and torsional moment respectively. The fourth column shows the mid-span deflections whereas the fifth column shows the angle of twist.

The ratios for the theoretical peak loads to experimental peak loads were 0.97, 1.02

and 0.99 for the pinned, fixed, and mixed boundary conditions. The maximum theoretical mid-span deflection was 7 percent and 13 percent lower than the experimental mid-span deflection for APUT with pinned and mixed boundary conditions. The maximum theoretical mid-span deflection for the same load type with fixed boundary condition was 7 percent higher than the maximum experimental mid-span deflection. Meanwhile, the ratios for the maximum theoretical angles of twist to maximum experimental angles of twist were 0.98, 0.93 and 0.92 for the pinned, fixed and mixed boundary conditions respectively.

4.5 Combined Axial Load, Biaxial Moment and Torsion under Ambient Temperature

Figures 119 -130 summarize the results of the combined axial load, biaxial moment and torsion for the boundary conditions used in this research. Tables 9-11 present theoretical results of load type APBT for pinned, fixed, and mixed boundary conditions. The first column shows the load type whilst the second, third and fourth present the axial loading, biaxial moment and torsional moment respectively. The fourth column shows the mid-span deflections whereas the fifth column shows the angle of twist.

The ratio for the theoretical peak loads to experimental peak loads were 0.93, 0.99 and 1.03 for the pinned, fixed, and mixed boundary conditions. The maximum theoretical mid-span deflections were 34 percent and two percent lower than the maximum experimental mid-span deflections for APBT with pinned and mixed boundary conditions. The maximum theoretical mid-span deflection for APBT with fixed boundary condition was three percent higher than the maximum experimental mid-span deflection. The ratios for the maximum theoretical angles of twist to experimental angles of twist were 0.94,1.02 and 1.08 for the pinned, fixed and mixed boundary conditions respectively.

4.6 Combined Axial Load and Torsion under Elevated Temperature

Figures 131 -139 present the results of the combined axial load and torsion for the boundary conditions used in this research. Tables 12-14 summarize theoretical results of load type HPT for pinned, fixed and mixed boundary conditions. The first column shows the load type whilst the second column and third present the axial load and torsional moment respectively. The fourth column shows the mid-span deflections whereas the fifth column shows the angle of twist. The ratio for the theoretical peak loads to experimental peak loads were 0.97, 1.02 and 0.97 for the pinned, fixed and mixed boundary conditions.

The maximum theoretical mid-span deflections were four percent, 8 percent and 11 percent lower than the experimental mid-span deflections for HPT with pinned, fixed and mixed boundary conditions. Meanwhile, the ratios of the maximum theoretical angle of twists to the experimental angles of twist were 1.08,1.03 and 1.10 for the pinned, fixed and mixed boundary conditions respectively.

4.7 Combined Uniaxial Moment and Torsion under Elevated Temperature

Figures 140 -145 present the results of the combined uniaxial moment and torsion for the boundary conditions used in this research. Tables 12-14 show the theoretical results of load type HUT for pinned, fixed and mixed boundary conditions. The first column shows the load type whilst the second column and third present the uniaxial moment and torsional moment respectively. The fourth column shows the mid-span deflections whereas the fifth column shows the angle of twist. The ratios for the theoretical peak loads to experimental peak loads were 1.03, 0.88 and1.08 for the pinned, fixed and mixed boundary conditions. The maximum theoretical mid-span deflections were 13 percent and 11 percent lower than the experimental mid-span deflection for HUT with pinned and fixed boundary conditions.

The maximum theoretical mid-span deflection with mixed boundary condition was

8 percent higher than the maximum experimental mid-span deflection. Meanwhile, the ratios of the maximum theoretical angles of twist to the experimental angles of twist were 0.93,0.95 and 1.12 for the pinned, fixed and mixed boundary conditions respectively.

4.8 Combined Biaxial Moment and Torsion under Elevated Temperature

Figures 146 -151 summarize the results of the combined biaxial moment and torsion at elevated temperatures for the boundary conditions used in this research. Tables 12-14 show theoretical results of load type HBT for pinned, fixed and mixed boundary conditions. The first column shows the load type whilst the second column and third present the biaxial moment and torsional moment respectively. The fourth column shows the mid-span deflections whereas the fifth column shows the angle of twist.

The ratio for the theoretical peak loads to experimental peak loads were 0.92, 1.11 and 1.01 for the pinned, fixed and mixed boundary conditions. The maximum theoretical mid-span deflections were 14 percent and five percent lower than the experimental mid-span deflections for HBT with fixed and mixed boundary conditions respectively. The theoretical mid-span deflection with pinned boundary condition was two percent higher than the mid-span deflection measured experimentally. Also, the ratios of the maximum theoretical angles of twist to the experimental angles of twist were 1.05,1.22 and 1.09 for the pinned, fixed and mixed boundary conditions respectively.

4.9 Combined Axial Load, Uniaxial Moment and Torsion under Elevated Temperature

Figure 152 -162 present the results of the combined axial load, uniaxial moment and torsion at elevated temperatures for the boundary conditions used in this research. Tables 12-14 show theoretical results of load type HPUT for pinned, fixed and mixed boundary conditions. The first column shows the load type whilst the second, third and fourth present the axial

loading, uniaxial moment and torsional moment respectively. The fourth column shows the mid-span deflections whereas the fifth column shows the angle of twist.

The ratios for the theoretical peak loads compared to the experimental peak loads were 0.98, 1.00 and 0.94 for the pinned, fixed and mixed boundary conditions. The maximum theoretical mid-span deflections were 14 percent lower than the experimental mid-span deflection for both the pinned and mixed boundary conditions. The theoretical mid-span deflection with fixed boundary condition was 6 percent higher than the mid-span deflection measured experimentally. Also, the ratios of the maximum theoretical angles of twist to the maximum experimental angles of twist were 0.99,1.25 and 1.10 for the pinned, fixed and mixed boundary conditions.

4.10 Combined Axial Load, Biaxial Moment and Torsion under Elevated Temperature

Figures 163 -174 present the results of the combined axial load, biaxial moment, and torsion for the boundary conditions used in this research. Table 12-14 show theoretical results of load type HPBT for pinned, fixed and mixed boundary conditions. The first column shows the load type whilst the second, third and fourth present the axial loading, biaxial moment and torsional moment respectively. The fourth column shows the mid-span deflections whereas the fifth column shows the angle of twist. The ratios for the theoretical peak loads to experimental peak loads were 0.97, 0.92 and 0.89 for the pinned, fixed and mixed boundary conditions.

The maximum theoretical mid-span deflection was 2% lower than the experimental mid-span deflection with pinned boundary conditions. The maximum theoretical mid-span deflections with fixed and mixed boundary condition were both 1% higher than the maximum experimental mid-span deflections. Also, the ratios of the maximum theoretical angle of twist to

the experimental angles of twist were 1.08,1.03 and 1.10 for the pinned, fixed and mixed boundary conditions.

CHAPTER 5

INTERACTION EXPRESSIONS FOR ELEVATED TEMPERATURE CONDITIONS

Presented in this chapter are interaction expressions for a biaxially loaded steel beam-columns with applied torsion at various elevated temperature conditions.

5.1 Ultimate Limit Load-Moment-Torsion Interaction Expressions

In this research, the beam-column interaction expressions are derived by using a non-linear load contour approximation approach to curve fit theoretical dimensionless interactions for HPUT and HPBT at elevated temperatures. The general form of the interaction expression is as follows [3]:

$$\left(\frac{P_u}{\phi_c P_n}+\frac{M_{ux}}{\phi_b M_{nx}}+\frac{M_{uy}}{\phi_b M_{ny}}\right)^{\alpha}+\left(\frac{T_u}{\phi_t T_n}\right)^{\alpha} \leq 1.00 \quad (62)$$

where P_u is the applied axial load, M_{ux} and M_{uy} being the flexural moments about x and y-axis respectively, T_u is the applied torque. Also, $\phi_c P_n$ is the design compressive strength, $\phi_b M_{nx}$ is the design flexural strength about the x-axis, $\phi_b M_{ny}$ is the design flexural strength about the y-axis and $\phi_t T_n$ is the design torsional strength.

For elevated temperatures,

$$\phi_c P_n = F_{cr}(T) \times A_g \quad (63)$$

where $F_{cr}(T)$ is the flexural buckling stress at elevated temperatures and A_g is the gross cross-sectional area of the member.

The flexural buckling stress at elevated temperatures $F_{cr}(T)$ is calculated based on the provisions of the AISC [89] as:

$$F_{cr}(T) = 0.42\left(\sqrt{\frac{F_{y(T)}}{F_{e(T)}}}\right)F_{y(T)} \quad (64)$$

$F_{y(T)}$ and $F_{e(T)}$ are the specified yield strength and the actual measured yield strength of the

member at elevated temperatures.

$$F_{e(T)} = \pi^2 E_{(T)}/\lambda^2 \quad (65)$$

Both $F_{y(T)}$ and $E_{(T)}$ are the temperature dependent yield strengths and elastic modulus obtained from Table A-4.2.1in the AISC [89]. λ represents the slenderness ratio (KL/r) in which K=1 for a pinned end member, L is the length of the member and r is the radius of gyration.

For a 1.5 x 1.5 x 0.125in. steel member of length 33.65in. with both ends pinned, the slenderness ratio is found to be 60.

In determining the design compressive strength at 900°F, the yield strength and elastic modulus at 900°F is found using the AISC [89];

$$F_{y(900°F)} = 0.82\ F_y \quad (66)$$

$$E_{(900°F)} = 0.62\ E \quad (67)$$

The yield strength and elastic modulus at ambient temperature F_y and E are 58.64 ksi and 29988 ksi respectively.

Hence, $F_{y(900°F)}$ and $E_{(900°F)}$ are computed to be 48.08 ksi and 18592.56 ksi using Equations 66 and 67.

From Equation (65), the actual measured yield strength $F_{e(900°F)}$ is found to be 50.97 ksi.

$$\frac{F_{y(900°F)}}{F_{e(900°F)}} = \frac{48.08\ \text{ksi}}{50.97\ \text{ksi}} = 0.94 \quad (68)$$

Also, the flexural buckling stress at high temperatures is determined from Equation 64 as

$$F_{cr(900°F)} = 0.42(\sqrt{(0.94)}) \text{ x } 48.08 \text{ ksi} \quad (69)$$

$$F_{cr(900°F)} = 20.73 \text{ ksi} \quad (70)$$

The compressive strength at elevated temperatures is also determined from Equation 63:

$$P_{n(900°F)} = 20.73 \text{ x } 0.6875 \text{ in}^2 \quad (71)$$

$P_{n(900°F)}$ = 15.14 kips (72)

Finally, the design compression strength $\phi_c P_{n(900°F)}$ is computed as:

$\phi_c P_{n(900°F)}$ = 0.90 x 15.14 , where ϕ_c = 0.90 (LRFD) (73)

$\phi_c P_{n(900°F)}$ = 13.6 kips (74)

Figure 175 shows the comparison of the design compressive strength, $\phi_c P_n$, and various slenderness ratios at ambient temperature, elevated temperatures of 900°F and 1650°F for both theoretical data and results obtained from the AISC equations [89].

Meanwhile, the design flexural and torsional strengths at elevated temperatures, $\phi_b M_n$ and $\phi_t T_n$ are determined from [89]:

$\phi_b M_{nx} = 0.90\ F_{y(T)}\ Z_x$ (75)

$\phi_b M_{ny} = 0.9\ F_{y(T)}\ Z_y$ (76)

$\phi_t T_n = 0.90\ F_{cr(T)}\ C_M$ (77)

where Z_x , Z_y are the plastic section modulus about x and y axes whereas C_M is the HSS torsional constant.

From Figure 175, the effect of elevated temperatures on the design compressive, flexural and torsional strengths can be expressed in the following form:

$\phi_c P_{n(700°F)} = 0.0011\lambda^2 - 0.3763\lambda + 35.28$ (78)

$\phi_b M_{n(700°F)} = 0.347\lambda$ (79)

$\phi_t T_{n(700°F)} = 0.2457\lambda$ (80)

$\phi_c P_{n(900°F)} = 0.0007\lambda^2 - 0.2476\lambda + 26.338$ (81)

$\phi_b M_{n(900°F)} = 0.2848\lambda$ (82)

$\phi_t T_{n(900°F)} = 0.2015\lambda$ (83)

$$\phi_c P_{n(1650°F)} = 0.0004\lambda^2 - 0.0147\lambda + 1.4646 \quad (84)$$

$$\phi_b M_{n(1650°F)} = 0.0208\lambda \quad (85)$$

$$\phi_t T_{n(1650°F)} = 0.0147\lambda \quad (86)$$

where λ is the slenderness ratio of the structural member subjected to elevated temperatures. Lateral torsional buckling is not considered in this research.

Figure 176 shows the theoretical dimensionless interaction curve, experimental curve and a nonlinear approximation for APBT. The interaction expression for APBT is as follows:

$$\left(\frac{P_u}{\phi_c P_n} + \frac{M_{ux}}{\phi_b M_{nx}} + \frac{M_{uy}}{\phi_b M_{ny}}\right)^{3.60} + \left(\frac{T_u}{\phi_t T_n}\right)^{1.20} \leq 1.00 \quad (87)$$

$$\text{where } \left(\frac{P_u}{\phi_c P_n} + \frac{M_{ux}}{\phi_b M_{nx}} + \frac{M_{uy}}{\phi_b M_{ny}}\right)^{3.60} = \Gamma_1 \quad (88)$$

Figure 177 shows the theoretical dimensionless interaction curve, experimental curve and a nonlinear approximation for HPBT at the temperature of 700°F. The interaction expression is:

$$\left(\frac{P_u}{\phi_c P_n} + \frac{M_{ux}}{\phi_b M_{nx}} + \frac{M_{uy}}{\phi_b M_{ny}}\right)^{3.40} + \left(\frac{T_u}{\phi t T_n}\right)^{1.60} \leq 1.00 \quad (89)$$

$$\text{where } \left(\frac{P_u}{\phi_c P_n} + \frac{M_{ux}}{\phi_b M_{nx}} + \frac{M_{uy}}{\phi_b M_{ny}}\right)^{3.40} = \Gamma_2 \quad (90)$$

The theoretical dimensionless interaction curve and the nonlinear approximation for HPBT at the temperature of 900°F is shown in Figure 178. The interaction expression is:

$$\left(\frac{P_u}{\phi_c P_n} + \frac{M_{ux}}{\phi_b M_{nx}} + \frac{M_{uy}}{\phi_b M_{ny}}\right)^{3.30} + \left(\frac{T_u}{\phi t T_n}\right)^{0.90} \leq 1.00 \quad (91)$$

$$\text{where } \left(\frac{P_u}{\phi_c P_n} + \frac{M_{ux}}{\phi_b M_{nx}} + \frac{M_{uy}}{\phi_b M_{ny}}\right)^{3.30} = \Gamma_3 \quad (92)$$

Figure 179 shows the theoretical dimensionless interaction curve and a nonlinear approximation for HPBT at the temperature of 1650°F. The interaction expression developed is:

$$\left(\frac{P_u}{\phi_c P_n} + \frac{M_{ux}}{\phi_b M_{nx}} + \frac{M_{uy}}{\phi_b M_{ny}}\right)^{2.90} + \left(\frac{Tu}{\phi tTn}\right)^{1.1} \leq 1.00 \quad (93)$$

where $\left(\frac{P_u}{\phi_c P_n} + \frac{M_{ux}}{\phi_b M_{nx}} + \frac{M_{uy}}{\phi_b M_{ny}}\right)^{2.90} = \Gamma_4$ (94)

The interaction expressions above are used to predict the interaction between the elevated temperature dependent strengths and design strengths.

CHAPTER 6

CONCLUSIONS AND FUTURE RESEARCH

6.1 Conclusions

The semi-analytical solution presented in this dissertation is in good agreement with the experimental results, with peak loads found to be within five percent of each other. Based on the materially nonlinear analysis and experiments conducted at both the ambient and high temperature conditions, the following conclusions are drawn:

A. Related to experimentally obtained member strength reduction at 700 degrees F in comparison with that at the ambient temperature:

1. The strength of members subjected to combined axial and torsional loading was reduced by 42 percent.
2. The strength of members subjected to combined biaxial moment and torsional loading was reduced by 33 percent.
3. The strength of members subjected to combined uniaxial moment and torsional loading decreased by 51 percent.
4. The strength of members subjected to combined axial loading, uniaxial moment and torsional moment decreased by 53 percent.
5. The strength of members subjected to combined axial loading, biaxial moment and torsional moment was reduced by 32 percent.

B. Related to the theoretical interaction curve in comparison with the interaction expressions at both ambient and elevated temperatures:

6. The theoretical interaction curve is within three percent of the interaction expression while the experimental interaction curve is within four percent of the interaction expression at ambient temperature.
7. The theoretical interaction curve is within five percent of the interaction expression while the experimental interaction curve is within seven percent of the interaction expression at 700 degrees F.
8. The theoretical interaction curve is within four percent of the interaction expression at 900 degrees F.
9. The theoretical interaction curve is within six percent of the interaction expression at 1650 degrees F.

C. Related to the theoretically predicted ultimate strength at 900 degrees F (referred to as Case 1 below), and 1650 degrees F (Case 2 below), respectively compared to that at the ambient temperature:

10. The strength of members subjected to combined axial and torsional loading was reduced by 54 percent, and 81 percent, respectively, for Cases 1 and 2.
11. The strength of members subjected to combined biaxial moment and torsional loading was reduced by 70 percent, and 88 percent, respectively, for Cases 1 and 2.
12. The strength of members subjected to combined uniaxial moment and torsional loading decreased by 72 percent, and 79 percent, respectively, for Cases 1 and 2.
13. The strength of members subjected to combined axial loading, uniaxial moment and torsional moment decreased by 66 percent, and 82 percent, respectively, for Cases 1 and 2.

14. The strength of members subjected to combined axial loading, biaxial moment and torsional moment was reduced by 72 percent, and 83 percent, respectively, for Cases 1 and 2.

The methodology presented in the dissertation is applicable to practical structural analysis or design of biaxially loaded beam-columns with applied torsion and subjected to high temperatures such as those encountered during a fire.

6.2 Future Research

Future studies can be conducted on the effect of post-fire conditions notably: cooling in air and water based methods on the behavior of biaxially loaded steel beam-columns with applied torsion. The effect of elevated temperatures on biaxially loaded steel members with singly symmetric and unsymmetric cross-sections with applied torsion will also need to be studied.

LIST OF REFERENCES

1.Darbhamulla, S. P., "Nonproportionally Loaded Steel Beam-Column and Flexibly- Connected Nonsway Frames," Ph.D. Dissertation, Old Dominion University, May, 1990.

2. Zhao, Yanhong., "Thermo-Elasto-Plastic Behavior of Biaxially Loaded Steel Beam- Columns Including Those From World Trade Center", Ph.D. Dissertation, Old Dominion University, 2013.

3. Konate, Mamadou.,"Inelastic Behavior and Strength of Steel Beam-Columns With Applied Torsion", Ph.D. Dissertation, Old Dominion University,2015.

4. Eidan, S. A., "Inelastic Stability of Nonproportionally Loaded Steel Sway Beam- Columns and Space Frames," Ph.D. Dissertation, Old Dominion University, 1992.

5. Ketter, R. C., "Stability of Beam-Columns above the Elastic Limit", *Proc. ASCE,* Vol.81, No.692, October 1955.

6. Galambos, T.V. and R.L. Ketter., "Columns Under Combined Bending and Thrust", Proceedings. ASCE, Vol. 85, EM2, 1959.

7. Mason, R. E., G.P. Fisher and G. Winter., "Eccentrically Loaded Hinged Steel Columns", ASCE, Vol. 84, EM4, 1958.

8. Birnstiel, C. "Experiments on H-Columns under Biaxal Bending", Journal of Structural Divison, October, 1968.

9. Birnstiel,C.,and Michalos,J., Ultimate Load of H-Columns Under Biaxial Bending, Journal of Structural Division,1963.

10. Galambos,T.V.,Adams,P.F. and Fukomot,Y., "Further Studies On The Lateral-Torsional Buckling Of Steel Beam-Columns", Fritz Engineering Laboratory Report, Lehigh University,1965.

11. Galambos, T. V. and Prasad, J., “Ultimate Strength Tables for Beam-columns,” Fritz Engineering Laboratory Report, No. 287 3, Lehigh University Institute of Research, January 1962.

12. Milner, H. R., “The Elastic Plastic Stability of Stanchions Bent about Two Axes”, Ph.D. Dissertation, Imperial College, University of London, December 1965.

13. Harstead,G.A.,Birnstiel,C., and Leu,K.C., Inelastic H-columns Under Biaxial Bending, Journal of Structural Division,1968.

14. Razzaq, Z., “Theoretical and Experimental Investigation of Biaxially Loaded Rectangular Tubular Columns”, *M.S. Thesis,* University of Windsor, Windsor, Ontario, Canada, 1968.

15. Marshall, P. J. and Ellis, J. S., “The Ultimate capacity of Biaxially Loaded Box Steel Columns”, *The Royal Military College of Canada,* Kingston, Ontario, Canada, February 1969.

16. Sakda, S. and Chen W.F., “Analysis of Biaxially Loaded Columns”, Fritz Engineering Laboratory Report No.331.12, September 1970.

17. Baseheart, T.M., “A Solution Procedure For Biaxially Loaded Beam-Columns”, Ph.D. Dissertation, University of Cincinnati, 1973.

18. Thompson,L.E., “Behavior of Steel Beam-Columns Subjected to Alternative Strains”, Ph.D. Dissertation, Rice University, 1971.

19. Hobbs,R.E., and Jowharzadeh,A.M., An Incremental Analysis Of Beam-Columns And Frames Including Finite Deformations And Bilinear Elasticity, Computer & Structures,1978,pp.323-330.

20. Razzaq, Z., and McVinnie, W. W., “Rectangular Tubular Steel Columns Loaded Biaxially,”*Journal of Structural Mechanics,*Vol,X,No.4, 1982.

21. Razzaq, Z., and McVinnie, W. W., “Theoretical and Experimental Behavior of Biaxially Loaded Inelastic Columns,” *Journal of Structural Mechanics,* Vol. 14, No. 3, March, 1986.

22. Han,D.J. and Chen,W.F., “Buckling and Cyclic Inelastic Analysis of Steel Tubular Beam-Columns”, Engineering Structures,1983.

23. Chen, W.F., “Design of Beam-Columns in Steel Frames in the United States”,Thin-Walled Structures, 1991, pp.1-83.

24. Dawe,J.L., and Kulak,G.L., Local Buckling Behavior of Beam-Columns, Journal of Structural Engineering,1986,pp.2447-2461.

25. Yang,K.C.,and Hsu,R., Structural Behavior of Centrally Loaded Steel Columns at Elevated Temperature, Journal of Constructional Steel Research, 2009,pp.2062-2068.

26. Hancock,G.J., and Rasmussen,K.J.R., “Recent Research on Thin-Walled Beam-Columns”, Thin-Walled Structures,198,pp.3-18.

27. Torkamani,M.A.M, and Sonmez,M., Inelastic Large Deflection Modeling of Beam-Columns,Journal of Structural Engineering,2001,pp.876-887.

28. Boissonnade,N.et al, Improvement Of The Interaction Formulae For The Beam-Columns In Eurocode 3, Computer and Structures,2002,pp.2375-2385.

29. Trahair, N.S., and Pi. Y. L.,“ Torsion, Bending and Buckling of Steel Beams,” *Engineering Structures,* ASCE, Vol. 19, No. 5, 1997, pp. 372-377.

30. Hasham,A.S., and Rasmussen,K.J.R., Section Capacity of Thin-Walled I-Section Beam-Columns, Journal of Structural Engineering,1998,pp.351-359.

31. Law,K.H., and Gardner,L., “Global Instability Of Elliptical Hollow Section Beam-Columns under Compression and Biaxial Bending”, International Journal of Steel Structures,2013,pp.745-759.

32. Marques,L.,et al, “Extensions of EC3-1-1 Interaction Formulae For The Stability Verification of Tapered Beam-Columns”, Journal of Constructional Steel Research,2014,pp.122-135.

33. Kucukler,M., Gardner,L., and Yidu,B., Flexural-Torsional Buckling of Austenitic Stainless Steel I-section Beam-Columns: Testing, Numerical Modelling and Design, Journal of Constructional Steel Research,2016.

34. Zhao,O.,”Structural Behavior of Stainless Steel Elements Subjected to Combined Loading”, Ph.D. Dissertation, Imperial College London and The University of Hong Kong,2015.

35. Zhao,O., Gardner,L., and Young,B., “Experimental Study of Ferritic Stainless Steel Tubular Beam-Column Members Subjected To Unequal End Moments”, Journal of Structural Engineering,2016.

36. Gizejowski,M.A., et al, “Out-of-Plane Buckling Resistance of Rolled Steel H-section Beam-Columns under Unequal End Moments”, Journal of Constructional Steel Research, pp.153-168.

37. Konate,M., and Razzaq,Z., “Yield Limit Interaction Relations For Biaxially Loaded Non-Sway Steel Beam-Columns with Applied Torsion”, Journal of Constructional Steel Research,2019,pp.182-191.

38. Kucukler,M.,Bu,Y.and Gardner,L., Flexural-Torsional Buckling of Austenitic Stainless Steel I-section Beam-Columns: Testing, Numerical Modelling and Design, Thin-Walled Structures,2020.

39. Liew, J.Y.R., “Advanced inelastic analysis of frame structures”, Journal of Constructional Steel Research 55,2000, pp.245-265.

40. Vila Real,P.M.M., The Effect of Residual Stresses In the Lateral-Torsional Buckling of Steel I-Beams at Elevated Temperature, Journal of Constructional Steel Research,60,2004,pp.783-793.

41. Lopes, N., Villa Real, P.M.M., Simoes da Silva, L., and Franssen, J.M.,“Stainless steel beam-columns in case of fire,” Proceedings of the fifth International Conference on Structures in Fire, 2008, pp.1-8.,

42. Knobloch,M.,Fontana,M., and Frangi,A., Steel Beam-Columns Subjected to Fire,Steel Construction,2008,pp.51-58.

43. Kodur,V.K.R., and Dwaikat,M.M.S., Response of Steel Beam-Columns Exposed to Fire, Engineering Structures, 2009,pp.369-379.

44. Chloe,L, et al, “Fundamental Behavior of Steel Beam-Columns and Columns Under Fire Loading: Experimental Evaluation”, Journal of Structural Engineering,2011,pp.954-966.

45. Chloe,L, et al, “Experimental Investigation of Steel Beam-Columns Under Fire Loading”, Structures Congress,2010,pp. 1604-1613.

46. Lopes, N., Villa Real, P.M.M., Simoes da Silva, L., and Franssen, J.M.,“ Duplex stainless steel columns and beam-columns in case of fire,” Proceedings of the fifth International Conference on Structures in Fire, 2008,pp.90-100.

47. Kucukler,M.,Gardner,L.,and Macorini,L., Flexural-Torsional Buckling assessment of Steel Beam-Columns Through a Stiffness Reduction Method, Engineering Structures,2015.

48. Abramyan,B.L., “Torsion and Bending of Prismatic Rods of Hollow Rectangular Section”, Techincal Memorandum 1319,1950.

49. Gaydon,F.A., and Nuttal,H., On The Combined Bending and Twisting of Beams of Various Sections,1957,pp.17-26.

50. Iwegwu, E. O., “Combined Plastic Bending and Torsion,” *Journal of the Mechanics and Physics of Solids,* Vol.10, 1962, pp.277-282.

51. Iwegwu, E. O., “Plastic Flexure and Torsion,” *Journal of the Mechanics and Physics of Solids,* 1960, pp.141-146.

52. Boulton,N.S., Plastic Twisting and Bending of an I-Beam in which the warp is Restricted, International Journal of Mechanical Science,1962,pp.491-502.

53. Nethercot,D.A., Torsional Rigidity of Rolled Steel Sections, International Journal of Mechanical Science,1974,pp.565-572.

54. May,I.M., and Al-Shaarbaf,A.S., Elasto-Plastic Analysis of Torsion Using A Three-Dimensional Finite Element Model, Computers & Structures, 1989,pp.667-678.

55. Trahair,N.S. and Bild,S. “Elastic Biaxial Bending and Torsion of Thin-Walled Members”, Thin-Walled Structures,1990,pp.269-307.

56. Billinghurst,J.R.L., et al, Inelastic Torsion Of Steel Members, Computers & Structures,1992,pp.887-894.

57. Chen,G., and Trahair,N.S., “Inelastic Nonuniform Torsion of Steel I-Beams”, Journal of Constructional Steel Research,1992,pp.189-207.

58. Zheng, B.,Hua,X.,and Shu,G.,”Tests of Cold-Formed and welded Stainless Steel Beam-Columns”, Journal of Constructional Steel Research,2015,pp.1-10.

59. Rowan,M.B,]., et al, Torsional Properties of Stainless Steel and Nickel-Titanium Endodontic Files,Journal of Endodontics,1996,pp.341-345.

60. Pi,Y.L., and Trahair,N.S., Non-Linear Inelastic Analysis of Steel Beam-Columns. I-Theory, Journal of Structural Engineering,1994,pp.2041-2061.

61. Trahair,N.S., and Pi,Y.P., “Torsion, Bending and Buckling of Steel Beams”, Engineering Structures,1997,pp.372-377.

62. Wagner,W., and Gruttmann,F., “Finite Element Analysis of Saint-Venant Torsion Problem With Exact Integration of The Elastic-Plastic Constitutive Equations”, Computer Methods in Applied Mechanics and Engineering, 2001, pp.3831-3848.

63. Gotluru,B.P., Schafer,B.W., and Pekoz,T., “Torsion in Thin-Walled Cold Formed Steel Beams”, Thin-Walled Structures,2000,pp.127-145.

64. Trahair,N.S., and Teh,L.H., Second Order Moments In Torsion Members, Engineering Structures,2001,pp.631-642.

65. Ridley-Ellis,D.J., Owen,J.S., and Davies,G., “Torsional Behavior of Rectangular Hollow Sections”, Journal of Constructional Steel Research,2003,pp.641-663.

66. Lee,Y.H.,et al, “Finite Element Formulation of A Composite Double T-Beam Subjected To Torsion”, Engineering Structures,2007,pp.2935-2945.

67. Gosowski,B.,”Non-uniform Torsion Of Stiffness Open Thin-Walled Members Of Steel Members”, Journal of Constructional Steel Research,2007,pp.849-865.

68. Melcher,J., and Karmazionova,M., On Problems of Torsion Analysis of Steel Members With Open Cross Sections, Steel Structures and Bridges,2012,pp.262-267.

69. Mahata,A.K., et al, “Room Temperature Torsional Behavior of 15-Cr-15Ni Titanium Modified Austenitic Stainless Steel”, 1st International Conference on Structural Integrity,2014,pp.166-172.

70. Peterman,K.D., Bian,G., and Schafer,B.W., “Experimental and Computational Analysis of Direct Torsion In Cold-Formed Steel Lipped Channels”, Proceedings of the Annual Stability Conference Structural Stability Research Council,2014,pp.332-345.

71. Wan,H.X.,”Behavior and strength of hollow flange channel sections under torsion and bending”, Thin-Walled Structures,94,2015,pp. 612-623.

72. Peterman,K.D., Bian,G.and Schafer, B.W. “Experimental and Computational Analysis of Direct Torsion In Cold-Formed Steel Lipped Channels”, Proceedings of the Annual Stability Conference Structural Stability Research Council,2014.

73. Aminbaghai,M.,et al, “Torsional Warping Eigenmodes Including The effect of The Secondary Torsion Moment on The Deformations”, Engineering Structures,2016,pp.299-316.

74. Lorkowski, P. and Gosowski, B., “Experimental and Numerical Research of The Torsion Problem of Built-up Steel Columns Laced In A Single Plane”, Engineering Structures,2018,pp.566-580.

75. Ahmad, M. et al, “Design of Steel Wide-Flange Members for Torsion Applied Through One Flange”, Journal of Constructional Steel Research, 141,2018,pp.50-62.

76. Devi,S.V.et al, Cold-Formed Steel Square Hollow Members With Circular Perforations Subjected to Torsion, Journal of Constructional Steel Research,162,2019.

77. Nandhakumar,C.S., Ramesh, R., and Sreevidya,V., “Investigation Of Cold Formed Steel Beam Subjected To Torsion”, Materials Today:Proceedings,2020,pp.425-429.

78. Gil,B.,et al.,“Major Axis Steel Joint Under Torsion: Stiffness and Strength Characterization”, Engineering Structures,2019,pp.586-602.

79. Winkler,R.,et al, Redistribution of Internal Torsional Moments caused by Plastic Yielding of Structural Steel Members, Structures,2019,pp.21-33.

80. Devi,S.V., and Singh,K.D., “Finite Element Study of Lean Duplex Stainless Steel Semi-Elliptical Hollow Section Members With Circular Perforation Subjected To Torsion”, Thin-Walled Structures,2020.

81. Angella,G.,et al, “Microstructure Evolution of AISI 316L In Torsion At High Temperature”, Acta Materialia,2005,pp.1263-1275.

82. Matheron,P.,et al, “Tension-Torsion ratcheting Tests on 9Cr Steel at High Temperature”,Nuclear Engineering and Design, 2015,pp.207-214.

83. Razzaq, Z., and Calash, A. Y., “Imperfect Columns with Biaxial Partial Restraints,” *Journal of Structural Engineering,* ASCE, Vol. III, No. 4, April, 1985, pp. 758-776.

84. Mcvinnie, W.W.,”Elastic and Inelastic Buckling of an Orthogonal Space Frame”, Ph.D. Dissertation, University of Illinois at Urbana-Champaign,1966.

85. Ballio, G. and Bampanini, G., “Equivalent Bending Moments for Beam-Columns”, *Journal of Constructional Steel Research*, Vol. 1, No. 3, May 1981.

86. Von, M., “Mechanik der festen Korper im plastisch deformablen Zustand. Gottin,” *Nachr. Math.* Phys., vol. 1, pp. 582-592, 1931.

87. European Committee for Standardization, (2005), “General rules- Structural Fire Design, En 1993-1-2.” Eurocode 3, Brussels.

88. AS 4100. Steel structures [S]. Sydney: Standards Australian, 1998.

89. American Institute of Steel Construction Inc., “Steel Construction Manual”. 15th Edition, 2015, ISBN I-56424-055-X

90. Sakumoto Y, Nakazato T, Matsuzaki A. High-Temperature Properties of Stainless Steel for Building Structures [J]. Journal of Structural Engineering, 1996, 122(4):399-406.

91. Gardner L, Insausti A, Ng K T, et al. Elevated temperature material properties of stainless steel alloys [J]. Journal of Constructional Steel Research, 2010, 66(5): 634-647.

92. Kirby B R. The Behaviour of High-Strength Grade 8.8 Bolts in Fire [J]. Journal of Constructional Steel Research, 1995, 33(1-2): 3-38.

93. Zhao B. Material behaviour at elevated temperatures: Work package 5.1 [R]. U K: The Steel Construction Institute, 2000.

94. Galambos, T. V., “Stability Design Criteria for Metal Structures”, Fifth Edition, *John Wiley <&Sons*, Inc., New York, 1998.

95. ASTM E119-98, “Fire Tests of Building Construction and Material”, Project No. 16410-108710, May 2, 2001.

96. EN 10002-5.”Tensile Testing of Metallic Materials- Method of Test at Elevated Temperatures”, Switzerland: ISO copyright office, 1992.

APPENDIX A: LIST OF FIGURES

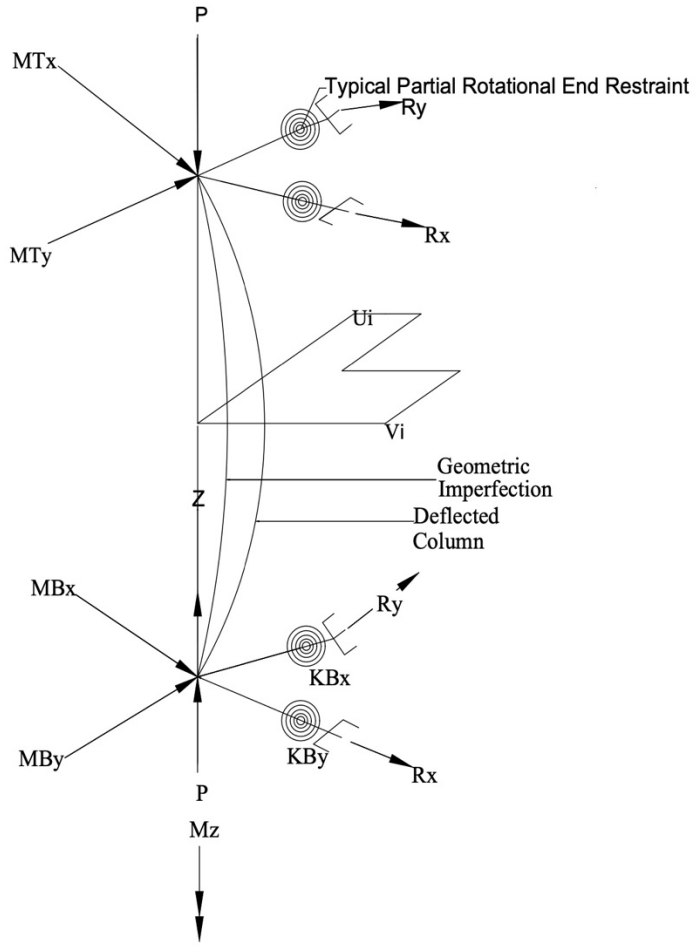

Figure 1.Biaxially Loaded Beam-Column Subjected to Applied Torque

From reference [2,3]

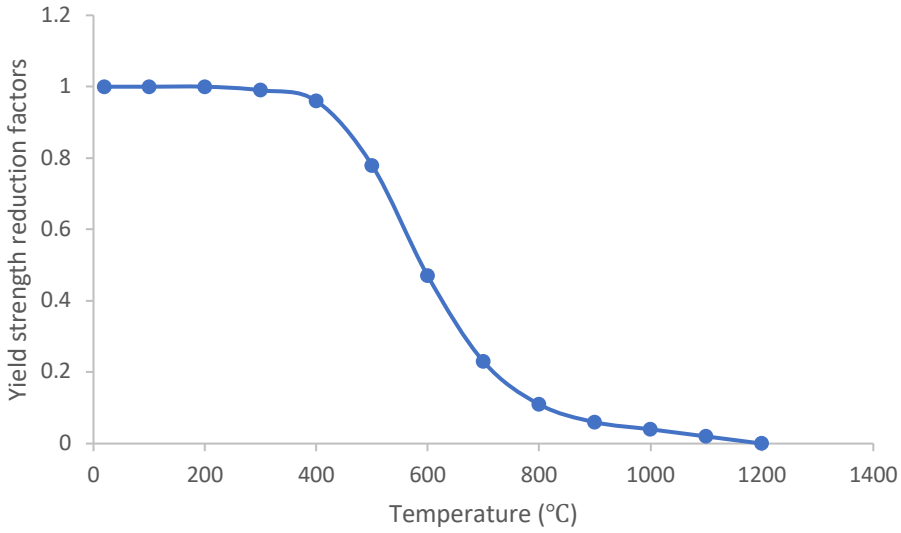

Figure 2.Yield Strength Reduction Factors at High Temperatures

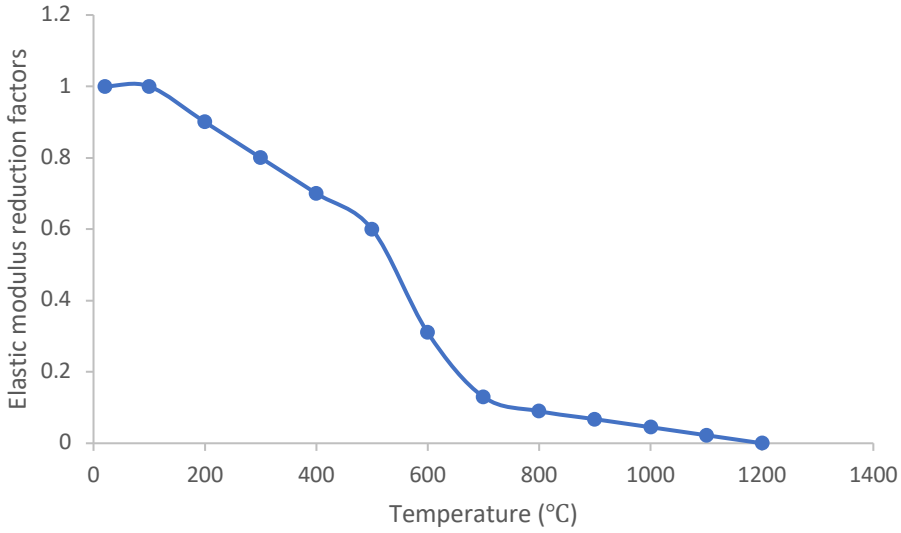

Figure 3.Elastic Modulus Reduction Factors at High Temperatures

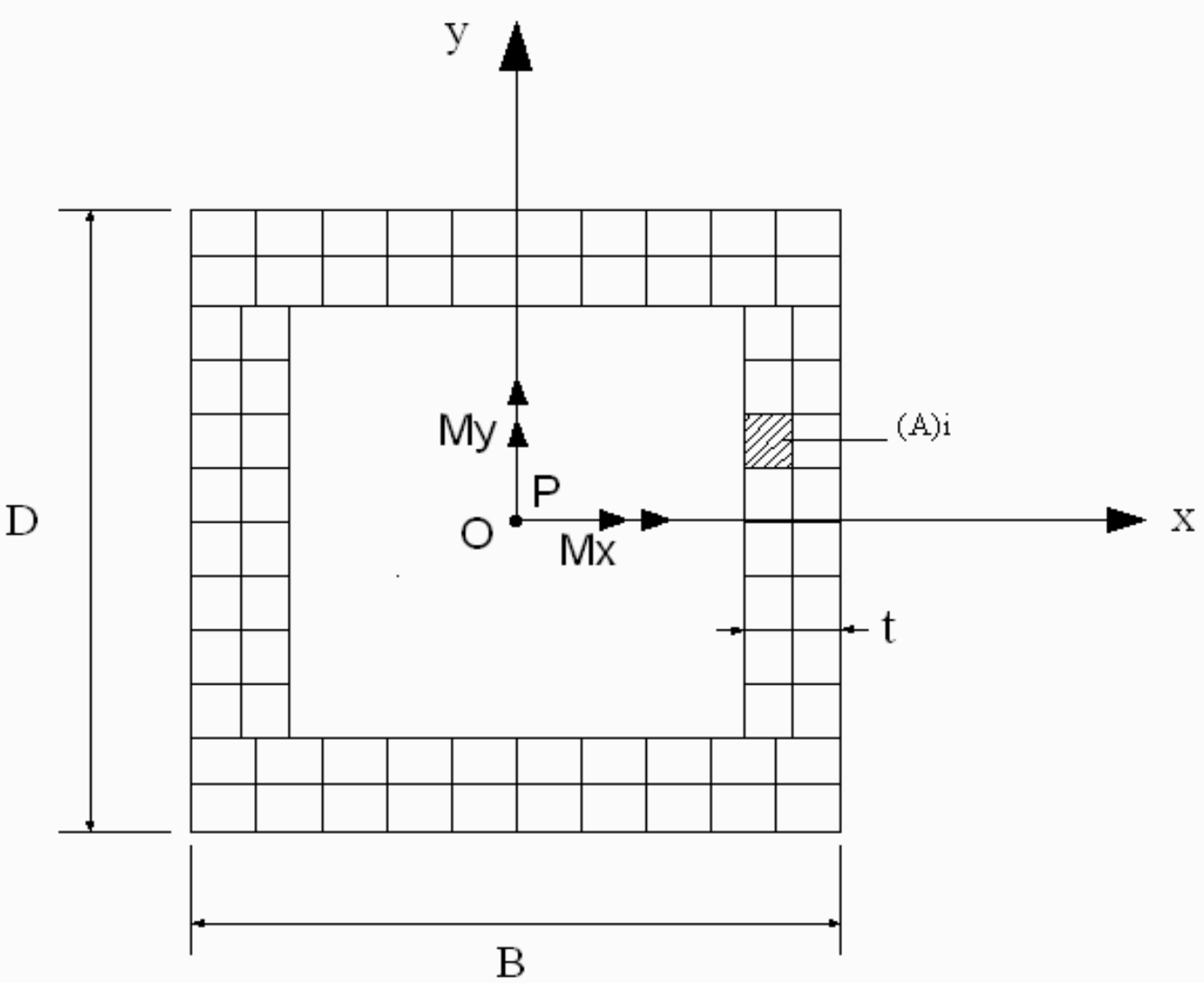

Figure 4.Discretized Hollow Rectangular Cross-section

From reference [2,3]

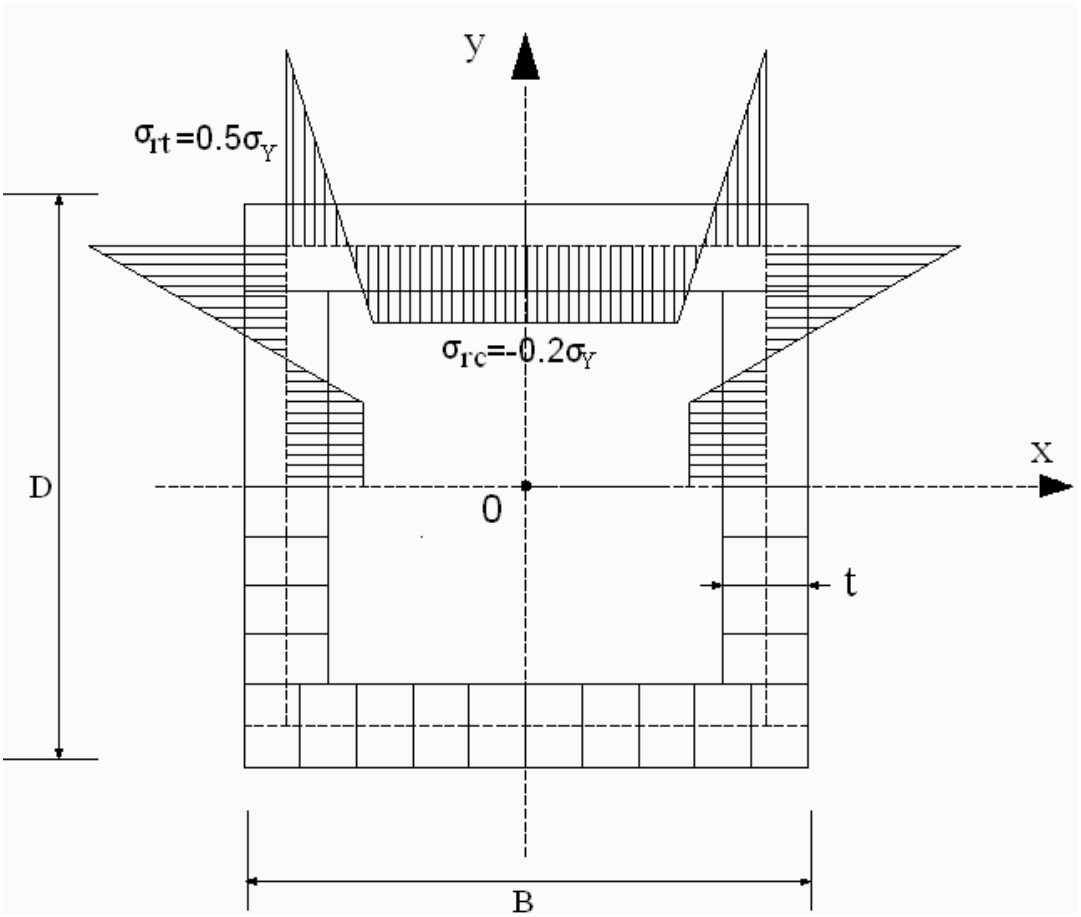

Figure 5.Residual Stress Distribution

From reference [2,3]

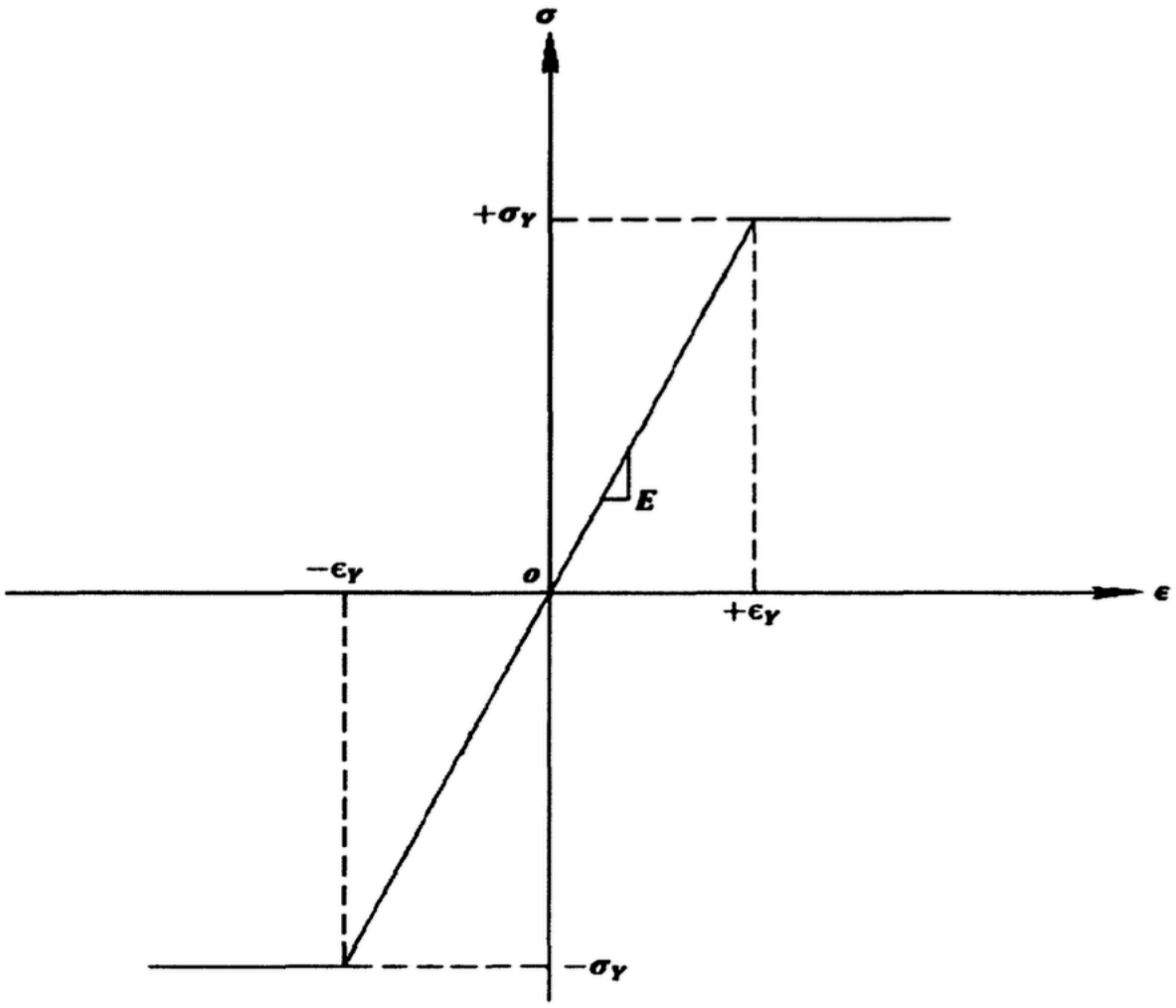

Figure 6.Stress Strain Relationship

From reference [3]

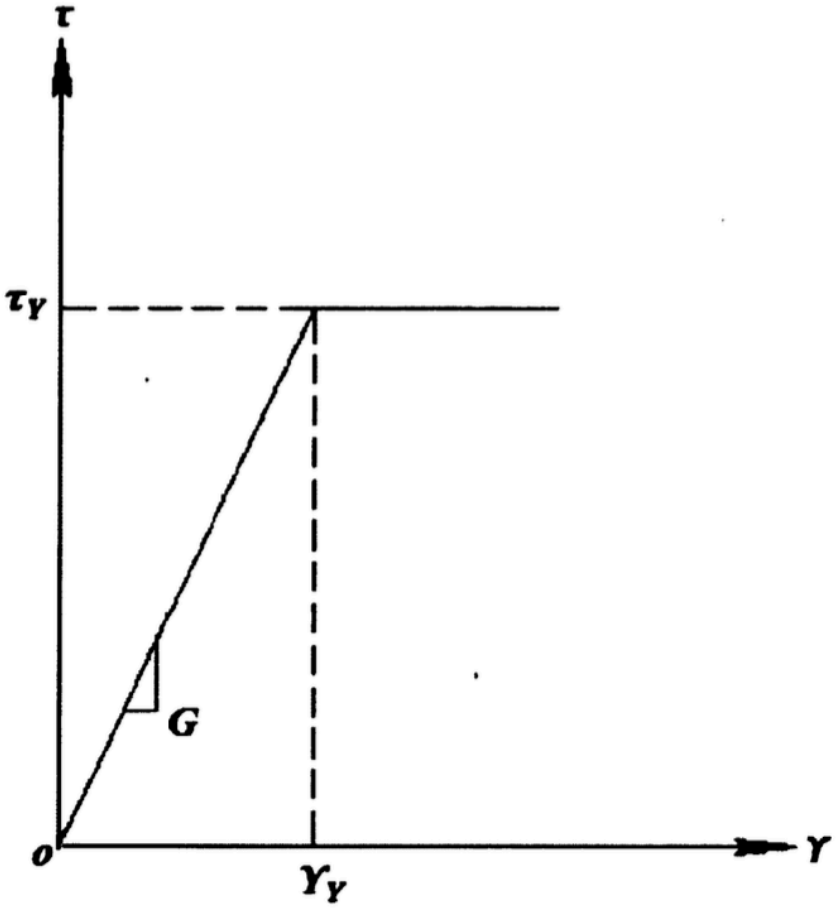

Figure 7.Shear-Stress-Shear Strain Relationship

From reference [2]

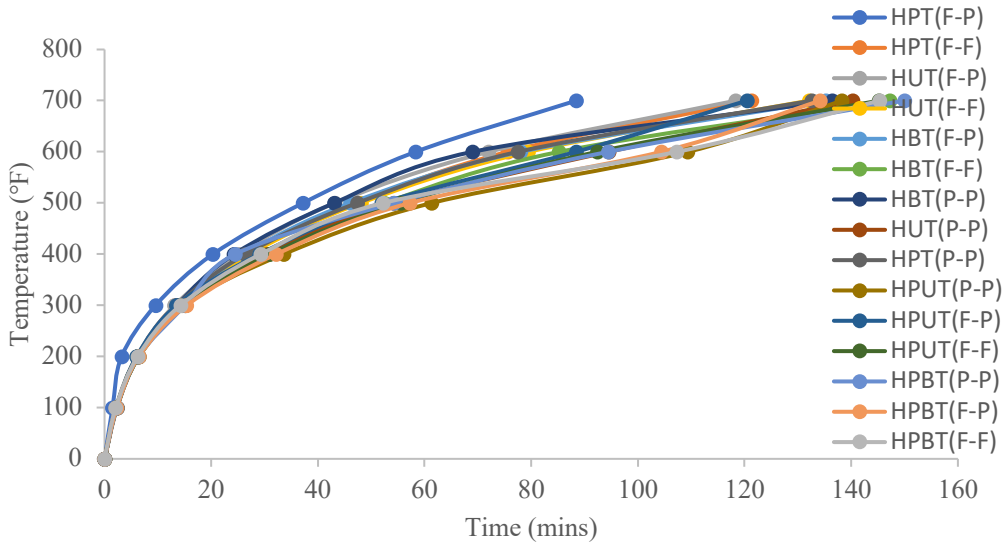

Figure 8.Temperature-Time Relationship

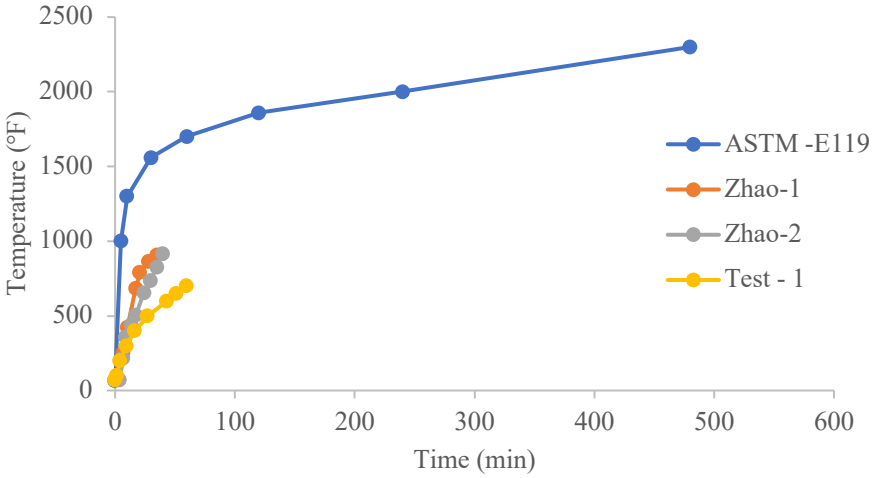

Figure 9.Temperature-Time Relationship

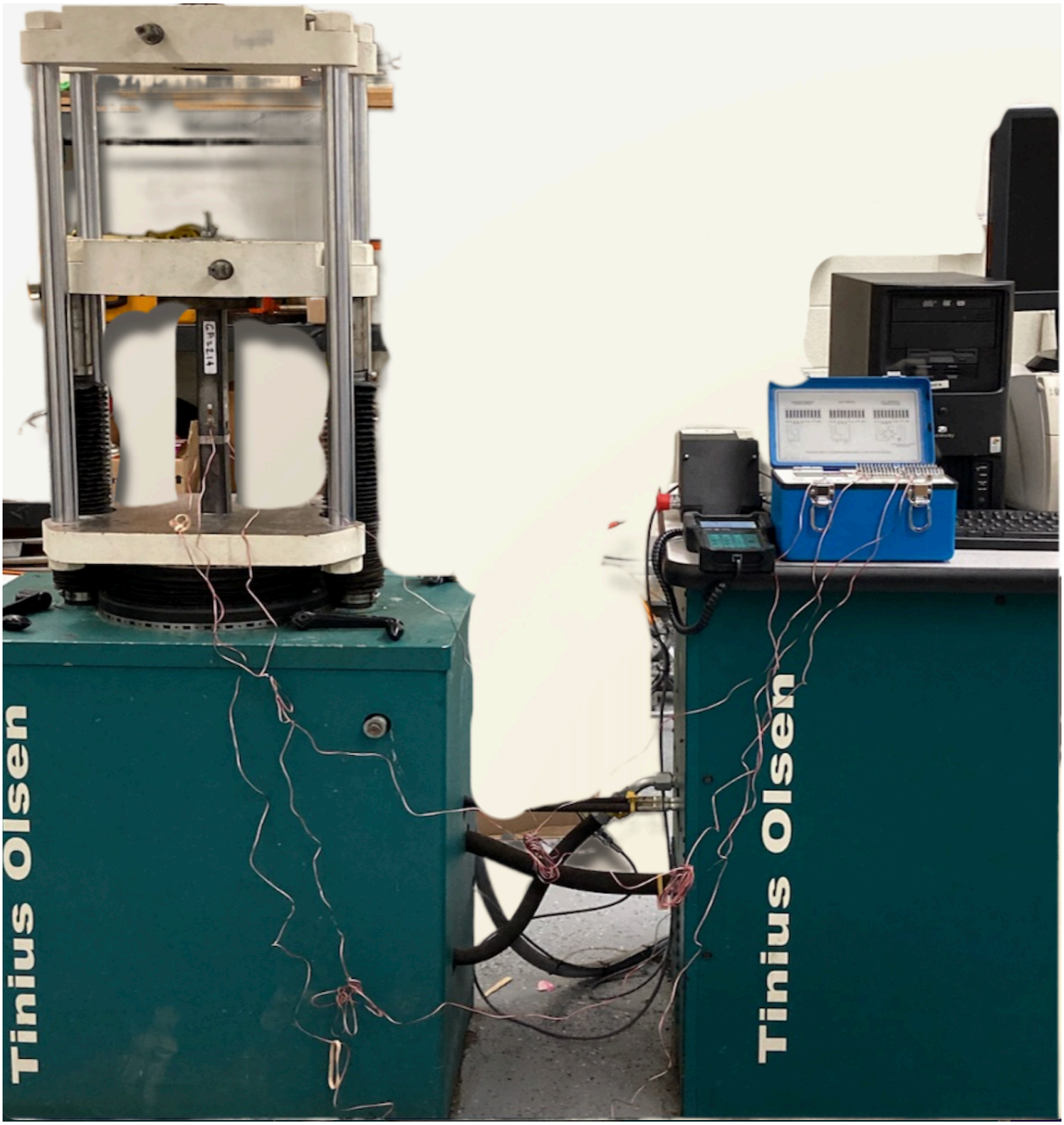

Figure 10.400K Capacity Tinius Olsen

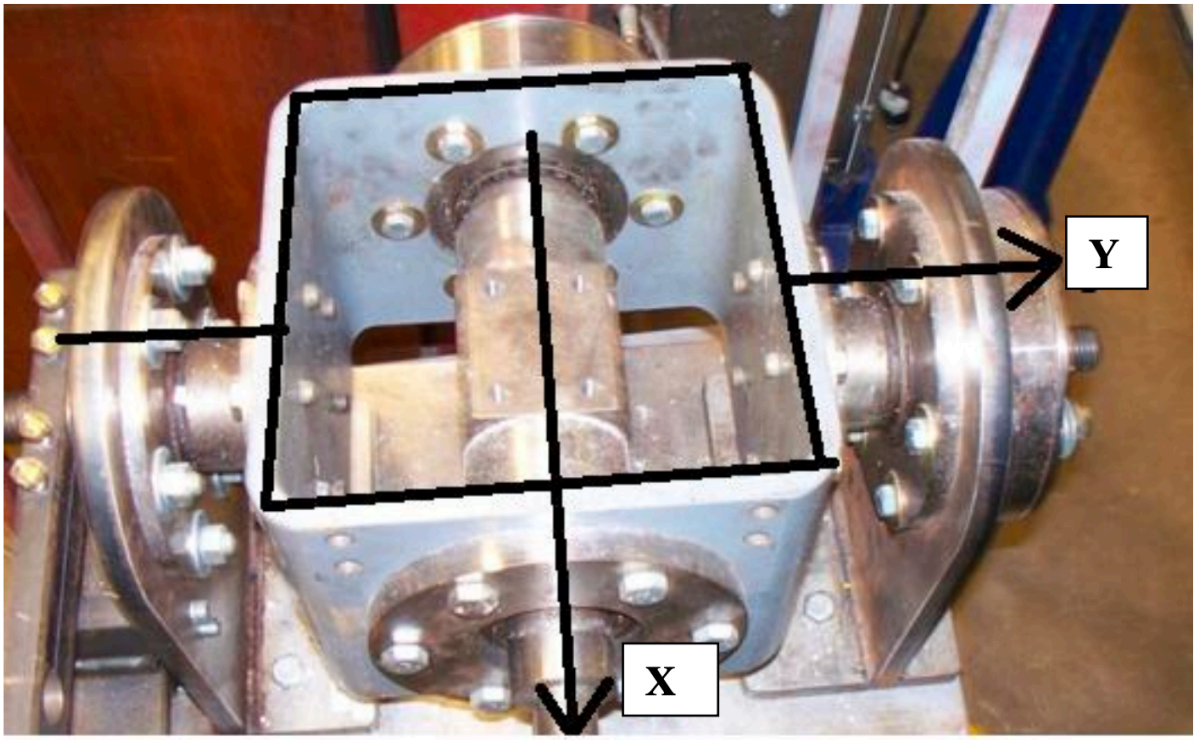

Figure 11.Lower Fixture Simulating Load and Moment Application

From reference [2]

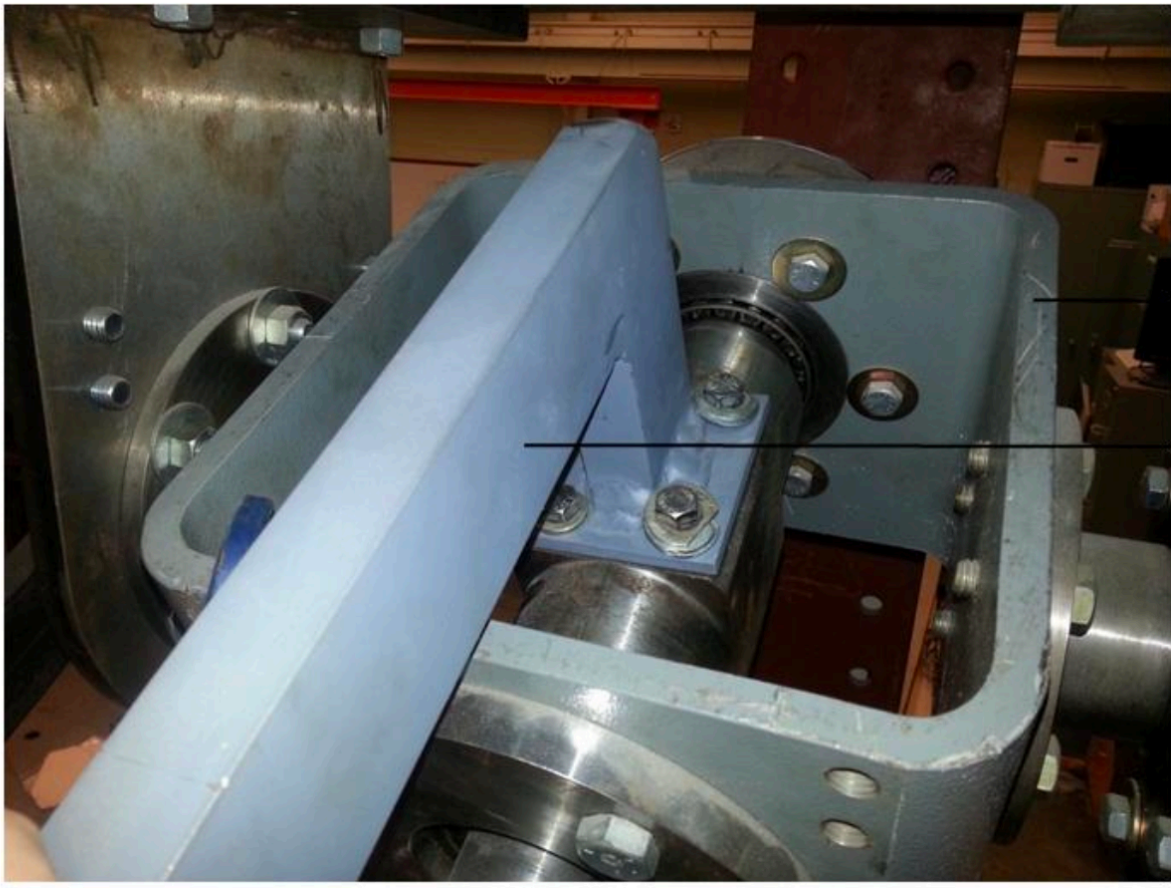

Figure 12.Upper Fixture Connected to a Moment Arm to Simulate Uniaxial and Biaxial Moment

From reference [2]

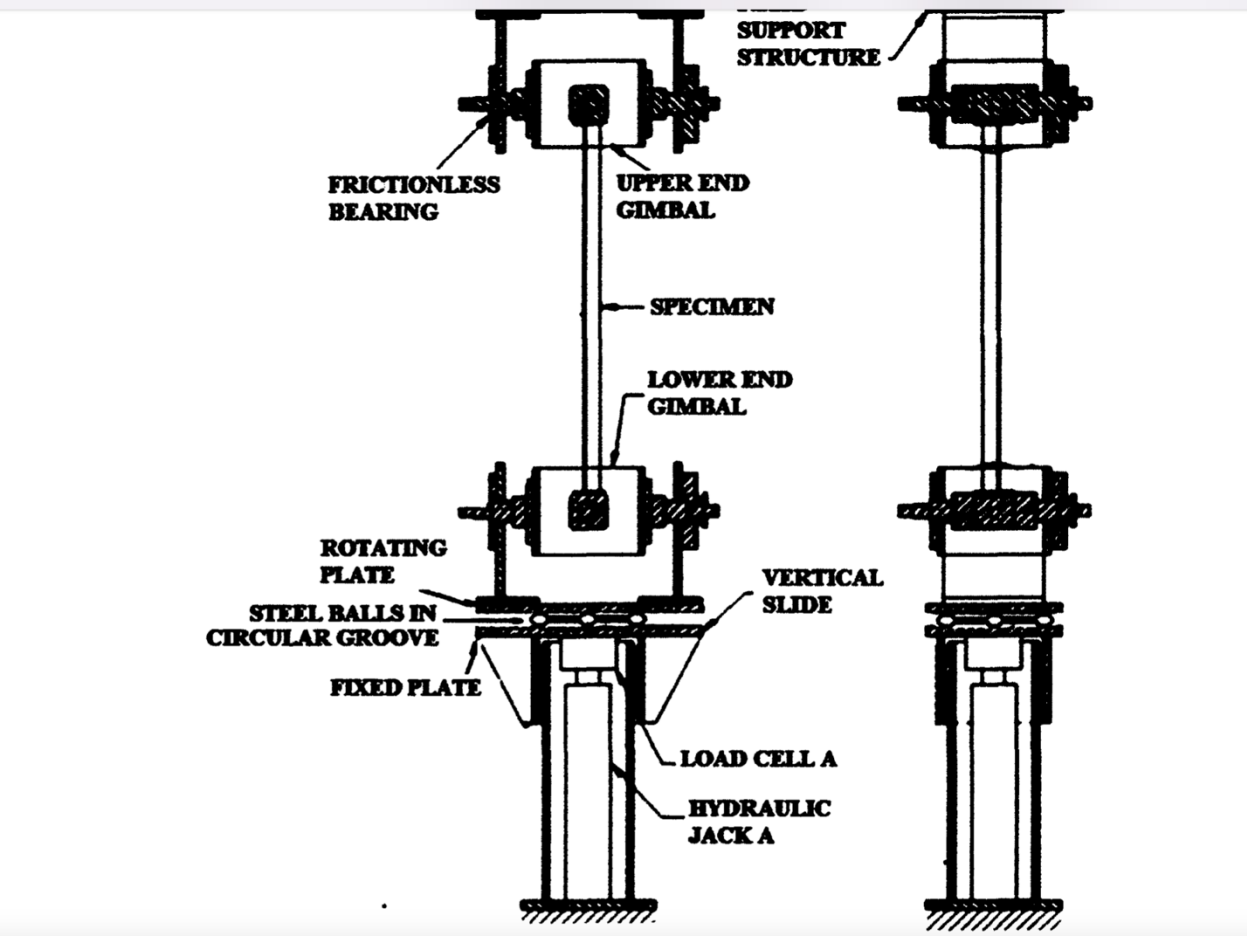

Figure 13.Biaxial and Torsional Moment Setup

From reference [3]

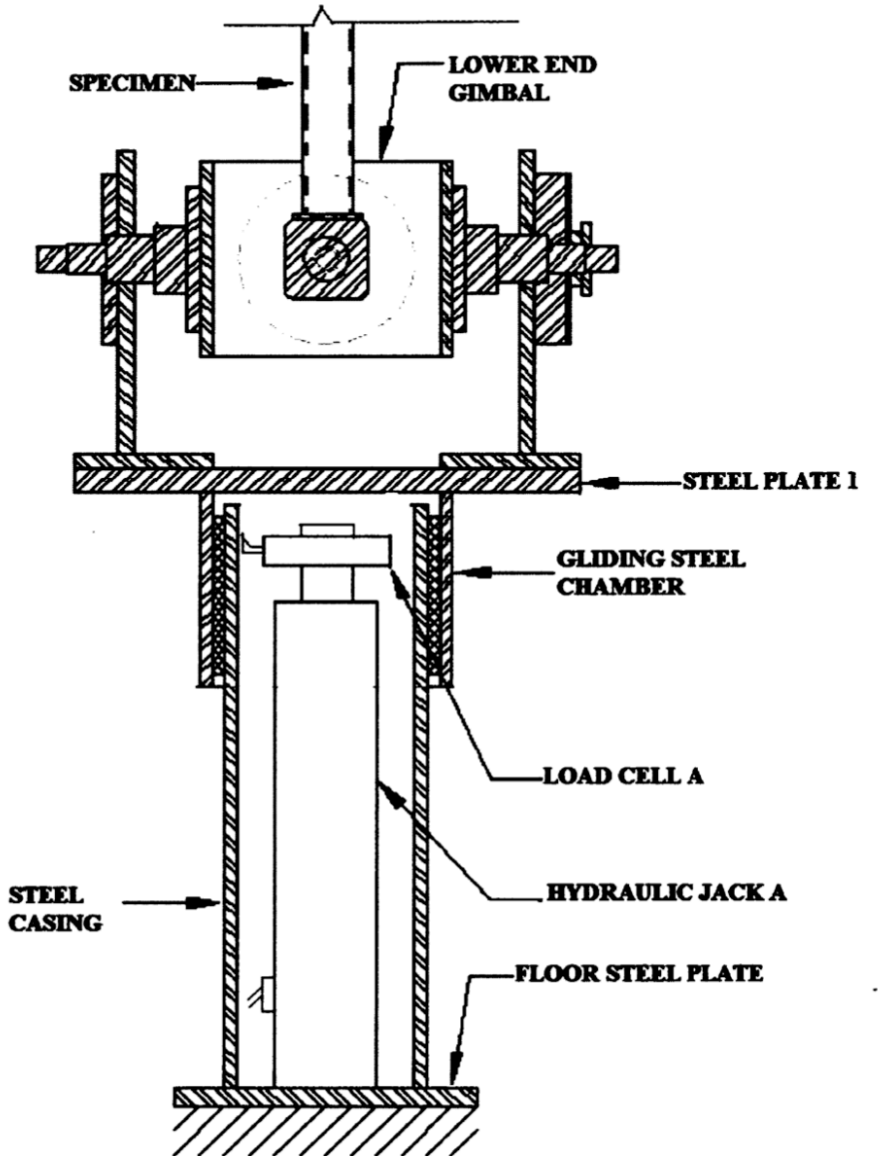

Figure 14.Schematic Diagram of Lower part of Axial and Bending Moment Setup

From Reference [3]

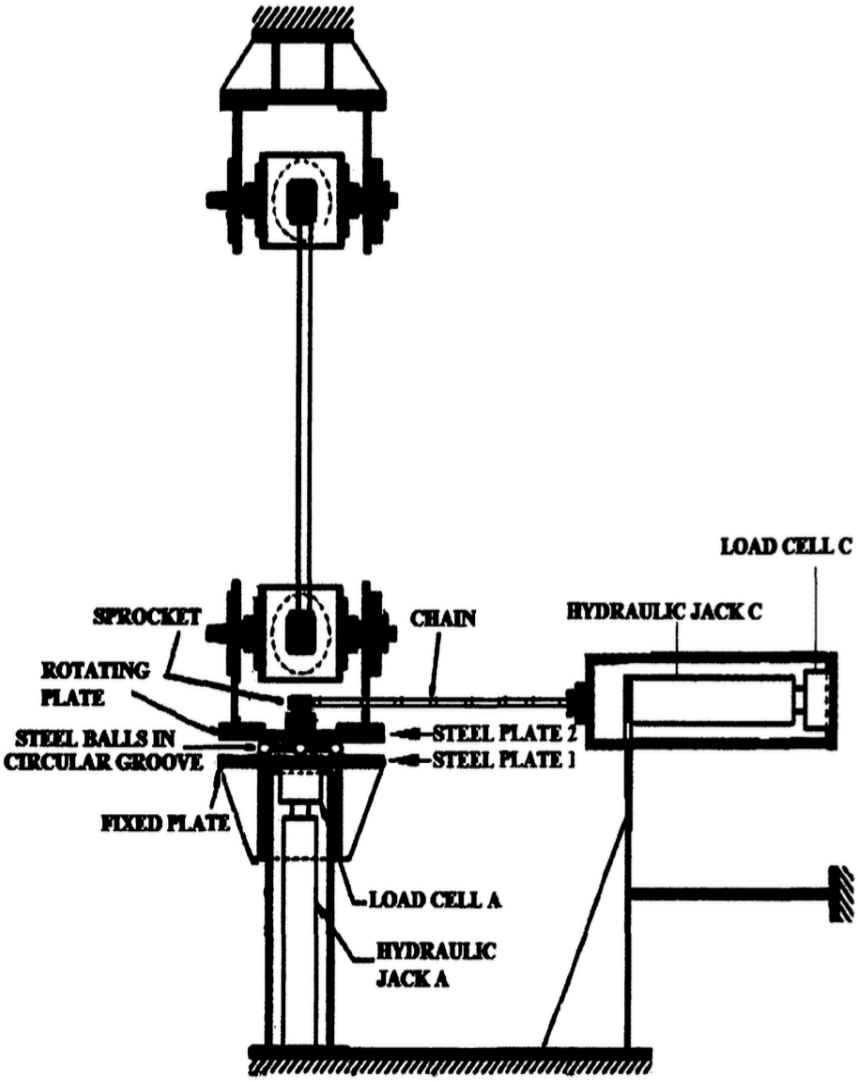

Figure 15.Axial, Bending and Torsion Setup Schematic Diagram

From reference [3]

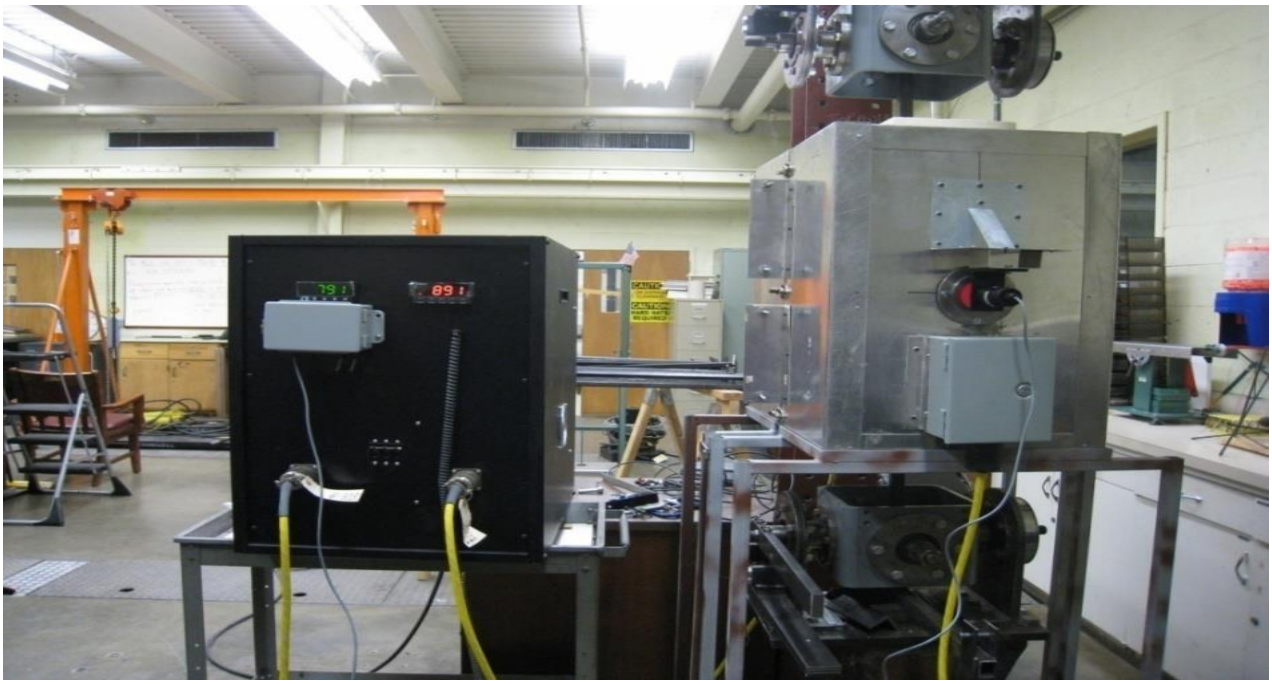

Figure 16.Electric Furnace and Controller

From reference [2]

Figure 17.A513 Type -1 Beam-Column Specimens

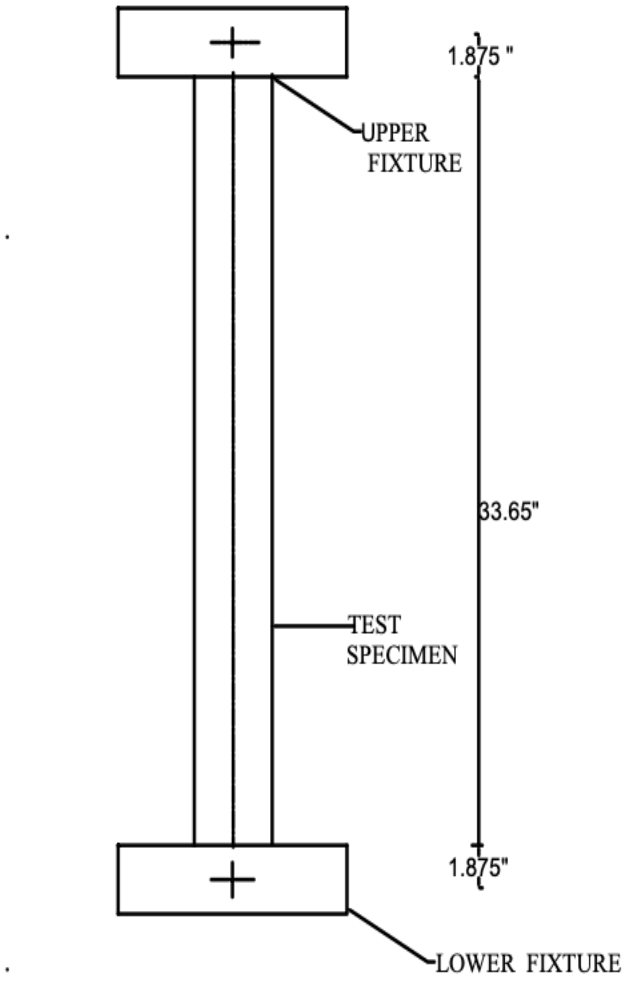

Figure 18.Schematic of Specimen End Fixtures

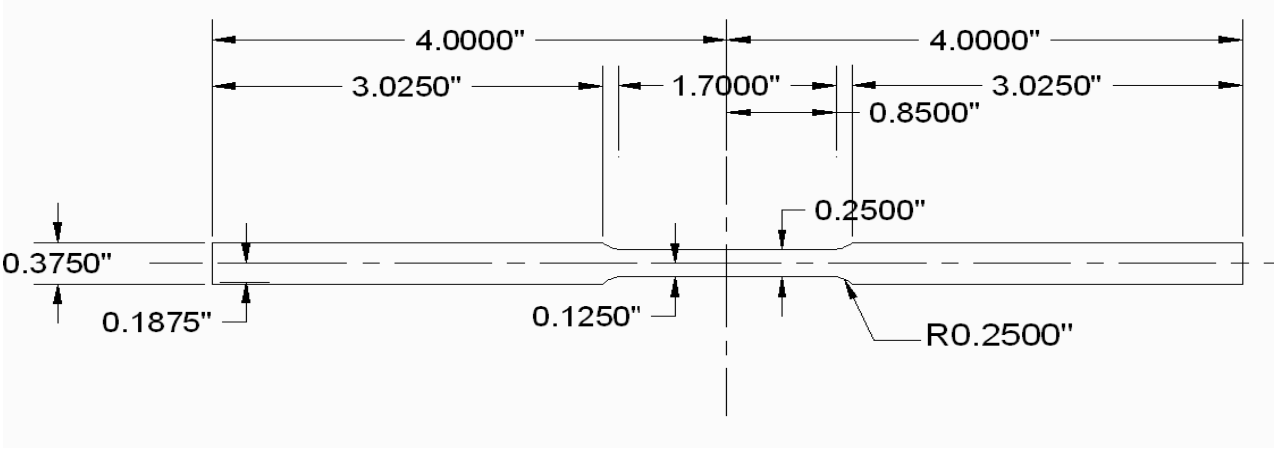

Figure 19.Tensile Coupon Specification

From reference [2]

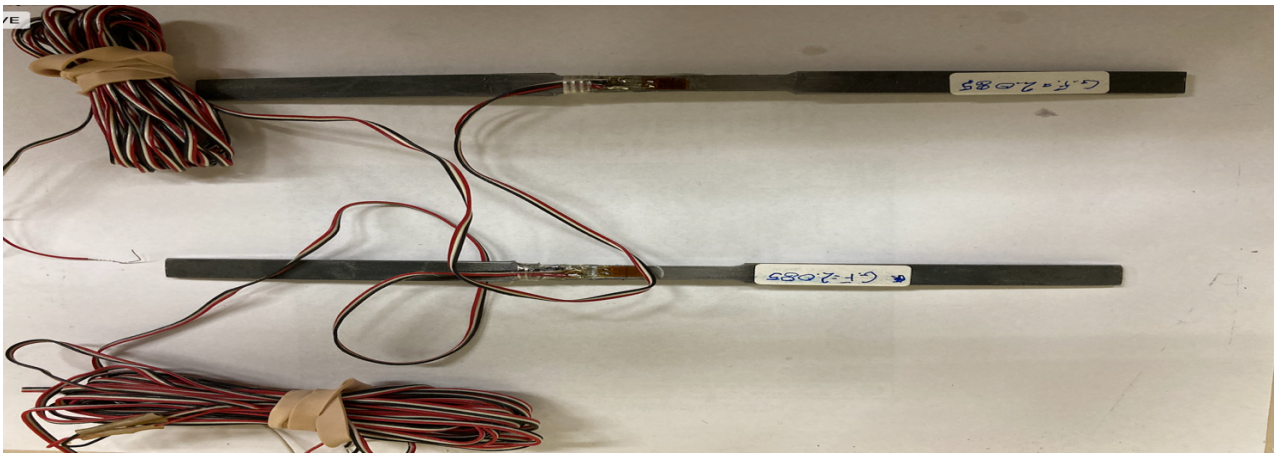

Figure 20.Tensile Coupon Specimens

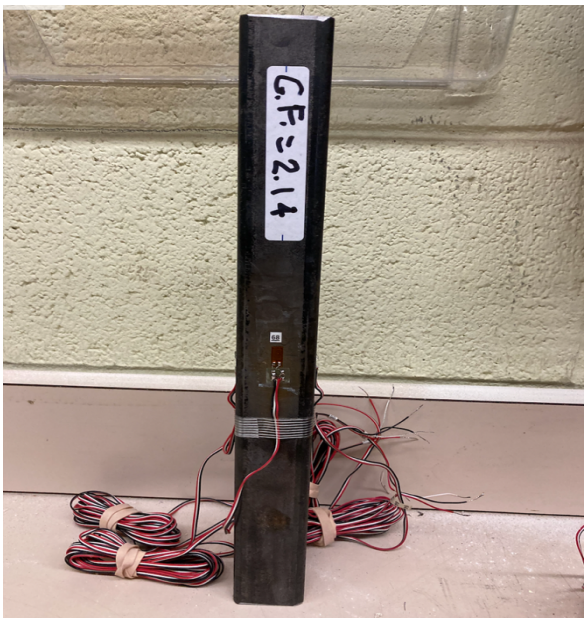

Figure 21.Stub Column Specimen

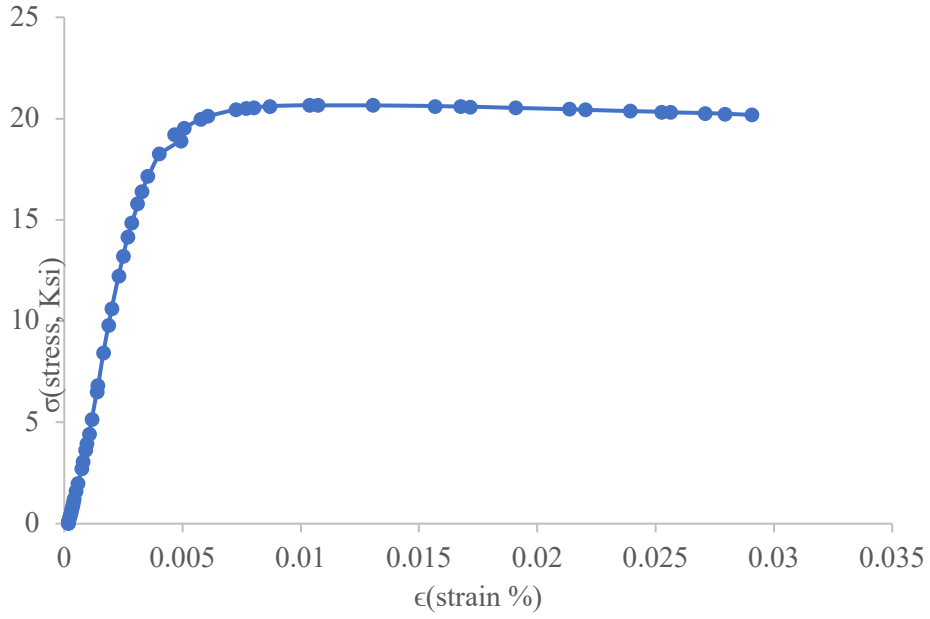

Figure 22.Stress-Strain Relationship for Stub Column Test

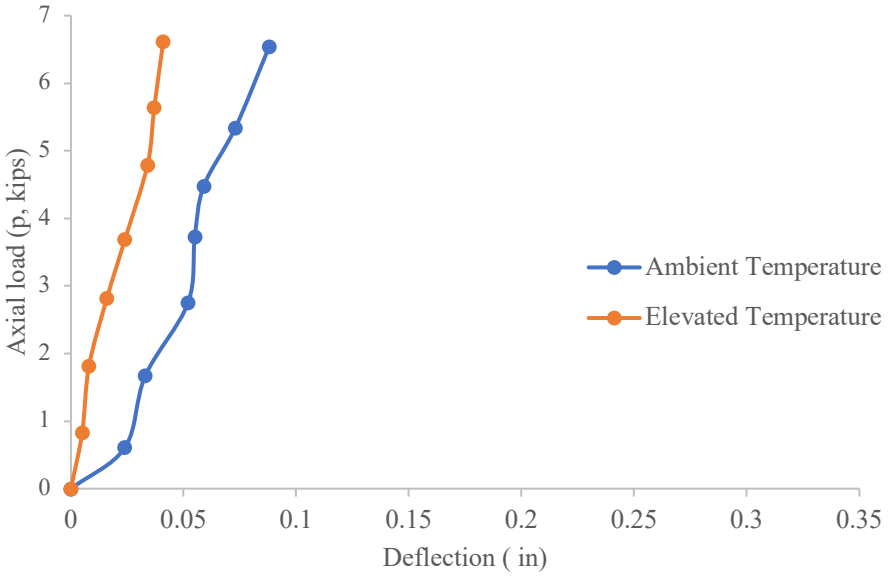

Figure 23. Experimental Curves for Axial load vs. Deflection (APT & HPT-Fixed-Pinned)

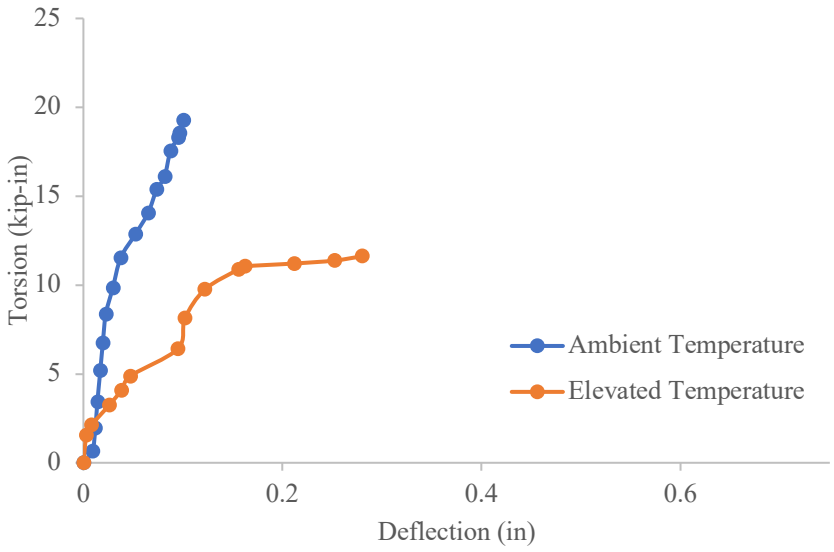

Figure 24. Experimental Curves for Torque vs. Deflection (APT & HPT-Fixed-Pinned)

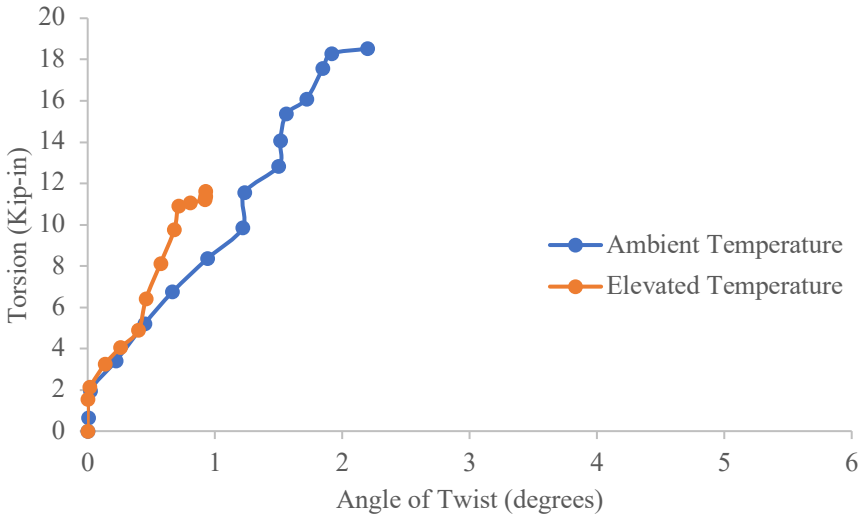

Figure 25. Experimental Curves for Torque vs. Angle of Twist (APT & HPT-Fixed-Pinned)

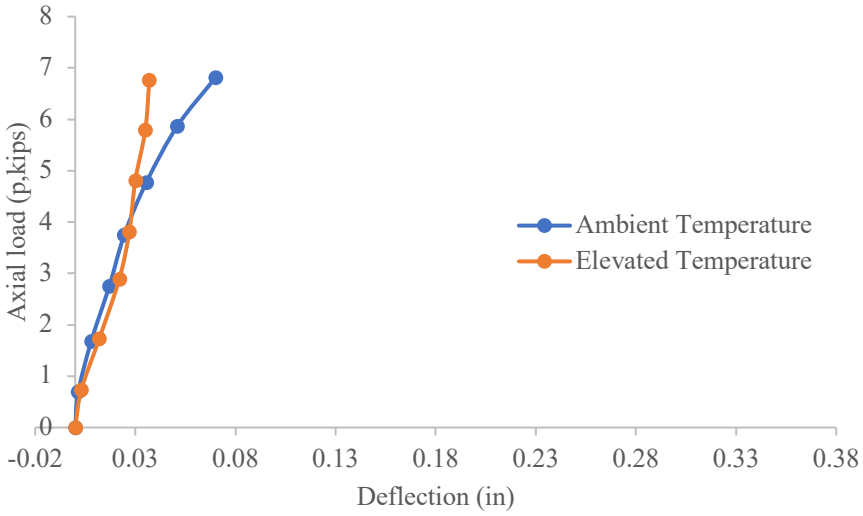

Figure 26. Experimental Curves for Axial load vs. Deflection (APT & HPT-Fixed-Fixed)

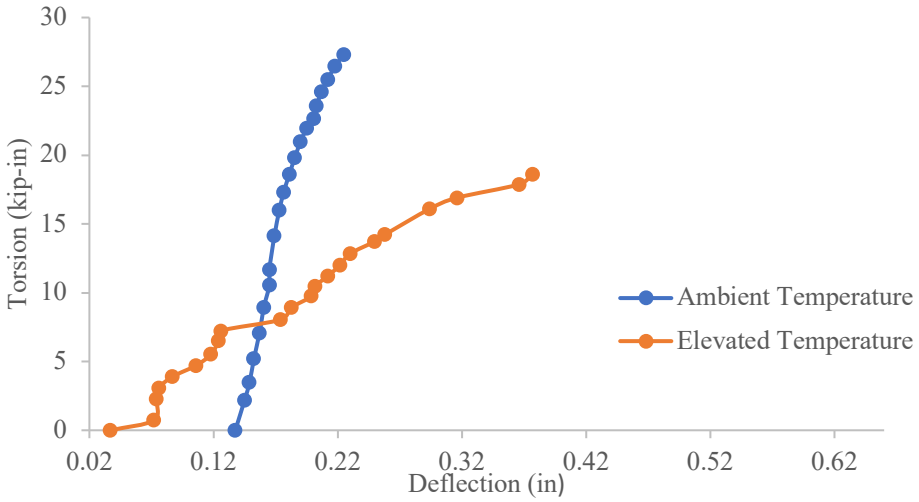

Figure 27. Experimental Curves for Torque vs. Deflection (APT & HPT-Fixed-Fixed)

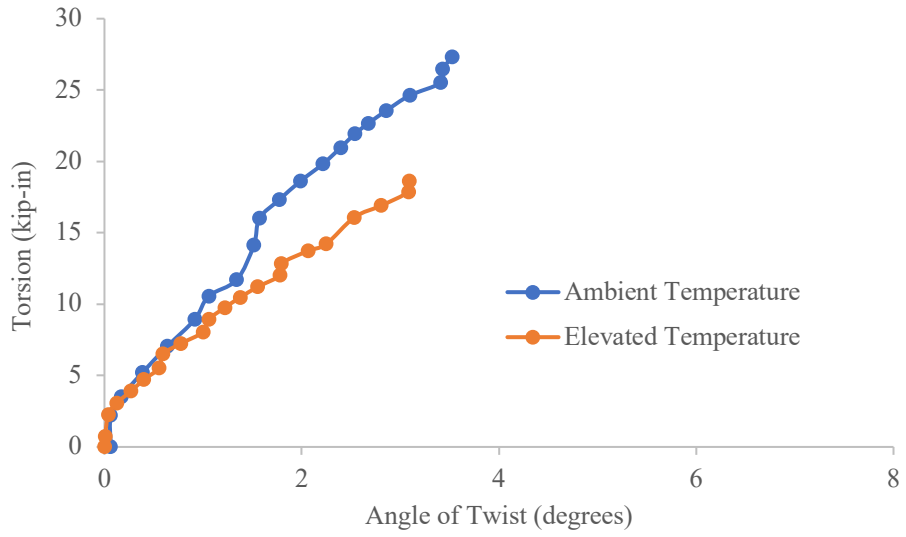

Figure 28. Experimental Curves for Torque vs. Angle of Twist (APT & HPT-Fixed-Fixed)

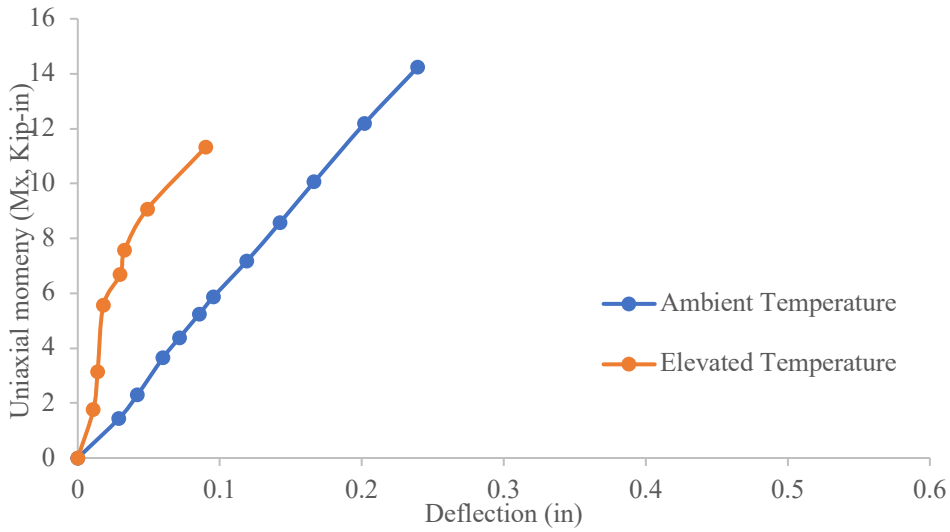

Figure 29. Experimental Curves for Moment vs. Deflection (AUT & HUT-Fixed-Pinned)

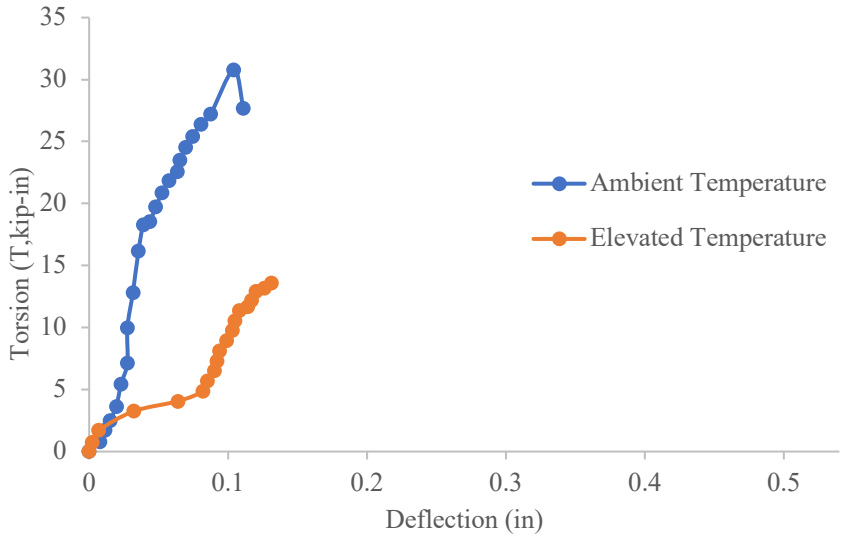

Figure 30. Experimental Curves for Torque vs. Deflection (AUT & HUT-Fixed-Pinned)

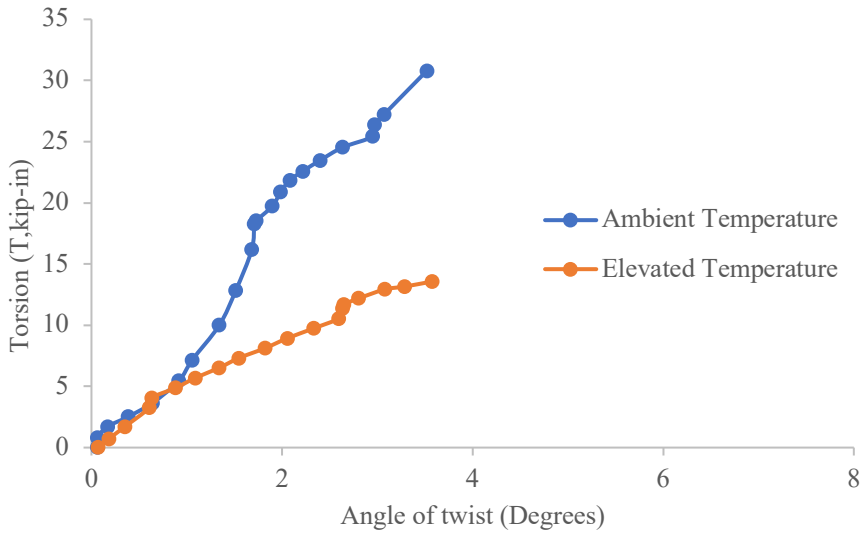

Figure 31. Experimental Curves for Torque vs. Angle of Twist (AUT & HUT-Fixed-Pinned)

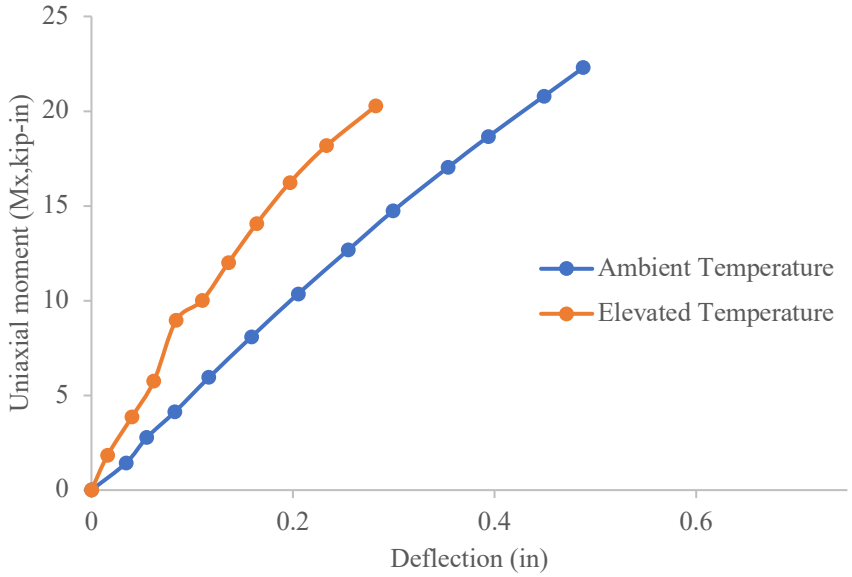

Figure 32. Experimental Curves for Moment vs. Deflection (AUT & HUT-Fixed-Partially Fixed)

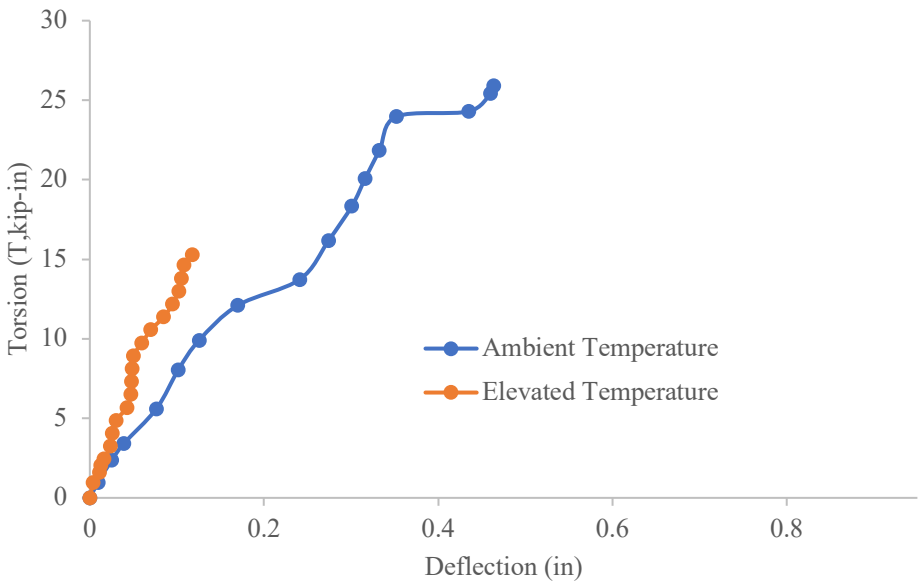

Figure 33. Experimental Curves for Torque vs. Deflection (AUT & HUT-Fixed-Partially Fixed)

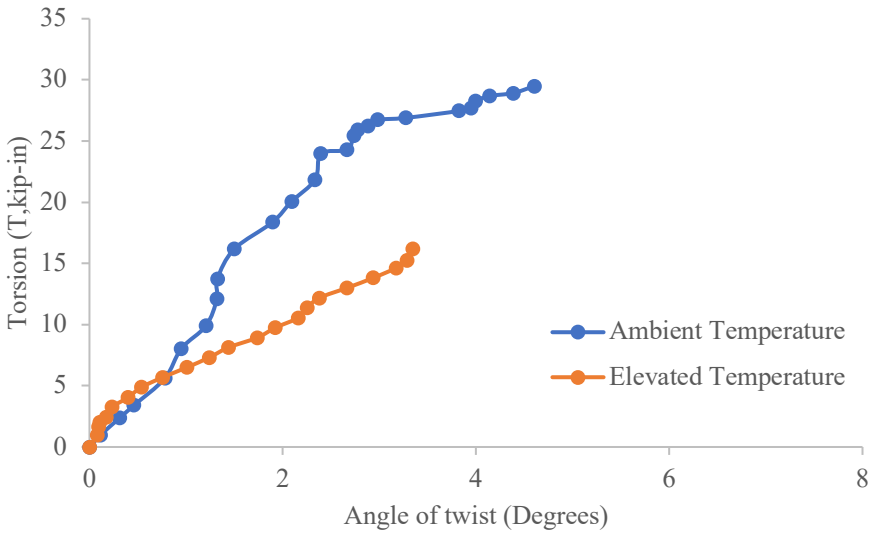

Figure 34. Experimental Curves for Torque vs. Angle of Twist (AUT & HUT-Fixed-Partially Fixed)

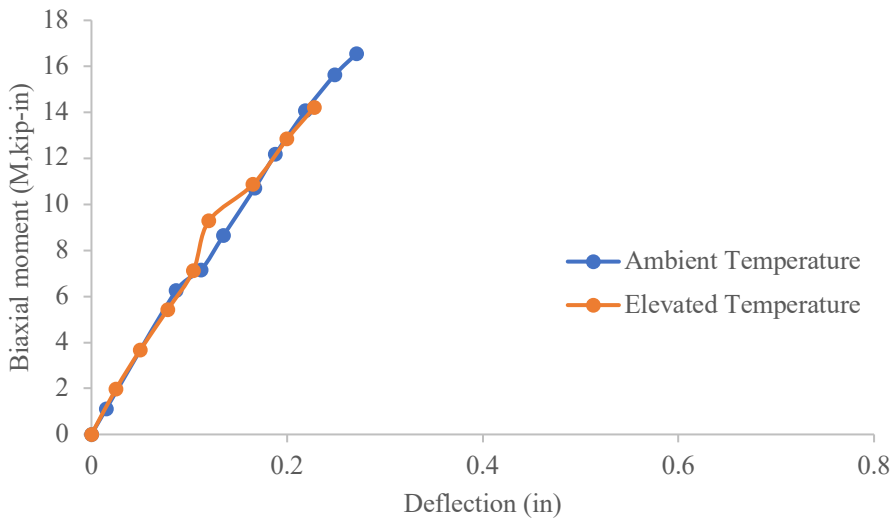

Figure 35. Experimental Curves for Moment vs. Deflection (ABT & HBT-Fixed-Partially Fixed)

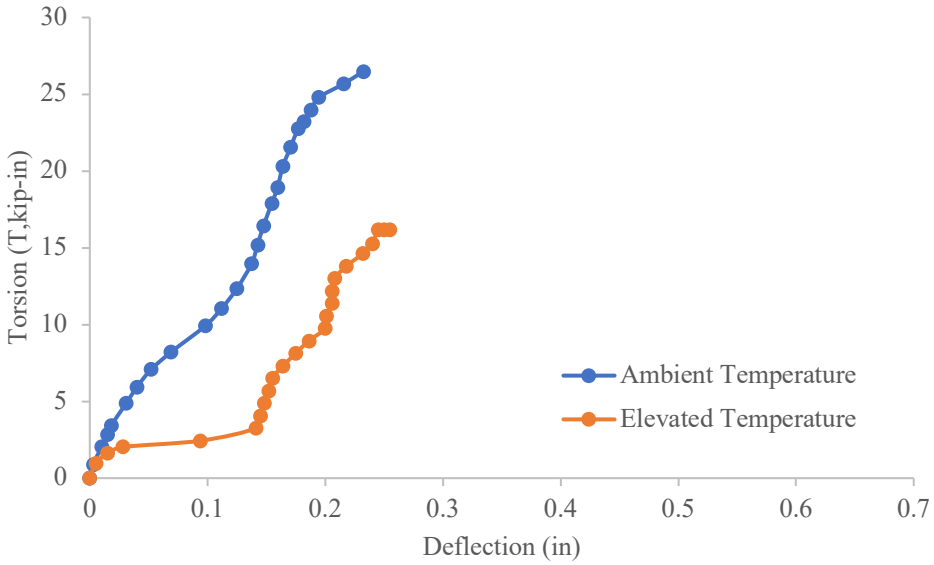

Figure 36. Experimental Curves for Torsion vs. Deflection (ABT & HBT-Fixed-Partially Fixed)

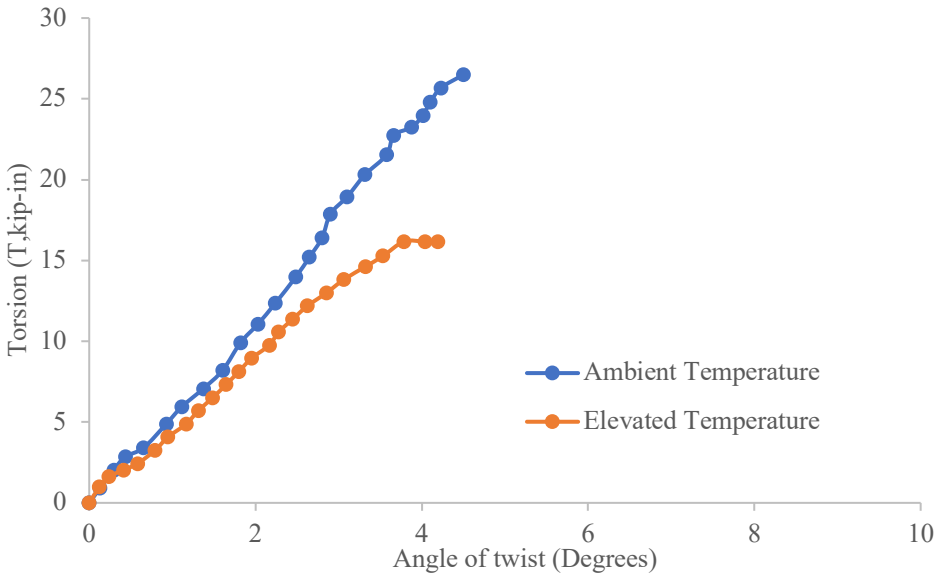

Figure 37. Experimental Curves for Torsion vs. Angle of Twist (ABT & HBT-Fixed-Partially Fixed)

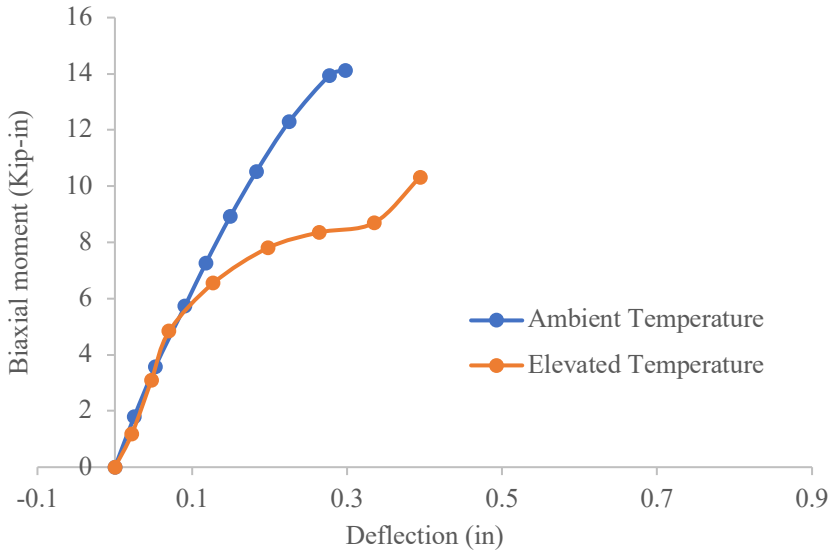

Figure 38. Experimental Curves for Biaxial Moment vs Deflection (ABT & HBT-Fixed-Partially Fixed)

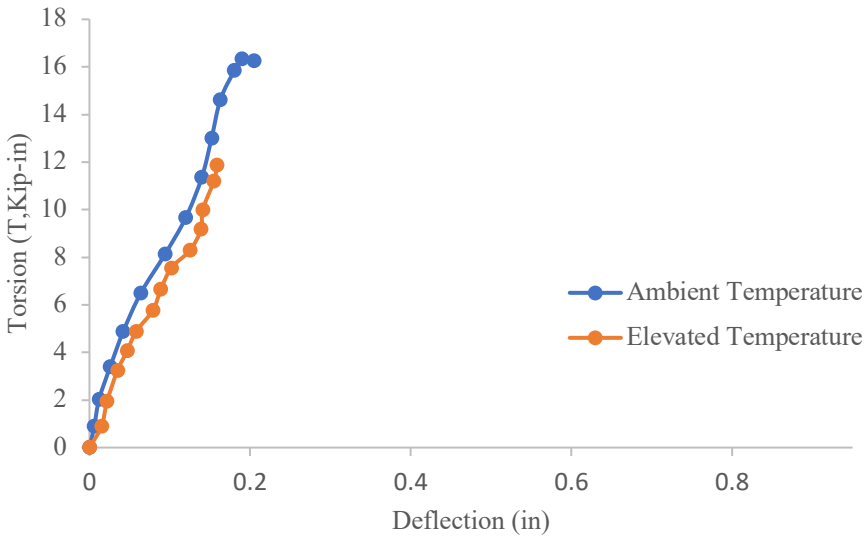

Figure 39. Experimental Curves for Torsion vs. Deflection (ABT & HBT-Fixed-Partially Fixed)

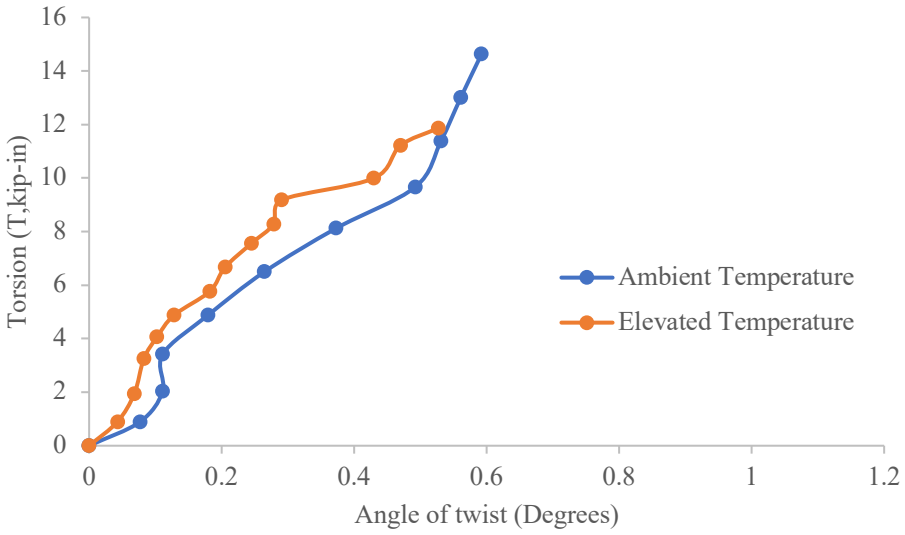

Figure 40. Experimental Curves for Torsion vs. Angle of Twist (ABT & HBT-Fixed-Partially Fixed)

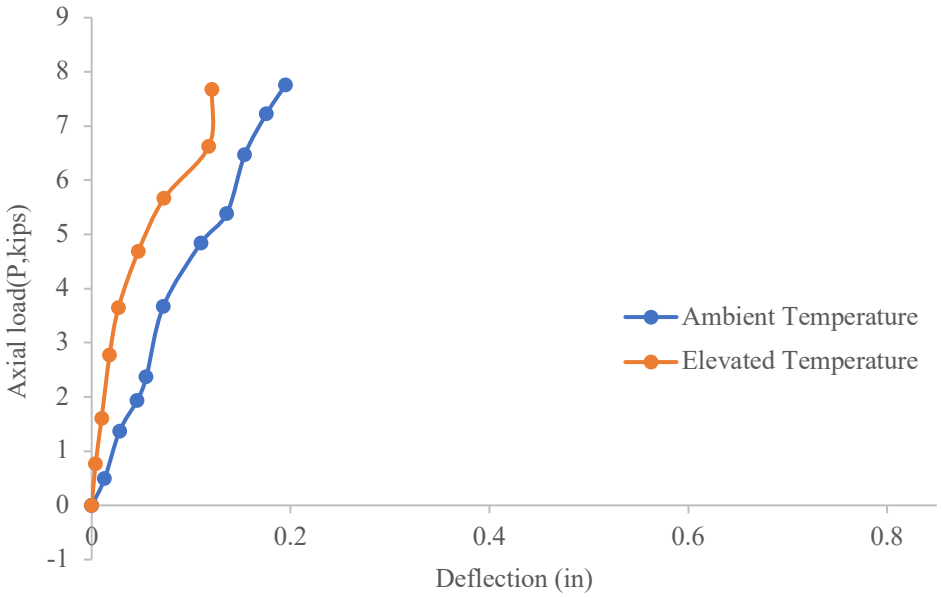

Figure 41. Experimental Curves for Axial load vs. Deflection (APT & HPT-Pinned-Pinned)

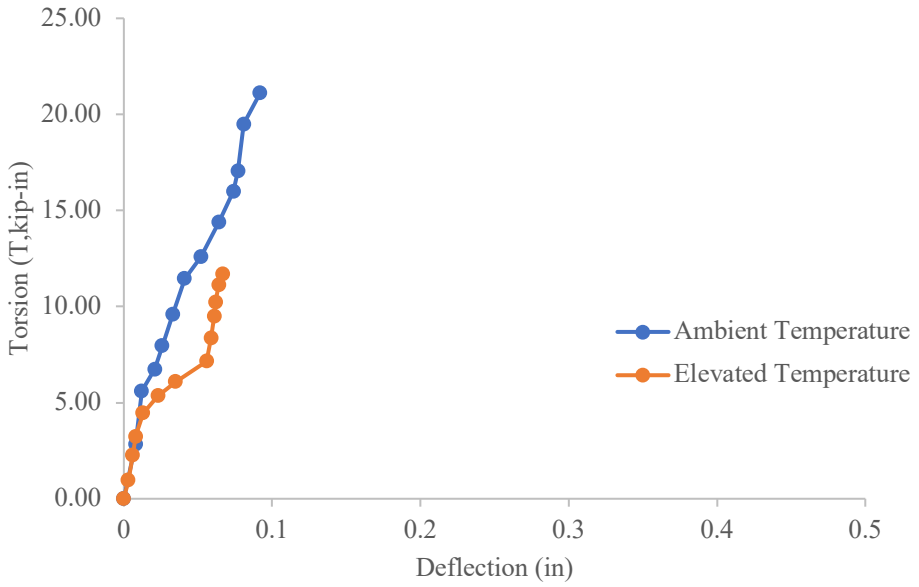

Figure 42. Experimental Curves for Torsion vs. Deflection (APT & HPT-Pinned-Pinned)

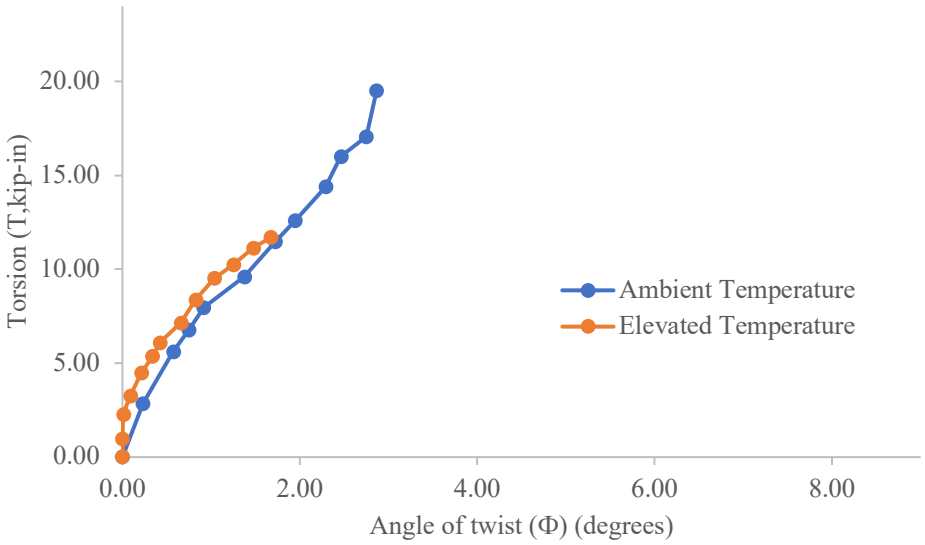

Figure 43. Experimental Curves for Torsion vs. Angle of Twist (APT & HPT-Pinned-Pinned)

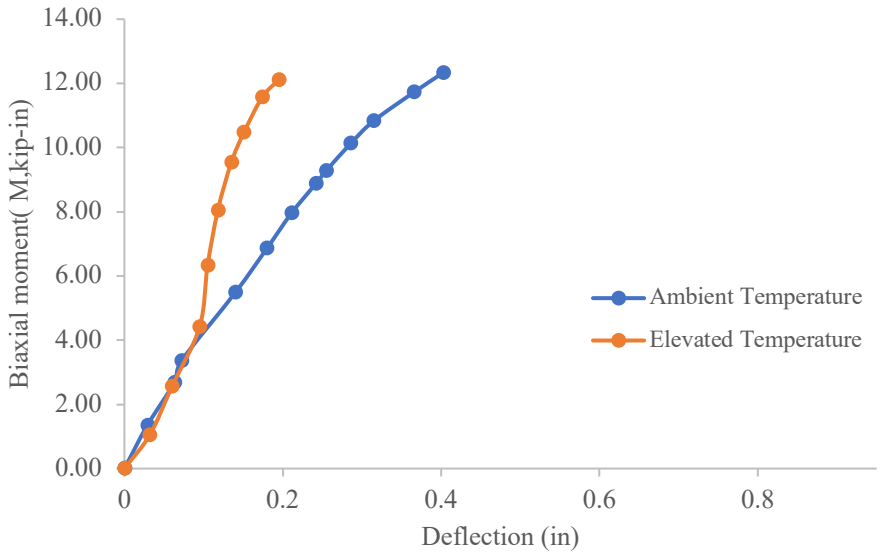

Figure 44. Experimental Curves for Biaxial Moment vs. Deflection (ABT & HBT-Pinned-Pinned)

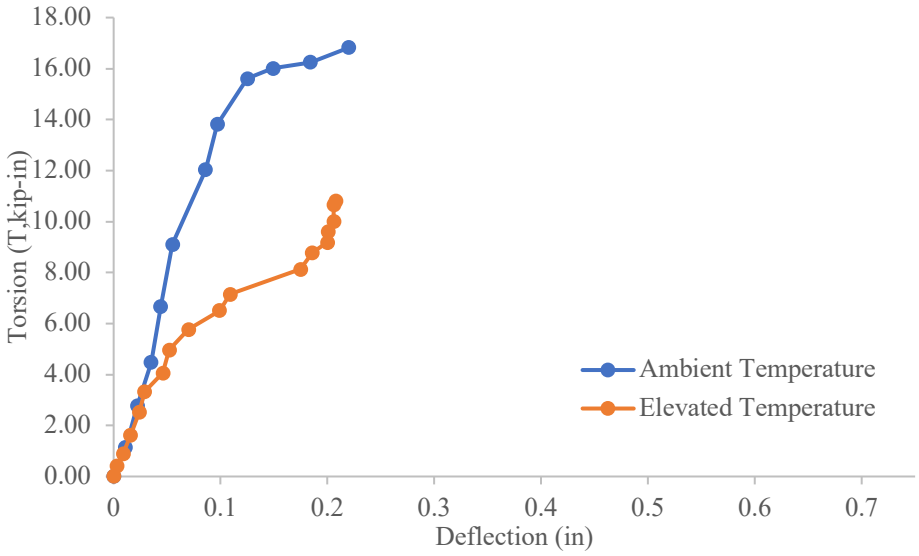

Figure 45. Experimental Curves for Torsion vs. Deflection (ABT & HBT-Pinned-Pinned)

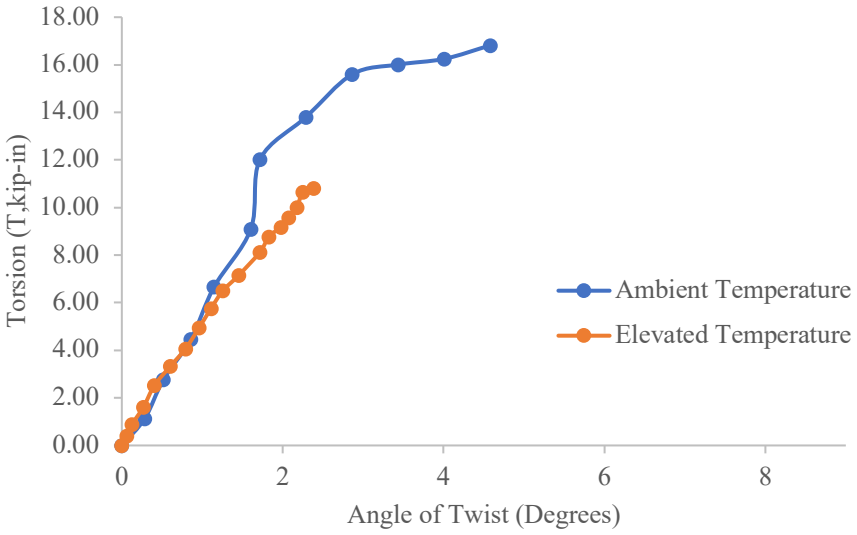

Figure 46. Experimental Curves for Torsion vs. Angle of Twist (ABT & HBT-Pinned-Pinned)

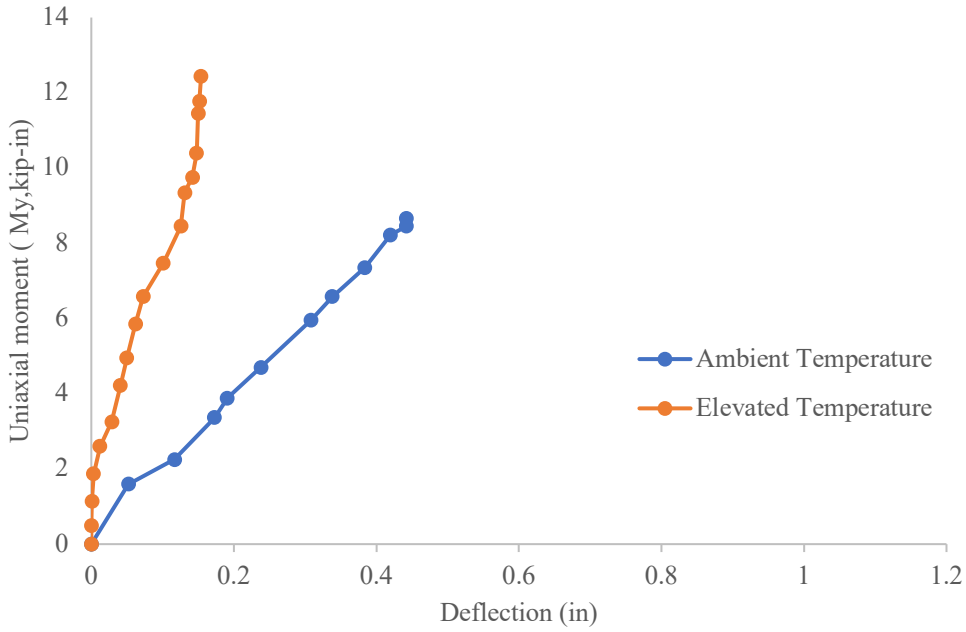

Figure 47. Experimental Curves for Moment vs. Deflection (AUT & HUT-Pinned-Pinned)

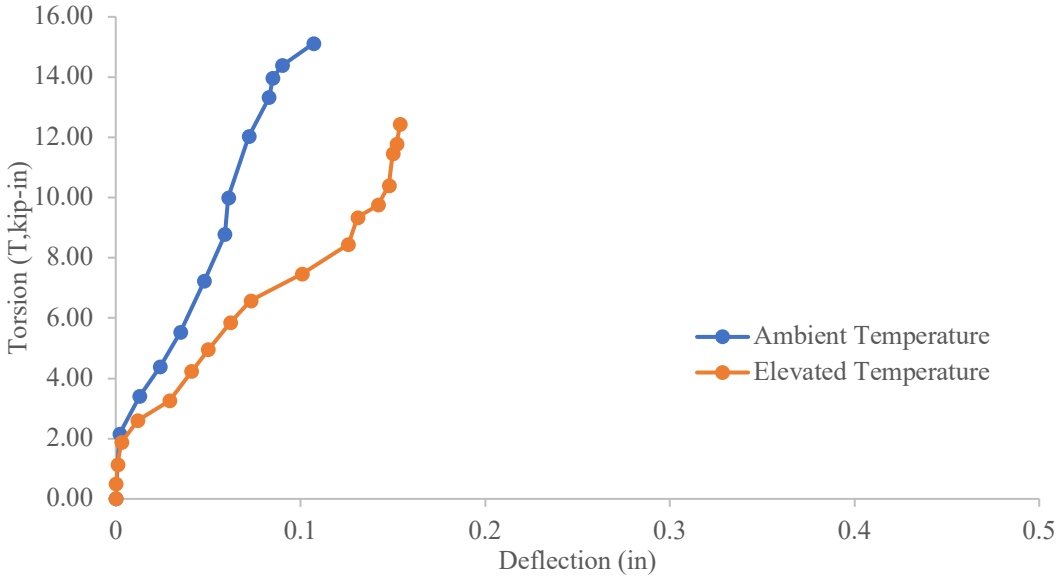

Figure 48. Experimental Curves for Torsion vs. Deflection (AUT & HUT-Pinned-Pinned)

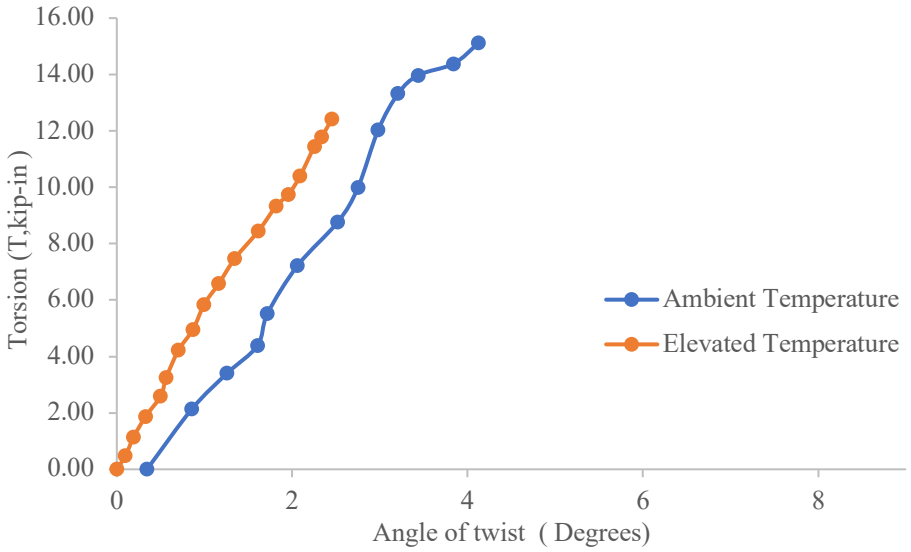

Figure 49. Experimental Curves for Torsion vs. Angle of Twist (AUT & HUT-Pinned-Pinned)

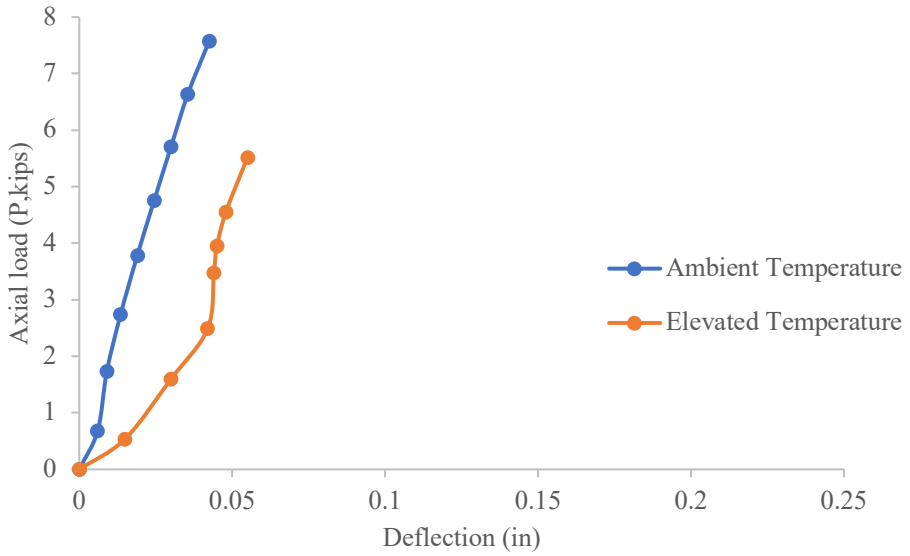

Figure 50. Experimental Curves for Axial Load vs. Deflection (APUT & HPUT-Pinned-Pinned)

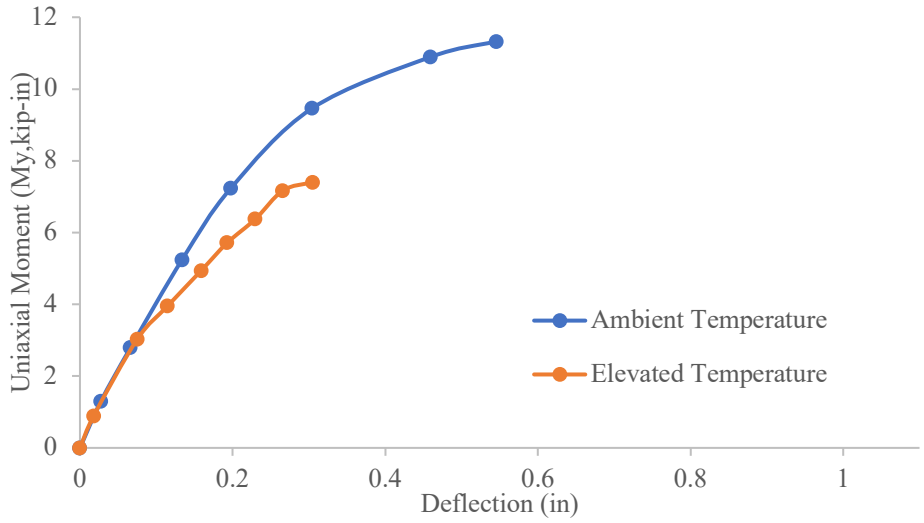

Figure 51. Experimental Curves for Uniaxial Moment vs. Deflection (APUT & HPUT-Pinned-Pinned)

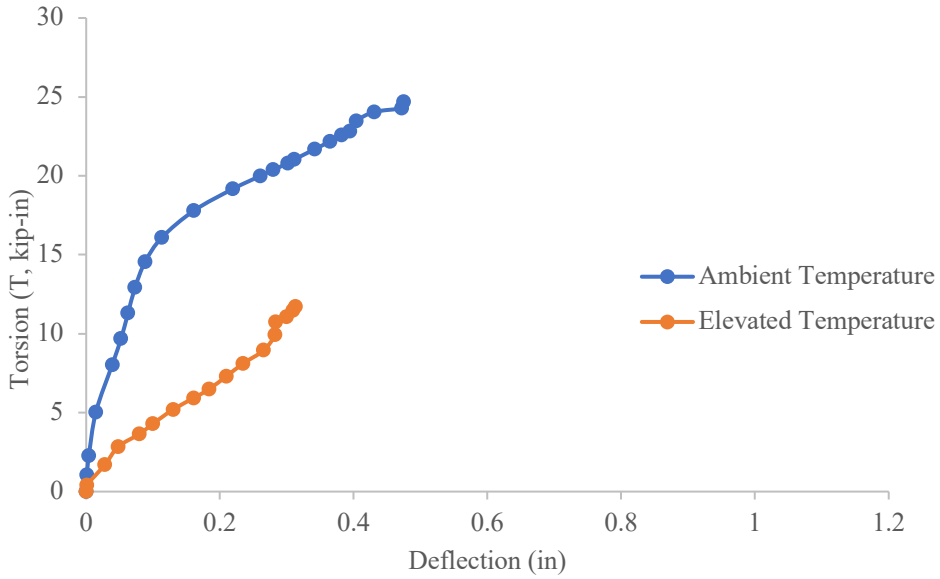

Figure 52. Experimental Curves for Torsion vs. Deflection (APUT & HPUT-Pinned-Pinned)

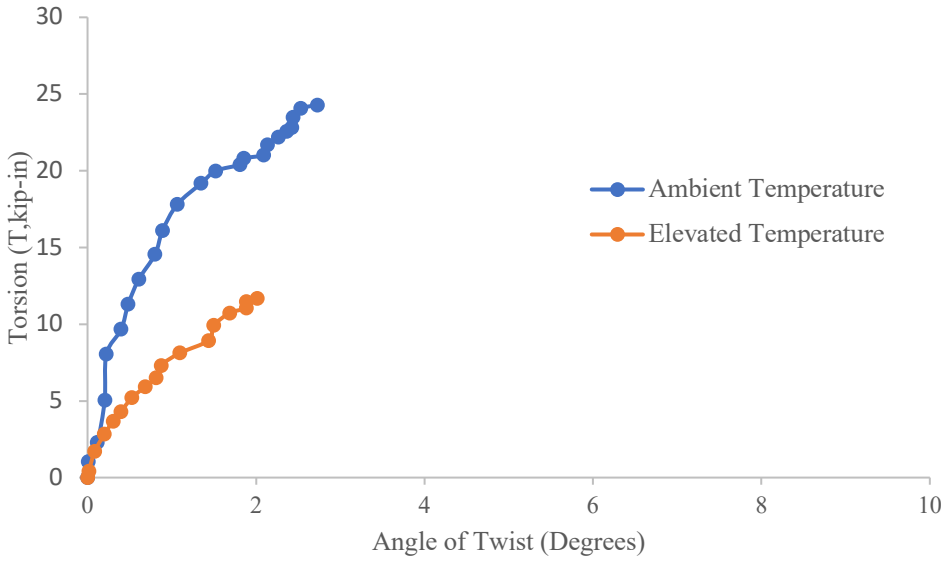

Figure 53. Experimental Curves for Torsion vs. Angle of Twist (APUT & HPUT-Pinned - Pinned)

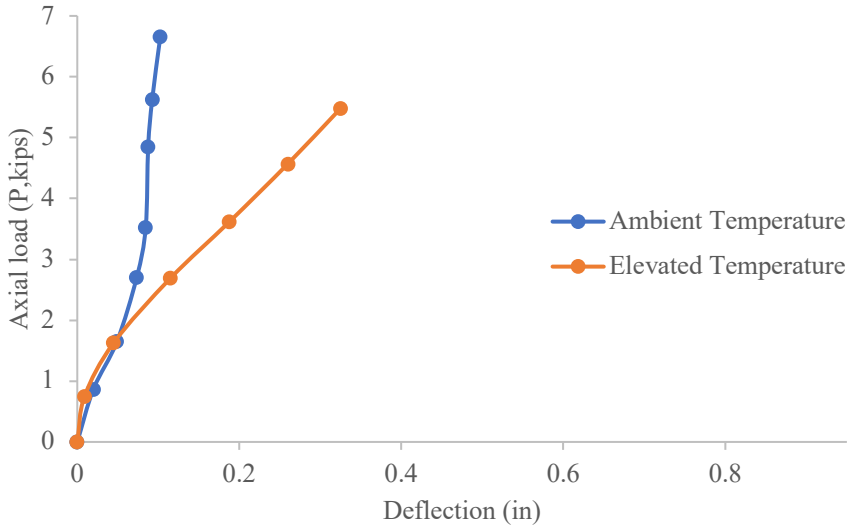

Figure 54. Experimental Curves for Axial load vs. Deflection (APUT & HPUT-Fixed-Pinned)

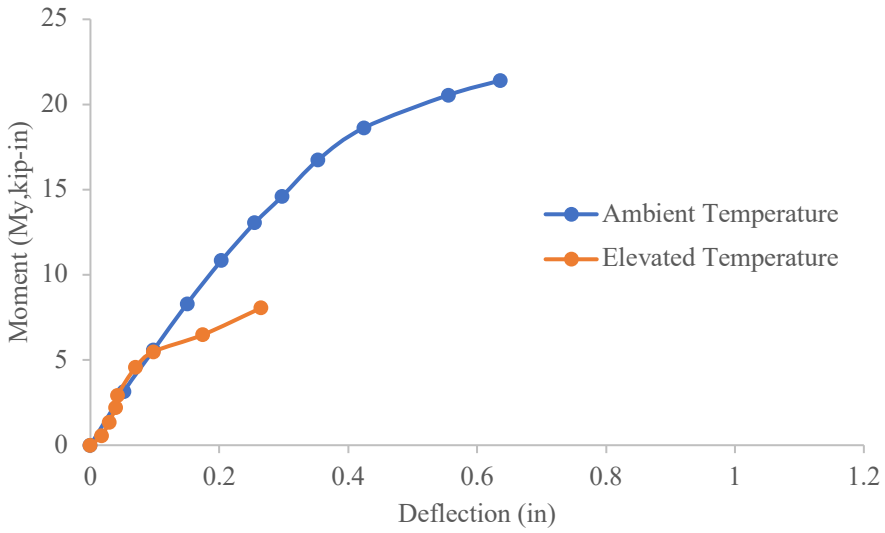

Figure 55. Experimental Curves for Uniaxial Moment vs. Deflection (APUT & HPUT-Fixed-Pinned)

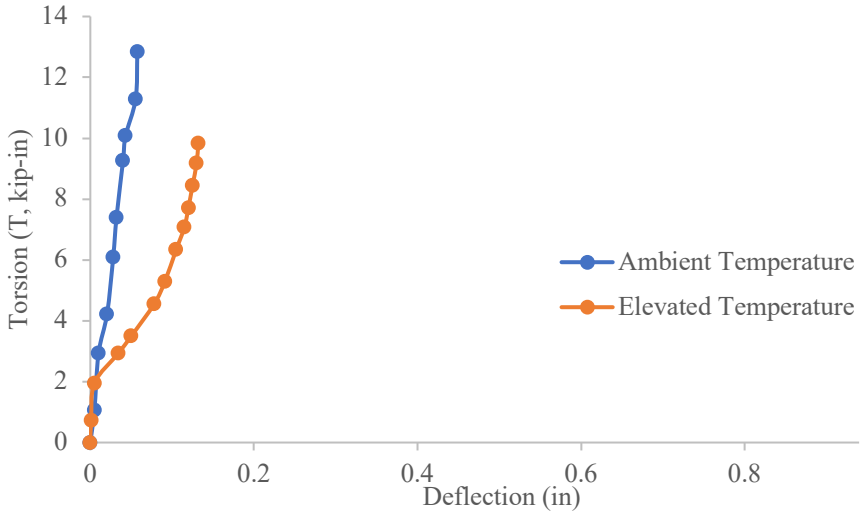

Figure 56. Experimental Curves for Torsion vs. Deflection (APUT & HPUT-Fixed-Pinned)

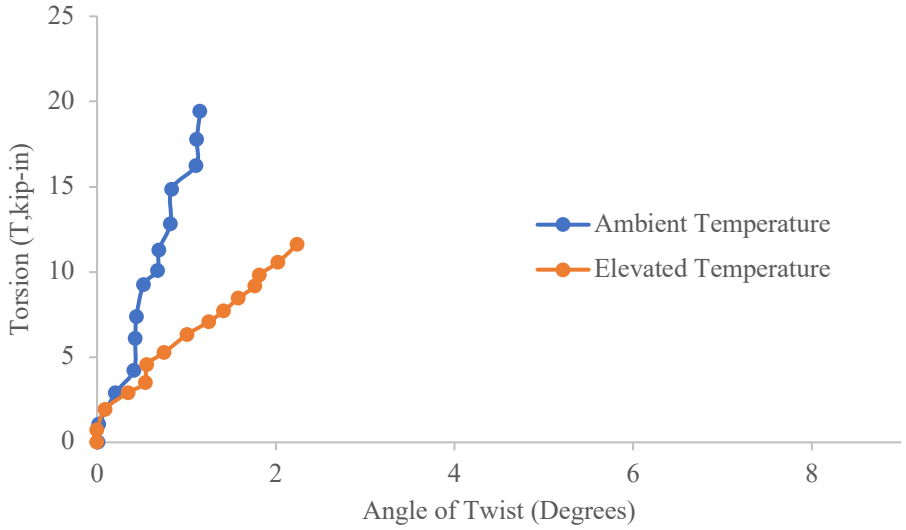

Figure 57. Experimental Curves for Torsion vs. Angle of Twist (APUT & HPUT-Fixed-Pinned)

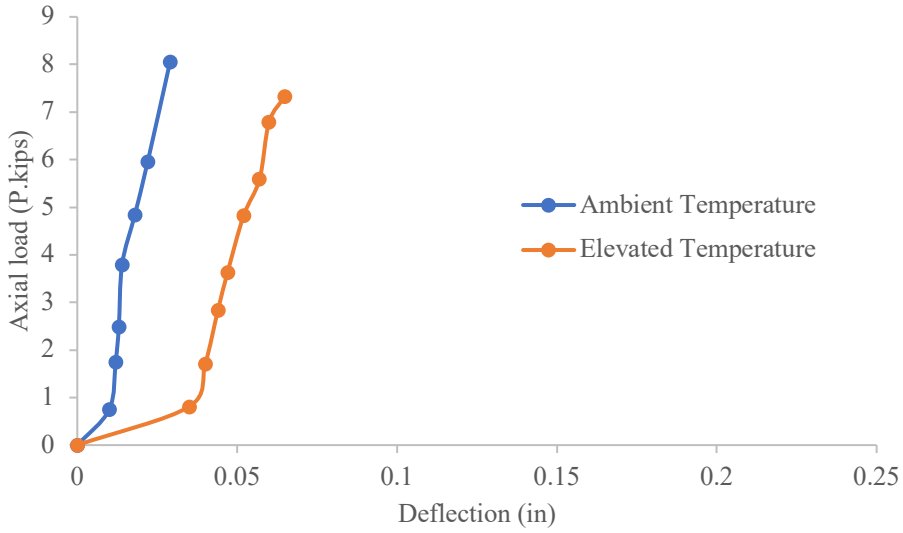

Figure 58. Experimental Curves for Axial Load vs. Deflection (APBT & HPBT-Fixed-Pinned)

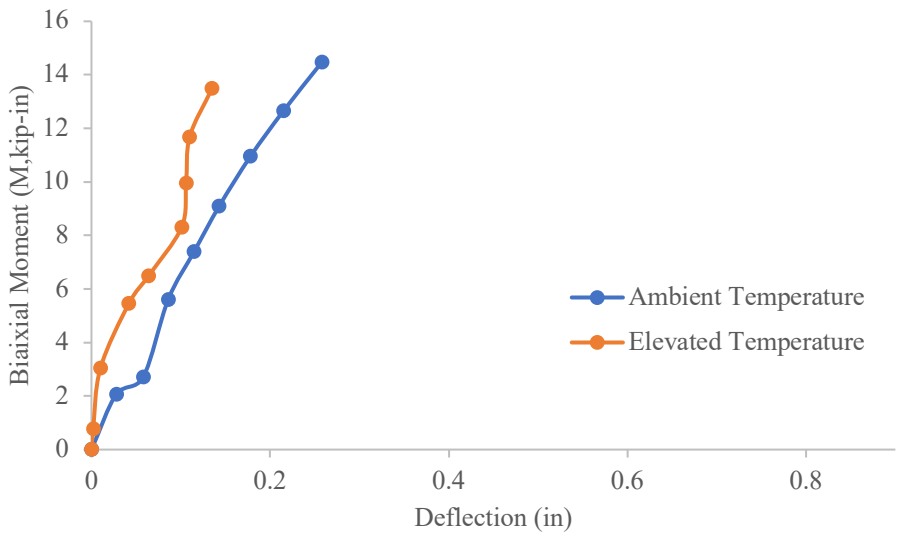

Figure 59. Experimental Curves for Biaxial Moment vs. Deflection (APBT & HPBT-Fixed-Pinned)

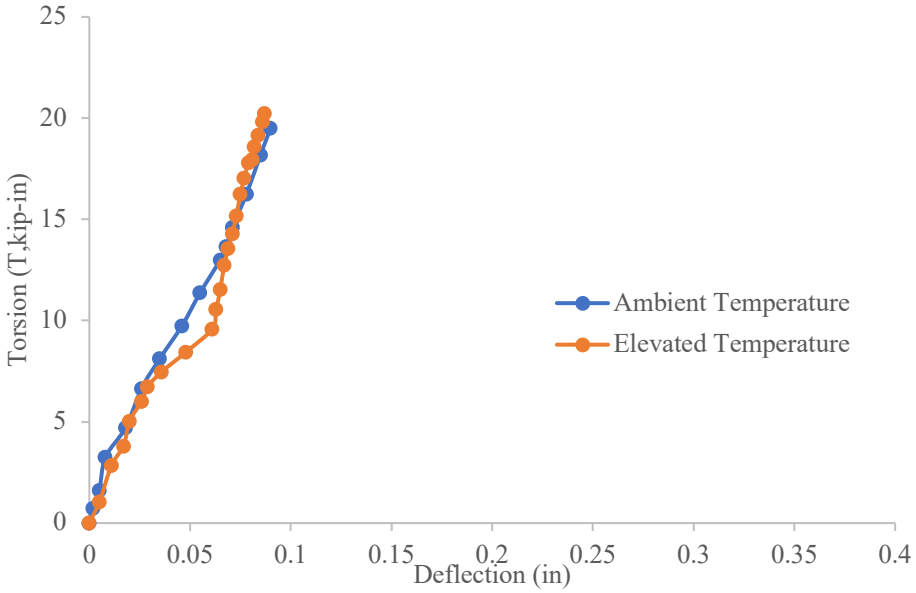

Figure 60. Experimental Curves for Torsion vs. Deflection (APBT & HPBT-Fixed-Pinned)

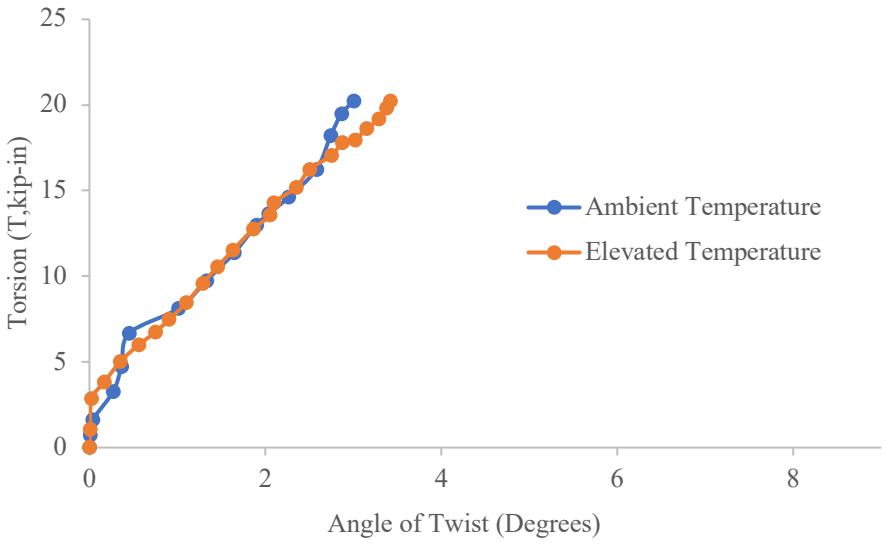

Figure 61. Experimental Curves for Torsion vs. Deflection (APBT & HPBT-Fixed-Pinned)

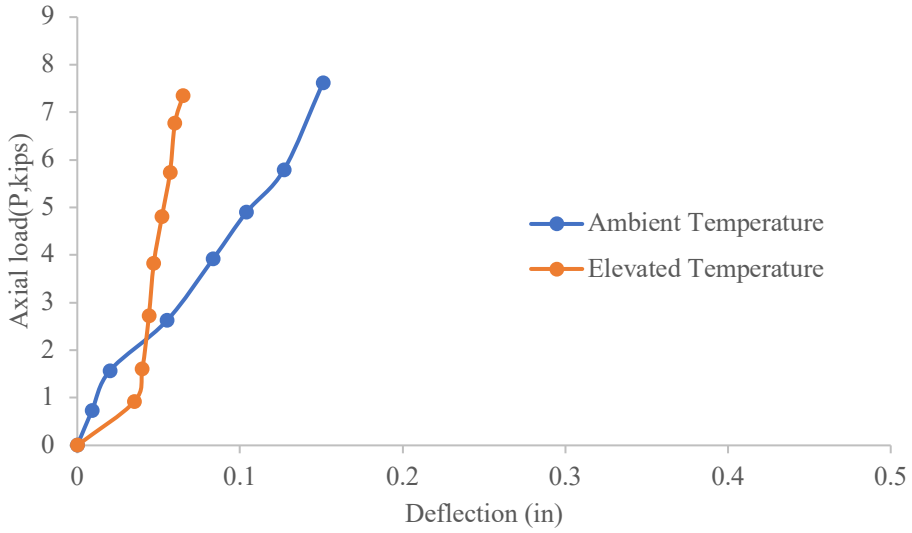

Figure 62. Experimental Curves for Axial Load vs. Deflection (APBT & HPBT-Fixed-Partially Fixed)

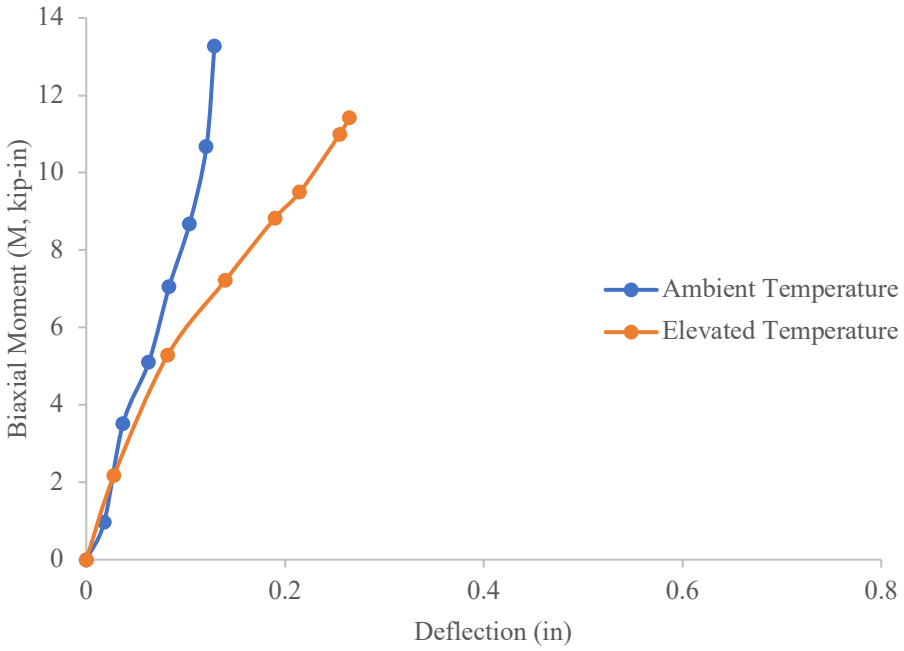

Figure 63. Experimental Curves for Biaxial Moment vs Deflection (APBT & HPBT-Fixed-Partially Fixed)

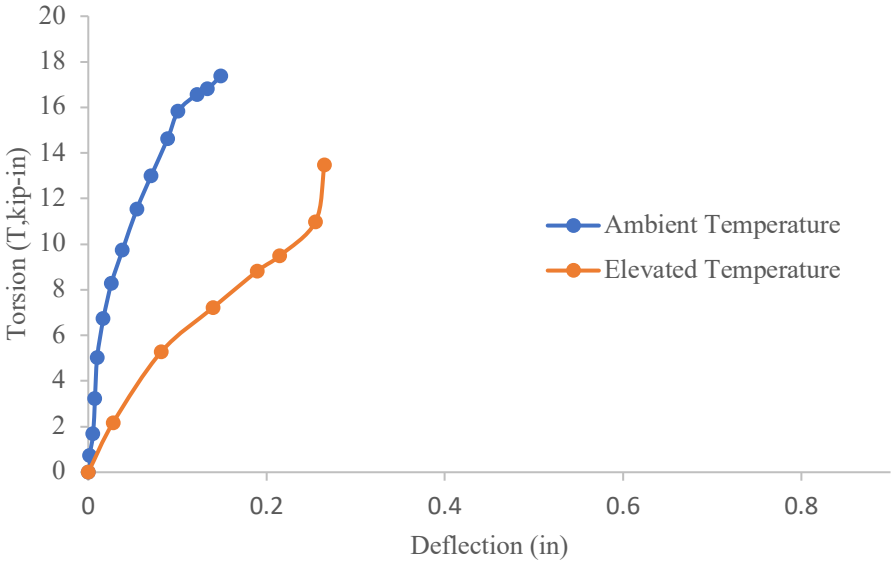

Figure 64. Experimental Curves for Torsion vs. Deflection (APBT & HPBT-Fixed-Partially Fixed)

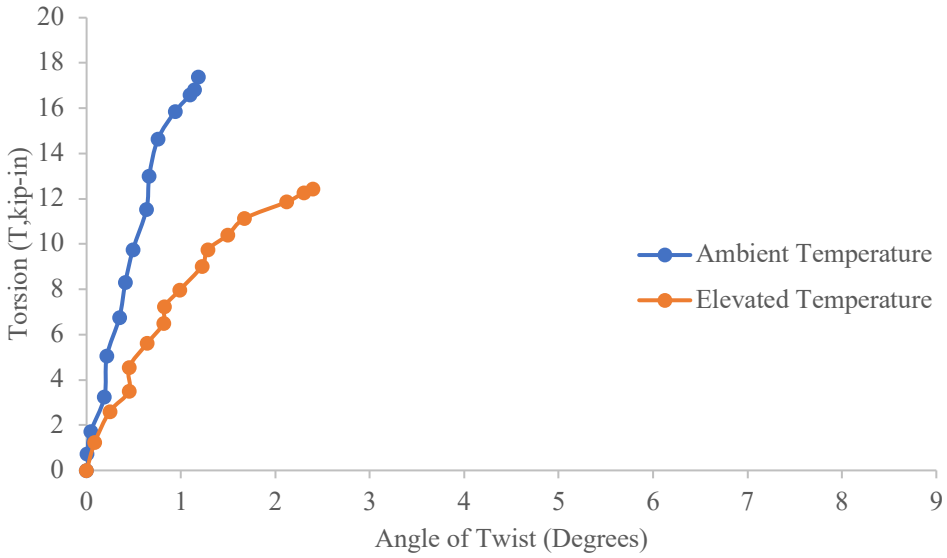

Figure 65. Experimental Curves for Torsion vs. Angle of Twist (APBT & HPBT-Fixed-Partially Fixed)

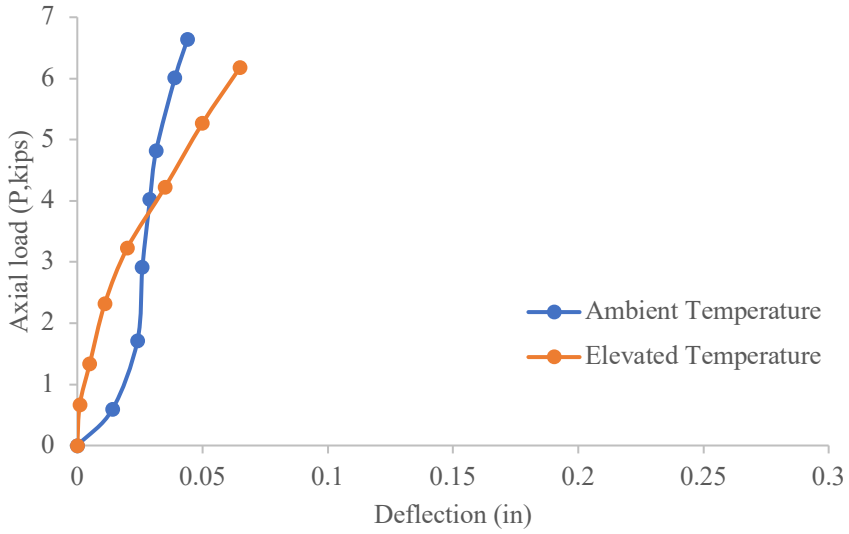

Figure 66. Experimental Curves for Axial load vs. Deflection (APBT & HPBT-Pinned-Pinned)

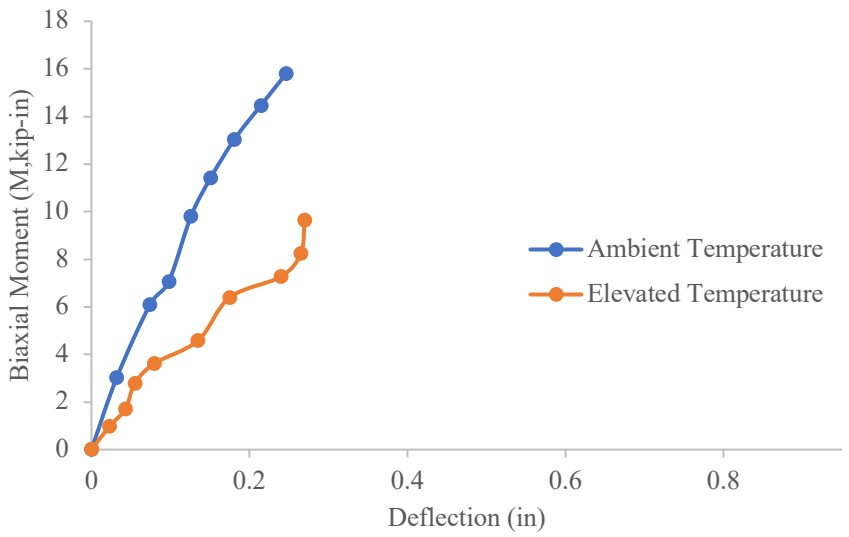

Figure 67. Experimental Curves for Biaxial Moment vs. Deflection (APBT & HPBT-Pinned-Pinned)

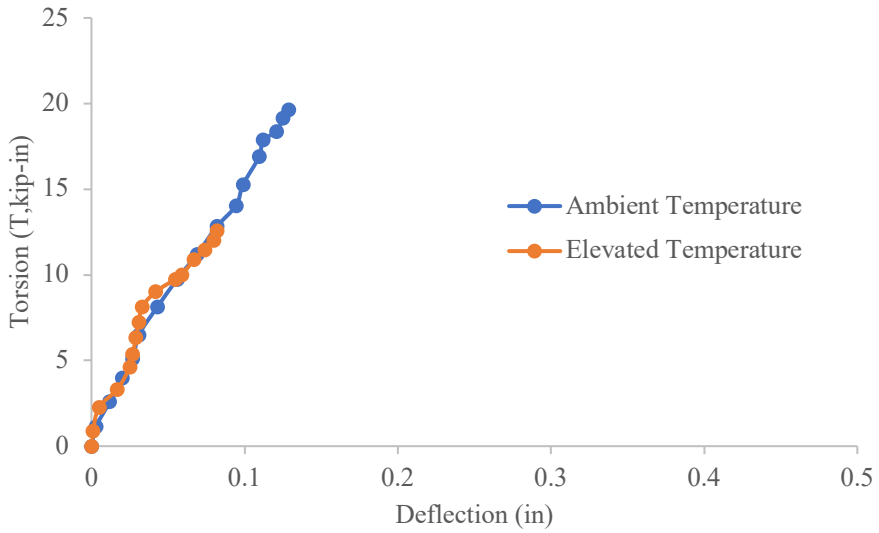

Figure 68. Experimental Curves for Torsion vs. Deflection (APBT & HPBT-Pinned-Pinned)

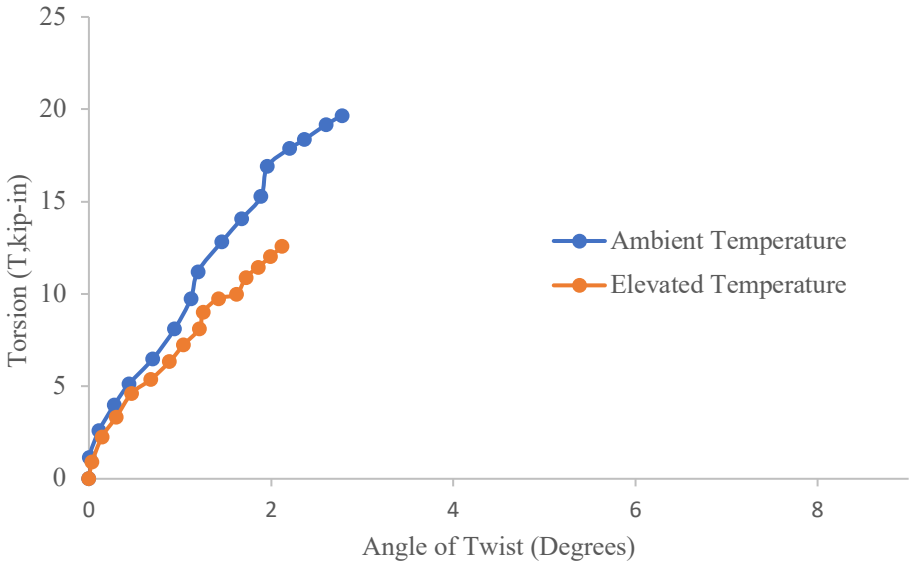

Figure 69. Experimental Curves for Torsion vs. Angle of Twist (APBT & HPBT-Pinned-Pinned)

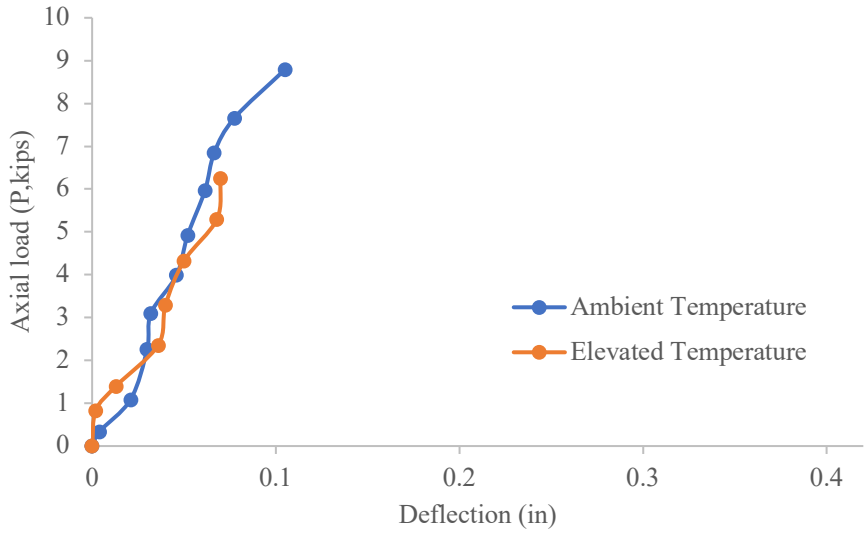

Figure 70. Experimental Curves for Axial load vs. Deflection (APUT & HPUT-Fixed-Partially Fixed)

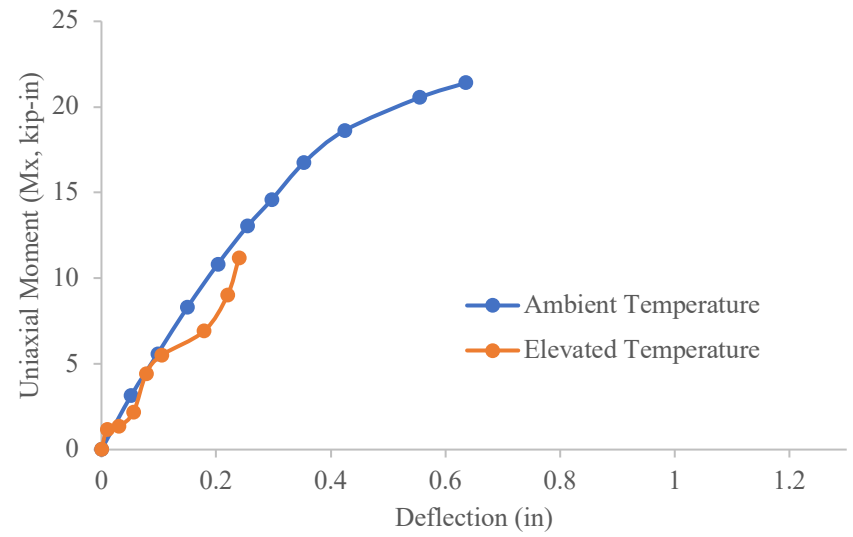

Figure 71. Experimental Curves for Uniaxial Moment vs. Deflection (APUT & HPUT-Fixed-Partially Fixed)

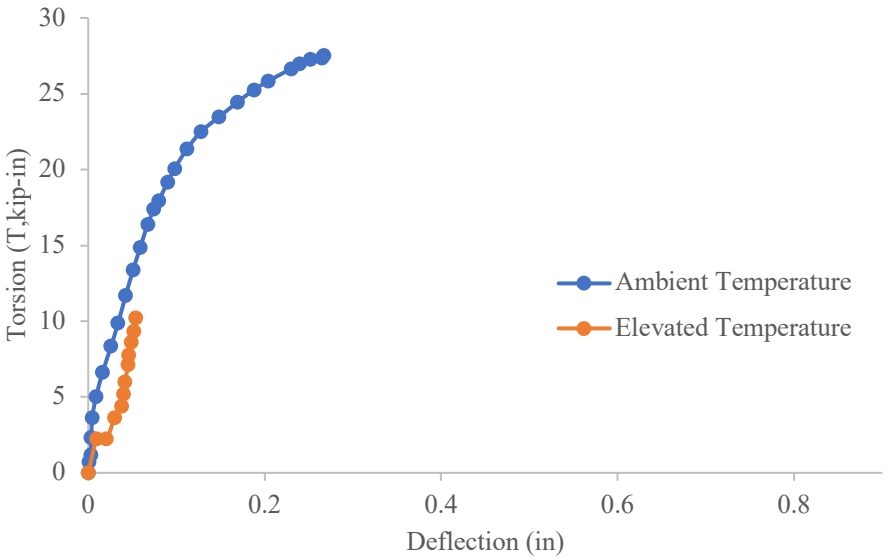

Figure 72. Experimental Curves for Torsion vs. Deflection (APUT & HPUT-Fixed-Partially Fixed)

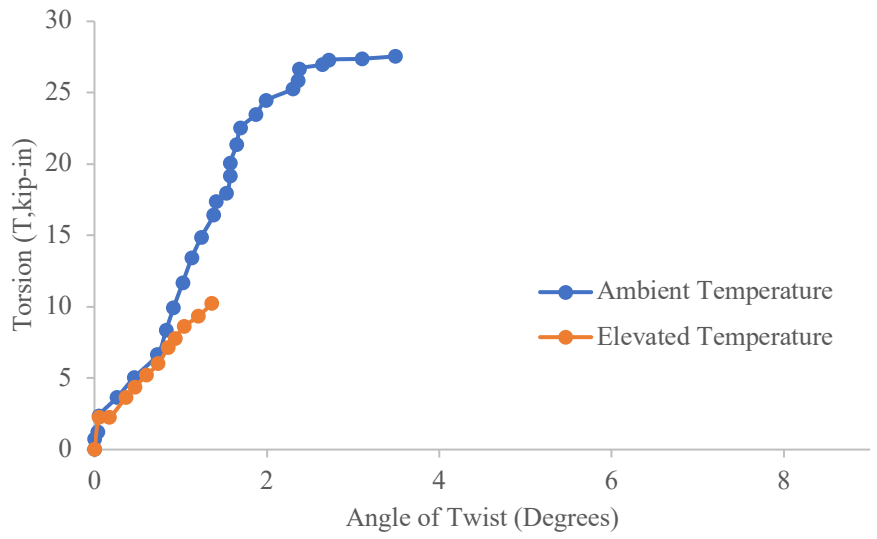

Figure 73. Experimental Curves for Torsion vs. Angle of Twist (APUT & HPUT-Fixed-Partially Fixed)

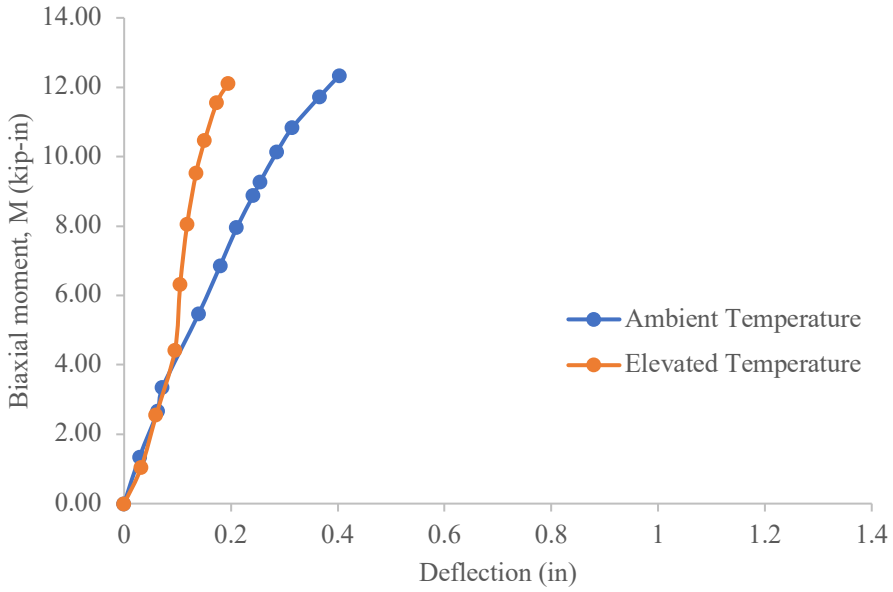

Figure 74. Experimental Curves for Biaxial Moment vs. Deflection (ABT & HBT-Pinned - Pinned)

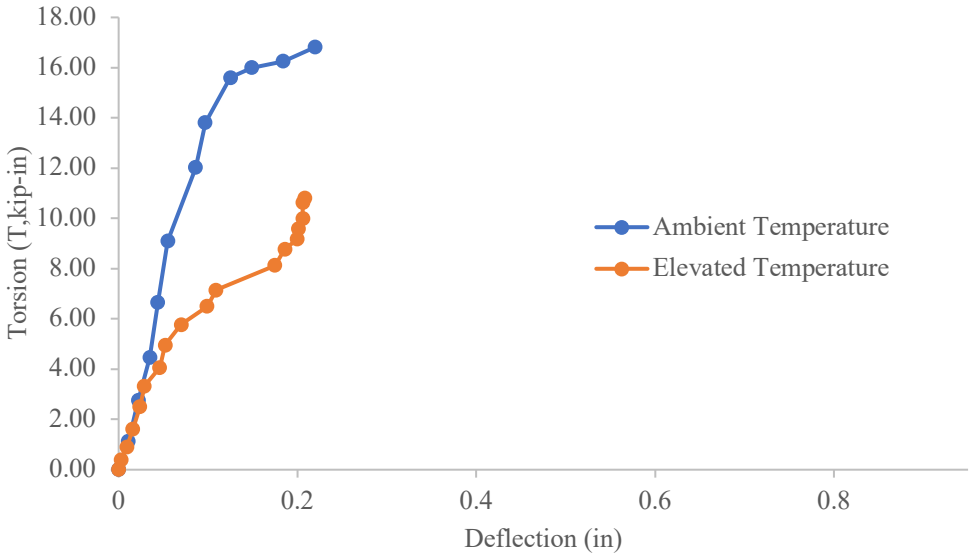

Figure 75. Experimental Curves for Torsion vs. Deflection (ABT & HBT-Pinned -Pinned)

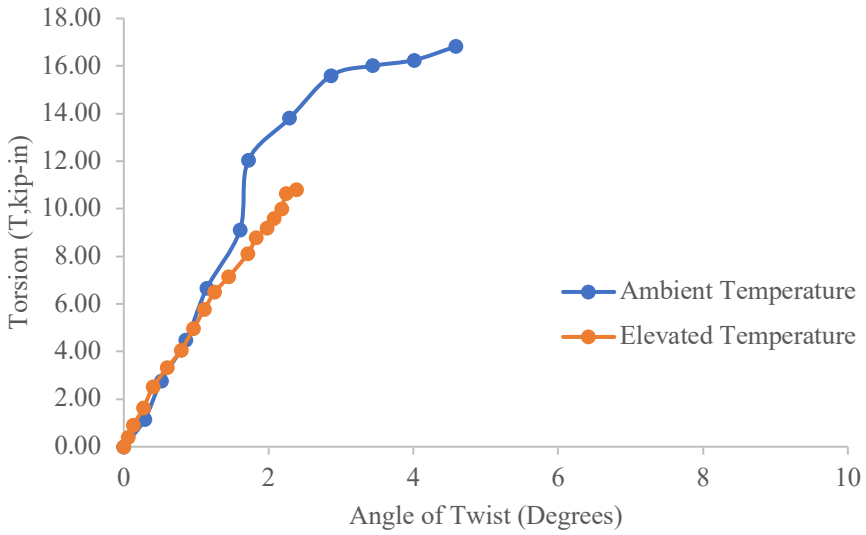

Figure 76. Experimental Curves for Torsion vs. Deflection (ABT & HBT-Pinned -Pinned)

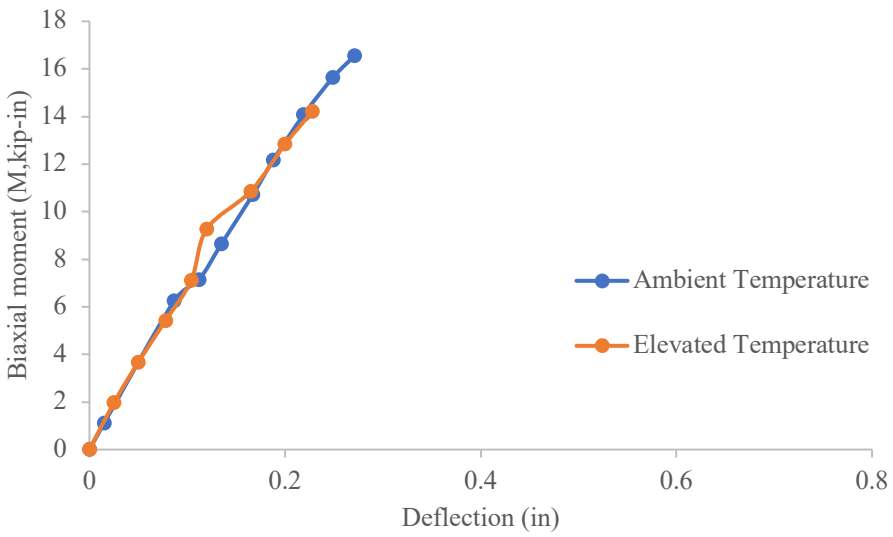

Figure 77. Experimental Curves for Biaxial Moment vs Deflection (ABT & HBT-Pinned - Pinned)

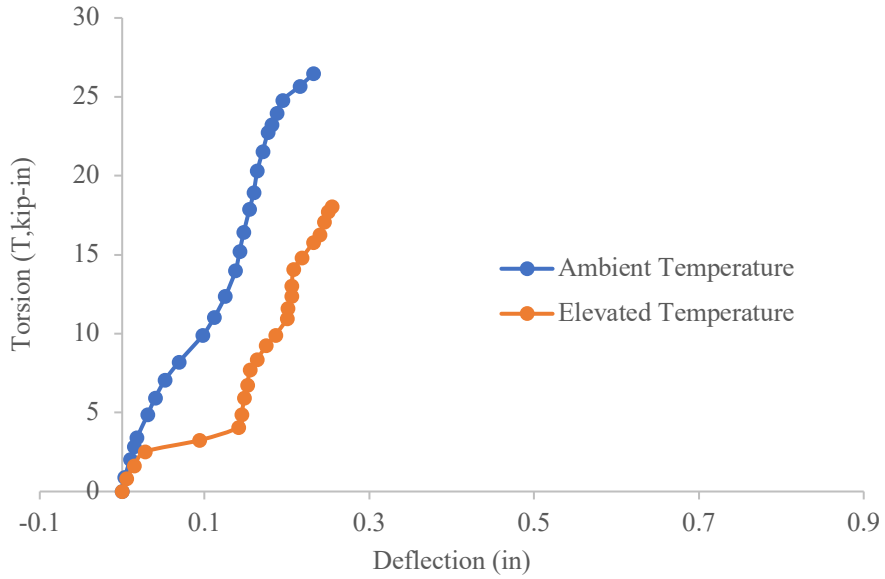

Figure 78. Experimental Curves for Torsion vs. Deflection (ABT & HBT-Pinned -Pinned)

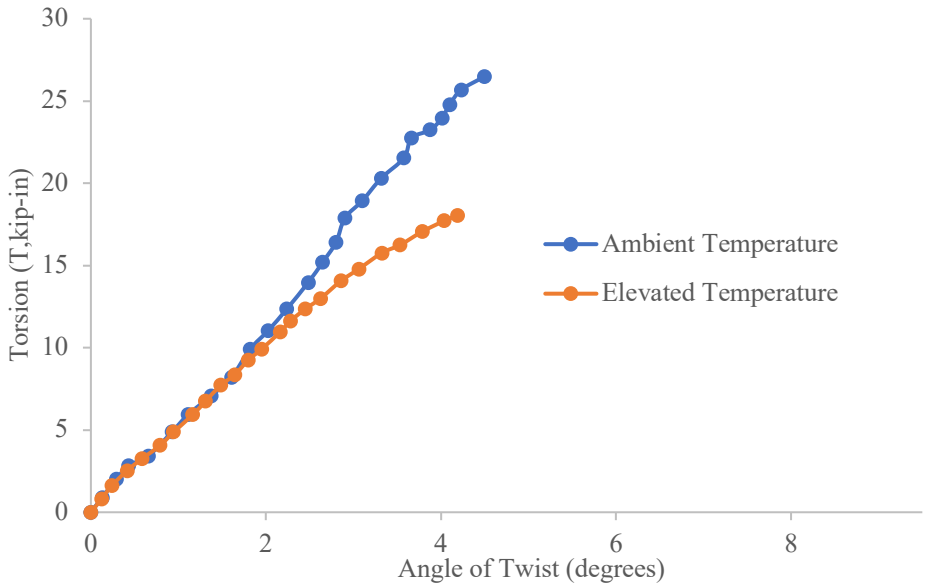

Figure 79. Experimental Curves for Torsion vs. Angle of Twist (ABT & HBT-Pinned -Pinned)

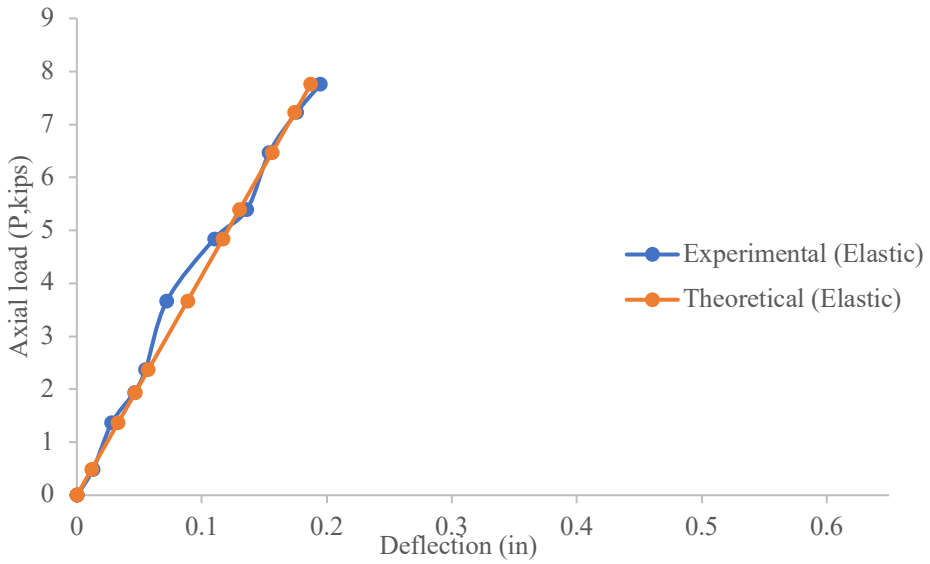

Figure 80. Axial Load vs. Deflection (APT- Pinned-Pinned)

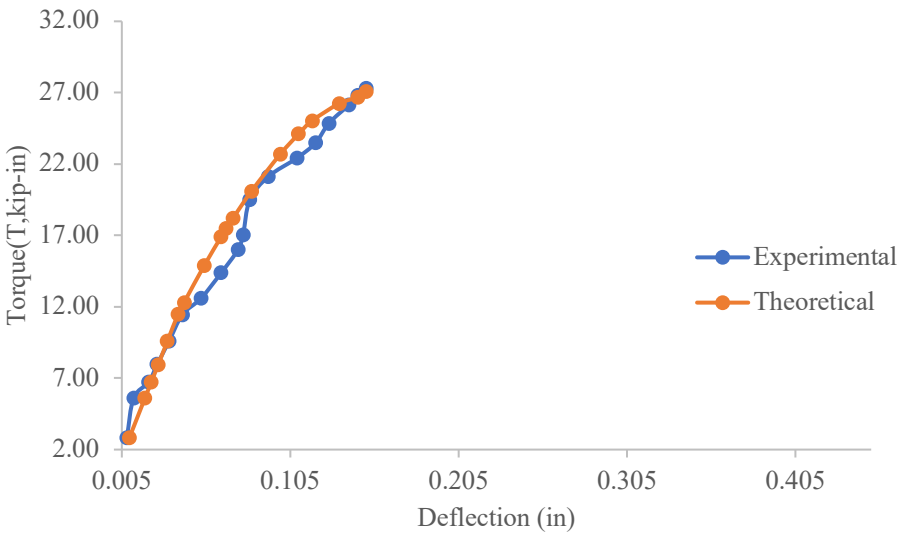

Figure 81. Torque vs. Deflection (APT- Pinned-Pinned)

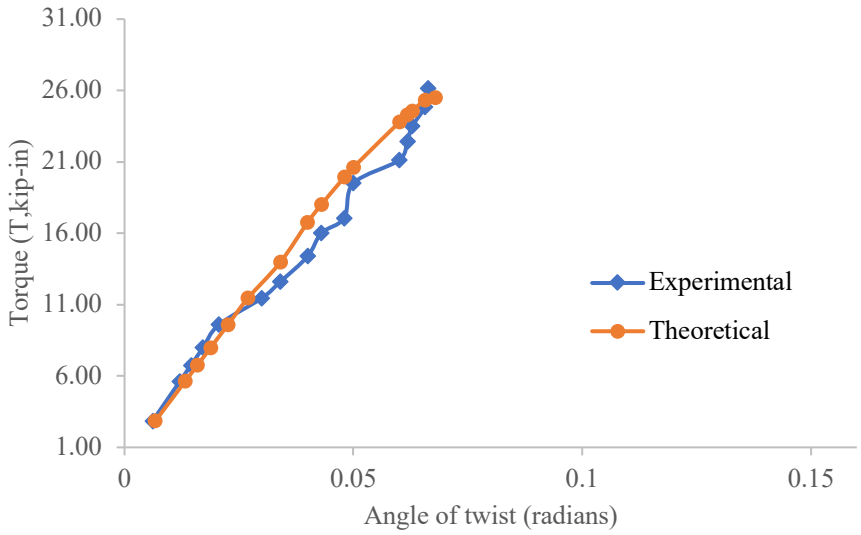

Figure 82. Torque vs. Angle of Twist (APT- Pinned-Pinned)

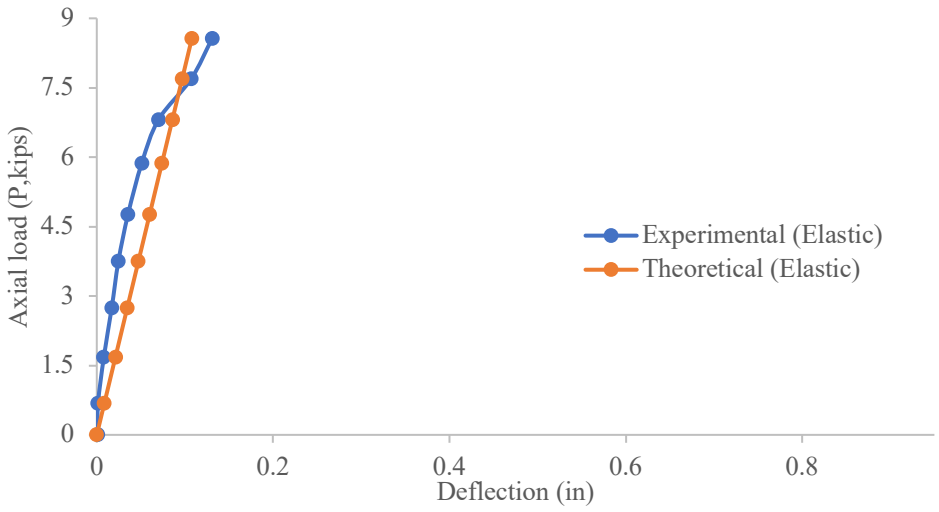

Figure 83. Axial Load vs. Deflection (APT- Fixed-Fixed)

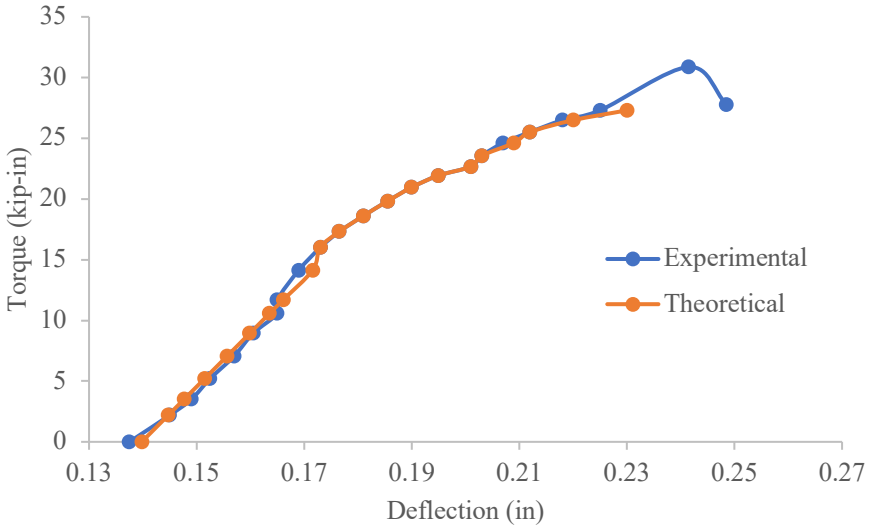

Figure 84. Torque vs. Deflection (APT- Fixed-Fixed)

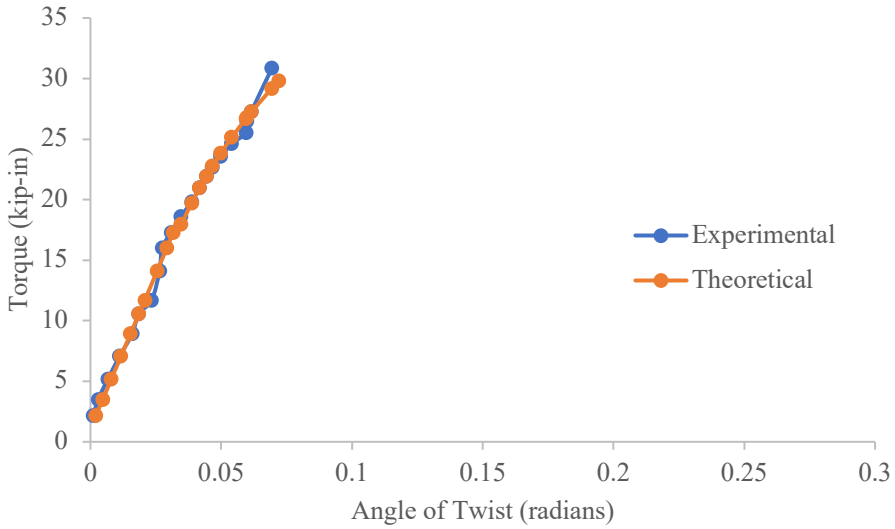

Figure 85. Torque vs. Angle of Twist (APT- Fixed-Fixed)

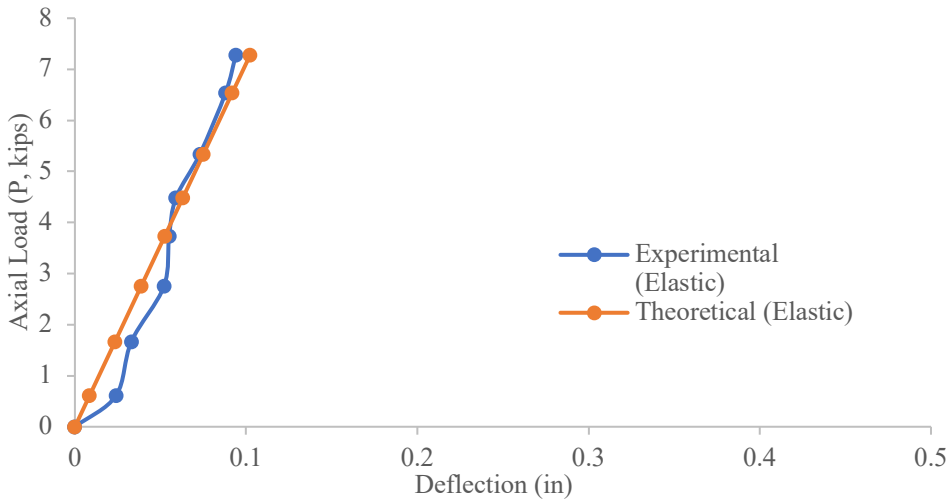

Figure 86. Axial Load vs. Deflection (APT- Fixed-Pinned)

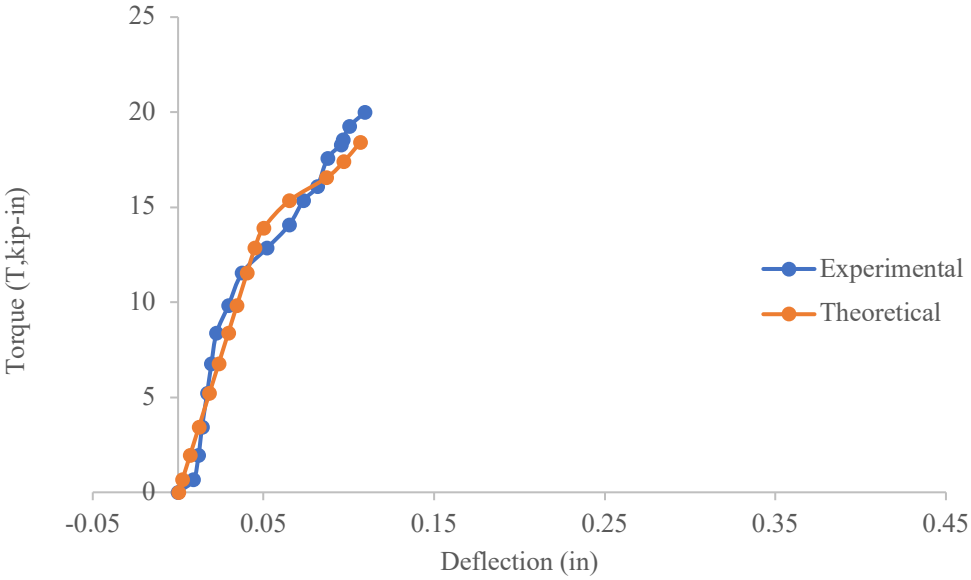

Figure 87. Torque vs. Deflection (APT- Fixed-Pinned)

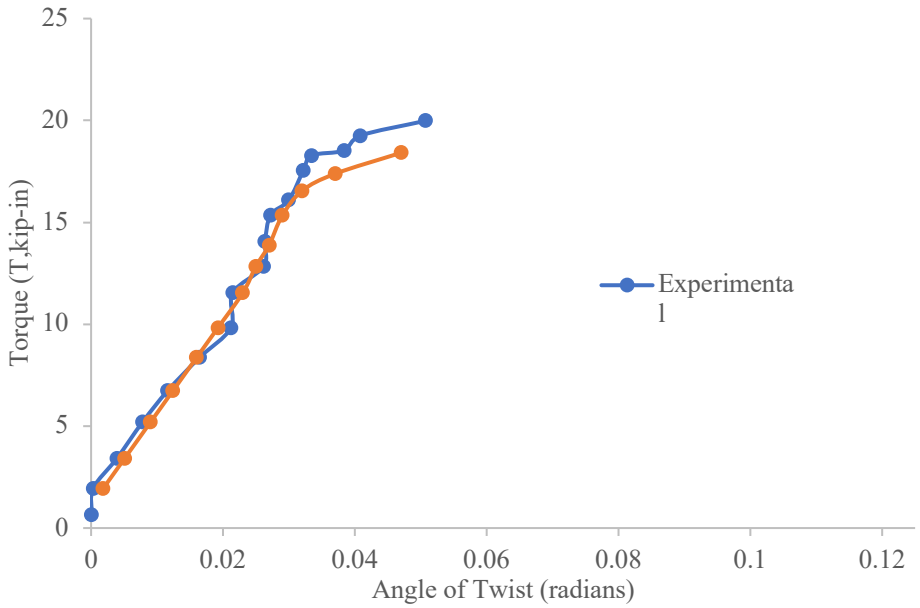

Figure 88. Torque vs. Angle of Twist (APT- Fixed-Pinned)

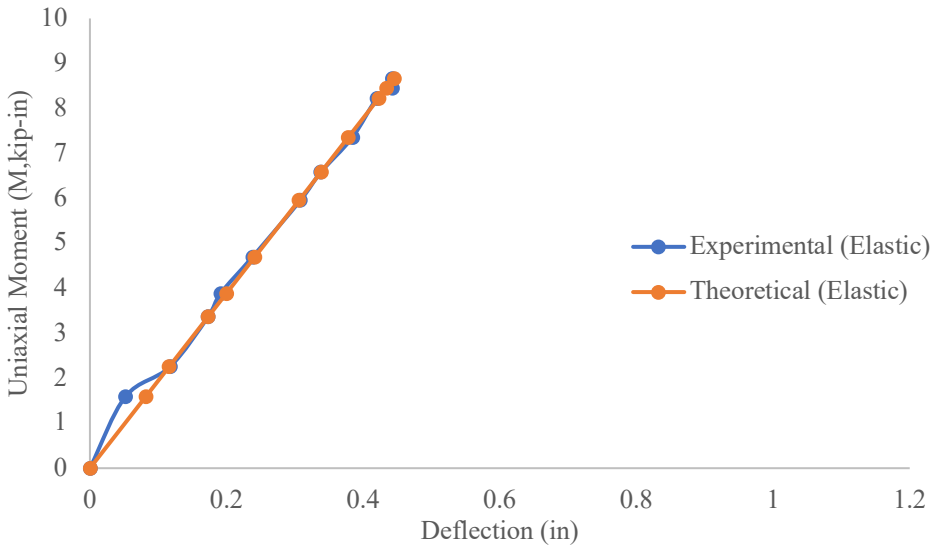

Figure 89. Uniaxial Moment vs. Deflection (AUT- Pinned-Pinned)

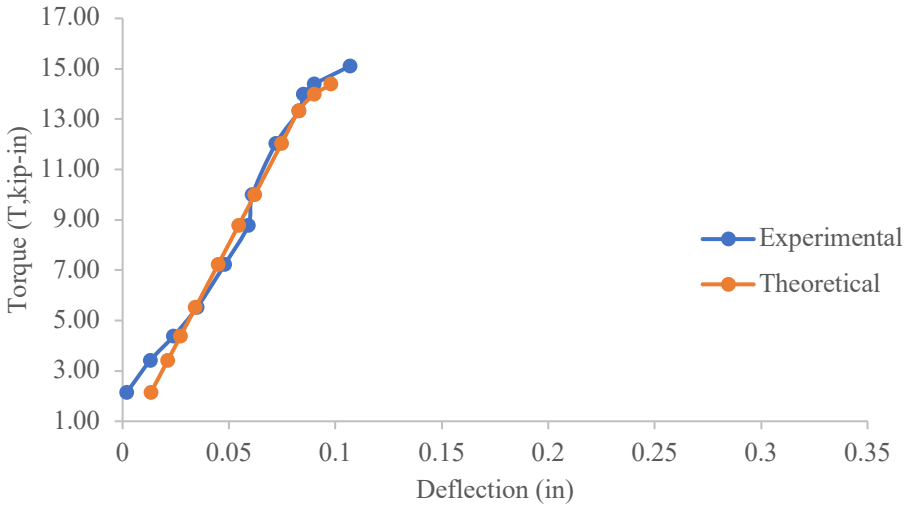

Figure 90. Torque vs. Deflection (AUT- Pinned-Pinned)

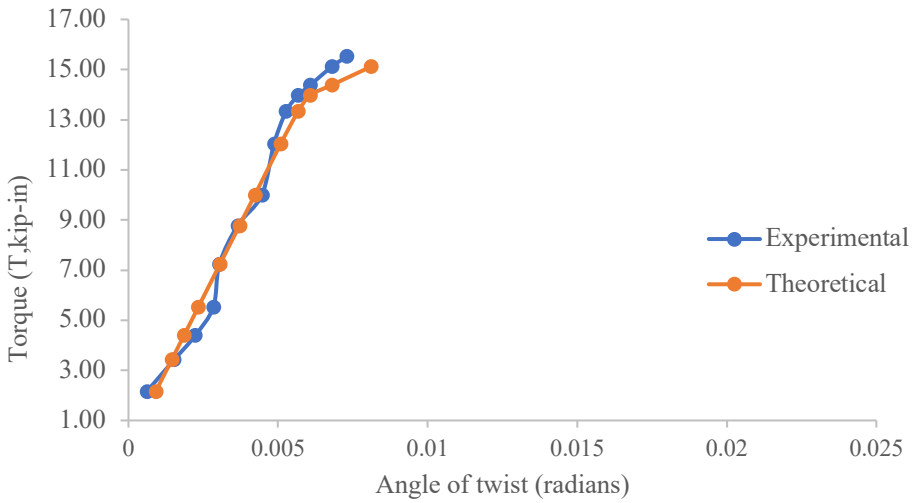

Figure 91. Torque vs. Angle of Twist (AUT- Pinned-Pinned)

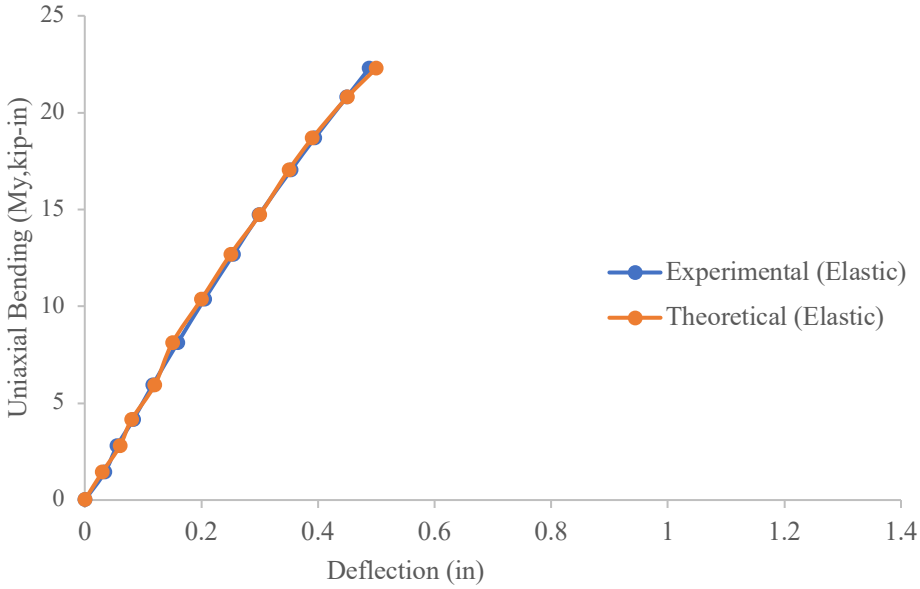

Figure 92. Uniaxial Moment vs. Deflection (AUT- Fixed-Fixed)

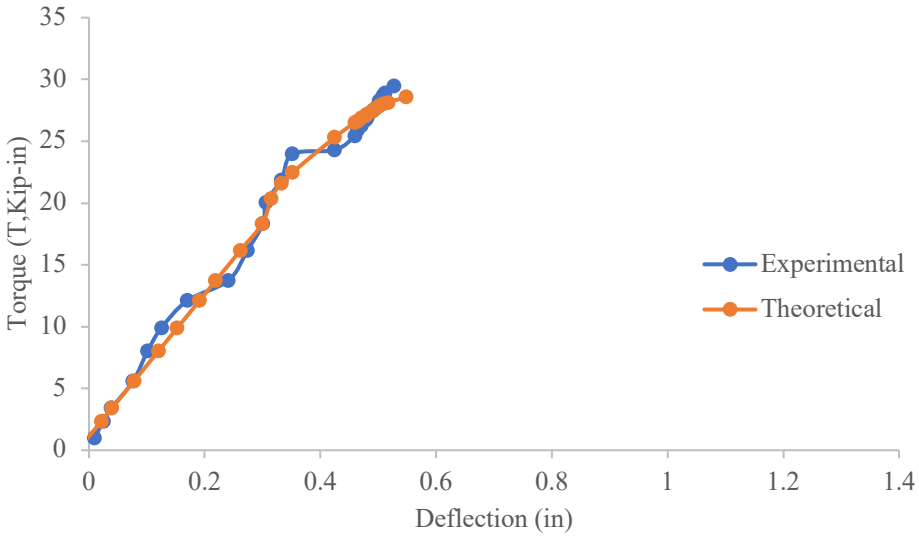

Figure 93. Torque vs. Deflection (AUT- Fixed-Fixed)

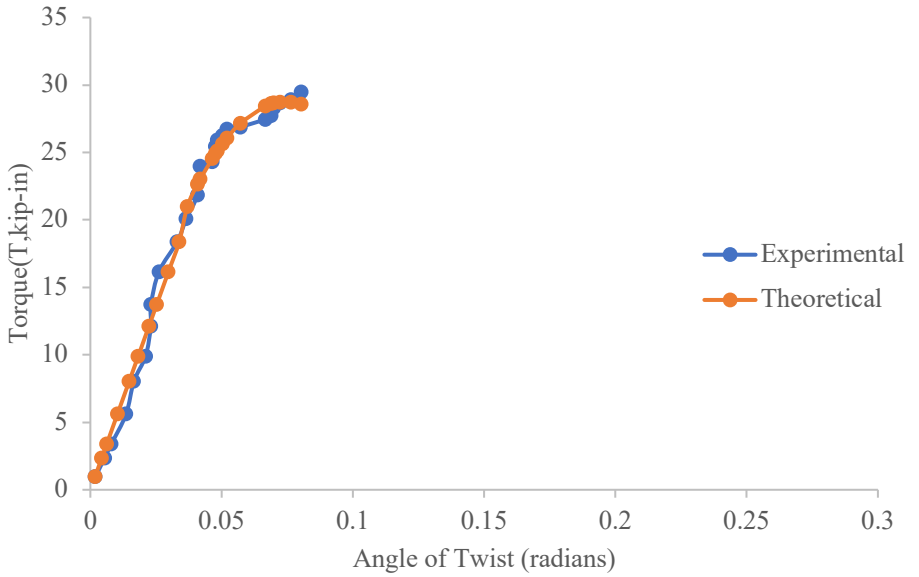

Figure 94. Torque vs. Angle of Twist (AUT- Fixed-Fixed)

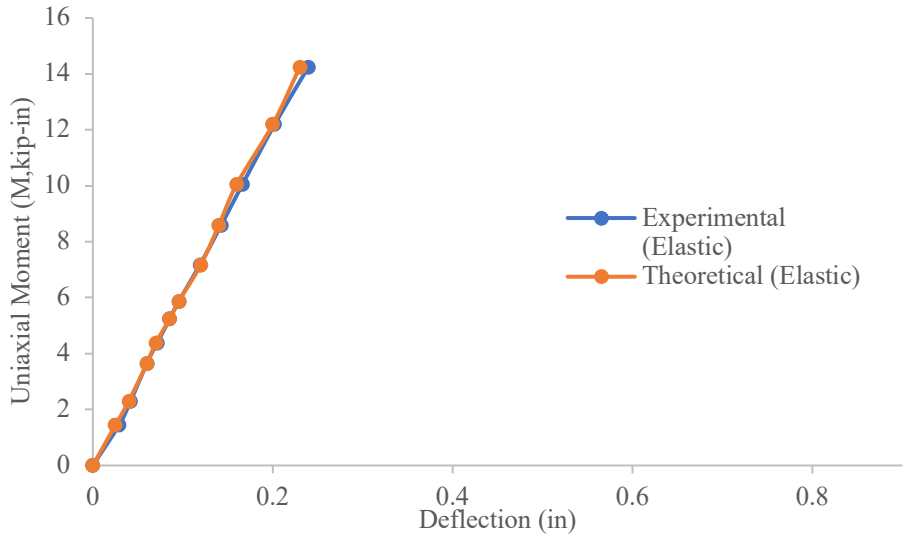

Figure 95. Uniaxial Moment vs. Deflection (AUT- Fixed-Pinned)

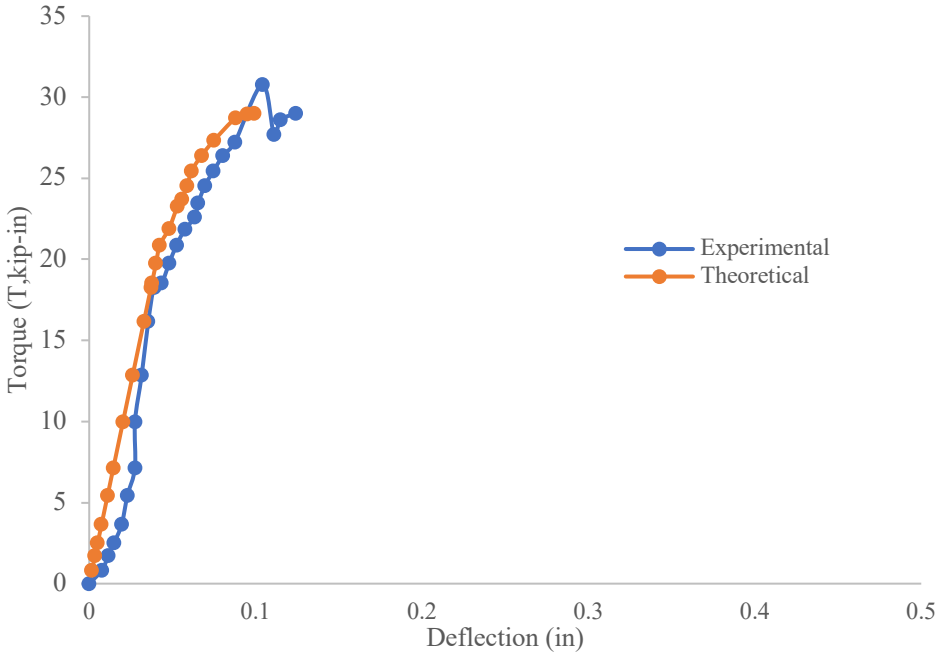

Figure 96. Torque vs. Deflection (AUT- Fixed-Pinned)

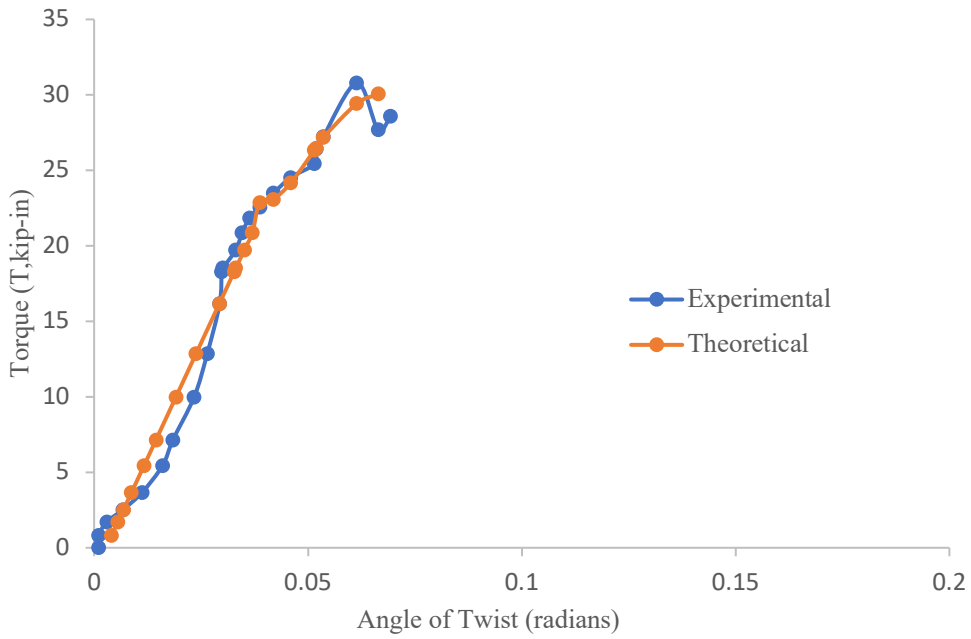

Figure 97. Torque vs. Angle of Twist (AUT- Fixed-Pinned)

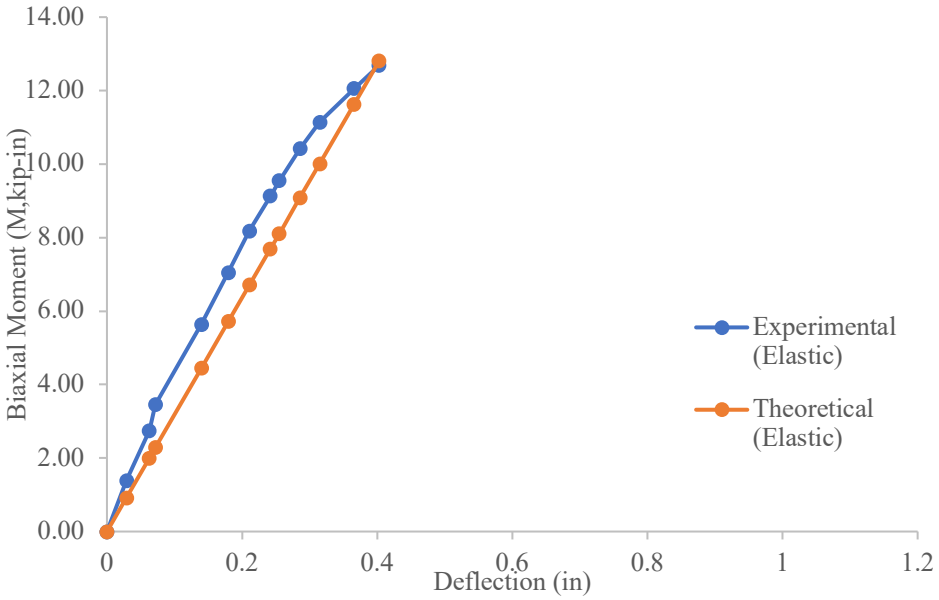

Figure 98. Biaxial Moment vs. Deflection (ABT- Pinned-Pinned)

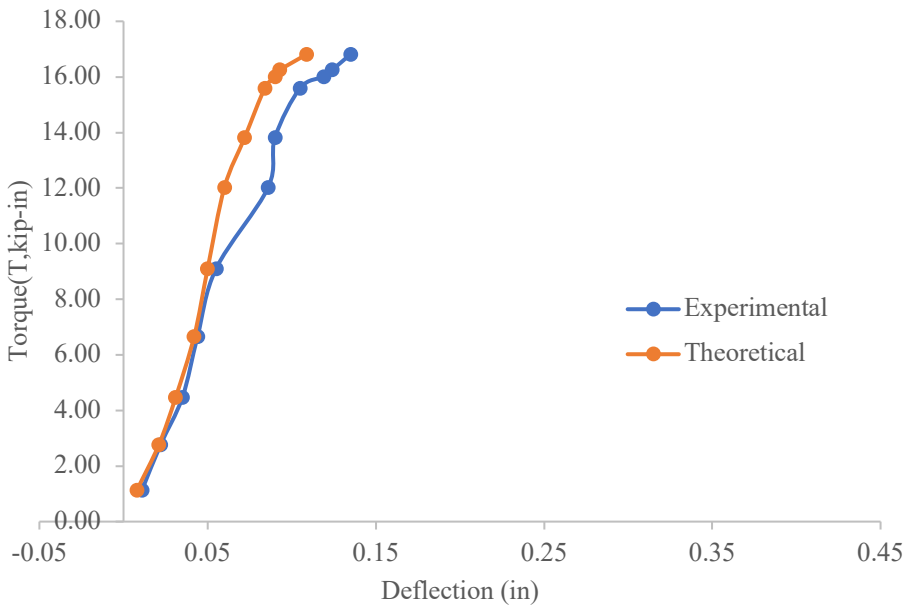

Figure 99. Torque vs. Deflection (ABT- Pinned-Pinned)

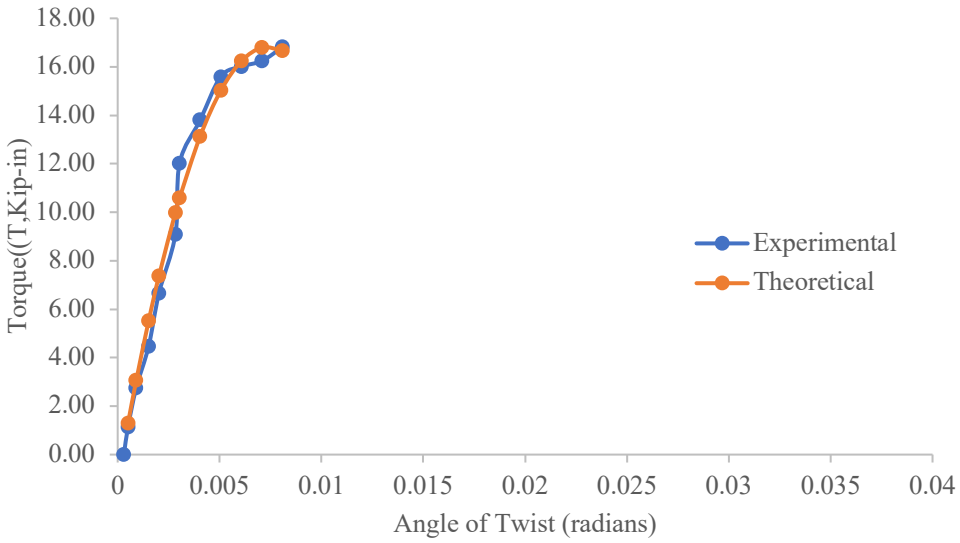

Figure 100. Torque vs. Angle of Twist (ABT- Pinned-Pinned)

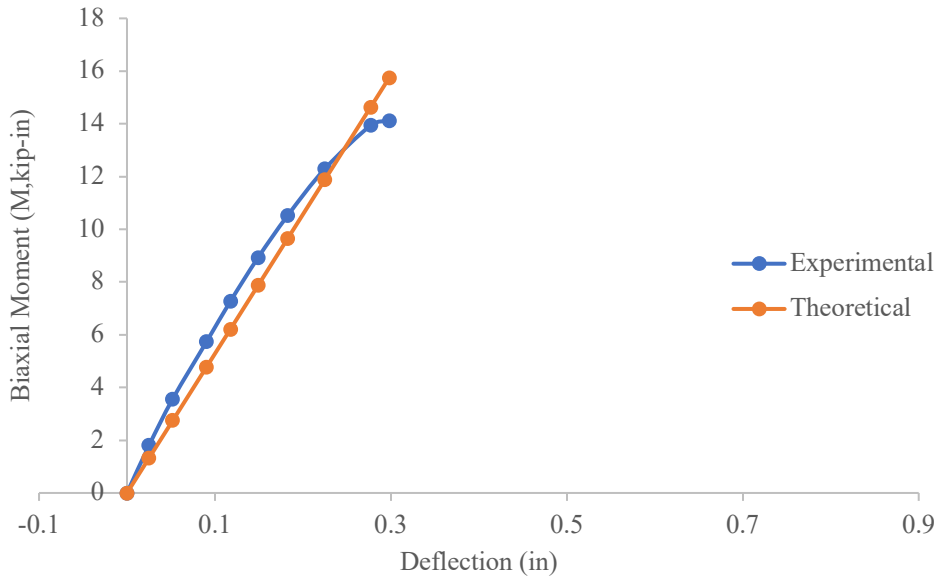

Figure 101. Biaxial Moment vs. Deflection (ABT- Fixed-Fixed)

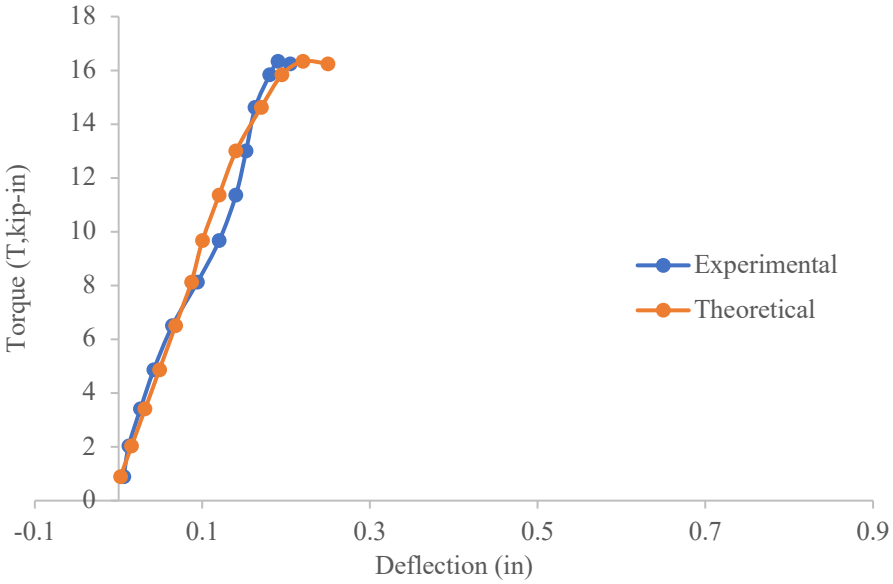

Figure 102. Torque vs. Deflection (ABT- Fixed-Fixed)

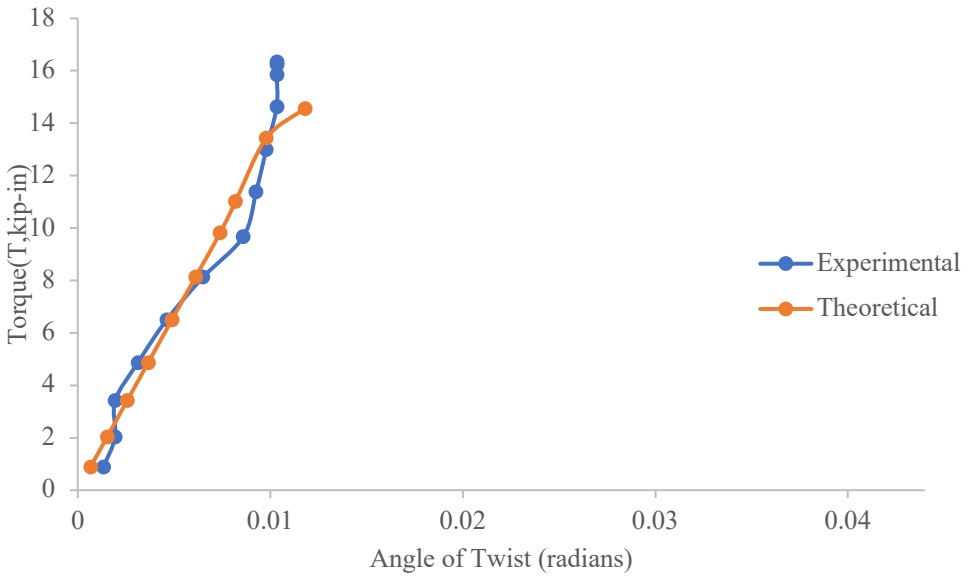

Figure 103. Torque vs. Angle of Twist (ABT- Fixed-Fixed)

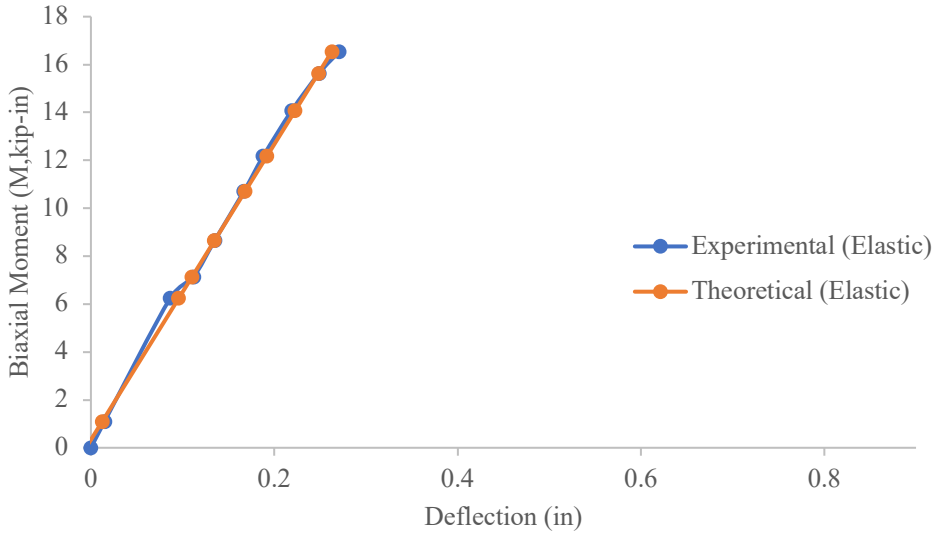

Figure 104. Biaxial Moment vs. Deflection (ABT- Fixed-Pinned)

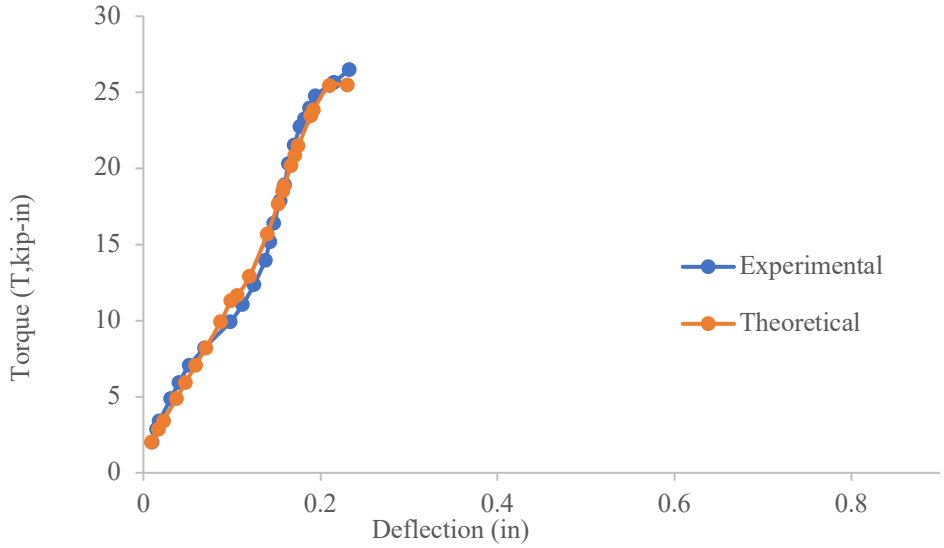

Figure 105. Torque vs. Deflection (ABT- Fixed-Pinned)

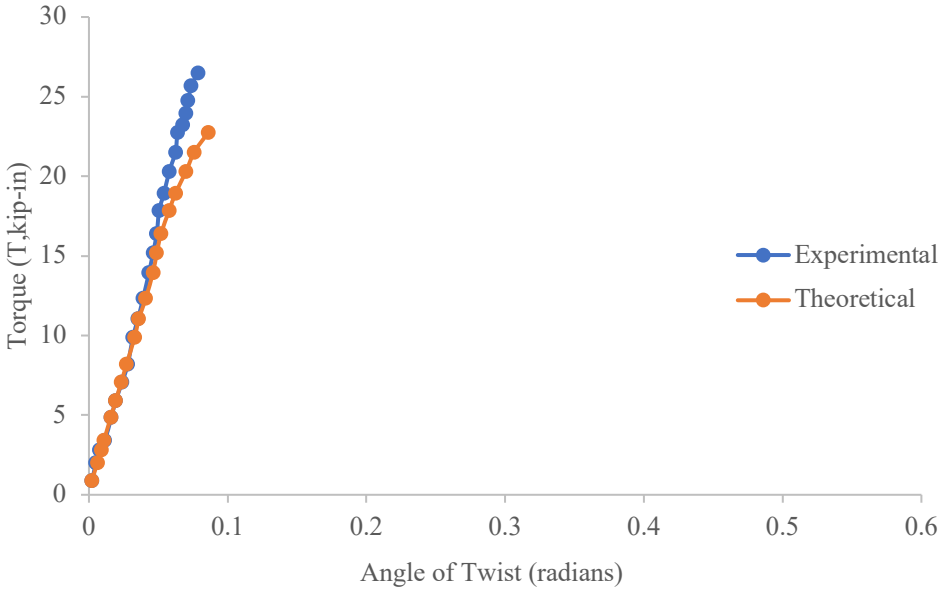

Figure 106. Torque vs. Angle of Twist (ABT- Fixed-Pinned)

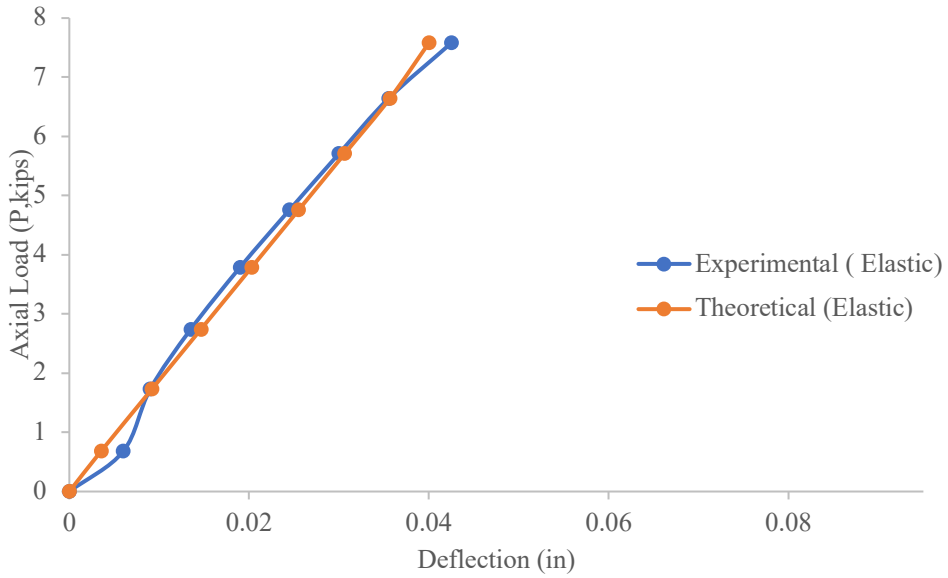

Figure 107. Axial Load vs. Deflection (APUT- Pinned-Pinned)

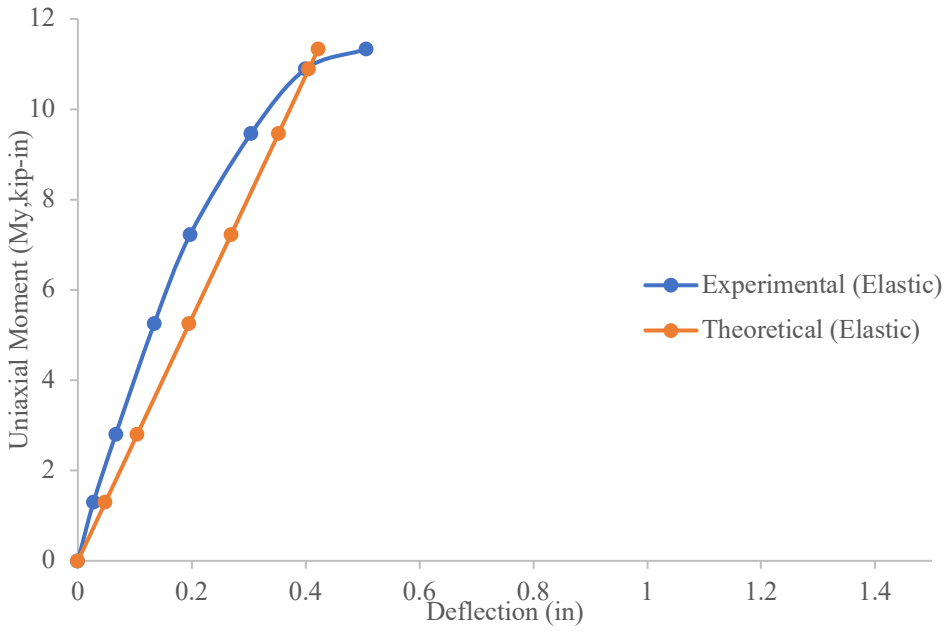

Figure 108. Uniaxial Moment vs. Deflection (APUT- Pinned-Pinned)

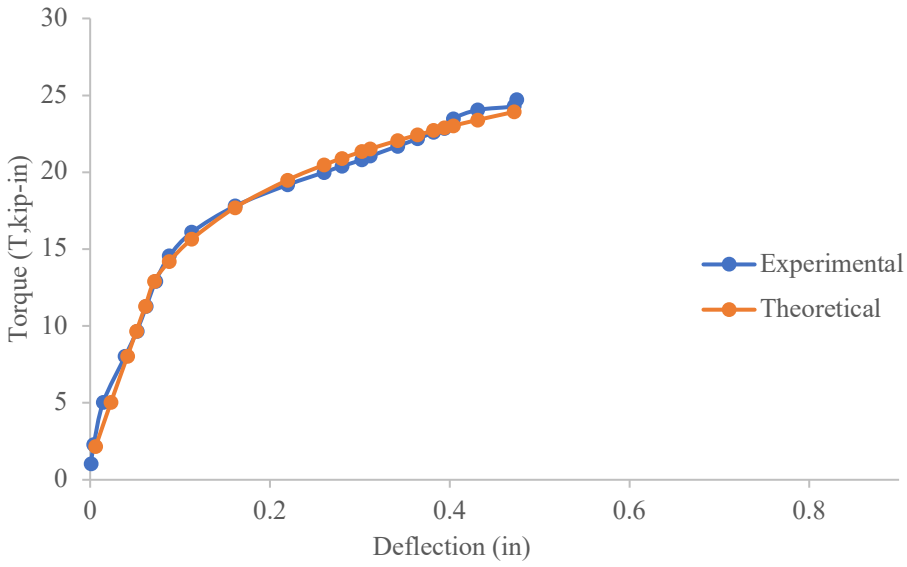

Figure 109. Torque vs. Deflection (APUT- Pinned-Pinned)

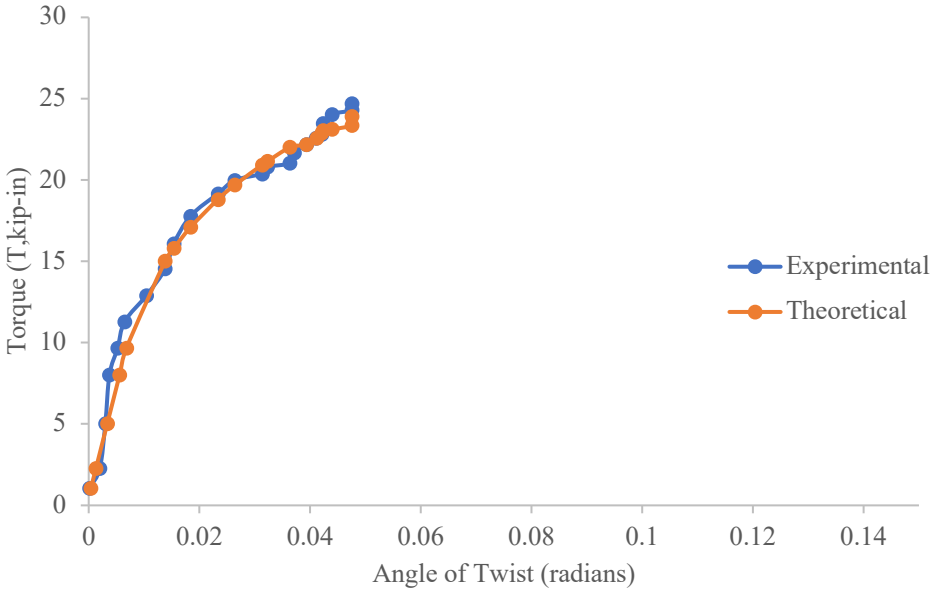

Figure 110. Torque vs. Angle of Twist (APUT- Pinned-Pinned)

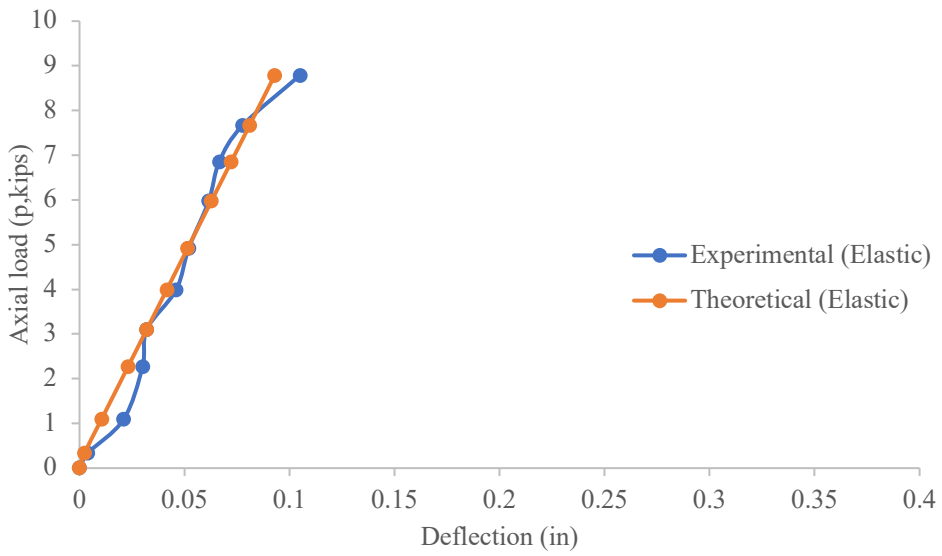

Figure 111. Axial Load vs. Deflection (APUT- Fixed-Fixed)

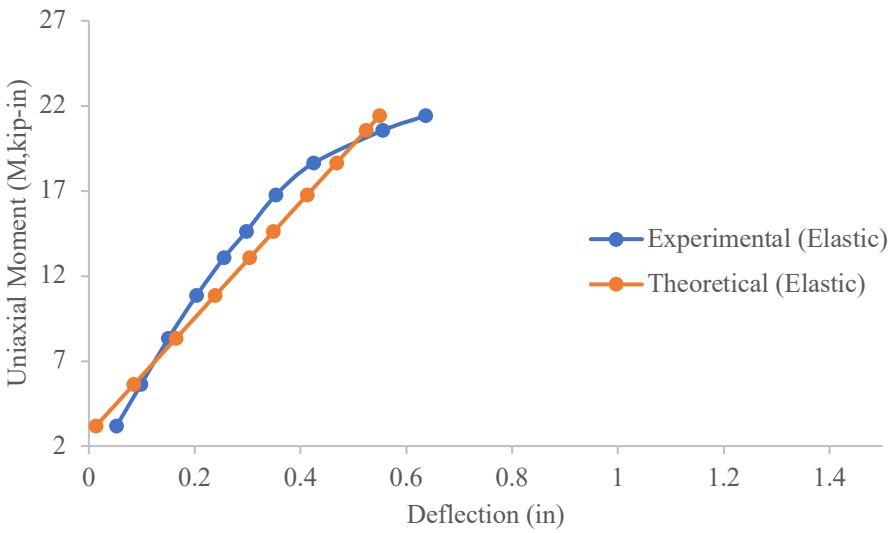

Figure 112. Axial Load vs. Deflection (APUT- Fixed-Fixed)

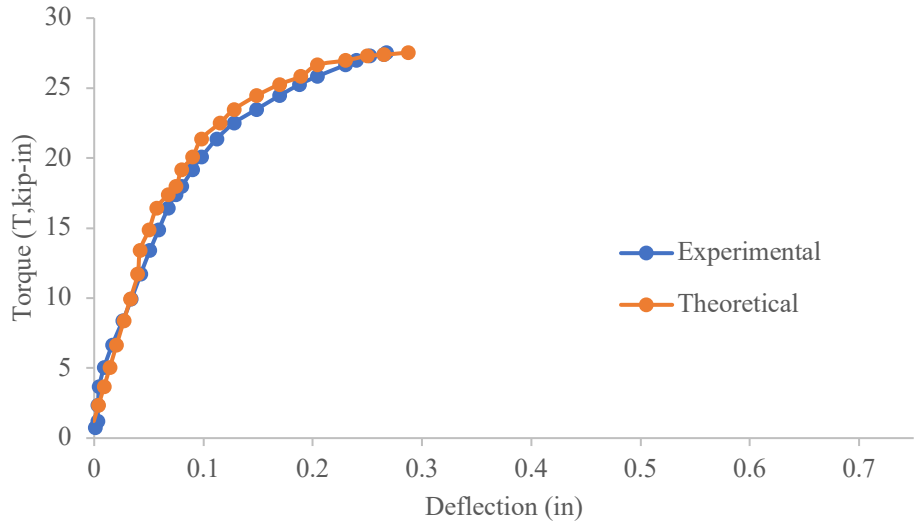

Figure 113. Torque vs. Deflection (APUT- Fixed-Fixed)

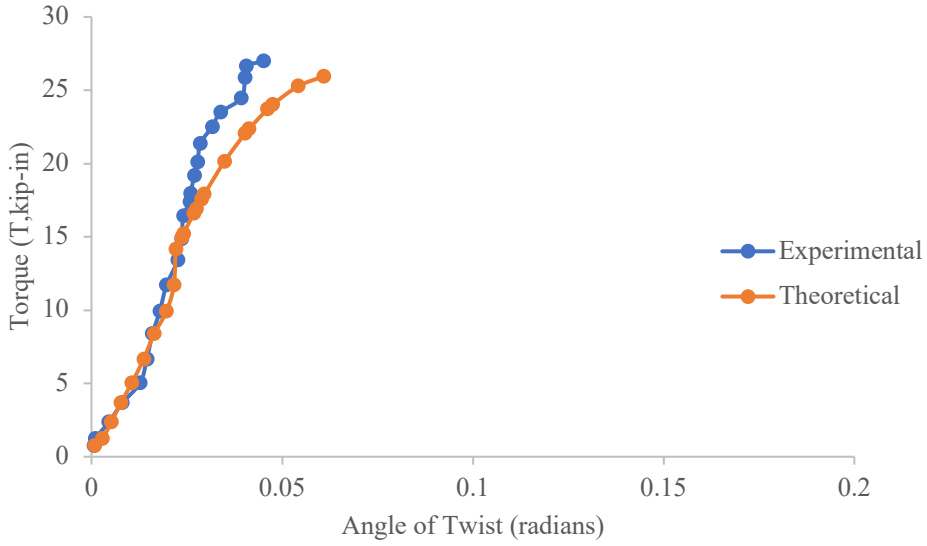

Figure 114. Torque vs. Angle of Twist (APUT- Fixed-Fixed)

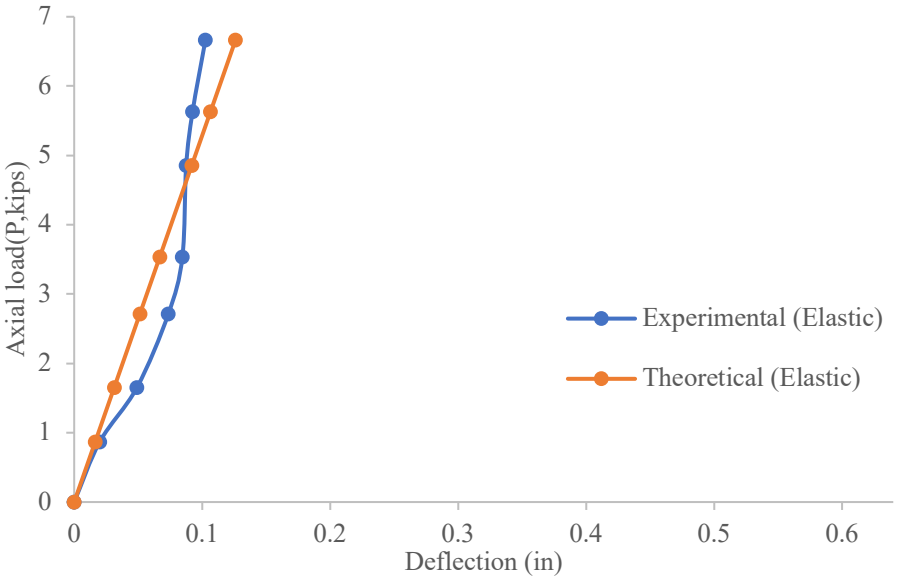

Figure 115. Axial Load vs. Deflection (APUT- Fixed-Pinned)

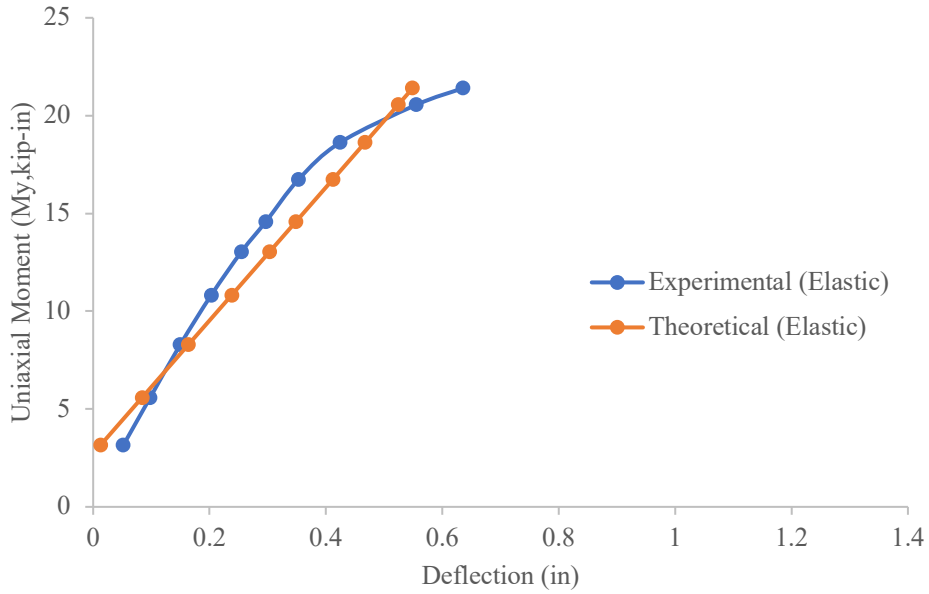

Figure 116. Uniaxial Moment vs Deflection (APUT- Fixed-Pinned)

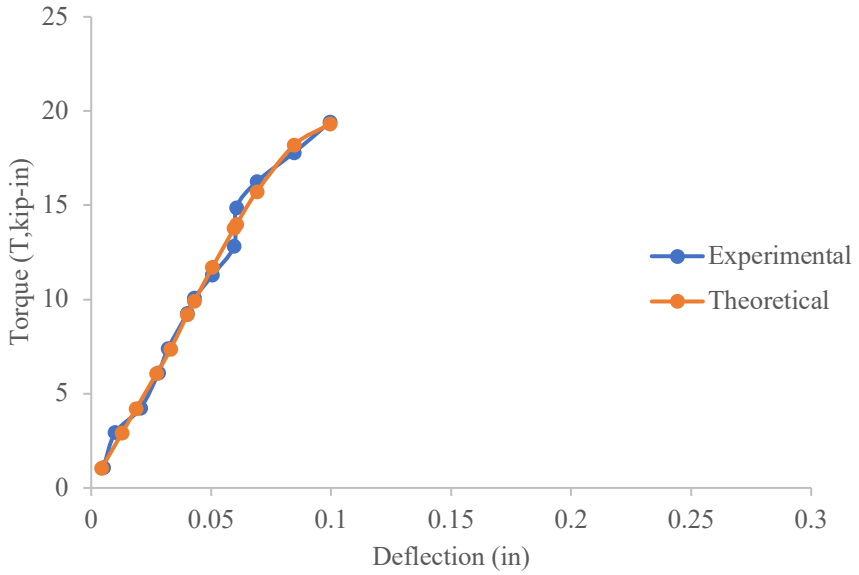

Figure 117. Torque vs. Deflection (APUT- Fixed-Pinned)

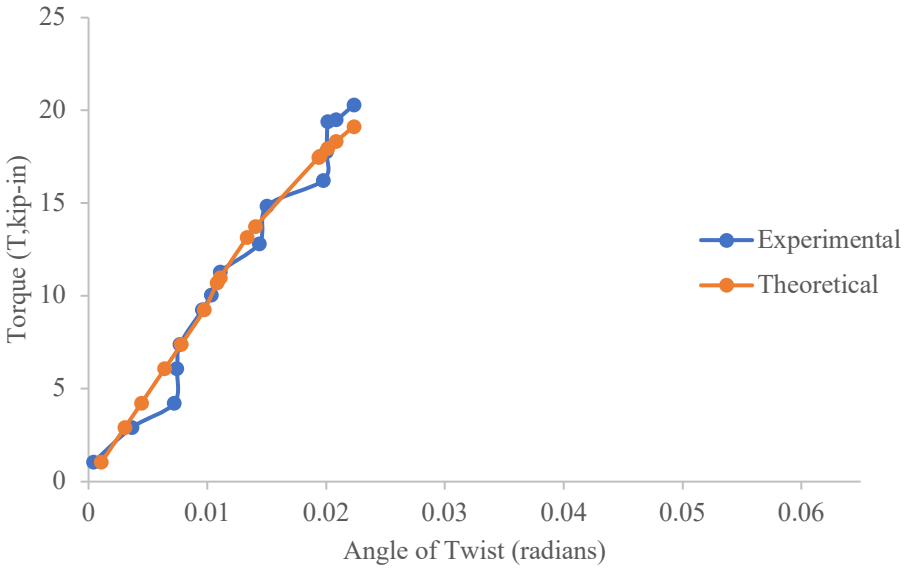

Figure 118. Torque vs. Angle of Twist (APUT- Fixed-Pinned)

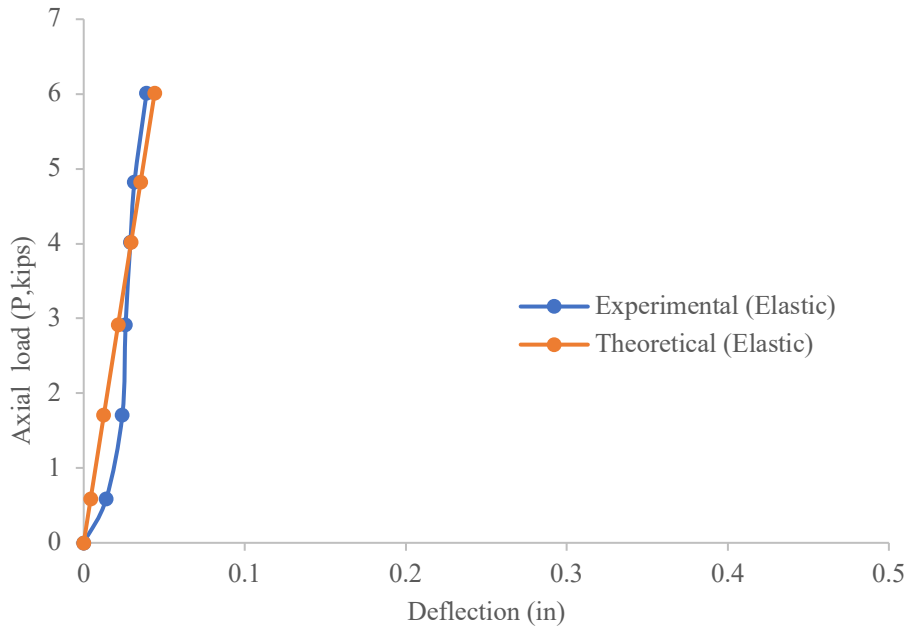

Figure 119. Axial Load vs. Deflection (APBT- Pinned-Pinned)

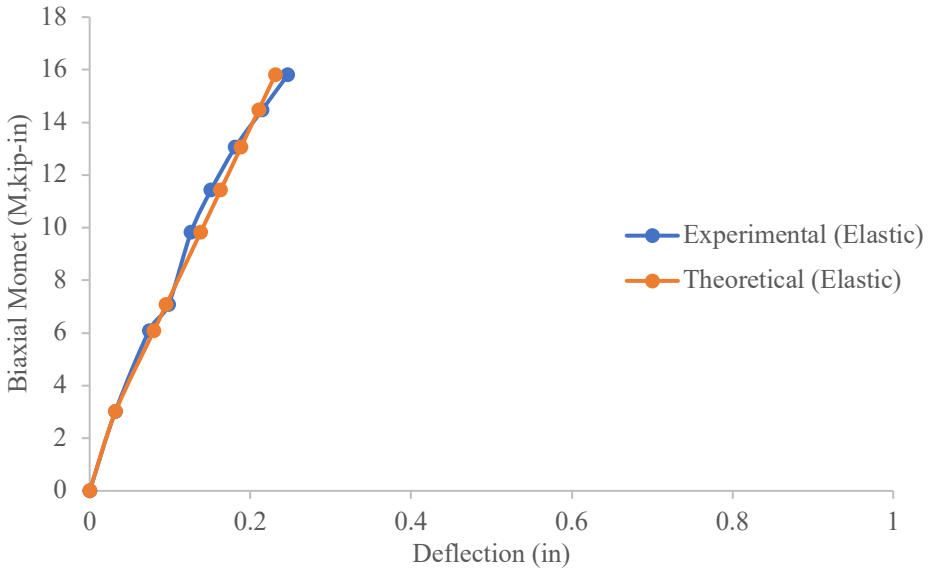

Figure 120. Biaxial Moment vs. Deflection (APBT- Pinned-Pinned)

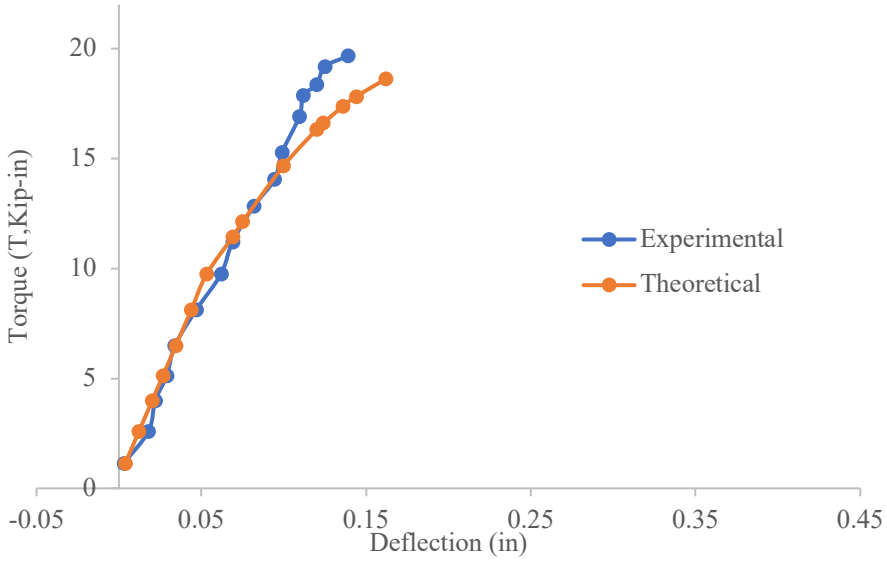

Figure 121. Torque vs. Deflection (APBT- Pinned-Pinned)

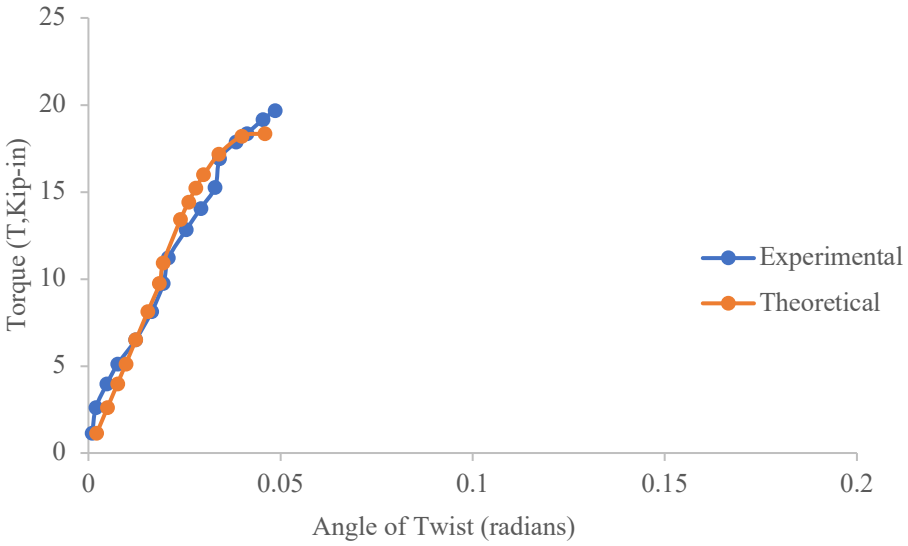

Figure 122. Torque vs. Angle of Twist (APBT- Pinned-Pinned)

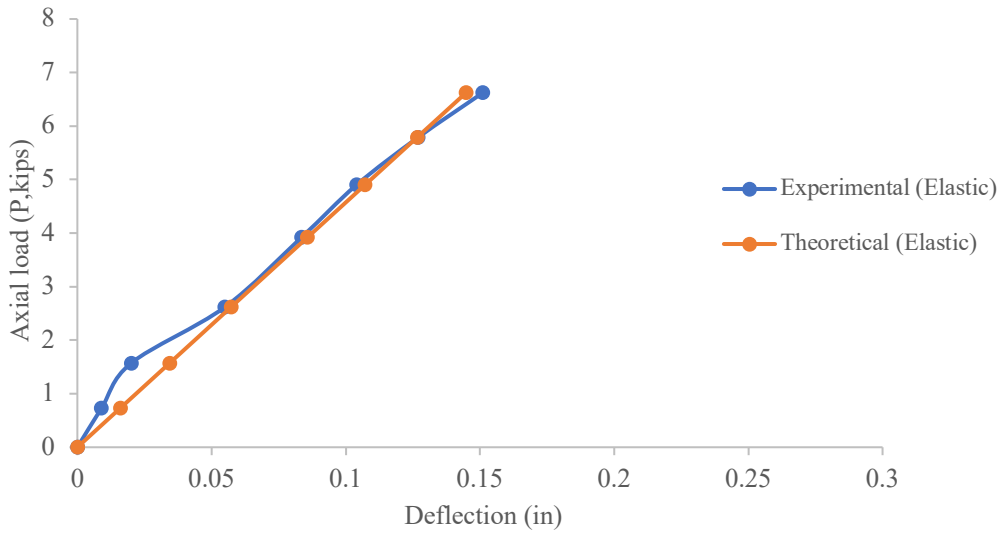

Figure 123. Axial Load vs. Deflection (APBT- Fixed-Fixed)

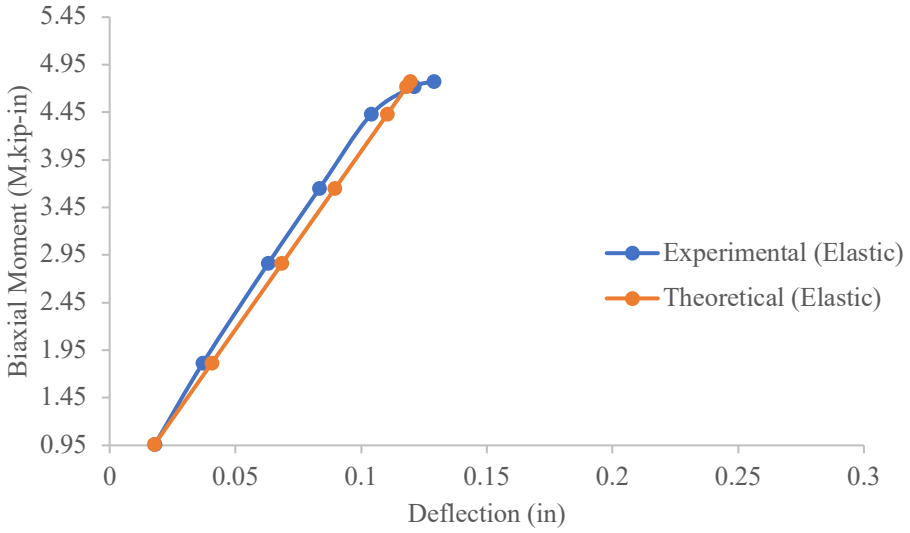

Figure 124. Biaxial Moment vs. Deflection (APBT- Fixed-Fixed)

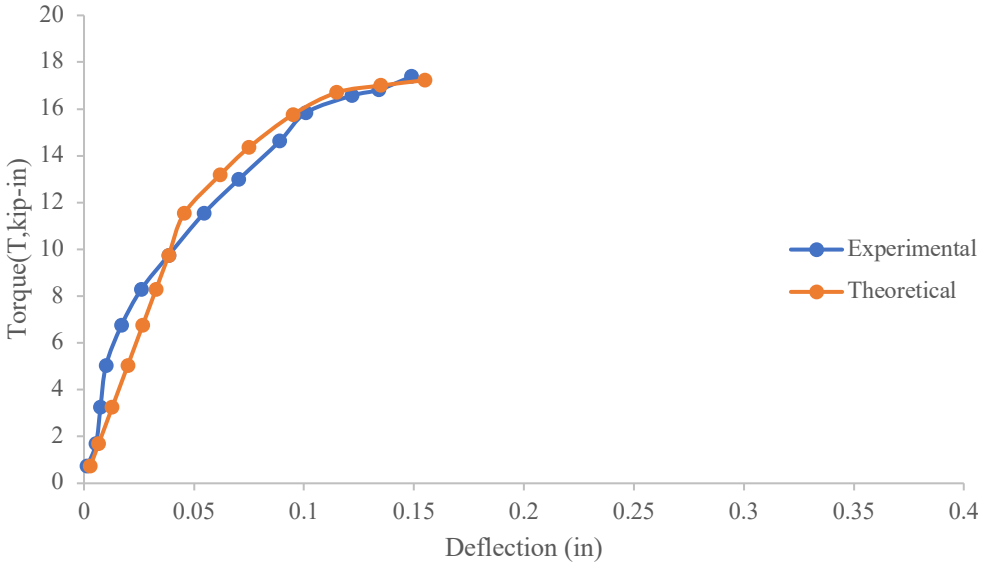

Figure 125. Torque vs. Deflection (APBT- Fixed-Fixed)

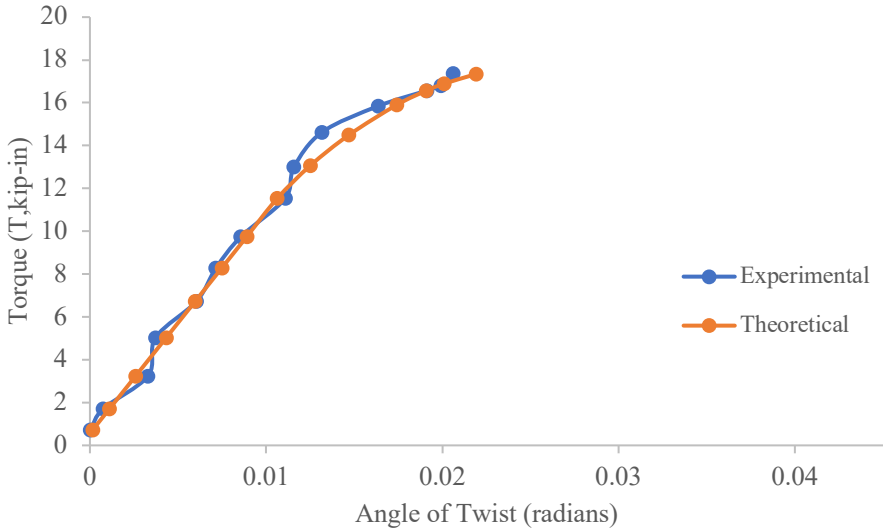

Figure 126. Torque vs. Angle of Twist (APBT- Fixed-Fixed)

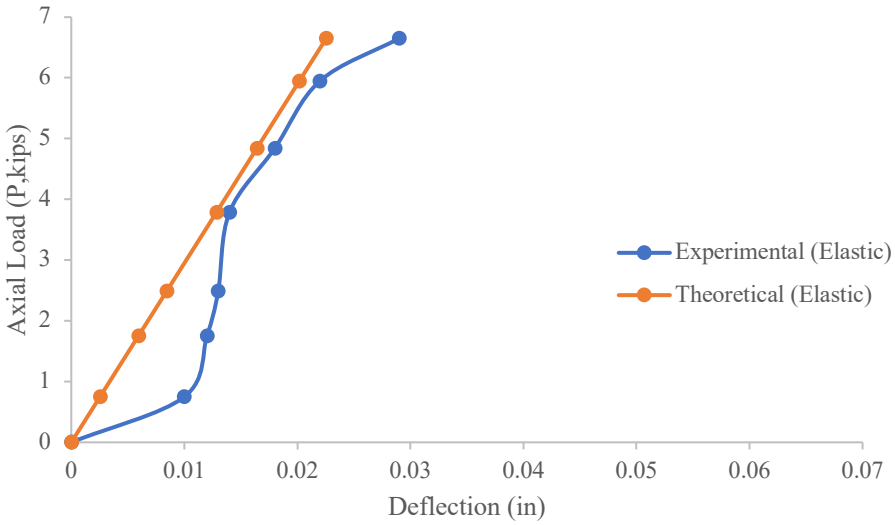

Figure 127. Axial Load vs. Deflection (APBT- Fixed-Pinned)

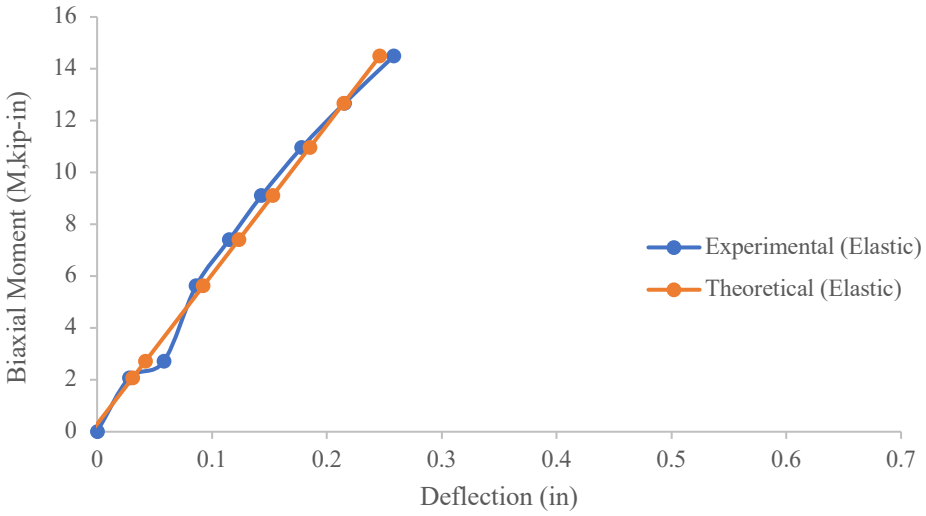

Figure 128. Biaxial Moment vs. Deflection (APBT- Fixed-Pinned)

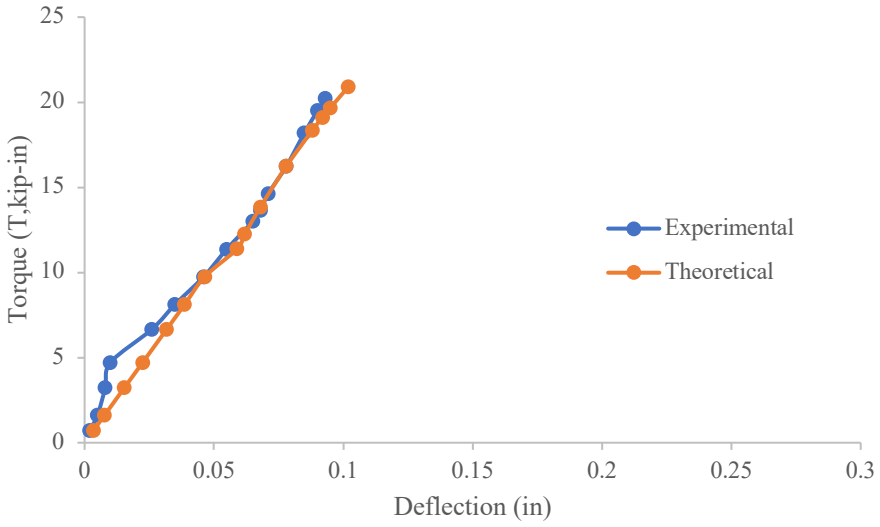

Figure 129. Torque vs. Deflection (APBT- Fixed-Pinned)

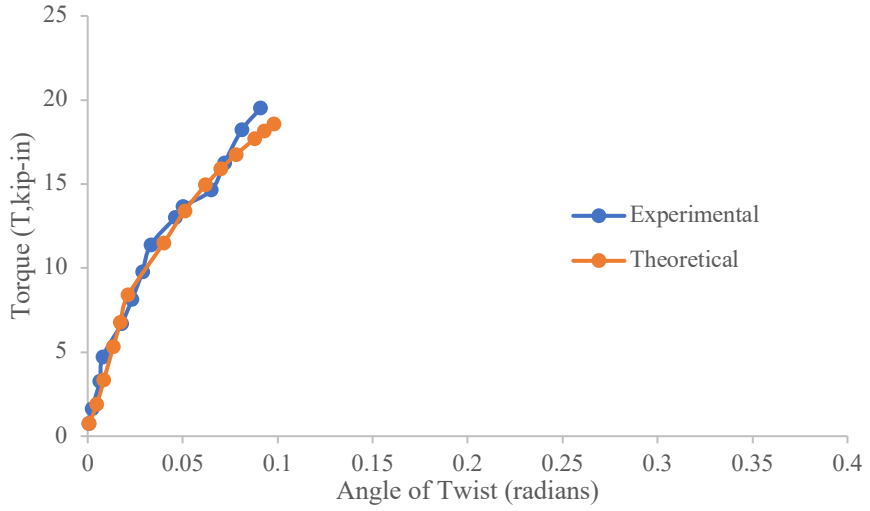

Figure 130. Torque vs. Angle of Twist (APBT- Fixed-Pinned)

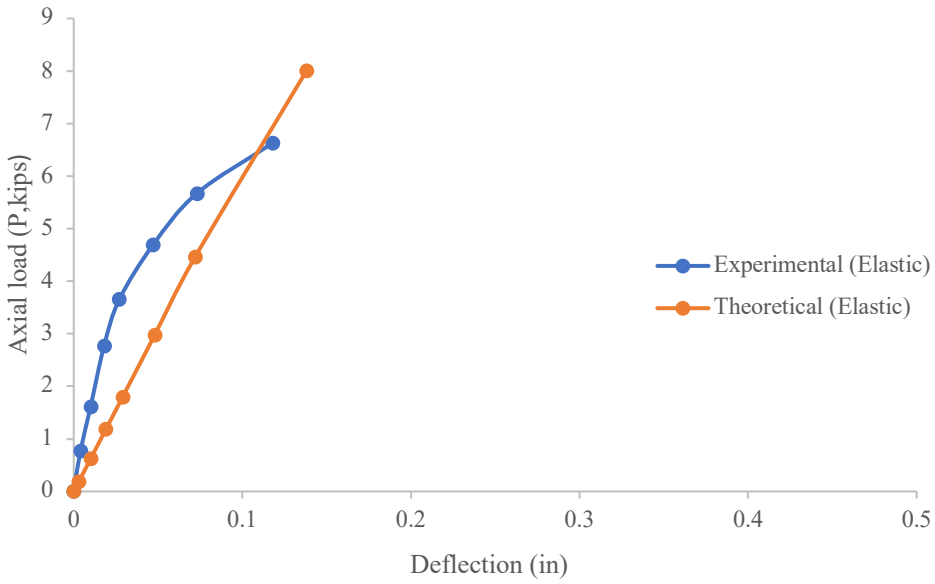

Figure 131. Axial load vs. Deflection (HPT- Pinned-Pinned)

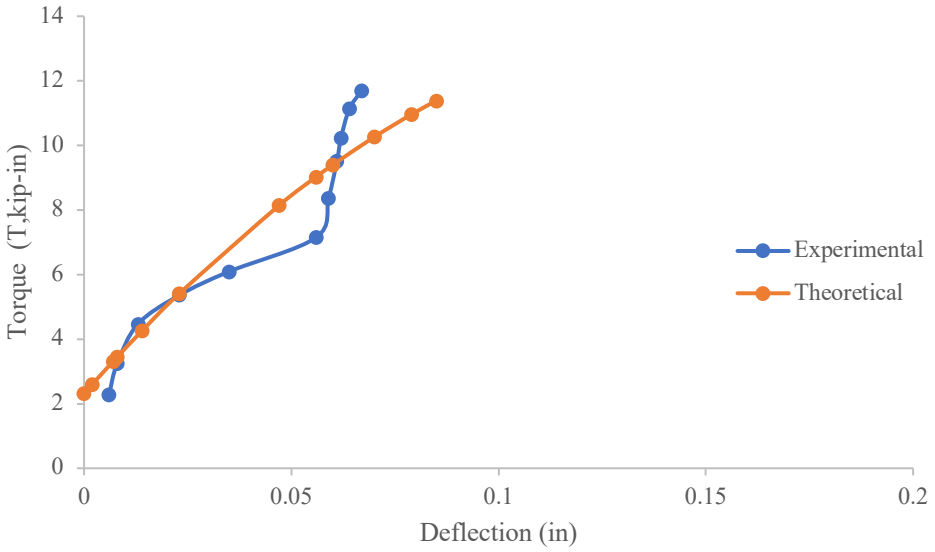

Figure 132. Torque vs. Deflection (HPT- Pinned-Pinned)

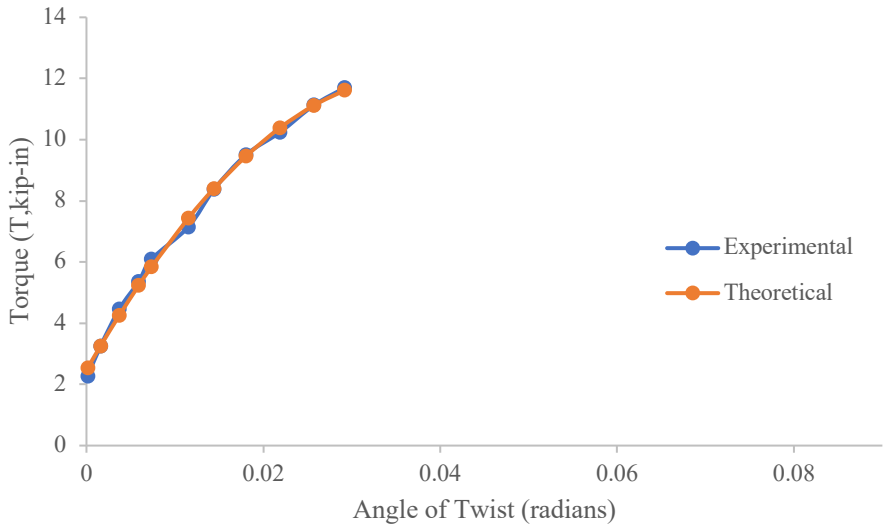

Figure 133. Torque vs. Angle of Twist (HPT- Pinned-Pinned)

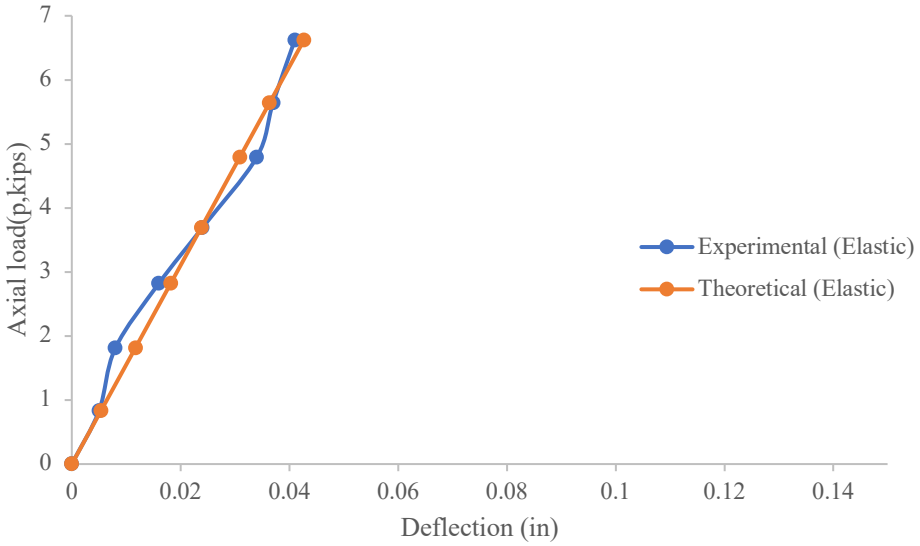

Figure 134. Axial Load vs. Deflection (HPT- Fixed-Pinned)

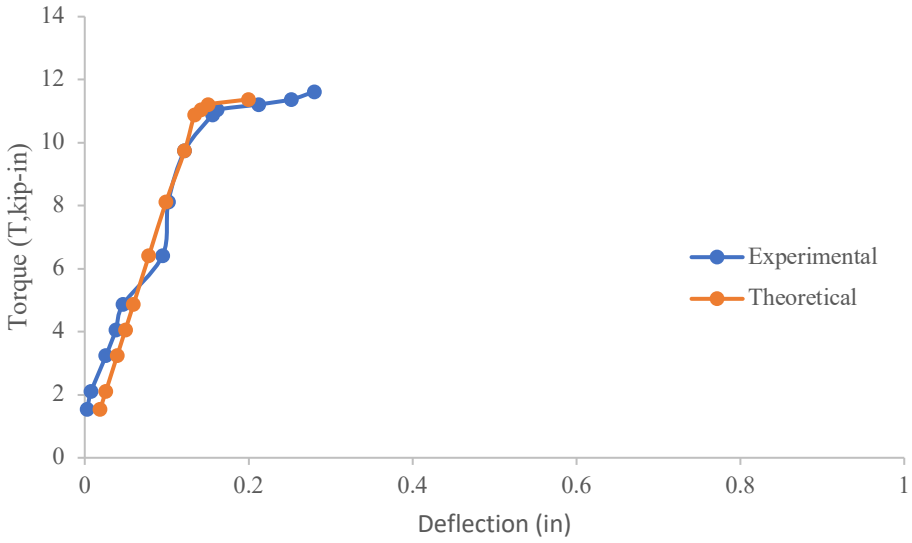

Figure 135. Torque vs. Deflection (HPT- Fixed-Pinned)

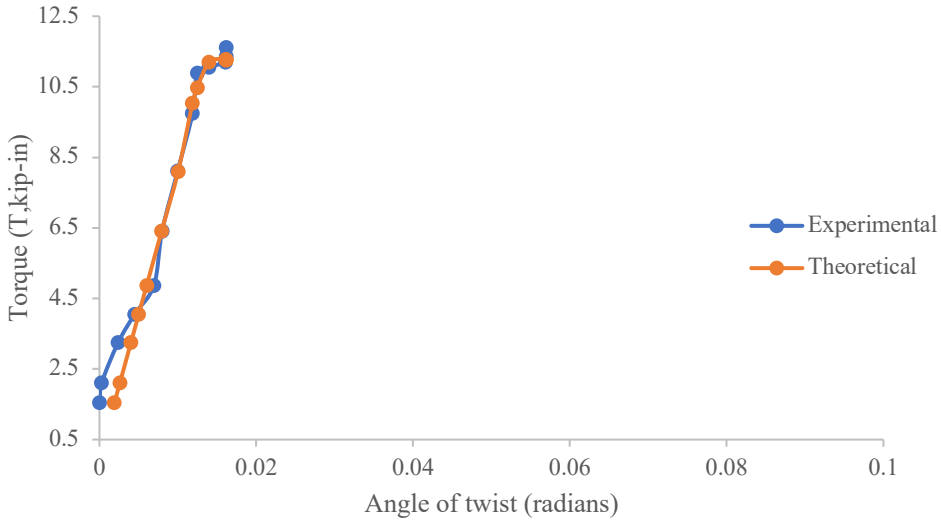

Figure 136. Torque vs. Angle of Twist (HPT- Fixed-Pinned)

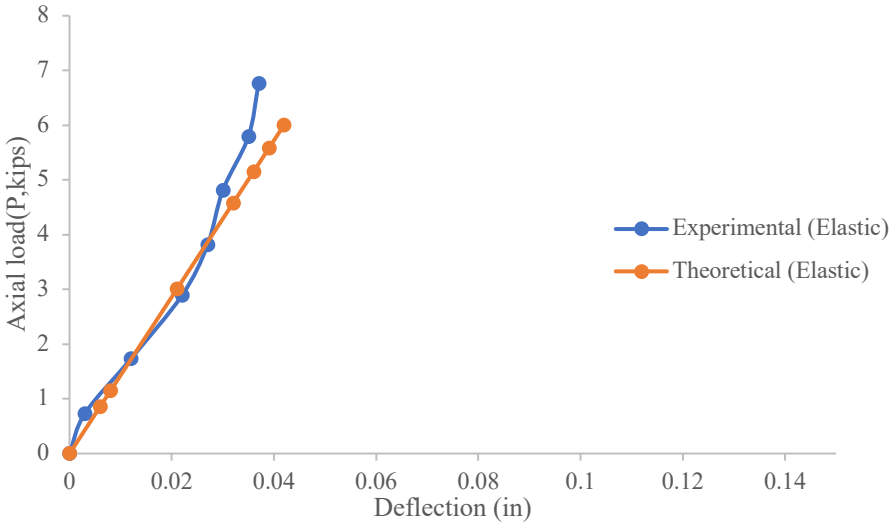

Figure 137. Axial load vs. Deflection (HPT- Fixed-Fixed)

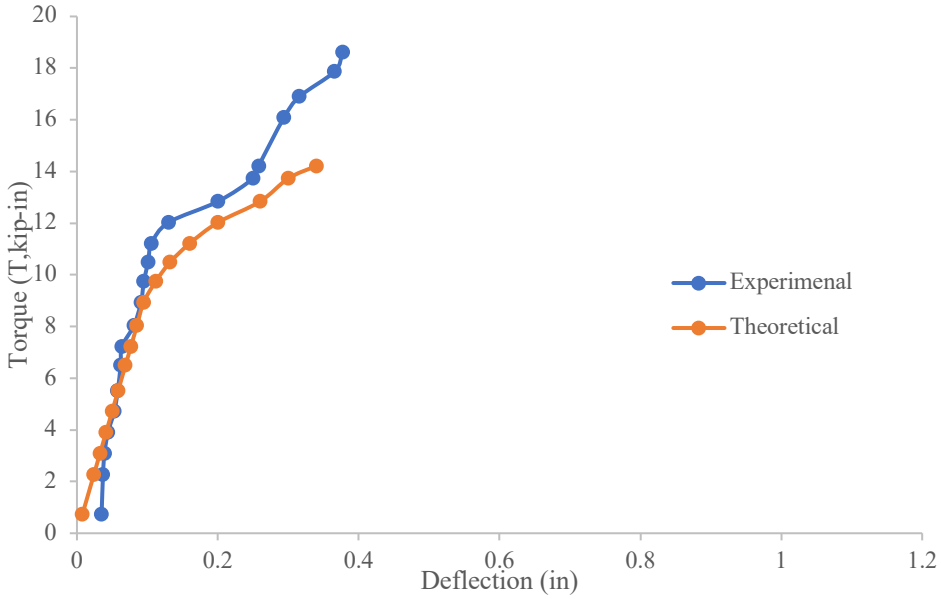

Figure 138. Torque vs. Deflection (HPT- Fixed-Fixed)

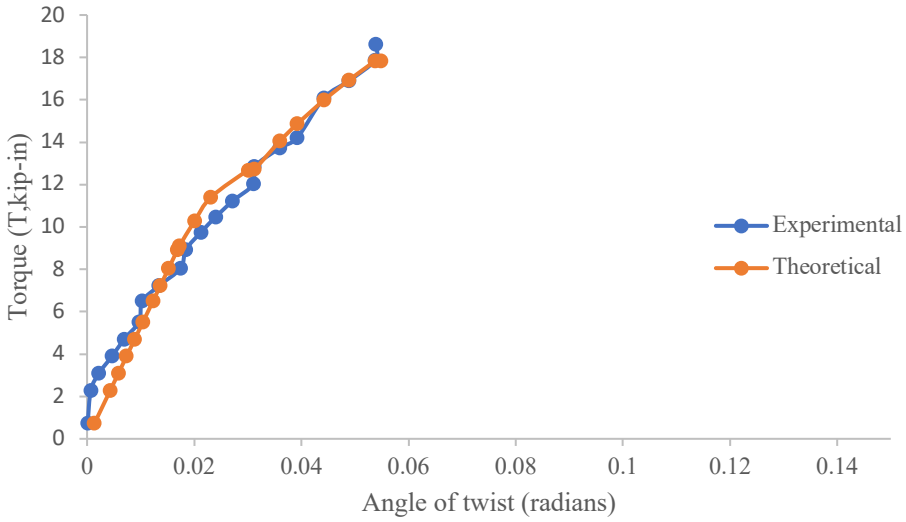

Figure 139. Torque vs. Angle of Twist (HPT- Fixed-Fixed)

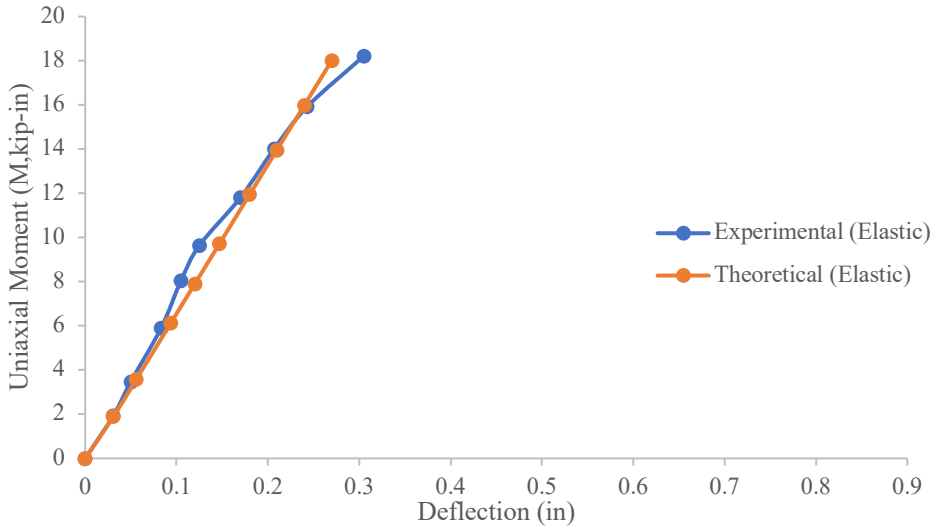

Figure 140. Uniaxial Moment vs. Deflection (HUT- Pinned-Pinned)

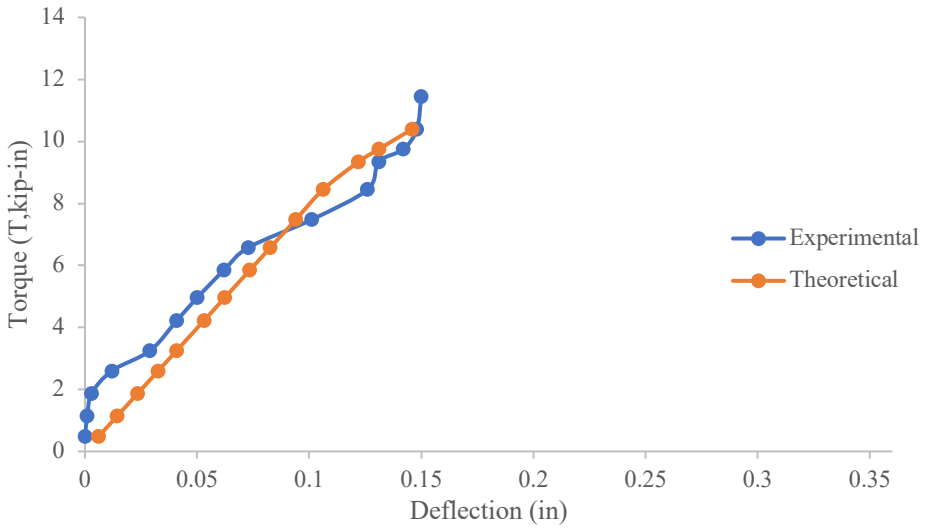

Figure 141. Torque vs. Deflection (HUT- Pinned-Pinned)

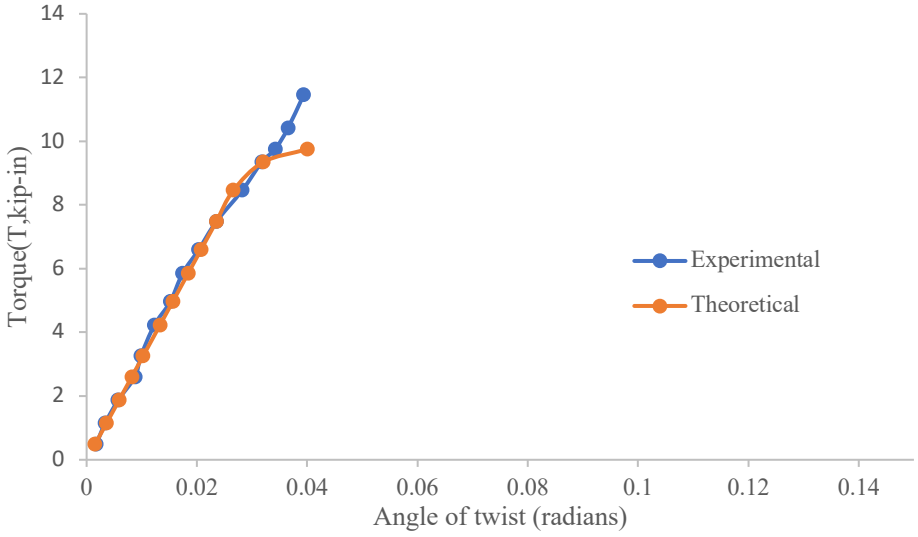

Figure 142. Torque vs. Angle of Twist (HUT- Pinned-Pinned)

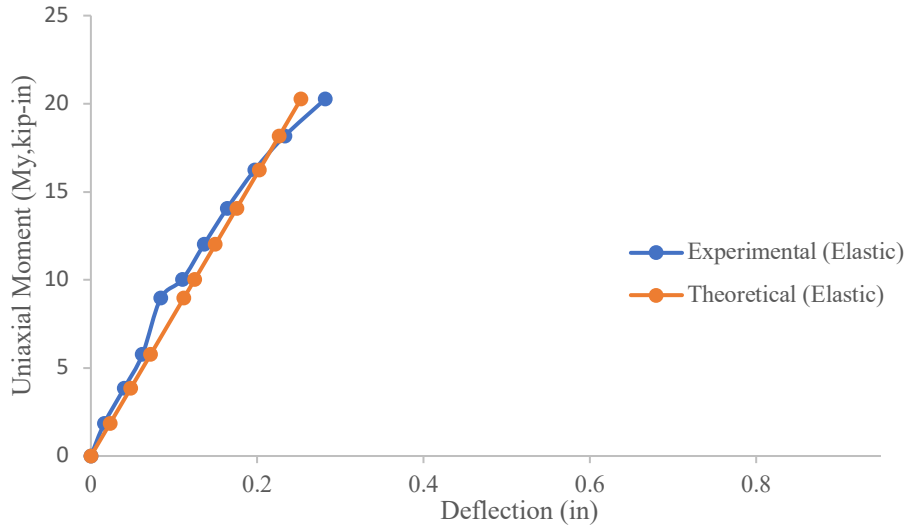

Figure 143. Uniaxial Moment vs. Deflection (HUT- Fixed-Pinned)

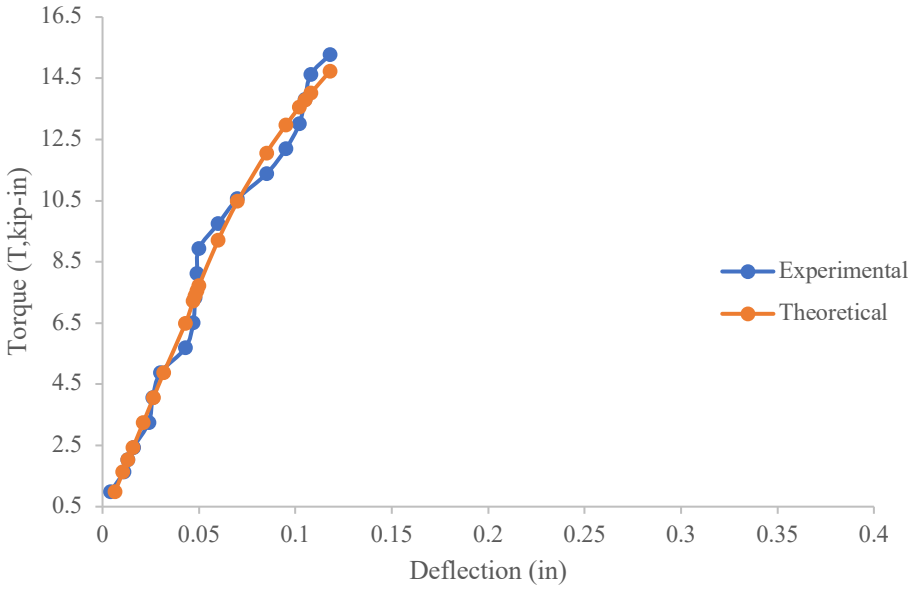

Figure 144. Torque vs. Deflection (HUT- Fixed-Pinned)

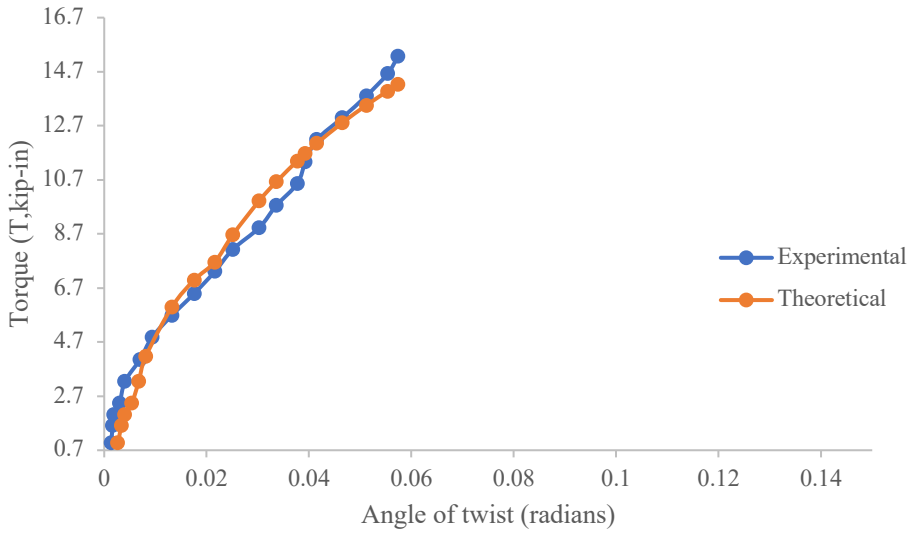

Figure 145. Torque vs. Angle of Twist (HUT- Fixed-Pinned)

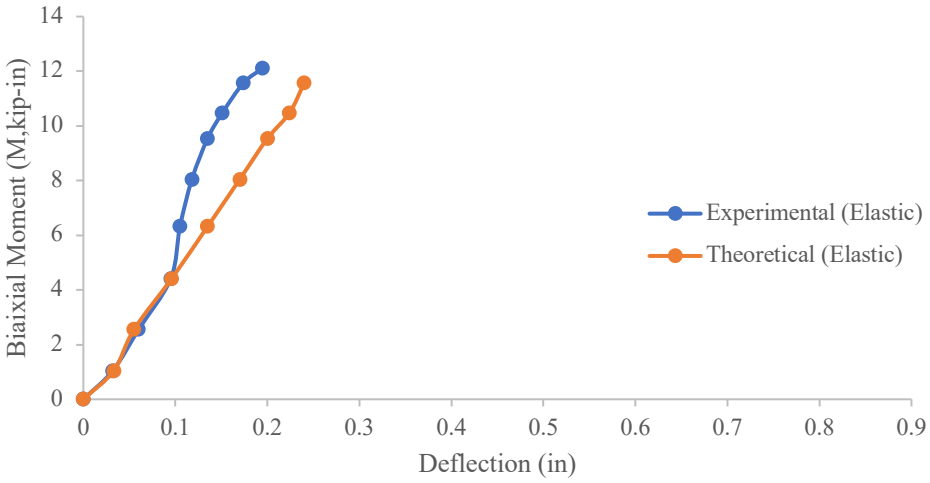

Figure 146. Biaxial Moment vs. Deflection (HBT- Pinned-Pinned)

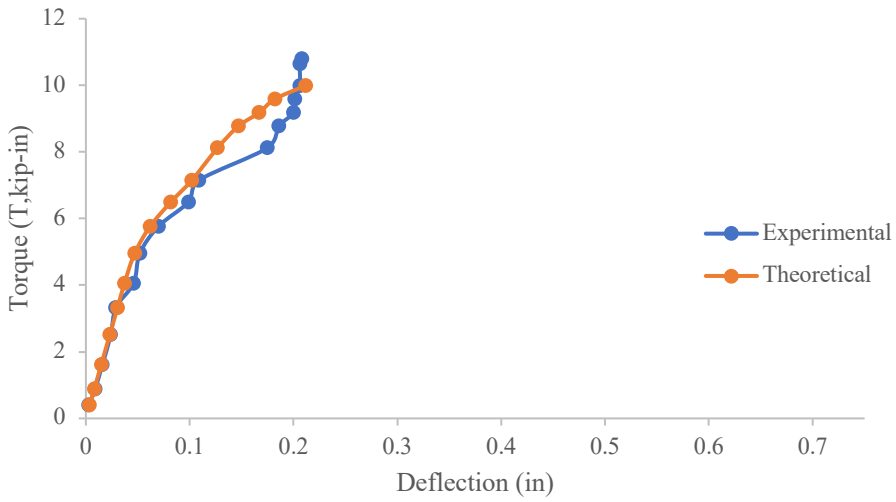

Figure 147. Torque vs. Deflection (HBT- Pinned-Pinned)

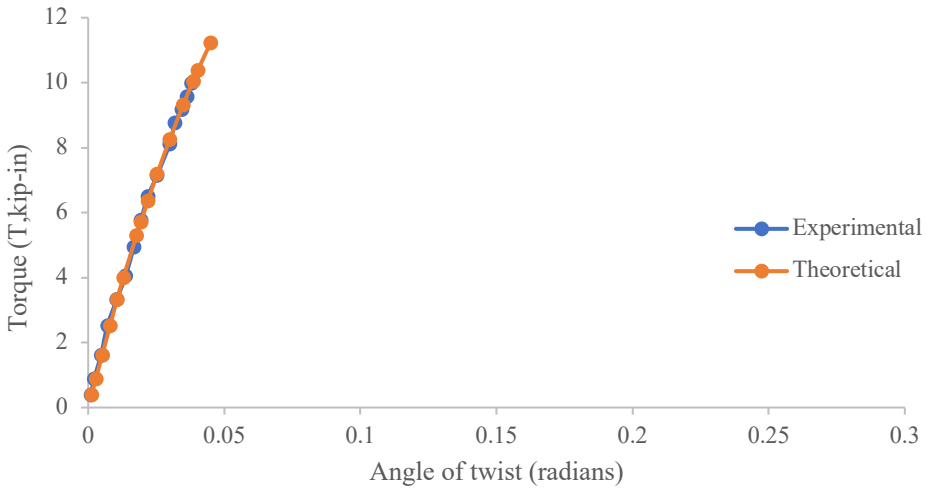

Figure 148. Torque vs. Angle of Twist (HBT- Pinned-Pinned)

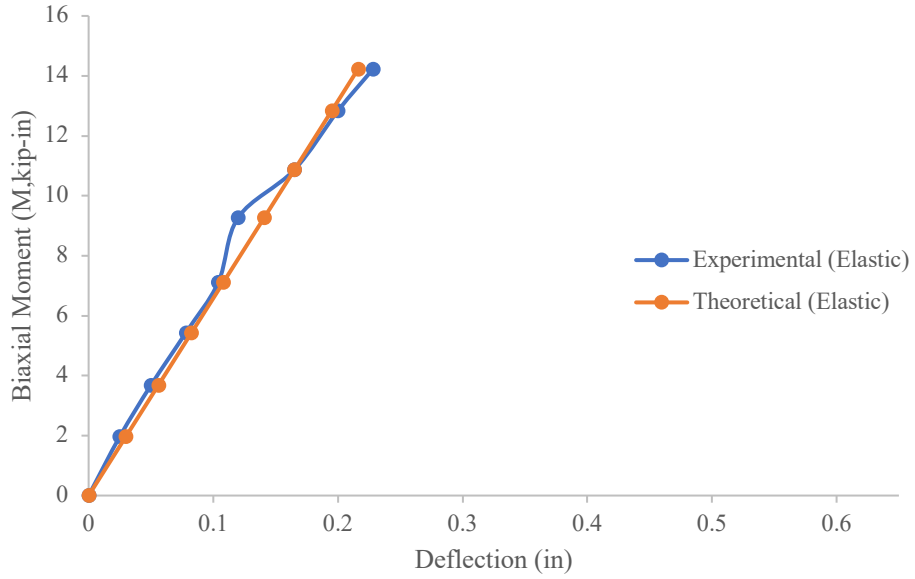

Figure 149. Biaxial Moment vs. Deflection (HBT- Fixed-Pinned)

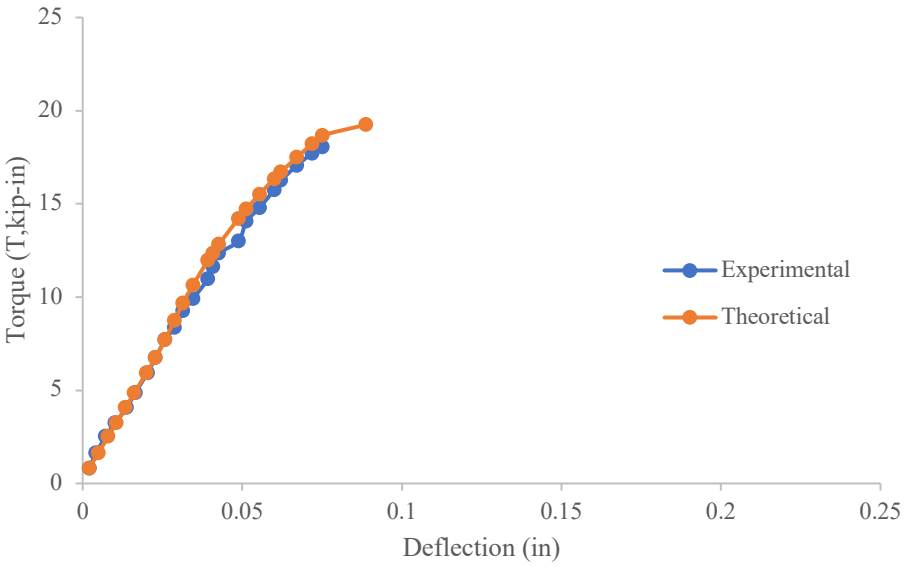

Figure 150. Torque vs. Deflection (HBT- Fixed-Pinned)

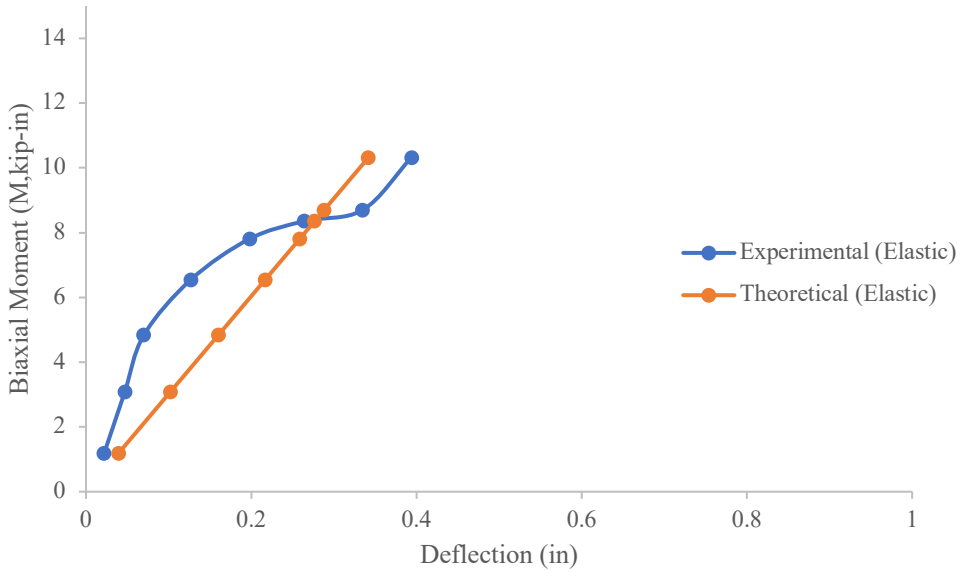

Figure 151. Torque vs. Deflection (HBT- Fixed-Pinned)

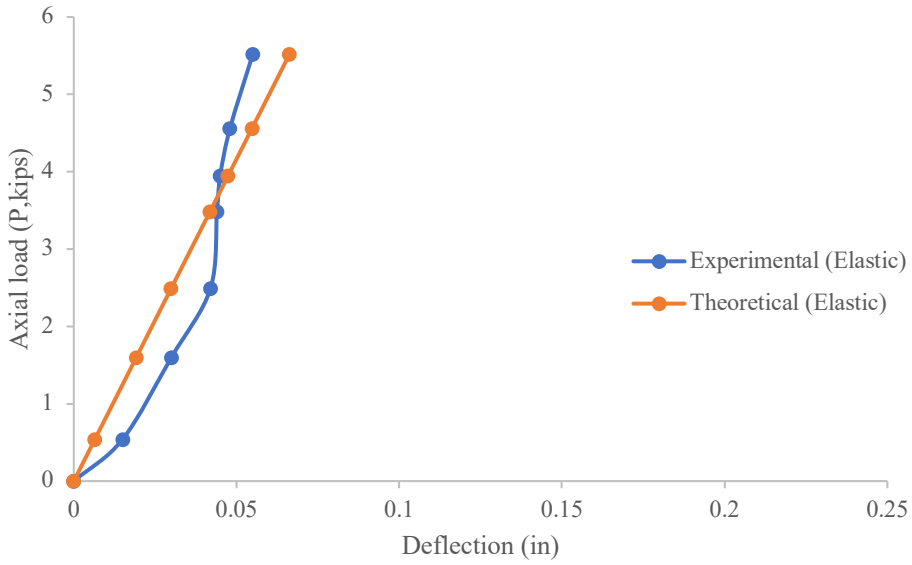

Figure 152. Axial Load vs. Deflection (HPUT- Pinned-Pinned)

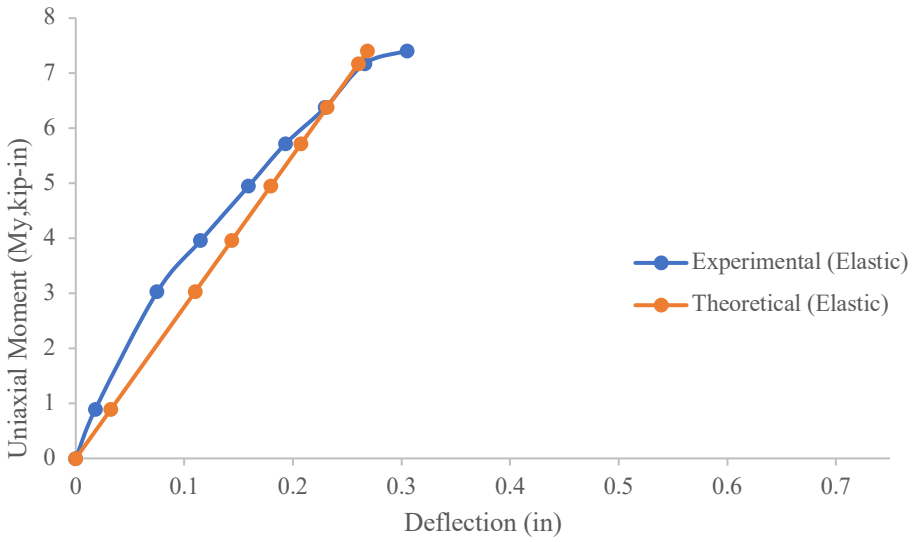

Figure 153. Uniaxial Moment vs. Deflection (HPUT- Pinned-Pinned)

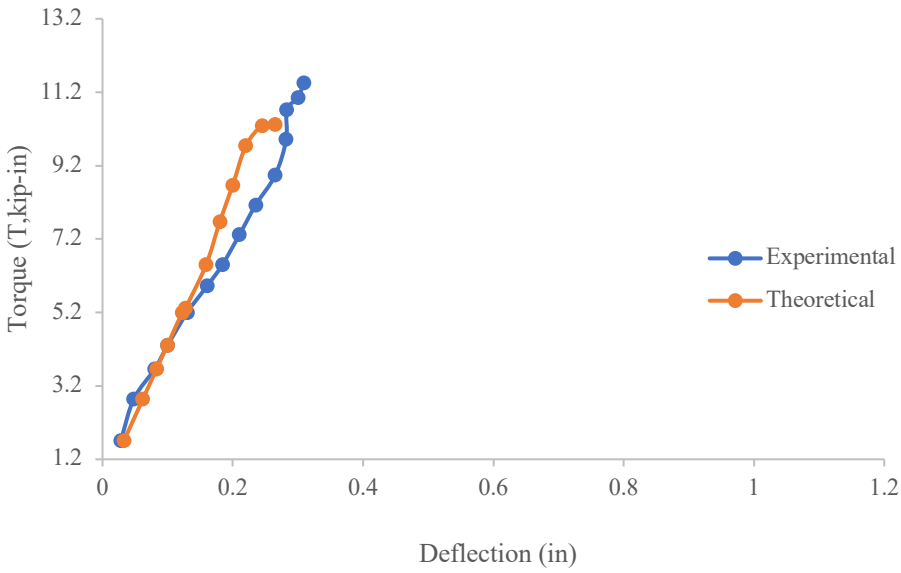

Figure 154. Torque vs. Deflection (HPUT- Pinned-Pinned)

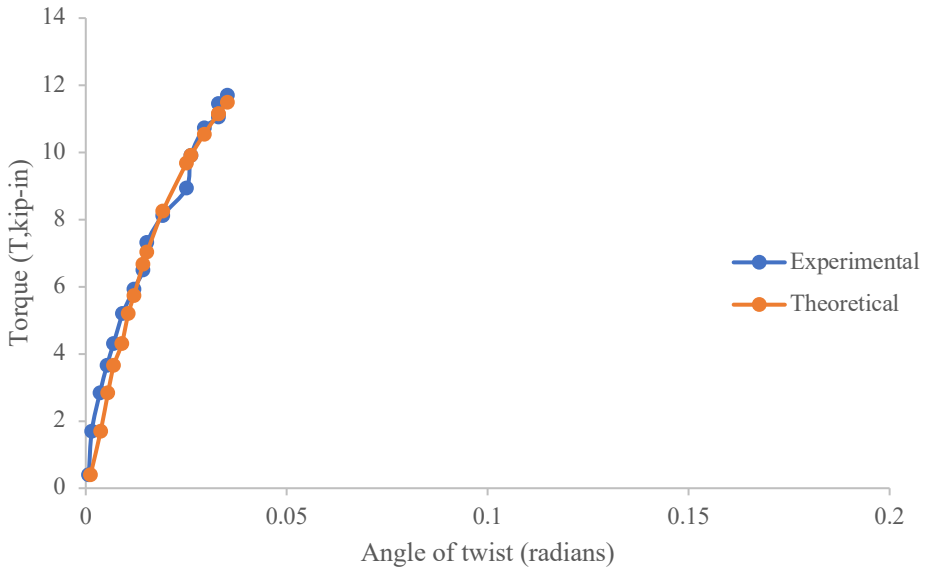

Figure 155. Torque vs. Angle of twist (HPUT- Pinned-Pinned)

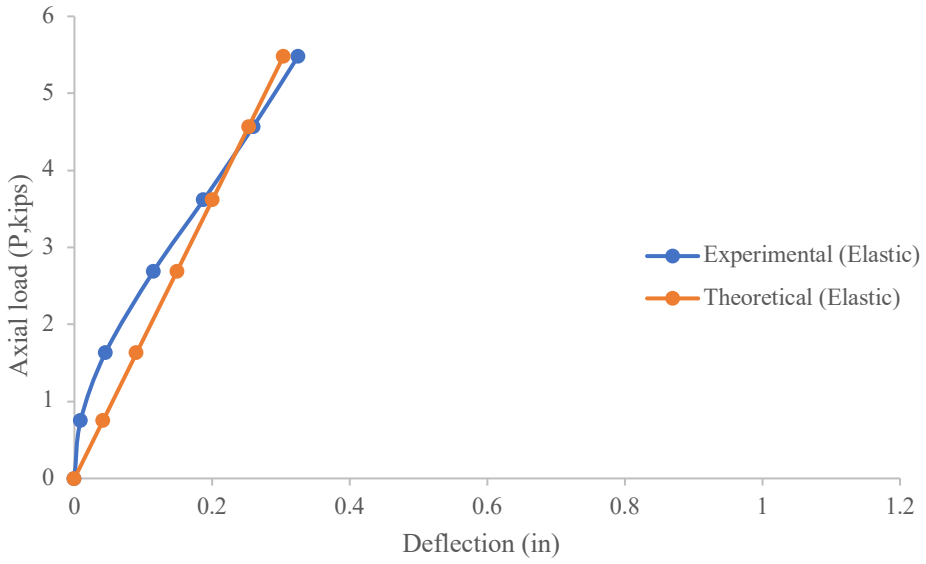

Figure 156. Torque vs. Angle of twist (HPUT- Fixed-Pinned)

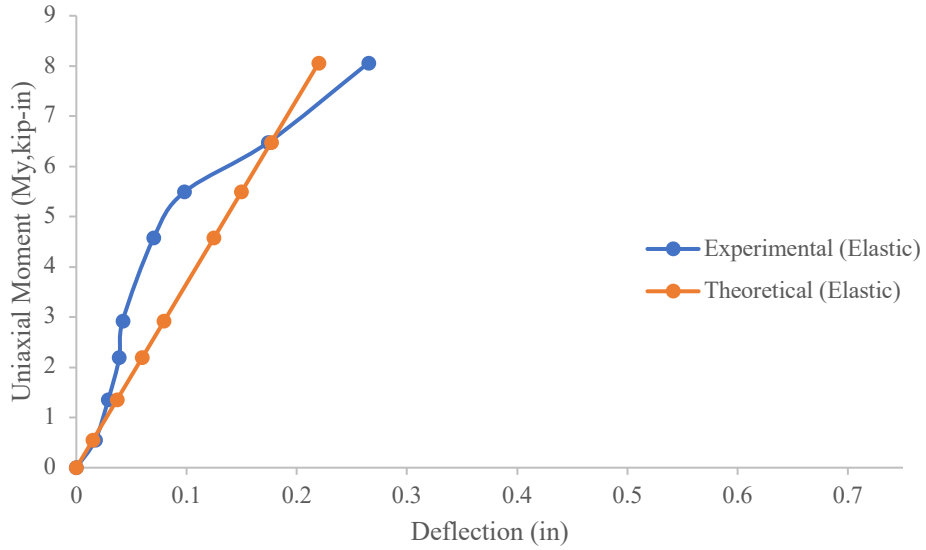

Figure 157. Uniaxial Moment vs. Deflection (HPUT- Fixed-Pinned)

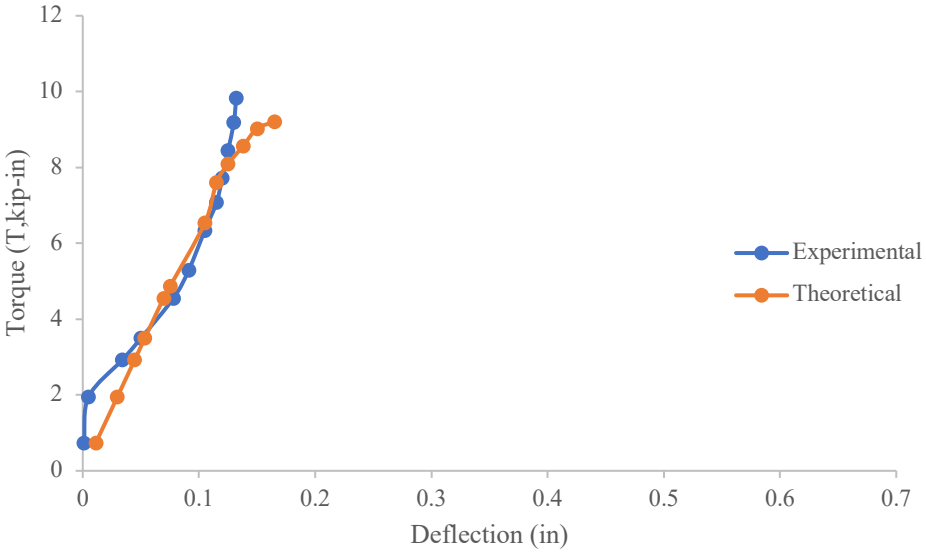

Figure 158. Torque vs. Deflection (HPUT- Fixed-Pinned)

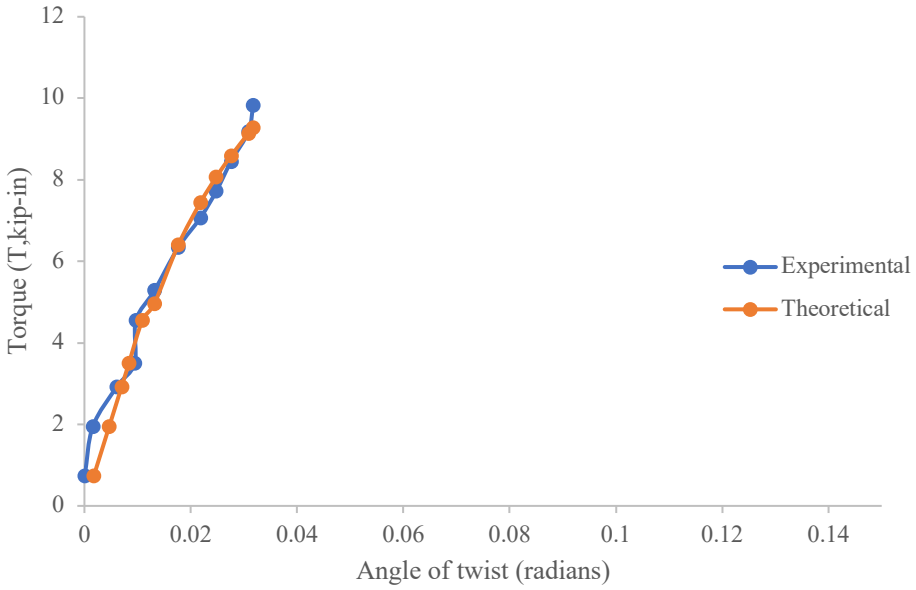

Figure 159. Torque vs. Angle of Twist (HPUT- Fixed-Pinned)

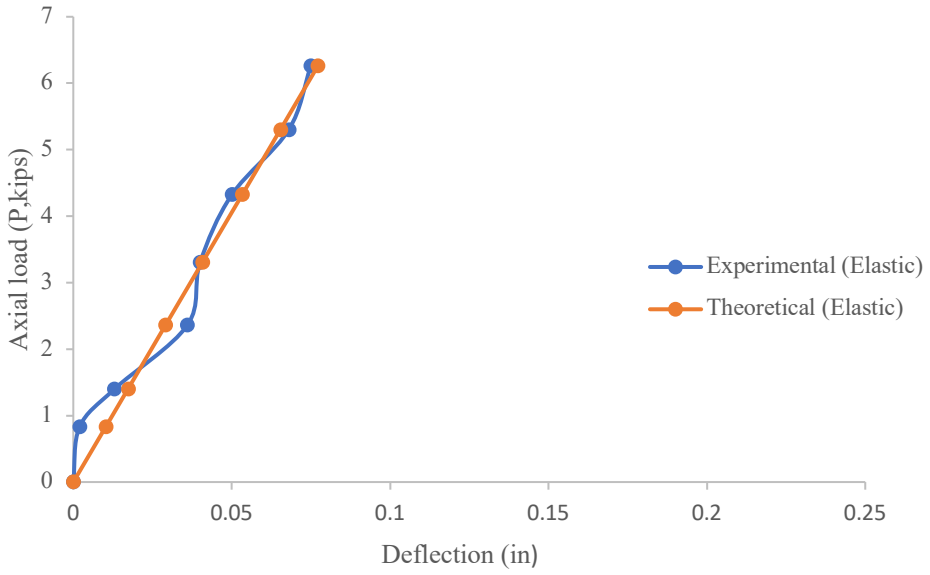

Figure 160. Axial Load vs. Deflection (HPUT- Fixed-Fixed)

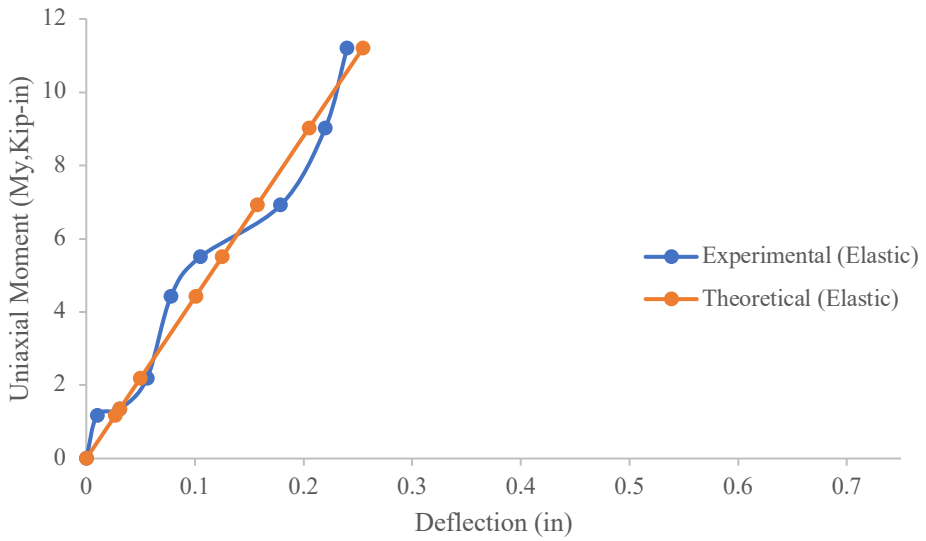

Figure 161. Uniaxial Moment vs. Deflection (HPUT- Fixed-Fixed)

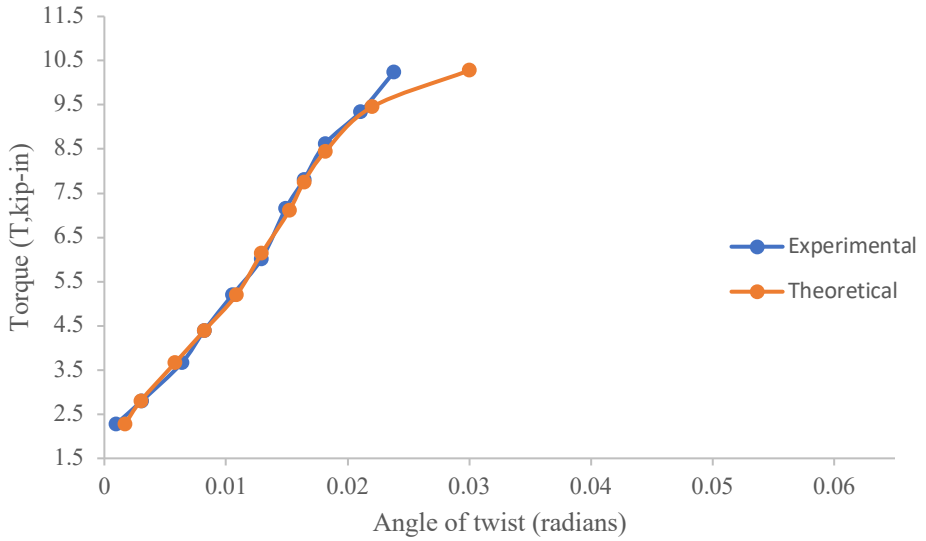

Figure 162. Torque vs. Angle of twist (HPUT- Fixed-Fixed)

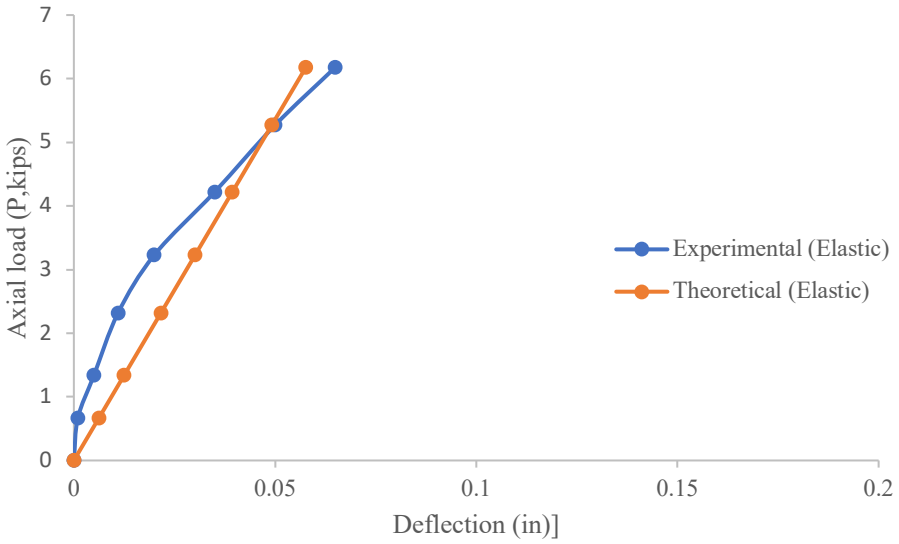

Figure 163. Axial Load vs. Deflection (HPBT- Pinned-Pinned)

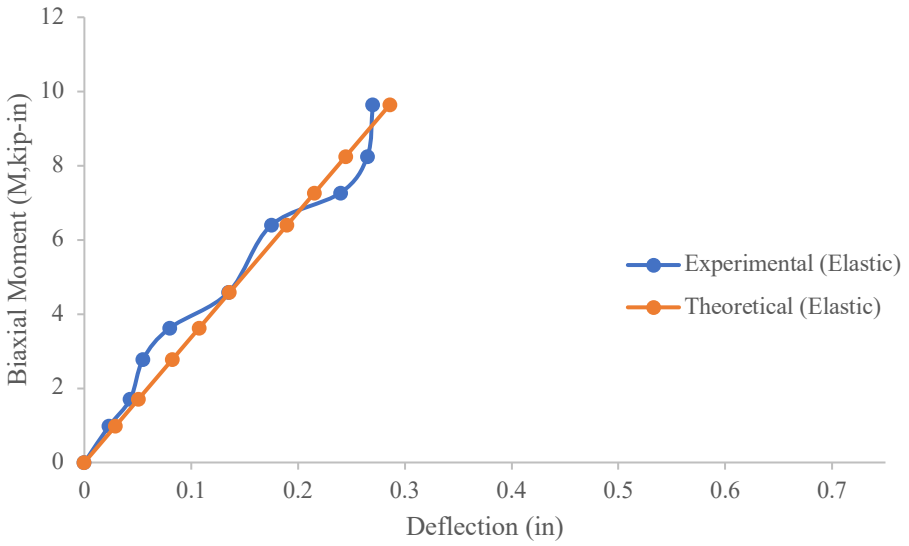

Figure 164. Biaxial Moment vs. Deflection (HPBT- Pinned-Pinned)

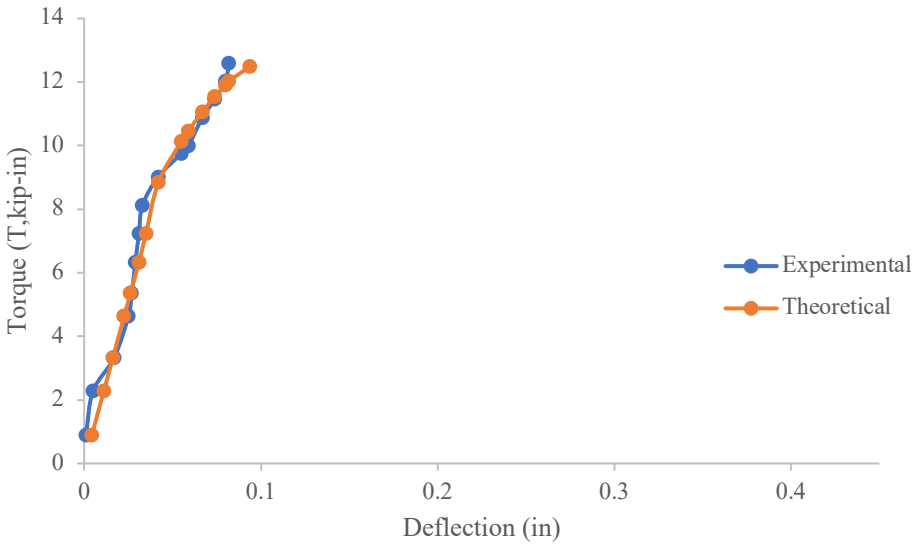

Figure 165. Biaxial Moment vs. Deflection (HPBT- Pinned-Pinned)

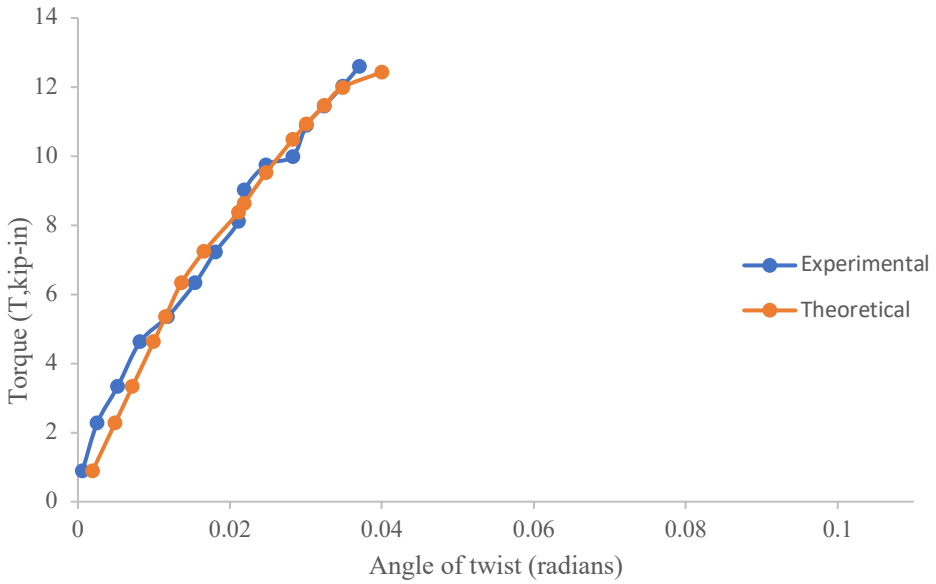

Figure 166. Biaxial Moment vs. Deflection (HPBT- Pinned-Pinned)

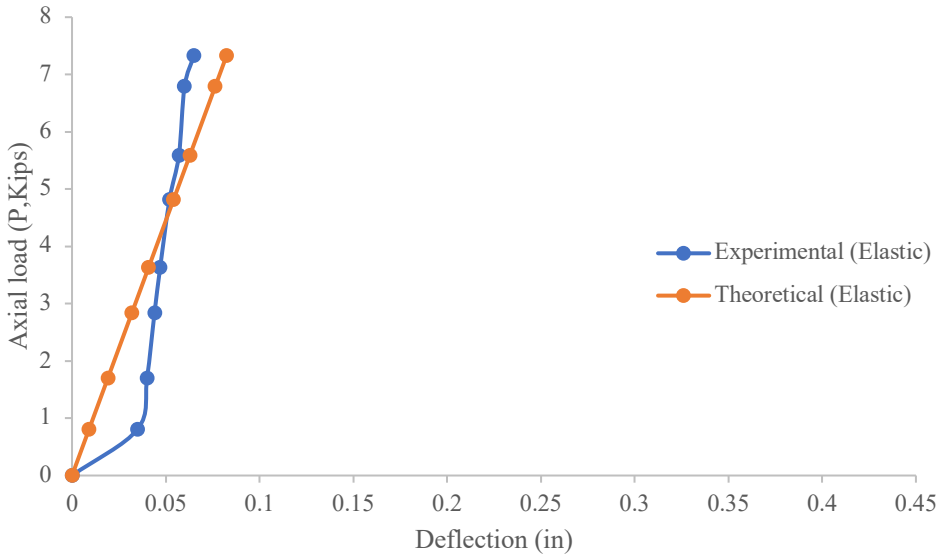

Figure 167. Axial Load vs. Deflection (HPBT- Fixed-Pinned)

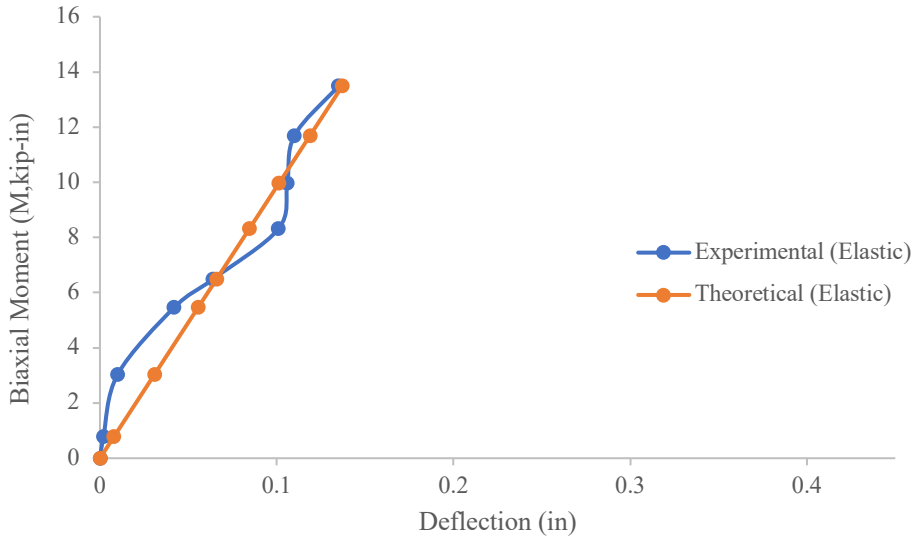

Figure 168. Biaxial Moment vs. Deflection (HPBT- Fixed-Pinned)

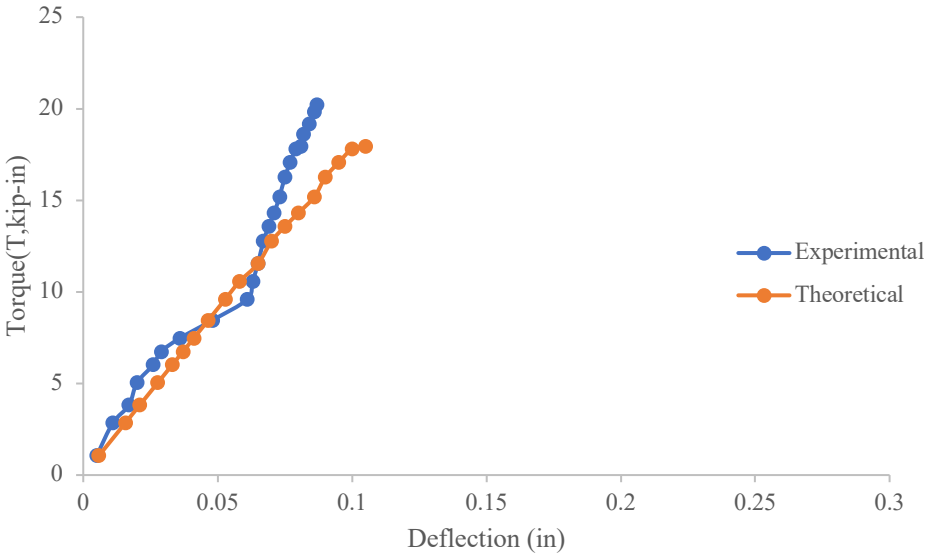

Figure 169. Torque vs. Deflection (HPBT- Fixed-Pinned)

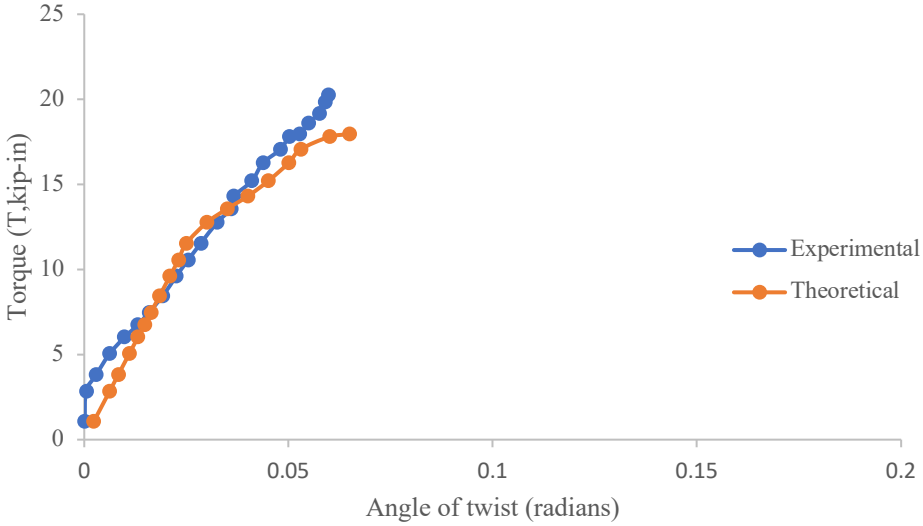

Figure 170. Torque vs. Angle of Twist (HPBT- Fixed-Pinned)

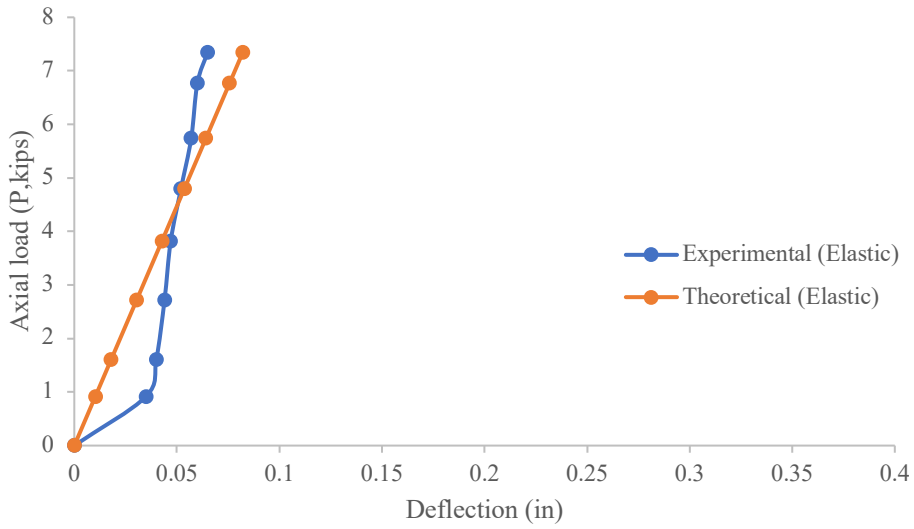

Figure 171. Axial Load vs. Deflection (HPBT- Fixed-Fixed)

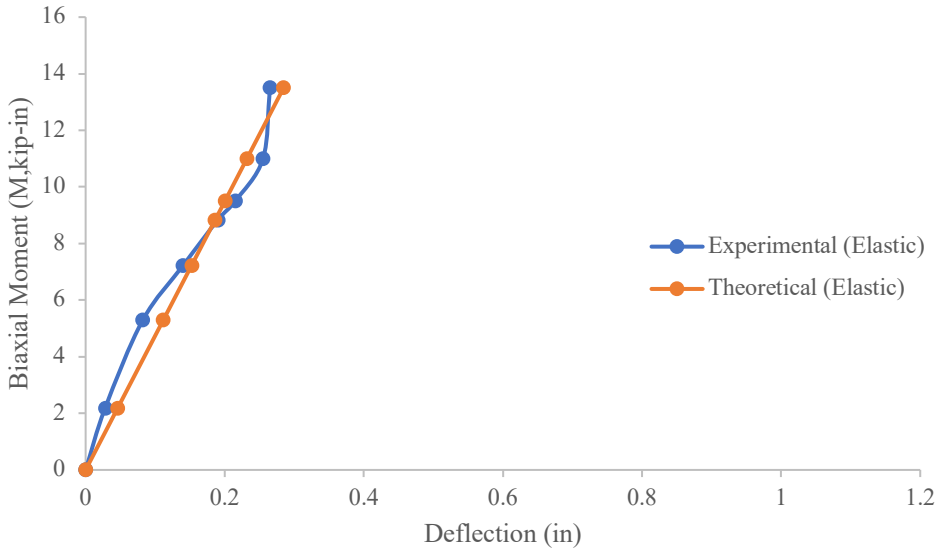

Figure 172. Biaxial Moment vs. Deflection (HPBT- Fixed-Fixed

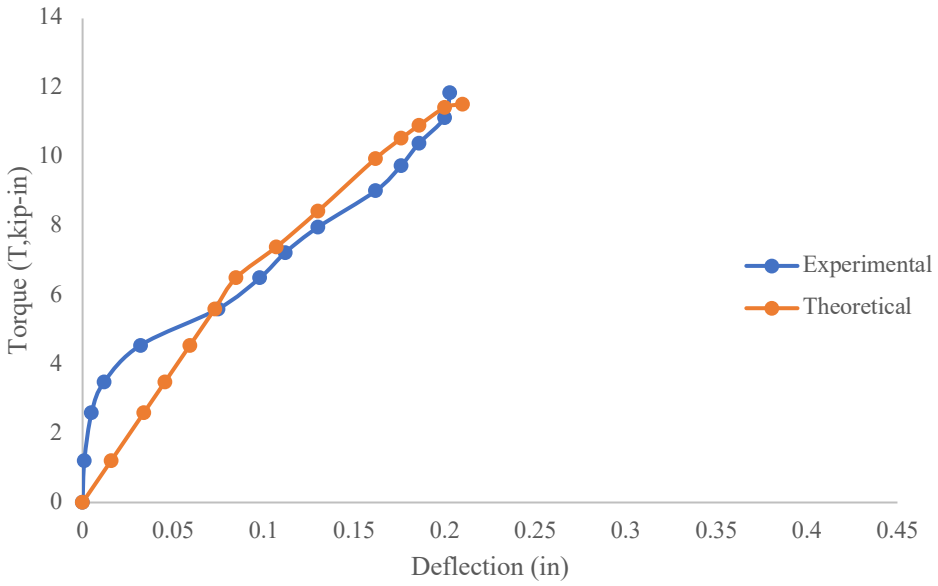

Figure 173. Torque vs. Deflection (HPBT- Fixed-Fixed)

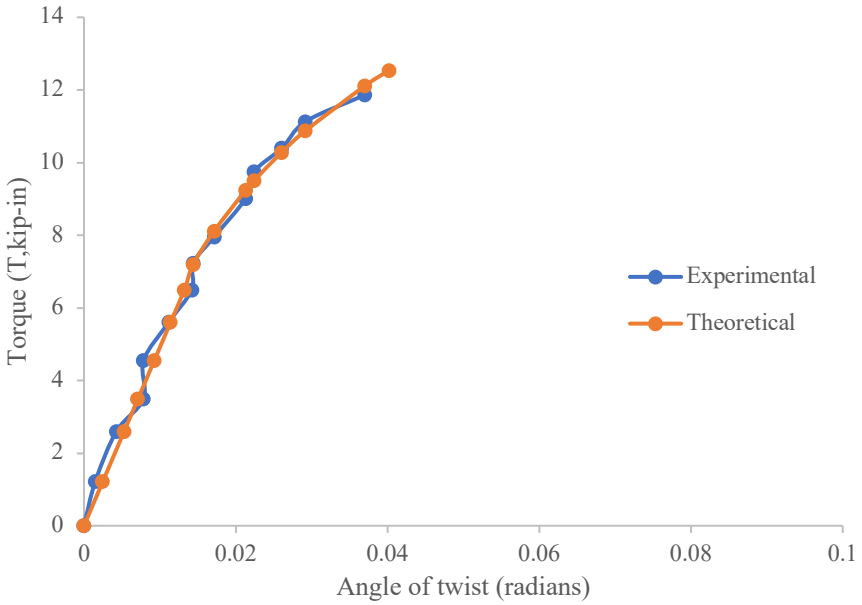

Figure 174. Torque vs. Angle of Twist (HPBT- Fixed-Fixed)

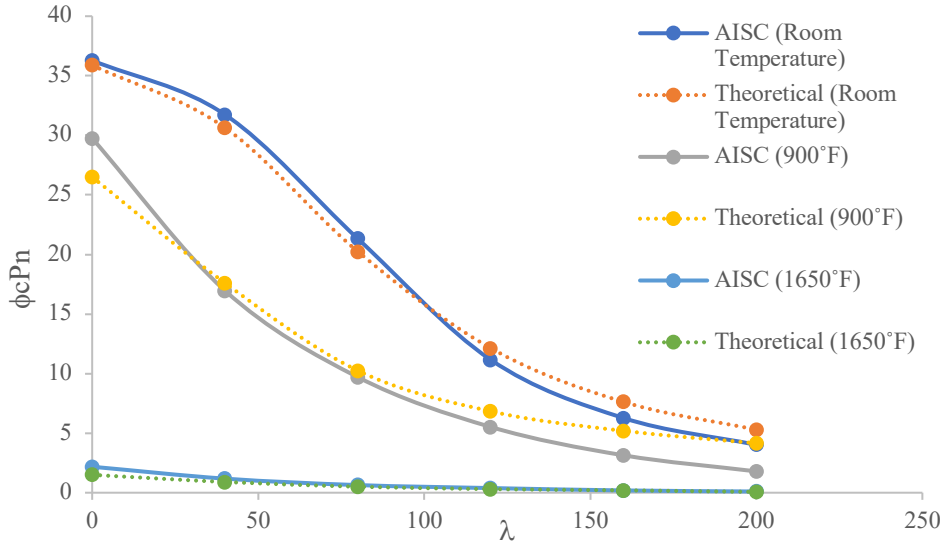

Figure 175. Design strength vs Slenderness ratio

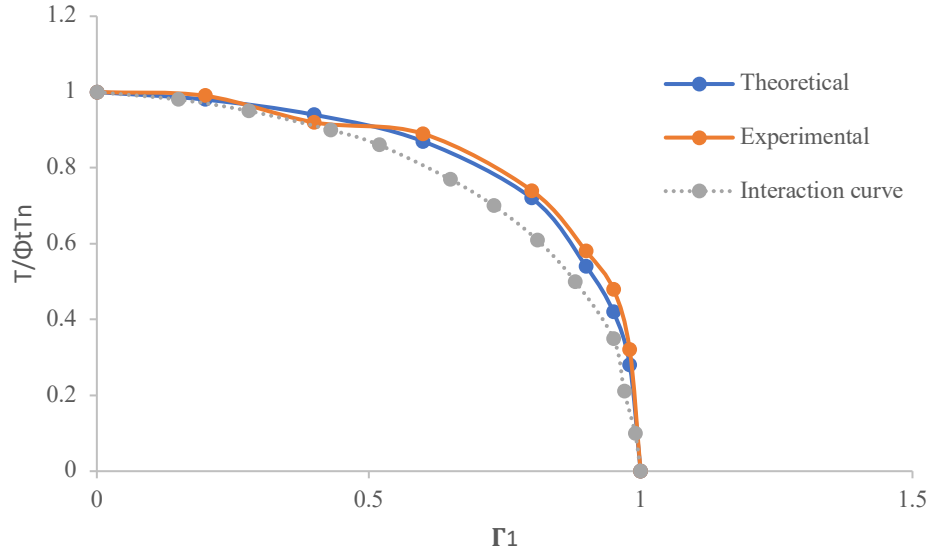

Figure 176. Comparison of Theoretical and Experimental Interaction Curves for APBT

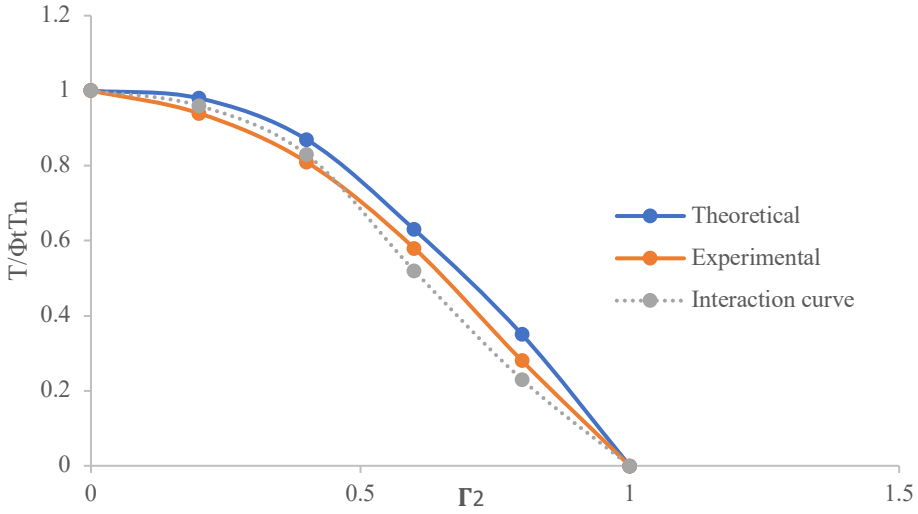

Figure 177. Comparison of Theoretical and Experimental Interaction Curves for HPBT (700°F)

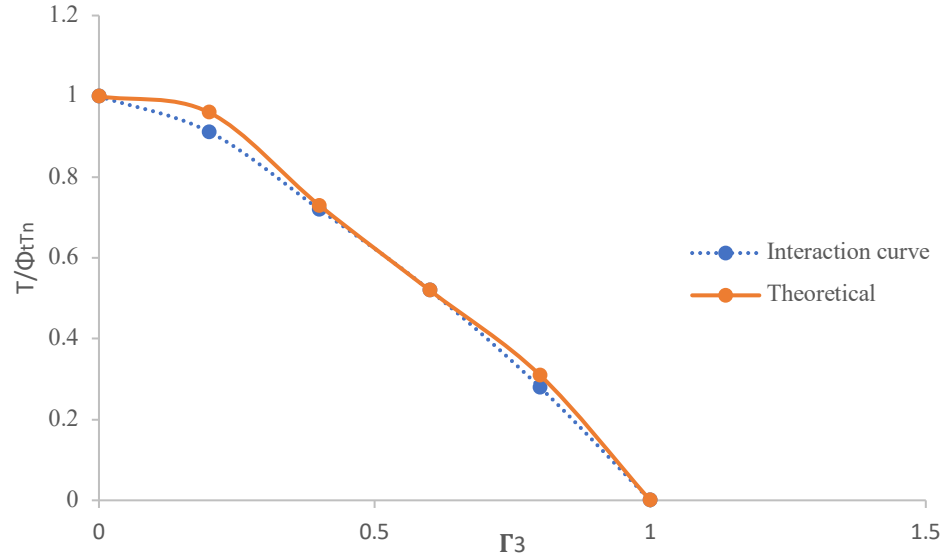

Figure 178. Comparison of Theoretical and Experimental Interaction Curves for HPBT (900°F)

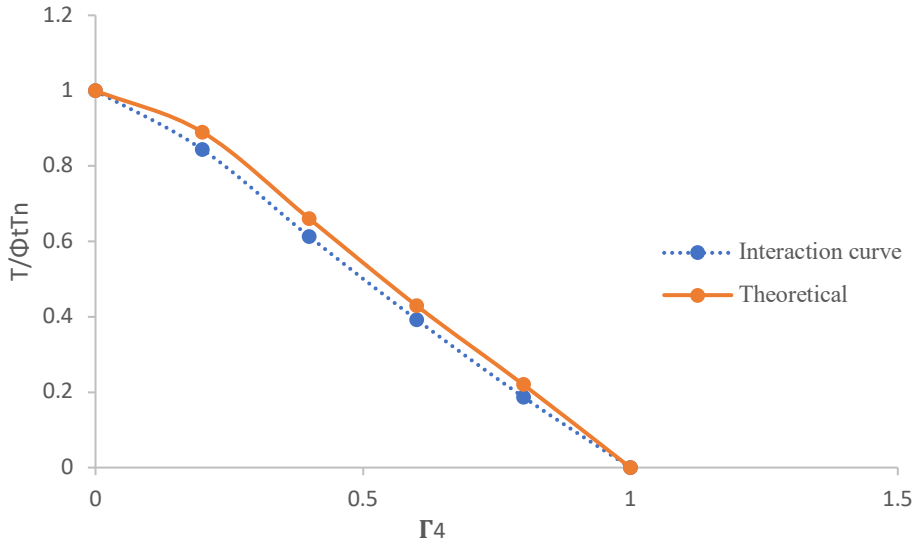

Figure 179. Comparison of Theoretical and Experimental Interaction Curves for HPBT (1650°F)

APPENDIX B: LIST OF TABLES

Table 1. Chemical Composition of A513 Type-1 Specimens

	C	Mn	P	S	Si	Al	Cu	Cb	Mo	Ni	Cr	V	Ti	B	N	Cn
Mat. Report	0.06	0.33	0.006	0.003	0.03	0.03	0.1	0.001	0.01	0.04	0.09	0.01	0.001	0	0.007	0.002
A513 Standards	0.2 – 0.15	0.30 – 0.60	0.035	0.035												

Table 2. List of Experimental Tests

Item	Load case	Load Type	Boundary Conditions	Temperature
1.	APT	Axial load + Torsion	Pinned - Pinned	Ambient
2.	AUT	Uniaxial Bending + Torsion	Pinned - Pinned	Ambient
3.	ABT	Biaxial Bending + Torsion	Pinned - Pinned	Ambient
4.	APUT	Axial load + Uniaxial Bending + Torsion	Pinned - Pinned	Ambient
5.	APBT	Axial load + Biaxial Bending + Torsion	Pinned - Pinned	Ambient
6.	APT	Axial load + Torsion	Fixed - Pinned	Ambient
7.	AUT	Uniaxial Bending + Torsion	Fixed - Pinned	Ambient
8.	ABT	Biaxial Bending + Torsion	Fixed - Pinned	Ambient
9.	APUT	Axial load + Uniaxial Bending + Torsion	Fixed - Pinned	Ambient
10.	APBT	Axial load + Biaxial Bending + Torsion	Fixed - Pinned	Ambient
11.	APT	Axial load + Torsion	Fixed - Fixed	Ambient
12.	AUT	Uniaxial Bending + Torsion	Fixed – Fixed on y-axis	Ambient
13.	ABT	Biaxial Bending + Torsion	Fixed – Fixed on y-axis	Ambient
14.	APUT	Axial load + Uniaxial Bending + Torsion	Fixed – Fixed on y-axis	Ambient
15.	APBT	Axial load + Biaxial Bending + Torsion	Fixed – Fixed on y-axis	Ambient
16.	APT	Axial load + Torsion	Pinned - Pinned	700°F
17.	AUT	Uniaxial Bending + Torsion	Pinned - Pinned	700°F
18.	ABT	Biaxial Bending + Torsion	Pinned - Pinned	700°F
19.	APUT	Axial load + Uniaxial Bending + Torsion	Pinned - Pinned	700°F
20.	APBT	Axial load + Biaxial Bending + Torsion	Pinned - Pinned	700°F
21.	APT	Axial load + Torsion	Fixed - Pinned	700°F
22.	AUT	Uniaxial Bending + Torsion	Fixed - Pinned	700°F
23.	ABT	Biaxial Bending + Torsion	Fixed - Pinned	700°F
24.	APUT	Axial load + Uniaxial Bending + Torsion	Fixed - Pinned	700°F
25.	APBT	Axial load + Biaxial Bending + Torsion	Fixed - Pinned	700°F
26.	APT	Axial load + Torsion	Fixed - Fixed	700°F
27.	AUT	Uniaxial Bending + Torsion	Fixed – Fixed on y-axis	700°F
28.	ABT	Biaxial Bending + Torsion	Fixed – Fixed on y-axis	700°F

Table 3. List of Experimental Tests Continued

Item	Load case	Load Type	Boundary Conditions	Temperature
29.	APUT	Axial load + Uniaxial Bending + Torsion	Fixed – Fixed on y-axis	700°F
30.	APBT	Axial load + Biaxial Bending + Torsion	Fixed – Fixed on y-axis	700°F

Table 4. Experimental Results for Ambient Temperature Tests (Pinned Boundary Condition)

Load Type	Maximum Axial Load (kips)	Maximum Bending Moment (kip-in)	Maximum Torsional Moment (kip-in)	Maximum Deflection (in)	Maximum Angle of Twist (radians)
APT	6.63	0	11.70	0.118	0.029
AUT	0	8.66	16.09	0.442	0.007
ABT	0	12.11	10.81	0.208	0.004
APUT	7.58	11.33	24.70	0.506	0.048
APBT	6.01	15.80	19.67	0.247	0.049

Table 5. Experimental Results for Ambient Temperature Tests (Fixed Boundary Condition)

Load Type	Maximum Axial Load (kips)	Maximum Bending Moment (kip-in)	Maximum Torsional Moment (kip-in)	Maximum Deflection (in)	Maximum Angle of Twist (radians)
APT	8.57	0	27.78	0.25	0.069
AUT	0	22.29	29.49	0.53	0.084
ABT	0	14.13	16.23	0.30	0.010
APUT	8.79	21.41	27.00	0.27	0.069
APBT	6.62	4.47	17.39	0.151	0.021

Table 6.Experimental Results for Ambient Temperature Tests (Mixed Boundary Condition)

Load Type	Maximum Axial Load (kips)	Maximum Bending Moment (kip-in)	Maximum Torsional Moment (kip-in)	Maximum Deflection (in)	Maximum Angle of Twist (radians)
APT	7.20	0	19.98	0.11	0.051
AUT	0	14.27	28.60	0.24	0.069
ABT	0	16.50	26.49	0.27	0.079
APUT	6.66	21.41	19.42	0.64	0.024
APBT	6.65	14.47	20.23	0.26	0.091

Table 7.Experimental Results for Elevated Temperature Tests (Pinned Boundary Condition)

Load Type	Maximum Axial Load (kips)	Maximum Bending Moment (kip-in)	Maximum Torsional Moment (kip-in)	Maximum Deflection (in)	Maximum Angle of Twist (in)
HPT	6.63	0	11.70	0.144	0.029
HUT	0	18.21	11.46	0.31	0.04
HBT	0	12.11	10.81	0.21	0.04
HPUT	5.52	7.41	11.46	0.31	0.035
HPBT	6.18	9.64	12.59	0.27	0.037

Table 8.Experimental Results for Elevated Temperature Tests (Fixed Boundary Condition)

Load Type	Maximum Axial Load (kips)	Maximum Bending Moment (kip-in)	Maximum Torsional Moment (kip-in)	Maximum Deflection (in)	Maximum Angle of Twist (radians)
HPT	6.76	0	18.25	0.37	0.05
HUT	0	20.27	15.28	0.28	0.06
HBT	0	10.32	10.09	0.39	0.009
HPUT	6.26	11.21	10.24	0.24	0.024
HPBT	7.35	13.49	20.23	0.135	0.087

Table 9. Experimental Results for Elevated Temperature Tests (Mixed Boundary Condition)

Load Type	Maximum Axial Load (kips)	Maximum Bending Moment (kip-in)	Maximum Torsional Moment (kip-in)	Maximum Deflection (in)	Maximum Angle of Twist (radians)
HPT	6.62	0	11.62	0.28	0.016
HUT	0	11.32	13.57	0.131	0.062
HBT	0	14.22	19.25	0.228	0.075
HPUT	5.48	8.06	20.31	0.636	0.020
HPBT	7.33	13.49	20.23	0.135	0.059

Table 10.Comparison of Experimental and Theoretical Results for Ambient Temperature Tests (Pinned Boundary Condition)

Load Type	Theo/Exp Axial Load	Theo/Exp Bending Moment	Theo/Exp Torsional Moment	Theo/Exp Deflection	Theo/Exp Angle of Twist
APT	1.21	0	0.97	1.17	1.07
AUT	0	1.00	0.89	1.01	1.14
ABT	0	0.96	0.92	1.02	1.13
APUT	1.00	1.00	0.97	0.93	0.98
APBT	1.00	1.00	0.93	0.66	0.94

Table 11.Comparison of Experimental and Theoretical Results for Ambient Temperature Tests (Fixed Boundary Condition)

Load Type	Theo/Exp Axial Load	Theo/Exp Bending Moment	Theo/Exp Torsional Moment	Theo/Exp Deflection	Theo/Exp Angle of Twist
APT	1.00	0	0.94	0.92	1.04
AUT	0	1.00	0.97	1.04	0.95
ABT	0	1.11	0.94	1.01	1.29
APUT	1.00	1.00	1.02	1.07	0.93
APBT	1.00	1.00	0.99	1.03	1.02

Table 12.Comparison of Experimental and Theoretical Results for Ambient Temperature Tests (Mixed Boundary Condition)

Load Type	Theo/Exp Axial Load	Theo/Exp Bending Moment	Theo/Exp Torsional Moment	Theo/Exp Deflection	Theo/Exp Angle of Twist
APT	1.01	0	0.92	0.97	0.92
AUT	0	1.00	1.14	0.96	1.43
ABT	0	1.00	0.99	0.96	1.09
APUT	1.00	1.00	0.99	0.87	0.92
APBT	1.00	1.00	1.03	0.98	1.08

Table 13.Comparison of Experimental and Theoretical Results for Elevated Temperature Tests (Pinned Boundary Condition)

Load Type	Theo/Exp Axial Load	Theo/Exp Bending Moment	Theo/Exp Torsional Moment	Theo/Exp Deflection	Theo/Exp Angle of Twist
HPT	1.20	0	0.97	0.96	0.93
HUT	0	0.99	1.03	0.87	0.93
HBT	0	0.96	0.92	1.02	1.05
HPUT	1.00	1.00	0.98	0.86	0.99
HPBT	1.00	1.00	0.97	0.98	1.08

Table 14.Comparison of Experimental and Theoretical Results for Elevated Temperature Tests (Fixed Boundary Condition)

Load Type	Theo/Exp Axial Load	Theo/Exp Bending Moment	Theo/Exp Torsional Moment	Theo/Exp Deflection	Theo/Exp Angle of Twist
HPT	0.90	0	1.02	0.92	1.02
HUT	0	1.00	0.88	0.89	0.95
HBT	0	1.00	1.11	0.86	1.22
HPUT	1.00	1.00	1.00	1.06	1.25
HPBT	1.00	0.71	0.92	1.01	1.03

Table 15. Comparison of Experimental and Theoretical Results for Elevated Temperature Tests (Mixed Boundary Condition)

Load Type	Theo/ Exp Axial Load	Theo/Exp Bending Moment	Theo/Exp Torsional Moment	Theo/Exp Deflection	Theo/Exp Angle of Twist
HPT	1.00	0	0.97	0.89	1.01
HUT	0	1.00	1.02	1.08	1.12
HBT	0	1.00	1.01	0.95	1.09
HPUT	1.00	1.00	0.94	0.86	1.1
HPBT	1.01	1.00	0.89	1.01	1.1

Table 16. Dimensionless Interactions for Axial Load, Biaxial Moment and Torsion at 900°F (HPBT)

Load Type	P	Mx	My	T
HPBT	0	0	0	1
HPBT	0.2	0.2	0.2	0.96
HPBT	0.4	0.4	0.4	0.73
HPBT	0.6	0.6	0.6	0.52
HPBT	0.8	0.8	0.8	0.31
HPBT	1.0	1.0	1.0	0.00

Table 17. Dimensionless Interactions for Axial Load, Biaxial Moment and Torsion at 1650°F (HPBT)

Load Type	P	Mx	My	T
HPBT	0	0	0	1
HPBT	0.2	0.2	0.2	0.87
HPBT	0.4	0.4	0.4	0.63
HPBT	0.6	0.6	0.6	0.41
HPBT	0.8	0.8	0.8	0.20
HPBT	1.0	1.0	1.0	0.00

APPENDIX C: LOAD AND MOMENT COEFFICIENTS

The coefficients g_{ij} used in this dissertation proposal are stated as follows:

$$g_{11} = EA_e \quad \text{(C-1)}$$

$$g_{12} = ES_x \quad \text{(C-2)}$$

$$g_{13} = ES_y \quad \text{(C-3)}$$

$$g_{14} = ES_{wx} \quad \text{(C-4)}$$

$$g_{21} = ES_x \quad \text{(C-5)}$$

$$g_{22} = EI_x \quad \text{(C-6)}$$

$$g_{23} = EI_{xy} \quad \text{(C-7)}$$

$$g_{24} = EI_{wy} \quad \text{(C-8)}$$

$$g_{31} = ES_y \quad \text{(C-9)}$$

$$g_{32} = EI_{xy} \quad \text{(C-10)}$$

$$g_{33} = EI_y \quad \text{(C-11)}$$

$$g_{34} = EI_{wx} \quad \text{(C-12)}$$

$$g_{41} = ES_{wx} \quad \text{(C-13)}$$

$$g_{42} = EI_{wy} \quad \text{(C-14)}$$

$$g_{43} = EI_{wx} \quad \text{(C-15)}$$

$$g_{44} = ES_{wy} \quad \text{(C-16)}$$

$$Ae = \int_{Ae} dA \quad \text{(C-17)}$$

$$S_x = \int_{Ae} y dA \quad \text{(C-18)}$$

$$S_y = \int_{Ae} x dA \quad \text{(C-19)}$$

$$S_{wx} = \int_{Ae} \omega_n dA \quad \text{(C-20)}$$

$$I_x = \int_{Ae} y^2 dA \quad \text{(C-21)}$$

$$I_y = \int_{Ae} x^2 \, dA \quad \text{(C-22)}$$

$$I_{wx} = \int_{Ae} \omega x \, dA \quad \text{(C-23)}$$

$$I_{wy} = \int_{Ae} \omega y dA \quad \text{(C-24)}$$

$$I_{xy} = \int_{Ae} xy \, dA \quad \text{(C-25)}$$

$$P_r = \int_{Ae} \sigma_r dA \quad \text{(C-26)}$$

$$P_p = \int_{Ap} \sigma_y dA \quad \text{(C-27)}$$

$$M_{xre} = \int_{Ae} \sigma_r \, y dA \quad \text{(C-28)}$$

$$M_{yre} = \int_{Ae} \sigma_r \, x dA \quad \text{(C-29)}$$

$$M_{xp} = \int_{Ap} \sigma_y \, y dA \quad \text{(C-30)}$$

$$M_{xp} = \int_{Ap} \sigma_y \, y dA \quad \text{(C-31)}$$

The bending stiffnesses are defined as follows:

$$B_{xx} = \left(\frac{g11g22 - g12g21}{g11} \right) \quad \text{(C-32)}$$

$$B_{xy} = \left(\frac{g11g23 - g21g13}{g11} \right) \quad \text{(C-33)}$$

$$B_{xw} = \left(\frac{g11g24 - g12g14}{g11} \right) \quad \text{(C-34)}$$

$$B_{yx} = \left(\frac{g11g32 - g12g31}{g11} \right) \quad \text{(C-35)}$$

$$B_{yy} = \left(\frac{g11g33 - g13g31}{g11} \right) \quad \text{(C-36)}$$

$$B_{yw} = \left(\frac{g11g34 - g14g31}{g11} \right) \quad \text{(C-37)}$$

The inelastic load and moment parameters are stated as follows:

$$P_{ep}^* = P_r + P_p \quad \text{(C-38)}$$

$$P_{ep} = P + P_{ep}^* \quad \text{(C-39)}$$

$$M_{xx(ep)} = M_{xre} + M_{xp} \quad \text{(C-40)}$$

$$M_{yy(ep)} = M_{yre} + M_{yp} \quad \text{(C-42)}$$

APPENDIX D: DERIVATION OF GOVERNING NONLINEAR DIFFERENTIAL EQUATIONS

APPENDIX D.1 Moment-Thrust-Curvature Relationship at Ambient Temperature

A discretized hollow rectangular section with width B, depth D and elemental area A_i is shown in Figure 2. The stress-strain as well as the shear stress-shear strain relationship for this experimental research follows the elastic-perfectly-plastic model including elastic unloading have also been shown in Figure 3 and 4 respectively. The residual stress distribution pattern [1,3,83] for the hollow rectangular section is shown in Figure 5. Considering a point (x,y) of the cross-section subjected to an axial load in addition to bending moments M_x and M_y about both the x and y axes, the normal strain ϵ is given by [1-4,14,16,83,84] as

$$\epsilon = \epsilon_0 + \phi_x y - \phi_y x + \epsilon_r + \epsilon_w \quad \text{(D-1)}$$

in which ϵ_0 represents the average strain, ϕ_x and ϕ_y represents the bending curvatures about the x and y axes respectively, ϵ_r denotes the residual strain and ϵ_w is the warping strain. For this research study, the normal stress-strain (σ-ϵ) relationships outlined below is applied:

$$\sigma = E\epsilon \qquad \text{for } -\epsilon_y < \epsilon < \epsilon_y \quad \text{(D-2)}$$

$$\sigma = +\sigma_y \qquad \text{for } \epsilon \geq \epsilon_y \quad \text{(D-3)}$$

$$\sigma = -\sigma_y \qquad \text{for } \epsilon \leq \epsilon_y \quad \text{(D-4)}$$

in which E is Young's modulus, σ_y is the normal yield stress and ϵ_y is the normal yield strain. Furthermore, the elastic normal stress at any point (x,y) on the selected cross-section is given as

$$\sigma = \frac{P}{A} + \frac{(Mx)y}{Ix} - \frac{(My)x}{Iy} + \sigma_r + \sigma_w \quad \text{(D-5)}$$

where P denotes axial load, M_x and M_y are the bending moments about the x and y axes, A is the cross-sectional area, I_x and I_y represents the moment of inertia of the member cross-section about the x and y axis, σ_r is the residual stress and σ_w is the warping normal stress. It is worth noting

that in the inelastic range, the normal stresses are determined iteratively and thus equation (D-5) is not applicable in that phase. The elastic-perfectly-plastic stress-strain relation is shown in Figure 3 and hence both the axial and biaxial moment equilibrium equations for the typical cross-section are expressed as follows [1,3,4,83-84]:

$$P = -\int_{Ae} \sigma_e \, dA - \int_{Ap} \sigma_y \, dA \quad \text{(D-6)}$$

$$M_x = \int_{Ae} \sigma_e \, y \, dA + \int_{Ap} \sigma_y \, y \, dA \quad \text{(D-7)}$$

$$M_y = -\int_{Ae} \sigma_e \, x \, dA - \int_{Ap} \sigma_y \, x \, dA \quad \text{(D-8)}$$

In the above equations, σ_e represents the normal elastic stress, $\int_{Ae}$ and $\int_{Ap}$ denotes the integrals over the elastic and plastic regions respectively whilst dA is the elemental area of the steel beam-column cross-section. A total of 2048 elemental areas which contributes to greater convergence (512 elemental areas per plate) was selected for each cross-section in this theoretical investigation.

APPENDIX D.2 Inelastic Differential Equation of Torsion under Ambient Temperature

The inclusion of torsion means that the influence of shear stresses cannot be ignored because without shear stresses an unsafe solution is obtained [3,16]. In the current study, an elastic-perfectly-plastic shear stress-strain relationship is implemented. The shear stress τ and shear strain Υ relationship utilized in this research investigation is as shown below:

$$\tau = G \, \Upsilon \qquad \text{for } -\Upsilon_Y < \Upsilon < \Upsilon_Y \quad \text{(D-9)}$$

$$\tau = \tau_Y \qquad \text{for } \Upsilon \geq \Upsilon_Y \quad \text{(D-10)}$$

From the above, G represents the shear modulus, Υ_Y is the shear yield strain whereas τ_Y represents the shear yield stress. Meanwhile, τ represents the elastic shear stress and this is shown by the general equation.

$$\tau = \frac{-AyQ}{hIx} - \frac{-AxQ}{hIy} + \tau_w + \tau_{sv} \quad \text{(D-11)}$$

Ax and Ay represent the shear forces about the x and y axis in the above equation whereas Q stands for the statical area moment, h in this context refers to the cross-sectional plate thickness. Also, τ_w is the warping shear stress and τ_{sv} is the Saint Venant shear stress. For this research investigation, the internal resisting torsional moment M_{zint} is revised to include inelastic behavior [3,15].

$$M_{zint} = (C_{te})\Phi' - C_{we}\Phi''' + M_{zp} \quad \text{(D-12)}$$

From the above equation, C_{te} and C_{we} are the Saint Venant torsional stiffness and warping stiffness for the elastic section of the beam-column cross-section respectively, Φ represents the angle of twist, Φ''' is the third derivative of the angle of twist whereas M_{zp} is the internal torsional moment for the plastic section of the beam-column cross-section. Warping effects have been ignored in the above analysis because of their minimal effects on both hollow and rectangular beam-column sections.

Subsequently, the Von Mises yield criterion [3,16,84-85] is utilized in the research investigation:

$$\sigma^2 + 3\tau^2 \leq \sigma_Y^2 \quad \text{(D-13)}$$

For a typical hollow rectangular cross-section, the internal resisting elastic-plastic torsional moment M_{zint} using Marshall's simplified equations [15] can be expressed in the following forms:

$$M_{zint} = \tau_Y C_{Mt} \quad \text{for yield limit} \quad \text{(D-14)}$$

$$M_{zint} = \tau_Y (C_{Mte} + C_{Mtp}) \quad \text{for inelastic} \quad \text{(D-15)}$$

$$M_{zint} = 2t\, A_E\, \tau_y \quad \text{for plastic} \quad \text{(D-16)}$$

where:

$$C_{Mt} = \frac{hcIt}{hhc+2Ae} \quad \text{(D-17)}$$

$$C_{Mte} = \frac{(1-\beta)hc,elastic\left(\frac{4hAe^2,elastic}{hc,elastic}+\frac{(1-\beta)^2h^3hc,elastic}{3}\right)}{(1-\beta)hhc,elastic+2Ae,elastic} \quad \text{(D-18)}$$

$$C_{Mtp} = 2\beta h(b-\beta h)(d-\beta h) - \frac{(4-\pi)(2ro-\beta(ro-ri)}{4} \quad \text{(D-19)}$$

where:

$$h_c = 2(((b-h) + (d-h))- (4-\pi)(r_o + r_i) \quad \text{(D-20)}$$

$$I_t = \frac{h^3hc}{3} + \frac{4hAe^2}{hc} \quad \text{(D-21)}$$

$$A_e = (b-h)(d-h)- \frac{(4-\pi)(ro + ri)^2}{4} \quad \text{(D-22)}$$

$$h_{c,elastic} = 2(b+d-2h-2\beta h) - (4-\pi)(r_o + r_i - \beta(r_o + r_i)) \quad \text{(D-23)}$$

$$A_{e,elastic} = (b-h-\beta h)(d-h-\tau Y h) - \frac{(4-\pi)(2ro-\beta(ro-ri)^2}{4} \quad \text{(D-24)}$$

$$\beta = \frac{1}{2} + \frac{Ae}{hhc} - \frac{\tau yL}{2G\Phi mh} \qquad \text{for } 0 \leq \beta \leq 1 \quad \text{(D-25)}$$

$$\Phi_M = \frac{L\tau yCM}{GIt} \quad \text{(D-26)}$$

From the above equations, C_{Mt} represents the torsion modulus constant, I_t equates to the torsion inertia constant, h_c is the mean perimeter, A_e is the enclosed area defined by the wall midline as figuratively shown in Figure 3, h is the cross-sectional wall thickness, C_{Mte} is the torsional modulus constant for the plastified section of the cross-section, β stands for the partial yielded portion of the beam-column cross-sectional area, Φ_M also stands for the angle of twist, C_M becomes equal to C_{Mt} for the yield limit and subsequently equal to (C_{Mte} + C_{Mtp}) for the inelastic phase. Meanwhile, the internal and external corner radii r_o and r_i represents the minute correction for the corner roundness of the rectangular hollow beam-column section. However, in this research investigation, the semi-analytical method applied ignores the effects of the inner and external corner radii in formulating the solution procedure.

APPENDIX D.3 Inelastic Equilibrium Equations for Biaxially Loaded Beam-Columns with Applied Torsion under Ambient Temperature

For the biaxially loaded steel beam-column with applied torque as shown in Figure 1, the displacements of the cross-section are as follows:

$u_Q = u + a\Phi\sin\alpha$ (D-27)

$v_Q = v - a\Phi\cos\alpha$ (D-28)

$\sin\alpha = (yo-y)/a$ (D-29)

$\cos\alpha = (xo-x)/a$ (D-30)

$u_Q = u + \Phi(yo-y)$ (D-31)

$v_Q = v - \Phi(xo-x)$ (D-32)

The displacements of the centroid become zero (x=y=0) and for doubly symmetric members xo and yo are equal to zero

$u_C = u$ (D-33)

$v_C = v$ (D-34)

The equilibrium equations based on the internal resisting moments at a distance z is as follows:

$Mx = -M_{BX} + R_{YZ} + Pv_C$ (D-35)

$My = -M_{BY} + R_{XZ} - Pu_C$ (D-36)

However, in the case of this biaxial setup, moments are only applied at the top end of the member. This makes M_{BX} and M_{BY} equal to zero.

where $R_XL = M_{TY}$ (D-37)

$R_YL = M_{TX}$ (D-38)

Hence, $Mx = z/L(M_{TX}) + Pv$ (D-39)

$My = z/L(M_{TY}) - Pu$ (D-40)

$$M_Z = M_{RZ} \quad \text{(D-41)}$$

Through translating and rotating the cross-section, a new set of rectilinear coordinates are obtained:

$$M_\xi = M_X + \Phi M_Y \quad \text{(D-42)}$$

$$M_\eta = M_Y - \Phi M_X \quad \text{(D-43)}$$

$$M_\varsigma = M_X u' + M_Y v' + P_{YO} u' - P_{XO} v' - \bar{K}\Phi' - v/L(M_{TY}) - u/L(M_{TX}) \quad \text{(D-44)}$$

Induced moments due to the presence of partial rotational end restraints in the member are introduced as follows:

$$m_{BX} = k_{BX}\theta_{BX} \quad \text{(D-45)}$$

$$m_{BY} = k_{BY}\theta_{BY} \quad \text{(D-46)}$$

$$m_{TX} = -k_{TX}\theta_{TX} \quad \text{(D-47)}$$

$$m_{TY} = -k_{TY}\theta_{TY} \quad \text{(D-48)}$$

where k_{BX}, k_{BY}, k_{TX}, k_{TY}, θ_{BX}, θ_{BY}, θ_{TX} and θ_{TY} represent the partial rotational stiffnesses and corresponding end slopes respectively.

$$\theta_{BX} = v'(0) \quad \text{(D-49)}$$

$$\theta_{BY} = u'(0) \quad \text{(D-50)}$$

$$\theta_{TX} = -v'(L) \quad \text{(D-51)}$$

$$\theta_{TY} = -u'(L) \quad \text{(D-52)}$$

Therefore, the induced moments are introduced into the new rectilinear coordinates ξ,η and ς of the displaced cross section as follows:

$$M_\xi = -m_{BX} + z/L(M_{TX} - m_{BX} + m_{BX}) + PV + \Phi(m_{BY} + z/L(M_{TY} + m_{TY} - m_{BY})) - M_{RZ}u' \quad \text{(D-53)}$$

$$M_\eta = m_{BY} + z/L(M_{TY} - m_{TX} + m_{BX}) - PU + \Phi(-m_{BX} + z/L(M_{TX} + m_{TY} - m_{BY})) - M_{RZ}v' \quad \text{(D-54)}$$

$M_\varsigma = u'(-m_{BX} + z/L(M_{TX} - m_{TX} + m_{BX}) + v'(m_{BY} + z/L(M_{TY} + m_{TY} - m_{BY}) - \bar{K}\Phi' - v/L(M_{TY} + m_{TY} - m_{BY}) - u/L(M_{TX} - m_{TX} - m_{BX}) + M_{RZ}$ (D-55)

From the above equations,

$K = \int_A \sigma a^2 dA$ (D-56)

where a^2 is defined as follows:

$a^2 = (x_o - x)^2 + (y_o - y)^2$ (D-57)

where a is defined as the distance between the point where σ acts and the shear center. By applying the fundamental rule of substituting equation 46 into equation 45, the resulting equation obtained is as follows:

$K = -Pr^2 + \beta_x M_{BX} - \beta_Y M_{BY}$ (D-58)

From the above equation:

$\beta_x = \frac{\int A\, y(x^2+y^2) dA}{Ix} - 2yo$ (D-59)

$\beta_y = \frac{\int A\, x(x^2+y^2) dA}{Iy} - 2xo$ (D-60)

Meanwhile, by introducing the curvature about x and y axes Φx and Φy as well as warping strain ϵ_w into equation

$\Phi_x = -v''$ (D-61)

$\Phi_y = u''$ (D-62)

$\epsilon_w = -\omega_n \Phi$ (D-63)

Hence, by substituting equations B-61 through B-63 into the general equation 1 we obtain the following as a result:

$\epsilon = \epsilon_o - v''y - u''x + \epsilon_r - \omega_n \Phi''$ (D-64)

By applying equations 2 through to 4 with equations D-38 into general equations 6 to 8, we obtain the underlisted following equations:

$$-g_{11}\epsilon_o + g_{12}v'' + g_{13}u'' + g_{14}\Phi'' - P_r - P_p = P \quad \text{(D-65)}$$

$$-g_{21}\epsilon_o + g_{22}v'' + g_{23}u'' + g_{24}\Phi'' - M_{xre} - M_{xp} = -M_x \quad \text{(D-66)}$$

$$-g_{31}\epsilon_o + g_{32}v'' + g_{33}u'' + g_{34}\Phi'' - M_{yre} - M_{yp} = M_y \quad \text{(D-67)}$$

$$(C_{te})\Phi' - C_{we}\Phi''' + M_{zp} = M_z \quad \text{(D-68)}$$

Equation 1 is used to solve for ϵ_o

$$\epsilon_o = \frac{\mathbf{1}}{\mathbf{g11}}(-P-P_p-P_r + g_{12}v'' + g_{13}u'' + g_{14}\Phi'') \quad \text{(D-64)}$$

By substituting equation (D-64) into equations (D-66) and (D-67), the resulting equations are as follows:

$$-g_{21}\frac{\mathbf{1}}{\mathbf{g11}}(-P-P_p-P_r + g_{12}v'' + g_{13}u'' + g_{14}\Phi'') + g_{22}v'' + g_{23}u'' + g_{24}\Phi'' - M_{xre} - M_{xp} = -M_x \quad \text{(D-69)}$$

$$-g_{31}\frac{\mathbf{1}}{\mathbf{g11}}(-P-P_p-P_r + g_{12}v'' + g_{13}u'' + g_{14}\Phi'') + g_{32}v'' + g_{33}u'' + g_{34}\Phi'' - M_{yre} - M_{yp} = M_y \quad \text{(D-70)}$$

$$v''(-g_{21}g_{12}+g_{11}g_{22})/g_{11} + u''(-g_{21}g_{13}+g_{11}g_{23})/g_{11} + \Phi''(-g_{21}g_{12}+g_{11}g_{24})/g_{11} - g_{21}(-P-P_p-P_r)/g_{11} - M_{xre} - M_{xp} = -M_x \quad \text{(D-71)}$$

$$v''(-g_{31}g_{13}+g_{11}g_{32})/g_{11} + u''(-g_{31}g_{13}+g_{11}g_{33})/g_{11} + \Phi''(-g_{31}g_{13}+g_{11}g_{34})/g_{11} - g_{31}(-P-P_p-P_r)/g_{11} - M_{yre} - M_{yp} = M_y \quad \text{(D-72)}$$

By substituting in the bending stiffnesses, load and moment parameters from equation (D-44)-(D-47), the resulting equation becomes:

$$B_{xx}v'' + B_{xy}u'' + B_{xw}\Phi'' + S_{xe}P_{ep} - A_eM_{xx(ep)} = -A_eM_{xx} \quad \text{(D-73)}$$

$$B_{yx}v'' + B_{yy}u'' + B_{yw}\Phi'' + S_{ye}P_{ep} - A_eM_{yy(ep)} = A_eM_{yy} \quad \text{(D-74)}$$

$$C_{te}\Phi' - C_{we}\Phi''' + M_{zp} = M_z \quad \text{(D-75)}$$

Hence by applying the second order approach, the equilibrium equations for the biaxial bending moments and torsional equations in this research investigation is expressed as follows:

$$M_\xi = PV - m_{BX} + \frac{z}{L}(M_{TX} - m_{TX} + m_{BX}) + \Phi(m_{BY} + \frac{z}{L}(M_{TY} + m_{TY} - m_{BY})) - M_{RZ}u' \quad \text{(D-76)}$$

$$M_{\eta} = - PU - m_{BY} + \frac{z}{L}(M_{TY} - m_{TX} + m_{BX}) + \Phi(-m_{BX} + \frac{z}{L}(M_{TX} + m_{TY} - m_{BY})) - M_{RZ}\, v' \qquad \text{(D-77)}$$

$$M_{\varsigma} = -K\Phi' + v'[m_{BY} + \frac{z}{L}(M_{TY} + m_{TY} - m_{BY}) + u'[-m_{BX} + \frac{z}{L}(M_{TX} - m_{TX} - m_{BX}) - \frac{v}{L}(M_{TY} + m_{TY} - m_{BY}) - \frac{u}{L}(M_{TX} - m_{TX} - m_{BX}) + M_{RZ} \qquad \text{(D-78)}$$

Substituting equations (D-73 -D-75) into (D-76 – D-78), we obtain the governing general nonlinear differential equations :

$$B_{xx}v'' + B_{xy}u'' + B_{xw}\Phi'' - A_eM_{RZ}u' + A_ePv + A_e\Phi(m_{BY} + \frac{z}{L}(M_{TY} - m_{TY} - m_{BY}) - A_em_{BX} + A_e\frac{z}{L}(-m_{TX} + m_{BX}) = - A_ePv_i - A_e\frac{z}{L}(M_{TX}) - S_{xe}P + S_{xe}P_{re} + A_eM_{xre} - S_{xe}P_p + A_eM_{xp} \qquad \text{(D-79)}$$

$$B_{yx}v'' + B_{yy}u'' + B_{yw}\Phi'' - A_eM_{RZ}v' + A_ePu + A_e\Phi(-m_{Bx} + \frac{z}{L}(M_{TX} - m_{TX} + m_{BX}) - A_em_{BY} - A_e\frac{z}{L}(m_{TY} - m_{BY}) = - A_ePu_i + A_e\frac{z}{L}(M_{TY}) - S_{ye}P - S_{ye}P_{re} + A_eM_{yre} - S_{ye}P_p + A_eM_{yp} \qquad \text{(D-80)}$$

$$C_{we}\Phi''' - (C_{te} + K)\Phi' + v'[m_{BY} + \frac{z}{L}(M_{TY} + m_{TX} - m_{BX}) + u'[-m_{BX} + \frac{z}{L}(M_{TX} - m_{TX} + m_{BX}) - \frac{v}{L}(M_{TY} + m_{TY} - m_{BY}) - \frac{u}{L}(M_{TX} - m_{TX} - m_{BX}) = - M_{RZ} + M_{zp} \qquad \text{(D-81)}$$

APPENDIX E: COMPUTER PROGRAM

```
clear all
clc
n = 64;
m = 1/8*n;
A = zeros(m,n);
X = zeros (m,n);
Y = zeros(m,n);
NA = n*m;
NB = m*n;
L = 33.75;
a = 1.5;
b = 1.5;
d = 1.5;
t = 0.125;
tf = 0.125;
tw = 0.125;
As = a*b-(a-2*tw)*(b-2*tf); % area of section
G= 11236;
Sigmay = 58.64;
Sigmar = 23.33;
tauy   = 32.56;
E = 29988;
ey = Sigmay/E;
Py = As*Sigmay;
Zx =  a*b^2/4-(a-2*tw)*(b-2*tf)^2/(4);
Zy =  b*a^2/4-(b-2*tf)*(a-2*tw)^2/(4);
Mpx = Zx*Sigmay;
Mpy = Zy*Sigmay;
Sx = 0.29125;
Sy = 0.29125;
xo = 0;
yo = 0;
Sx1 = 0.0039;        % Elastic section modulus about x-axis
Sx2 = 0.0352;        % Elastic section modulus about x-axis
Sx3 = 0.0352;        % Elastic section modulus about x-axis
Sx4 = 0.0039;        % Elastic section modulus about x-axis
Sy1 = 0.0039;        % Elastic section modulus about y-axis
Sy2 = 0.0352;        % Elastic section modulus about y-axis
Sy3 = 0.0352;        % Elastic section modulus about y-axis
Sy4 = 0.0039;        % Elastic section modulus about y-axis
Ix1 = 0.00024;       % Moment of inertia about x-axis
Ix2 = 0.0203;        % Moment of inertia about x-axis
Ix3 = 0.0203;        % Moment of inertia about x-axis
Ix4 = 0.00024;       % Moment of inertia about x-axis
```

```
Iy1 = 0.00024;       % Moment of inertia about x-axis
Iy2 = 0.0203;        % Moment of inertia about x-axis
Iy3 = 0.0203;        % Moment of inertia about x-axis
Iy4 = 0.00024;       % Moment of inertia about x-axis
Iw = (b^3*t^3)/36;   % warping constant
Iwy1 = (b^3*t^3)/36;  %
Iwy2 = (b^3*t^3)/36;  %
Iwy3 = (b^3*t^3)/36;  %
Iwy4 = (b^3*t^3)/36;  %
Iwx1 = (b^3*t^3)/36;  %
Iwx2 = (b^3*t^3)/36;  %
Iwx3 = (b^3*t^3)/36;  %
Iwx4 = (b^3*t^3)/36;  %
Ixy1 = 0.000;
Ixy2 = 0.000;
Ixy3 = 0.000;
Ixy4 = 0.000;
Swx1 = 0;        % Warping statical moment about x-axis
Swx2 = 0;        % Warping statical moment about x-axis
Swx3 = 0;        % Warping statical moment about x-axis
Swx4 = 0;        % Warping statical moment about x-axis
Swy1 = 0;        % Warping statical moment about y-axis
Swy2 = 0;        % Warping statical moment about y-axis
Swy3 = 0;        % Warping statical moment about y-axis
Swy4 = 0;        % Warping statical moment about y-axis
p  = 0;
p1 = 0;
p2 = 0;
p3 = 16;
pM = 100;
MxM= 100*sin(45);
MzM = 50;
e  = 8.125;
di = 24;
Mx = p3*sin(45)*di;
My = p3*sin(45)*di;
Mz = 0;
ho = L/10;
y = d/2;
x = b/2;
z= L;
MTx = Mx;            % moment at the top end of the column about x-axis
MTy = My;            % moment at the top end of the column about y-axis
MBx = 0;             % moment at the bottom end of the column about x-axis
MBy = 0;             % moment at the bottom end of the column about y-axis
mTx = 0;             % moment due to springs at the top end of the column about x-axis
```

```
mTy = 0;              % moment due to springs at the top end of the column about y-axis
mBx = 0;              % moment due to springs at the bottom end of the column about x-axis
mBy = 0;              % moment due to springs at the top end of the column about y-axis
Pr  =  Sigmar*As;      % residual axial load
Pp  =  Sigmay*As;      % internal plastic load
Pep = p1+Pr;
Pepstar = Pr;
Mxr = 0;              % residual bending moment about x-axis
Mxp = 0;              % internal plastic moment about x-axis
Myr = 0;              % residual bending moment about y-axis
Myp = 0;              % internal plastic moment about y-axis
Mxx = Mxr + Mxp;
Myy = Myr + Myp;
Mrz = Mz;          % reacting torsional moment
Mzp = 0;              % torsional moment due to plastification%%
AE1 = (b*tf);
AE2 = (b*tf);
AE3 = ((d-2*tf)*tw );
AE4 = ((d-2*tf)*tw );
Zx =  a*b^2/4-(a-2*tw)*(b-2*tf)^2/(4);          % Plastic section modulus about x-axis.
Zy =  b*a^2/4-(b-2*tf)*(a-2*tw)^2/(4);          % Plastic section modulus about y-axis.
% sigmay = sqrt((sigma)^2 + 3*(tauy^2));         % Shear yield stress.
ey    = Sigmay/E ;                    % Yield strain.
p1p   = p1/Py;
Mpy   = Zy*Sigmay ;                     % Plastic My.
Mpx   = Zx*Sigmay ;                     % Plastic Mx.
Mpz   = tauy*2*tf*As;
Ri    = 1.5*tf;                    % External corner radii
Ro    = 1.0*tf;                    % Internal corner radii
Ap    = (b-tf)*(d-tf)- (Ro^2+Ri^2*(4-pi))/4;    % Area enclosed by mean perimeter
pm    = 2*[(b-tf)+ (d-tf)] - (Ri-Ro)*(4-pi);    % Mean perimeter length
It    = (4*Ap^2*tf)/pm + (tf^3*pm)/3;          % Torsional constant
Cw    = E*Iw;                    % Warping stiffness
Kt    = (4*Ap^2*tf)/pm;
Ct    = G*Kt;
Cmt   = (pm*It)/(tf*pm + 2*Ap);              % Torsional modulus constant
Mzy   = tauy*Cmt;                    % Internal resisting moment for yield limit
phim  = (L*tauy*Cmt)/(G*It);                % angle of twist
Beta  = 0.5+(Ap/tf*pm)-(tauy*L)/(2*G*phim*tf);  % partial yielded cross-sections
pme   = 2*(b+d-2*tf-2*Beta*tf-(4-pi)*(Ro+Ri)-(Beta*Ro)+ (Beta*Ri));      % mean perimeter
elastic
Ape   = (b-tf-Beta*tf)*(d-tf-Beta*tf)-((4-pi)*(Ro^2+Ri^2-Beta^2*Ro^2+Ri^2))/4;          %
ACmte  = ((1-Beta)*pme*(4*pm*Ape^2/(pme) + (1-Beta)^2*tf^3*pme/3));
Cmte   = ACmte /(1-Beta*tf*pme + 2*Ape);
Cmtp   = 2*Beta*tf*(b-Beta*tf)*(d-Beta*tf)-((4-pi)*(2*Ro-Beta*Ro+Beta*Ri))/4;
```

```
Mzi    = tauy*(Cmte + Cmtp);                    % Internal resisting moment for
inelastic limit
Mzp    = 2*0.125*Ap*tauy;                       % Internal resisting moment for plastc
limit
voi    = L/10000;
uoi    = L/10000;
Vi     = voi*sin(pi*z/L);
Ui     = uoi*sin(pi*z/L);
Limit2  = Sigmay/E;

                        %% CROSS-SECTIONAL ANALYSIS %%
%% CALCULATION OF INTERNAL STRAINS AND STRESES
%% HORIZONTAL PLATES
for i = 1:m*n
   A(i) = (1.5/n)*(0.125/m);
   A2 = A;
end
Q1 = 0.5:1:n/2;
Q2 = (-n/2 + 0.5):1:n/2;
for i = 1:n
   j = 1:m;
   if i<(1+n/2)
      X(j,i)= -0.75+ Q1(i)*(1.5/n);
   else
      X(j,i)= Q2(i)*(1.5/n);
   end
   X2(j,i) = X(j,i);
end

Q3= 0.5:1:m;
for i = 1:m
   j = 1:n;
   Y(i,j)= 0.75-Q3(i)*(0.125/m);
   Y2(i,j)= -Y(i,j);
end

%% VERTICAL PLATES

A3 = zeros(n,m);
X3 = zeros(n,m);
Y3 = zeros(n,m);
for i = 1:m*n
   A3(i) = (0.75-2*0.125)/(n)*(0.125/m);
   A4 = A3;
end
Q4 = 0.5:1:m;
```

```
Q5 = (-m/2+0.5):1:m/2;
for i = 1:m
   j = 1:n;
   X3(j,i)= 0.75-Q4(i)*(0.125/m);
   X4(j,i)= -X3(j,i);
end

for i = 1:n
   j = 1:m;
   if i<(1+n/2)
   Y3(i,j)= (-0.625+Q1(i)*(1.25/n));
   else
   Y3(i,j)= -Q2(i)*(1.25/n);
   end
   Y4(i,j) = Y3(i,j);
end
Ae1 = A(1,1);
Ae2 = A2(1,1);
Ae3 = A3(1,1);
Ae4 = A4(1,1);


%% TANGENT STIFFNESS FORMULATION BASED ON PLATES
%% PLATE 1
g11P1  = E*Ae1;
g12P1  = E*Sx1;
g13P1  = E*Sy1;
g14P1  = E*Swx1;
g21P1  = E*Sx1;
g22P1  = E*Ix1;
g23P1  = E*Ixy1;
g24P1  = E*Iwy1;
g31P1  = E*Sy1;
g32P1  = E*Ixy1;
g33P1  = E*Iy1;
g34P1  = E*Iwx1;
g41P1  = E*Swx1;
g42P1  = E*Iwy1;
g43P1  = E*Iwx1;
g44P1  = E*Swy1;
%% PLATE 2
g11P2  = E*Ae2;
g12P2  = E*Sx2;
g13P2  = E*Sy2;
g14P2  = E*Swx2;
g21P2  = E*Sx2;
```

```
g22P2  = E*Ix2;
g23P2  = E*Ixy2;
g24P2  = E*Iwy2;
g31P2  = E*Sy2;
g32P2  = E*Ixy2;
g33P2  = E*Iy2;
g34P2  = E*Iwx2;
g41P2  = E*Swx2;
g42P2  = E*Iwy2;
g43P2  = E*Iwx2;
g44P2  = E*Swy2;
%% PLATE 3
g11P3  = E*Ae3;
g12P3  = E*Sx3;
g13P3  = E*Sy3;
g14P3  = E*Swx3;
g21P3  = E*Sx3;
g22P3  = E*Ix3;
g23P3  = E*Ixy3;
g24P3  = E*Iwy3;
g31P3  = E*Sy3;
g32P3  = E*Ixy3;
g33P3  = E*Iy3;
g34P3  = E*Iwx3;
g41P3  = E*Swx3;
g42P3  = E*Iwy3;
g43P3  = E*Iwx3;
g44P3  = E*Swy3;
%% PLATE 4
g11P4  = E*Ae4;
g12P4  = E*Sx4;
g13P4  = E*Sy4;
g14P4  = E*Swx4;
g21P4  = E*Sx4;
g22P4  = E*Ix4;
g23P4  = E*Ixy4;
g24P4  = E*Iwy4;
g31P4  = E*Sy4;
g32P4  = E*Ixy4;
g33P4  = E*Iy4;
g34P4  = E*Iwx4;
g41P4  = E*Swx4;
g42P4  = E*Iwy4;
g43P4  = E*Iwx4;
g44P4  = E*Swy4;
```

```
Ta = [ E*Ae1  E*Sx1 E*Sy1 E*Swx1 ; E*Sx1 E*Ix1 E*Ixy1 E*Iwy1; E*Sy1 E*Ixy1 E*Iy1
E*Iwx1; E*Swx1 E*Iwy1 E*Iwx1 E*Swy1];
Tb = [ E*Ae2  E*Sx2 E*Sy2 E*Swx2 ; E*Sx2 E*Ix2 E*Ixy2 E*Iwy2; E*Sy2 E*Ixy2 E*Iy2
E*Iwx2; E*Swx2 E*Iwy2 E*Iwx2 E*Swy2];
Tc = [ E*Ae3  E*Sx3 E*Sy3 E*Swx3 ; E*Sx3 E*Ix3 E*Ixy3 E*Iwy3; E*Sy3 E*Ixy3 E*Iy3
E*Iwx3; E*Swx3 E*Iwy3 E*Iwx3 E*Swy3];
Td = [ E*Ae4  E*Sx4 E*Sy4 E*Swx4 ; E*Sx4 E*Ix4 E*Ixy4 E*Iwy4; E*Sy4 E*Ixy4 E*Iy4
E*Iwx4; E*Swx4 E*Iwy4 E*Iwx4 E*Swy4];

TA = repmat(Ta,n*m);
TB = repmat(Tb,m*n);
TC = repmat(Tc,m*n);
TD = repmat(Td,n*m);
NA = n*m;

f = [p1;Mx;My;Mz];
EsA = pinv(Ta)*f;
EsB = pinv(Tb)*f;
EsC = pinv(Tc)*f;
EsD = pinv(Td)*f;

for i = 1:m
   j = 1:n;
   Esp1(i,j) = -Y(i,j)*EsA(1,1)+EsA(2,1);
   Sigma1(i,j) = Esp1(i,j)*E;
   if Esp1(i,j)> Sigmay/E
      Sigma1(i,j) = Sigmay;
   end
   if Esp1(i,j)<-Sigmay/29998
      Sigma1(i,j)= -Sigmay;
   end
Px1(i,j) = -Sigma1(i,j)*A(1,1);
Mx1(i,j) =  Sigma1(i,j).*Y(i,j)*A(1,1);
My1(i,j) =  Sigma1(i,j).*X(i,j)*A(1,1);

Esp2(i,j) = -Y2(i,j)*EsB(1,1)+EsB(2,1);
   Sigma2(i,j) = Esp2(i,j)*E;
   if Esp2(i,j)> Sigmay/E
      Sigma2(i,j) = Sigmay;
   end
   if Esp2(i,j)<-Sigmay/29998
      Sigma2(i,j)= -Sigmay;
   end
Px2(i,j) = -Sigma2(i,j)*A2(1,1);
Mx2(i,j) =  Sigma2(i,j).*Y2(i,j)*A2(1,1);
My2(i,j) =  Sigma2(i,j).*X2(i,j)*A2(1,1);
```

```
end

for i = 1:n
   j = 1:m;
Esp3(i,j) = -Y3(i,j)*EsC(1,1)+ EsC(2,1);
   Sigma3(i,j) = Esp3(i,j)*E;
   if Esp3(i,j)> Sigmay/E
      Sigma3(i,j) = Sigmay;
   end
   if Esp3(i,j)<-Sigmay/29998
      Sigma3(i,j)= -Sigmay;
   end
Px3(i,j) = -Sigma3(i,j)*A3(1,1);
Mx3(i,j) =  Sigma3(i,j).*Y3(i,j)*A3(1,1);
My3(i,j) =  Sigma3(i,j).*X3(i,j)*A3(1,1);


Esp4(i,j) = -Y4(i,j)*EsD(1,1)+EsD(2,1);
   Sigma4(i,j) = Esp4(i,j)*E;
   if Esp4(i,j)> Sigmay/E
      Sigma4(i,j) = Sigmay;
   end
```

VITA

George Adomako Kumi was born in Kumasi, Ghana. He graduated from Opoku Ware School, Kumasi in 2006. He received his Bachelor of Science in Building Technology from Kwame Nkrumah University of Science and Technology, Ghana in 2011 and subsequently worked with the Department of Urban Roads, Kumasi. He received the highly coveted Chinese Government Scholarship to continue his graduate studies at the prestigious Chongqing University, People's Republic of China from August 2014 to July 2018. He received a certificate in Chinese Language and Culture in July 2015 and subsequently his Master of Science in Civil Engineering (Structural Engineering Focus) after completing a 3 year graduate degree program in July 2018. Adomako Kumi started his Ph.D. in Civil Engineering at The Civil and Environmental Department of Old Dominion University (134 Kaufman Hall, Norfolk, VA,23529) in Fall 2018. The current dissertation "**THERMO-ELASTO-PLASTIC STABILITY OF BIAXIALLY LOADED HOLLOW RECTANGULAR SECTION STEEL BEAM-COLUMNS WITH APPLIED TORSION**" was supervised by Dr. Zia Razzaq.

He currently serves as the Secretary for the American Society of Civil Engineering (ASCE-Norfolk Branch). During his Ph.D studies, Kumi worked as a Research and Teaching assistant at The CEE Department of Old Dominion University (2019-2023) ,Civil Engineer Intern at the City of Virginia Beach Public Works Engineering QA/QC Department (Summer 2022), Field Engineer Intern for McLean Construction Company (Summer 2023) and Structural Engineering Intern for AECOM Technical Services (Fall 2023).